



PHD

**Intracellular Library Screening to Derive Novel Peptide-based Inhibitors of Toxicity in Alzheimer's Disease
(Alternative Format Thesis)**

Carver, Rebecca

Award date:
2022

Awarding institution:
University of Bath

[Link to publication](#)

Alternative formats

If you require this document in an alternative format, please contact:
openaccess@bath.ac.uk

Copyright of this thesis rests with the author. Access is subject to the above licence, if given. If no licence is specified above, original content in this thesis is licensed under the terms of the Creative Commons Attribution-NonCommercial 4.0 International (CC BY-NC-ND 4.0) Licence (<https://creativecommons.org/licenses/by-nc-nd/4.0/>). Any third-party copyright material present remains the property of its respective owner(s) and is licensed under its existing terms.

Take down policy

If you consider content within Bath's Research Portal to be in breach of UK law, please contact: openaccess@bath.ac.uk with the details. Your claim will be investigated and, where appropriate, the item will be removed from public view as soon as possible.

**Intracellular Library Screening to
Derive Novel Peptide-based
Inhibitors of Toxicity in
Alzheimer's Disease**

Rebecca Carver

A thesis submitted for the degree of Doctor of Philosophy

University of Bath

Department of Biology and Biochemistry

June 2022

Copyright Notice

Attention is drawn to the fact that copyright of this thesis/portfolio rests with the author and copyright of any previously published materials included may rest with third parties. A copy of this thesis/portfolio has been supplied on condition that anyone who consults it understands that they must not copy it or use material from it except as licenced, permitted by law or with the consent of the author or other copyright owners, as applicable.

Declarations

Declaration of any previous submission of the work

The material presented here for examination for the award of a higher degree by research has not been incorporated into a submission for another degree.

Rebecca Carver

Declaration of authorship

I am the author of this thesis, and the work described therein was carried out by myself personally, with the exception of the cell-based evaluations in Chapter Two, Three and Four where ~ 5 % of the work was carried out by other researchers in the preparation and culture of cells prior to some assays which was conducted by Kim Morris.

Rebecca Carver

Acknowledgements

I would first and foremost like to thank my supervisor Jody Mason for his dedicated help and guidance throughout this study. Thank you for all of your support over the years and your unlimited help solving the many issues faced within the lab. Without your dedication, help and guidance this study would not have been possible. I would also like to thank my secondary supervisor Robert Williams for helping me to explore the cellular aspects of this thesis and helping to optimise an exciting cell-based assay to greatly enhance the characterisation of our peptide hits.

I would also like to thank everyone in the Mason lab, in particular, Miao Yu, Hadi Mohammad, Sarah Madden, Andrew Brennan, Akello Agwa, Richard Meade and Kathryn Watt, all of whom have contributed greatly throughout my PhD and have all helped me to solve experimental issues across the multiple aspects of the study. If I ever had a question, you'd all be more than happy to help and offer as much advice as possible which made problem solving and troubleshooting a whole lot smoother having so many great, experienced people at hand! Thank you also goes to Kim Morris in the Williams lab for all of your help and support in developing the cell-based assay within the study, thank you for sharing all of your skills and knowledge and helping to establish the assay within your lab!

Finally, a thank you to Alzheimer's Society for their generosity in funding and providing me the means by which to carry out this PhD thesis.

Table of contents

Contents

Acknowledgements.....	3
Table of contents	4
Thesis Abstract.....	7
List of Abbreviations	8
Chapter One: Introduction.....	13
History of Alzheimer’s Disease	14
General overview of Alzheimer’s Disease and symptoms.....	14
Alzheimer’s Disease Epidemiology.....	16
Processing of Amyloidogenic Precursor Protein to produce A β	16
Amyloid Cascade Hypothesis.....	19
Pathological Role of oligomeric A β	21
Familial AD.....	22
Risk Factors in sporadic AD	27
Why target A β over Tau?.....	28
Structure/Fold of A β throughout aggregation.....	31
A β – a native role?	34
Towards AD Treatments.....	35
Peptide Therapies to target AD	38
Aim of the study.....	46
Chapter Two: Method developments carried out throughout the study to enable optimal experimental processes.....	47
Chapter Introduction.....	48
Method development steps for optimisation.....	49
Optimisation steps for Library Building	49
Library Screening in PCA platform	58
Peptide synthesis and purification	61
Expression and purification of A β (M1-42)	64
Monomeric A β (M1-42) isolated with Size Exclusion Chromatography.....	65
Methods to explore oligomerisation state of A β throughout aggregation	67
Optimisation of a cell-based toxicity assay to assess A β -induced toxicity.....	74
Optimisation of an A β 1-42-induced toxicity assay in differentiated SH-SY5Y cells	75

Abstract.....	75
Introduction	75
Materials and Methods.....	80
Results and discussion	84
Conclusions	94
Supporting Information.....	97
Supporting Results.....	97
Chapter Conclusions	98
Chapter Three: Identification of in-cell derived peptide inhibitors of A β aggregation and toxicity	99
Chapter Introduction.....	100
An in-cell derived peptide inhibitor of A β aggregation and toxicity	103
Abstract.....	103
Introduction	103
Materials and Methods.....	106
Results.....	110
Discussion	124
Conclusions	131
Supporting Information.....	133
Supporting Materials and Methods.....	133
Supporting Results.....	141
Chapter Conclusions	143
Chapter Four: Establishing a Transcription Block Survival screening assay to identify functional peptide antagonists of A β toxicity	144
Chapter Introduction.....	145
A Transcription Block Survival screening assay to identify functional peptide antagonists of A β toxicity.....	147
Abstract.....	147
Introduction	147
Materials and Methods.....	150
Results.....	153
Discussion	167
Conclusions	171
Supporting Information.....	174
Supplementary Materials and Methods	174
Supplementary Results.....	180
Chapter Conclusion.....	182

Chapter Five: Conclusions	184
Thesis Conclusions	185
Bibliography	190

Thesis Abstract

Alzheimer's disease (AD) is the most common form of dementia with around 520,000 individuals currently diagnosed in the UK. Despite the devastating impact of AD there are currently no successful therapeutic approaches to treat the condition. AD is characterised by the misfolding and aggregation of the Amyloid- β ($A\beta$) peptide. Whilst pinpointing the exact species of $A\beta$ that exerts toxicity is difficult, it is generally accepted that oligomeric forms of the peptide confer toxicity. Various oligomer sizes and conformers impart varying mechanisms of toxicity but ultimately, soluble oligomers of $A\beta$ initiate a cascade of downstream toxic events that eventually lead to the neuronal cell death responsible for AD. Recent application of cryogenic electron microscopy (cryo-EM) and solid-state NMR (ssNMR) techniques have revealed high-resolution structural information regarding the architecture of $A\beta$ within fibres.

Here, a semi-rational approach has been applied to design peptide libraries utilising one of these recent high-resolution structures as a template. In particular, we focus on two key regions, an outer β -sheet strand and the central dimeric interface, which are instrumental in formation of the Greek-key motif common to most amyloid folds. The intracellular Protein-fragment complementation assay (PCA) was employed, and a further novel transcription block survival (TBS) assay developed, along with successful proof-of-concept experiments, and applied to successfully identify peptide inhibitors of $A\beta_{1-42}$. The study utilised Thioflavin-T (ThT) fluorescence aggregation assays along with Circular Dichroism (CD), Transmission Electron Microscopy (TEM) and photoinduced crosslinking experiments to demonstrate the ability of the selected peptides to impact upon $A\beta$ aggregation. The study next sought to explore how the altered aggregation of $A\beta$ would translate within a cell-based assay. Therefore, an $A\beta$ -induced toxicity assay was optimised within a differentiated SH-SY5Y cell line applying low concentrations of $A\beta$. Upon application of the identified peptide hits it was observed both could partially rescue $A\beta$ -induced toxicity within the human derived neuronal-like cell line as measured by 3-(4,5-dimethylthiazol-2-yl)-2,5-diphenyltetrazolium-bromide (MTT) viability assays. The peptide sequences identified herein present exciting targets for potential therapeutic candidates to target $A\beta$ -induced toxicity in AD.

Overall, this study demonstrates the successful application of the PCA assay and the development and application of the novel, intracellular TBS screening platform to identify peptide hit sequences able to alter $A\beta$ -induced aggregation. Optimisation of an $A\beta$ -induced toxicity assay within a relevant human-derived cell line also provides a platform to assess the potential of future drug candidates and reveals the potential for the peptide sequences identified to partially rescue $A\beta$ -induced toxicity.

List of Abbreviations

1,2-Dimyristoyl-sn-glycero-3-phospho-L-serine (DMPS)

3-(4,5-dimethylthiazol-2-yl)-2,5-diphenyltetrazolium-bromide (MTT)

Acetylcholinesterase (AChE)

Adenosine Triphosphate (ATP)

Alanine (Ala) (A)

Alzheimer's Disease (AD)

Ammonium Persulphate (APS)

Ampicillin (Amp)(A)

Amyloid Cascade Hypothesis (ACH)

Amyloid Precursor Protein (APP)

Amyloid- β (A β)

Apolipoprotein E (APOE (gene)/ApoE (protein))

APP Intracellular Domain (AICD50)

Arginine (Arg) (R)

Asparagine (Asn) (N)

Aspartic Acid (Asp) (D)

A β _{17-40/42} fragment (p3)

Blood Brain Barrier (BBB)

Brain-Derived Neurotrophic Factor (BDNF)

Calcium (2+) (Ca²⁺)

Calcium-dependent Calmodulin Kinase IIa (CamKIIa)

Cell Penetrating Peptide (CPP)

Cellular Prion Protein (PrP^c)

Central Nervous System (CNS)

Cerebrospinal fluid (CSF)

Chloramphenicol (Cm)(C)

Circular Dichroism (CD)

Cryogenic electron microscopy (cryo-EM)

Cysteine (Cys) (C)

D-Enantiomeric peptides (D-peptides)

Deoxyribonucleic Acid (DNA)

Dihydrofolate Reductase (mDHFR)

Dimethyl sulfoxide (DMSO)

Dithiothreitol (DTT)

Down's Syndrome (DS)

Dulbecco's modified Eagle's medium (DMEM)

Escherichia coli (*E. coli*)

European Collection of Authenticated Cell Cultures (ECACC)

Excitatory amino acid transporter 2 (EAAT2)

Extracellular Matrix (ECM)

Familial AD (FAD)

Fetal Bovine Serum (FBS)

Food and Drug Administration (FDA)

Frontotemporal Dementia (FTD)

Glutamate (Glu) (E)

Glutamine (Glu) (Q)

Glycine (Gly) (G)

Glycogen Synthase Kinase-3 β (GSK3 β)

Green Fluorescent Protein (GFP)

Guanidine Hydrochloride (GuHCl)

High Performance Liquid Chromatography (HPLC)

Histidine (His) (H)

Human Amyloid Precursor Protein (hAPP)

Human Tau (hTau)

Insulin Degrading Enzymes (IDE)

Islet Amyloid Polypeptide (IAPP)

Isoleucine (Iso) (I)

Isopropyl β -D-1-thiogalactopyranoside (IPTG)

Kanamycin (Kan)(K)

L-Enantiomeric peptides (L-peptides)

Leucine (Leu) (L)

Long Term Depression (LTD)

Long Term Potentiation (LTP)

Lysine (Lys) (K)

Lysogeny Broth (LB)

Magic-angle Spinning (MAS)

Major Histocompatibility Complex (MHC)

Mass Spectrometry (MS)

Messenger RNA (mRNA)

Methionine (Met) (M)

Microtubule-associated Protein (MAP)

Mild Cognitive Impairment (MCI)

Neurofibrillary Tangles (NFT)

Neuron Specific Enolase (NSE)

Neuronal Nuclei protein (NeuN)

N-methyl-d-aspartate Receptors (NMDAR)

Nuclear magnetic resonance (NMR)

O-linked N-acetylglucosamine (O-GlcNAc)

Penicillin (Pen)

Phenylalanine (Phe) (F)

Phosphatidylinositol 3-kinase (PI3K)

Photo-induced Cross-linking of Unmodified Proteins (PICUP)

Polymerase Chain Reaction (PCR)

Positron Emission Tomography (PET)

Presenilin-1 (PSEN-1)

Presenilin-2 (PSEN-2)

Proliferative Cell Nuclear Antigen (PCNA)

Proline (Pro) (P)

Propidium Iodide-Hoe (PI/Hoe)

Protein Data Bank (PDB)

Protein Fragment Complementation Assay (PCA)

Protein-Protein Interaction (PPI)

Quantitative determination of Interference with A β aggregate size Distribution (QIAD)

Reactive Oxygen Species (ROS)

Retinoic Acid (RA)

Reverse-phase High Performance Liquid Chromatography (RP-HPLC)

Serine (Ser) (S)

Single Nucleotide Polymorphism (SNP)

Sodium dodecyl-sulfate Polyacrylamide Gel Electrophoresis (SDS-PAGE)

Solid-phase Peptide Synthesis (SPPS)

Solid-State NMR (ssNMR)

Soluble APP N-terminal fragment (sAPP)

Streptomycin (Strep)

Stress associated ER protein 1 (SERP-1)

Surface Plasmon Resonance (SPR)

Thioflavin-T (ThT)

Threonine (Thr) (T)

TPA Responsive Element (TRE)

Transcription Block Survival (TBS)

Transmission Electron Microscopy (TEM)

Trimethoprim (TMP)

Tris(2,2-bipyridyl)dichlororuthenium(II) hexahydrate (RuBpy)

Tryptophan (Trp) (W)

Tyrosine (Tyr) (Y)

United Kingdom (UK)

United States (US)

Valine (Val) (V)

β -site Amyloid Precursor Protein Cleaving enzyme 1 (BACE-1)

Chapter One: Introduction

History of Alzheimer's Disease

Alzheimer's Disease (AD) was first described over 100 years ago in 1906 by the German physician Dr. Alois Alzheimer after he performed an autopsy following the death of 51 years-old patient Auguste Dieter. Dieter had been displaying what we now associate with dementia-like symptoms including memory loss, confusion, aphasia, and hallucinations. Alzheimer documented dramatic brain shrinkage due to cerebral atrophy and observed the amyloid plaques and neurofibrillary tangles now considered the defining characteristics of AD. Following a poorly received lecture from Alzheimer describing his findings it was not until 1910 that AD got its name when Emil Kraepelin, a colleague of Alzheimer, described Alois' findings in a textbook referencing the disease as Alzheimer's disease. However, due to the rarity of AD at the time (Alzheimer identified just three further AD cases) the name Alzheimer and his research weren't greatly received and went mostly unnoticed. Later in 1976, AD was recognised as the most common cause of dementia and Glenner and Wong's isolation and identification of Amyloid- β (A β) in 1984 followed (Glenner and Wong, 1984). In 1995 Alzheimer's findings, including notes from his conversations with Auguste Dieter and other patients were found and re-evaluated using modern techniques (Möller and Graeber, 1998). Although Glenner and Wong guessed that A β was a causative factor of AD, it was not until later identification of inherited genes within familial AD (FAD) that influence the processing and production of the A β peptide that led to formation of the Amyloid Cascade Hypothesis (ACH) with A β denoted the instigating factor in the disease (Hippius and Neundörfer, 2003; Makin, 2018).

General overview of Alzheimer's Disease and symptoms

AD is a neurodegenerative disorder with a complicated disease progression. The aggregation of two proteins, A β and Tau, causes neuronal dysfunction and eventually leads to cell death and loss of neurons. The extent of this neuronal loss is depicted in the AD brain image shown in Figure 1 and has been compared to the weight of an orange (around 140 g) (ARUK, 2015). In most forms of AD, one of the areas within the brain that is damaged first is in and around the hippocampus within the temporal lobe, a region responsible for formation of day-to-day memory. This neuronal loss causes disruption in memory formation, in particular that of short-term memories in the early stages of the disease. Forms of less common AD may affect other regions of the brain first, meaning that the first sign of AD is not always short-term memory loss. For example, in Posterior Cortical Atrophy early neuronal loss and damage is often associated with the occipital and parietal lobes which enable processing of visual information and facilitate spatial awareness. Symptoms

developed throughout AD are dependent on the region of the brain affected. As the disease spreads throughout the brain, symptoms become vast and can impair language, reasoning, social behaviour, visuospatial awareness and cause a lack of concentration and fluctuations in mood, including anxiety and stress, depending on the region of the brain damaged (Figure 1). Eventually, symptoms become more severe once AD inflicts various regions of the brain and patients will lose the ability to independently live and function and require assistance with daily tasks and are often unaware of what is happening around them.

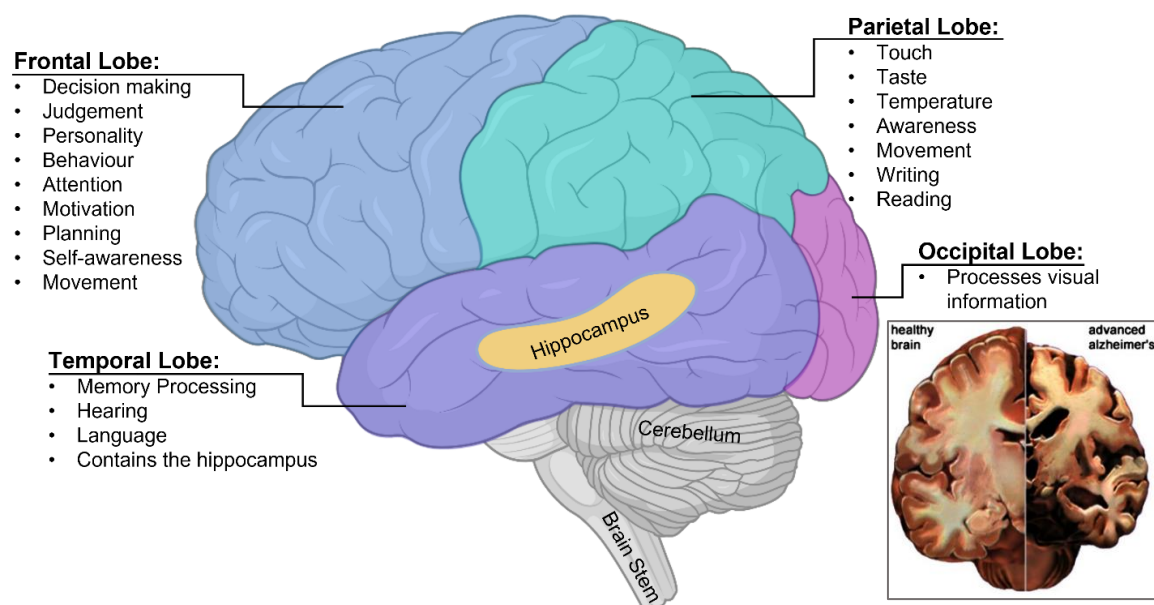


Figure 1: Structure and function of the brain. Surrounding the brain is a layer of cells called the cerebral cortex which is divided into four lobes as depicted above. The brain is constructed of two hemispheres, the left and the right. Each hemisphere has a 'set' of lobes which may differ slightly in their function but ultimately the two sides work synergistically. The functions of each lobe are listed. Damage to the various brain regions in AD results in a vast range of symptoms depending on the region of the brain that is damaged. The frontal lobe is situated at the forefront of the brain and is often damaged later in AD. The temporal lobe is largely associated with memory processing and contains the hippocampus which is responsible for formation of day-to-day memories. Towards the back of the brain are the parietal lobe, responsible for understanding the body's position, touch, taste, reading and writing, and the occipital lobe responsible for visual information. Beneath the cerebral cortex is the sub-cortex which contains various structures responsible for movement, emotions, balance and posture and survival functions such as heartbeat in the basal ganglia (located above the hippocampus region), limbic system (includes the hippocampus so surrounding hippocampus region), cerebellum (labelled) and brain stem (labelled) respectively. Information from (Society, 2022b). Image created using BioRender.com. Inset is an image of a cerebral slice of human healthy brain compared to AD brain to demonstrate extent of neuronal loss. Image credit: 2014 Alzheimer's Association. <http://www.alz.org>. from (Waser et al., 2016).

Alzheimer's Disease Epidemiology

Over 50 million individuals worldwide are affected by dementia with a staggering new diagnosis every three seconds across the globe (Patterson, 2018). In 2015 it was estimated that 1 in 3 people born in the United Kingdom (UK) will develop dementia in their lifetime. The societal impact of dementia has a price tag to match with the global cost coming in at around 1 trillion US\$. The biggest risk factor is age and with the ever-aging population this figure is predicted to double by 2030 where cases could be as high as 82 million and as high as 131 million by 2050 (Nguyen, 2018; Patterson, 2018). Dementia is a devastating disease not only for those diagnosed but also for their relatives. Much of the care provided is by family members with an estimated 82 billion hours of informal care carried out each year (Patterson, 2018) by around 16 million family members (Association, 2018), with 70 % of that care provided by women (WHO, 2021b). As well as in terms of care, dementia also implicates women disproportionately compared to men with women accounting for around 65% of dementia deaths (WHO, 2021b). AD is the most common form of dementia accounting for up to 70% of dementia cases (WHO, 2021a) and in total affecting around 10% of the population over 60 (Frank et al., 2003). In 2019, AD ranked 7th leading cause of death globally (WHO, 2020) which highlights the importance of research into prospective treatments and cures for the disease.

Processing of Amyloidogenic Precursor Protein to produce A β

There are two hallmark proteins responsible for the pathology observed in AD; an extracellular plaque composed mostly of the Amyloid- β (A β) peptide, and intracellular inclusions assembled largely by the cytoskeletal protein, Tau. Dysregulation of these proteins in AD leads to the production of neuritic plaques and neurofibrillary tangles (NFT), respectively. Both proteins have been extensively studied and both are important targets in the hunt for successful AD treatments. However, this study will focus on A β , a peptide of 37-43 amino acids, its role in AD pathology and its potential as a therapeutic target.

A β peptide is produced from proteolytic cleavage of the Amyloid Precursor Protein (APP). Alternative splicing of APP results in the production of three isoforms with varying lengths, APP₆₉₅, APP₇₅₁ and APP₇₇₀. Whilst the physiological role of APP is not clear, APP and its cleavage products are thought to play important roles in cell survival and signalling pathways (Leissring et al., 2002). APP undergoes either of two cleavage pathways, non-amyloidogenic or amyloidogenic cleavage (Figure 2). Whilst all isoforms are susceptible to amyloidogenic cleavage, APP₆₉₅ has been shown to undergo preferential amyloidogenic cleavage, resulting in elevated A β levels compared to the longer isoforms, and is primarily

expressed in neurons (Belyaev et al., 2010). APP₇₅₁ and APP₇₇₀, expressed at lower levels in the brain, are otherwise ubiquitous with increased expression also demonstrated in AD brain (Tanaka, Nakamura and Ueda, 1990; Wang et al., 2016).

In the non-Amyloidogenic pathway APP is cleaved within the A β fragment by α -secretase and produces a soluble APP N-terminal fragment (sAPP α) which has been shown to be important for neuronal protection, synaptogenesis and synaptic plasticity with no production of A β (Mattson et al., 1993; Mattson, 1997). α -secretase cleavage is followed by γ -secretase and often subsequent ϵ -secretase cleavage to release the APP intracellular domain (AICD50) (physiological role discussed below) and an A β _{17-40/42} fragment (p3) fragment of which no clear role has been established (Chow et al., 2010).

Alternatively, APP can undergo amyloidogenic cleavage in which β -secretase cleavage is followed by γ -secretase (a complex of enzymes in which Presenilin-1 and Presenilin-2 (PSEN-1/2) are the catalytic subunits) cleavage releasing the A β extracellularly (Robakis, 2011). This γ -secretase cleavage is not always specific and can cleave at various residues, resulting in multiple lengths of A β being produced, ranging from 37 to 43 amino acids, with 1-40 and 1-42 being the most predominant. In a healthy brain, A β ₁₋₄₀ is the more dominant species, however A β ₁₋₄₂ begins to accumulate in AD either as a result of increased processing of APP or the decreased clearance of A β ₁₋₄₂. A β ₁₋₄₂ is prone to aggregation and self-assembles much more readily than A β ₁₋₄₀ and is considered the more toxic isoform (Esbjörner et al., 2014). An extracellular APP cleavage product is also produced following the cleavage by β -secretase (sAPP β) which has been shown to play a role in synaptic pruning and neuronal cell death (Nikolaev et al., 2009). Additionally, an AICD50 is released following γ -secretase cleavage (with subsequent ϵ -secretase cleavage to create a 50 amino acid residue protein) which is thought to enter the nucleus where it acts as a transcription factor for genes such as p53, potentially altering calcium signalling leading to Long Term Depression (LTD) at neuronal synapses and eventually neurodegeneration (Alves da Costa et al., 2006; Berridge, 2010; Chow et al., 2010). The AICD50 fragment has also been shown to upregulate production of the A β -degrading enzyme Nepilysin by increasing transcription of the gene that encodes the protein (Belyaev et al., 2010; Grimm et al., 2015).

Interestingly, A β has been suggested to act via a feedback loop to increase amyloidogenic processing of APP by influencing membrane fluidity. Oligomeric A β ₁₋₄₀ is thought to bind to neuronal membranes and decrease the fluidity. This decreased fluidity provides favourable conditions for cleavage of APP by β -secretase and γ -secretase as opposed to α -secretase, thus A β stimulates its own production in this feedback circle (Peters et al., 2009).

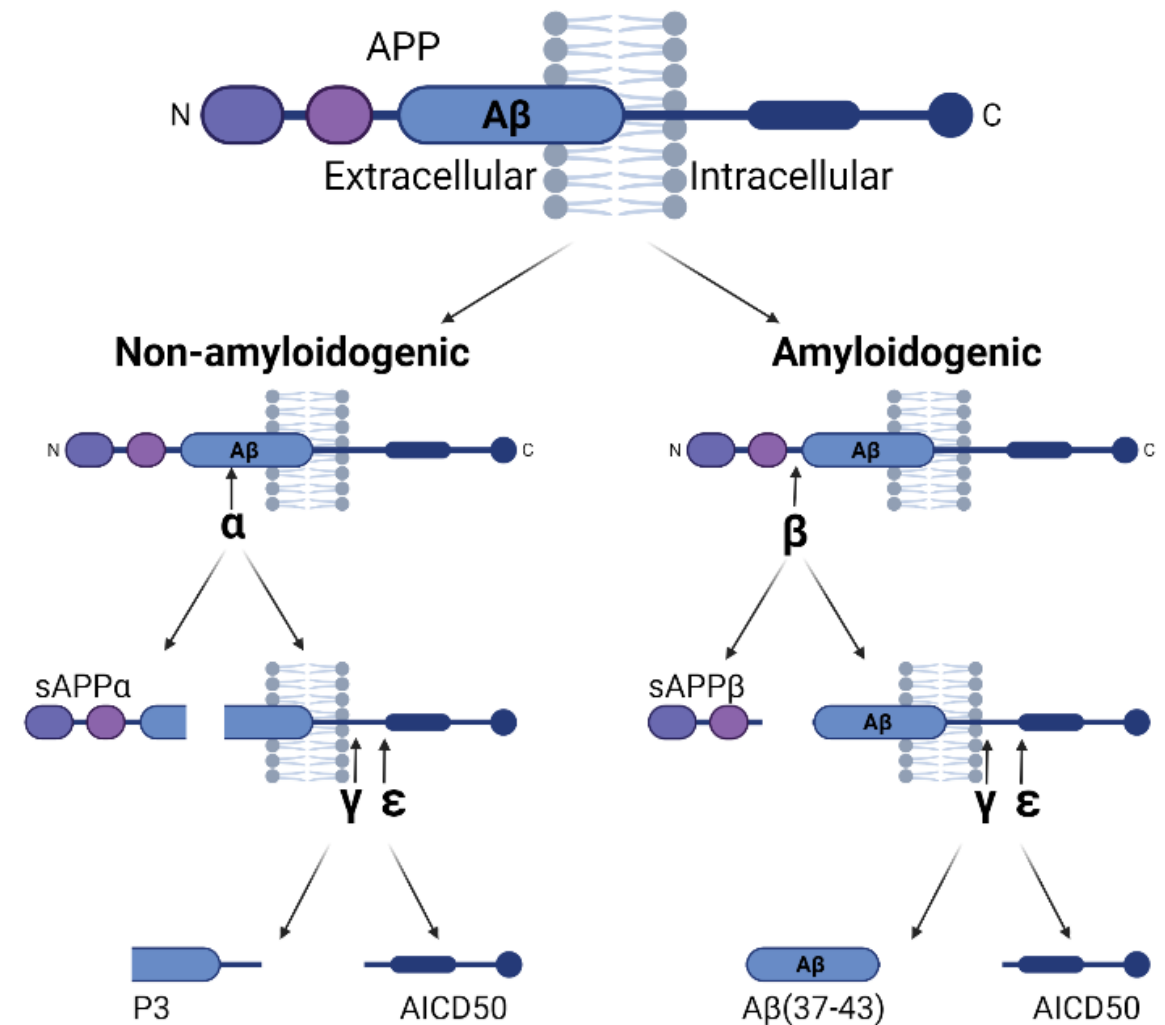


Figure 2: Processing Pathway of Amyloid Precursor Protein. Amyloid Precursor Protein (APP) can undergo non-Amyloidogenic cleavage in which APP is cleaved by α -secretase, releasing an extracellular sAPP α fragment, followed by γ -secretase cleavage to release an intracellular C-terminal fragment. This intracellular fragment is often also cleaved by ϵ -secretase to remove a few residues and create the AICD50 fragment which translocates to the nucleus where it influences transcription of genes such as p53 and Nephrilysin. Alternatively, APP can be cleaved by β -secretase to release the N-terminus as an sAPP β fragment which has a role in synaptic pruning and neuronal cell death. Subsequent cleavage by γ -secretase releases the extracellular A β peptide and the AICD50 domain (after trimming of a few residues by ϵ -secretase). This image was influenced from (Chow et al., 2010; Kumar and Walter, 2011). Image created using BioRender.com.

Amyloid Cascade Hypothesis

The progression of AD is complex, and the disease develops as a result of the interplay between multiple cellular pathways and proteins with aberrations in these amyloid proteins occurring at least 20 years before clinical diagnosis (Figure 4). The Amyloid Cascade Hypothesis (ACH) attempts to explain this and was proposed by Hardy and Higgins nearly 30 years ago. All autosomal dominant mutations identified within FAD fall within APP (bundled around the cleavage sites for production of A β) (Goate et al., 1991) or PSEN-1/2 (Scheuner et al., 1996). Therefore, FAD mutations demonstrated that the processing of APP to produce A β is vital to the disease progression and hinted towards the crucial role of A β in AD (Figure 3) (Table 1).

The ACH hypothesis suggests that A β is the instigating factor in AD and alterations in the processing or clearance of A β lead to accumulation of the peptide. Accumulation of A β leads to its aggregation and subsequent production of toxic species that initiate a cascade of downstream events from altering Calcium (2+) (Ca²⁺) levels and the formation of Tau NFT to activation of the immune system and eventually neuronal cell death (Hardy, J.A. and Higgins, 1992) (Figure 3). Initially, the insoluble plaques of A β were believed to be the disease-causing agent, however these did not correlate well with disease progression and cognitive symptoms. Whilst the exact species of A β that is toxic is not fully understood, it is currently accepted to be the soluble oligomer (Mroczko et al., 2018). A β oligomers may have greater toxicity compared to fibrillar A β due to their smaller size and exposed surface hydrophobicity, thus increased affinity to bind and alter membranes and undergo subsequent internalisation compared to aggregates in which the hydrophobic regions have been internalised in the core of the plaque (Mannini et al., 2014; Vadukul et al., 2020). Many now agree that the amyloid plaque may stand as an inert reservoir for toxic A β species that may be intentionally constructed by microglia as a defence mechanism to sequester pathologic A β (Huang, Y. et al., 2021).

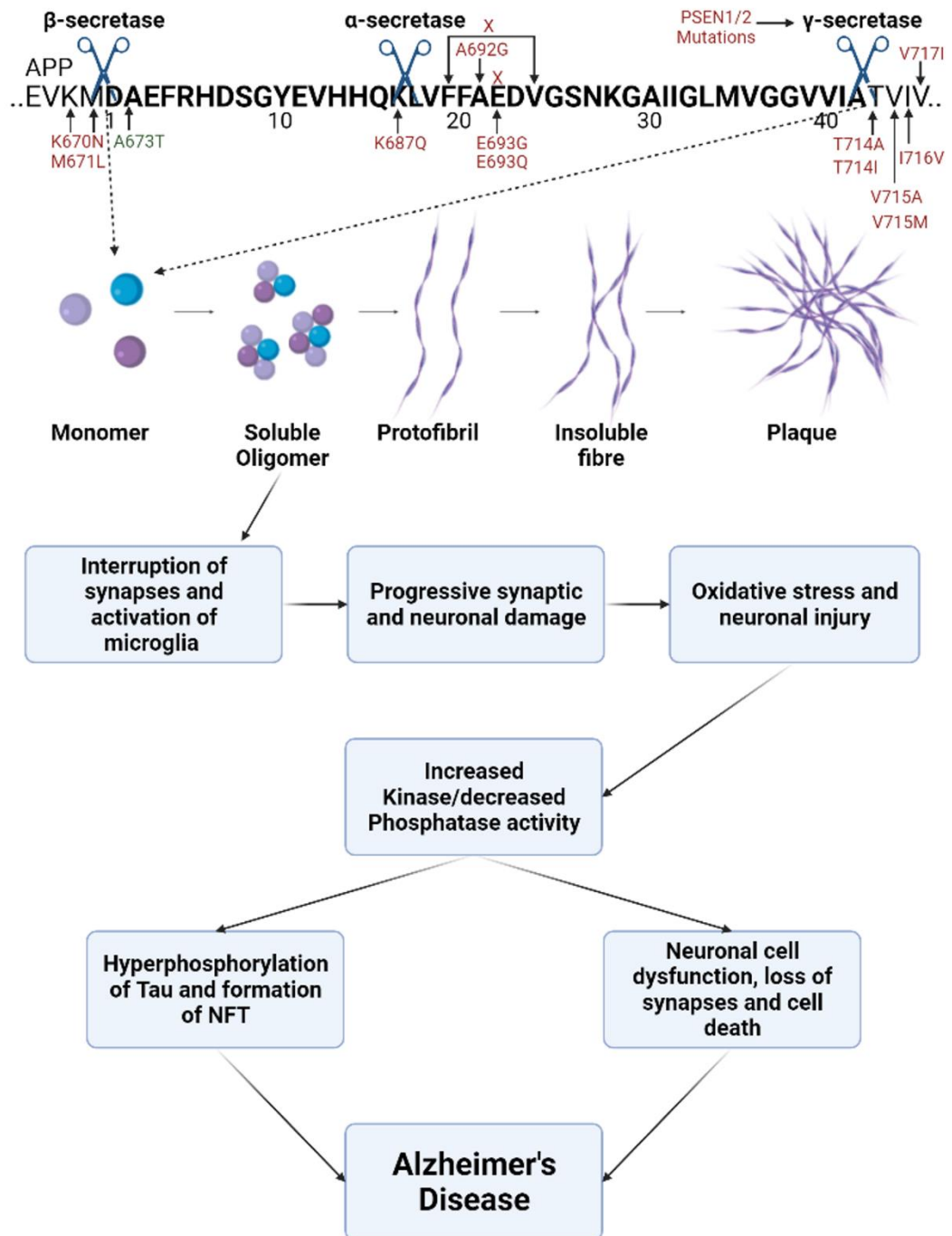


Figure 3: The Amyloid Cascade Hypothesis. Across the top of the figure is part of the sequence of Amyloid Precursor Protein (APP) with the residue numbers for A β shown beneath. Cleavage sites for β , α and γ (γ -secretase cleavage can alter by a few residues to alter the length of A β peptide produced) are shown. Mutations in genes coding for proteins involved in the metabolism of the transmembrane protein APP result in the accumulation of A β and its subsequent aggregation. Pathogenic mutations are shown in red and protective mutations in green and deletions represented as X. The toxic oligomers confer toxicity of A β and result in a cascade of events involving interruption of synapses and microglial activation, synaptic damage and oxidative stress that eventually lead to the activation of kinases. These Kinases subsequently phosphorylate Tau to produce NFT and result in neuronal cell damage and eventually death. NFT = Neurofibrillary tangle. This image was influenced from (Hardy, J. and Selkoe, 2002; Rocchi et al., 2003; Kumar and Walter, 2011). Image created using BioRender.com. More information on the mutations shown can be found in Table 1.

Pathological Role of oligomeric A β

There are many isoforms of the dynamic A β soluble oligomer and various forms have been studied to elucidate the mechanism behind A β toxicity. It is currently understood that smaller A β oligomers (ranging from 8-70 kDa) and dimers (~7 kDa) are more toxic than larger oligomers or plaques which may stand as inert species (Yang, T. et al., 2017). Whilst this may be the case it is important to note that 'spill-over' from these plaques by toxic oligomer species which exist in equilibrium surrounding the plaques can exert toxicity to surrounding neurons. Also, microglia and astrocytes recruited to the site of the plaque cause neuroinflammation and cell stress leading to neuronal damage, thus plaques do not stand as entirely inert species (Benilova, Karran and De Strooper, 2012).

Numerous forms of A β oligomer exert varying mechanisms of toxicity and it is likely that the AD brain contains a heterogeneous mix of toxic oligomeric species. One example of such specifically revealed the role of A β 56 (a 56kDa oligomer of A β) and its interaction with *N*-methyl-d-aspartate receptors (NMDAR) to increase NMDAR-mediated Ca²⁺ influx. This results in the activation of Calcium-dependent kinases which proceed to phosphorylate Tau, leading to the formation of NFT and Tau-induced toxicity (Amar et al., 2017). Oligomer-induced influx of Ca²⁺ into neurons also activates mitochondrial uptake of Ca²⁺ to prevent an overload in the cytosol. However, elevated levels of Ca²⁺ within the mitochondria result in the production of Reactive Oxygen Species (ROS), inhibition of Adenosine Triphosphate (ATP) synthesis, activation of caspases (in particular A β oligomers have been shown to activate caspase-3 (Marín et al., 2000)) and apoptosis of the cell, all of which contribute towards AD pathology (Calvo-Rodriguez et al., 2020). Therefore, A β oligomers contribute to Tau hyperphosphorylation and mitochondrial dysfunction via elevated levels of Ca²⁺.

Toxic dimers and oligomers have been shown to exert a range of potentially neurotoxic effects including inhibition of Long Term Potentiation (LTP), activation of microglia and blocking the reuptake of glutamate from synapses (Yang, T. et al., 2017; Brinkmalm et al., 2019). Specifically, dimers have been reported to trigger hyperexcitability in neurons by blocking glutamate reuptake at the synapse. The mechanism by which is uncertain but has been suggested to be via obstruction of the Excitatory amino acid transporter 2 (EAAT2) which clears glutamate from the synapse (Zott et al., 2019). In addition, dimers have been reported to directly impair synaptic plasticity thus memory formation (Shankar et al., 2008) and induce Tau phosphorylation (Jin et al., 2011). Oligomers are also thought to cause vasoconstriction by production of ROS which ultimately activate pericytes (via Endothelin-1) to initiate constriction of capillaries (Nortley et al., 2019).

When studying FAD mutations in APP, Wolfe et. al. found that longer A β peptides (45 residues or more) could be produced that confer toxicity by remaining locked to the

membrane. The group speculated that these membrane anchored, long A β peptides formed oligomers which result in the formation of pores in the membrane (Devkota, Williams and Wolfe, 2021).

In addition to oligomer conformation, size, or peptide length, post translational modifications may also alter toxicity of A β peptides. An N-terminally truncated (removal of residues Asp and Ala), pyroglutamated (side chain of N-terminal Glu cyclises) form of A β has been shown to initiate pathways of toxicity leading to synaptic dysfunction independent to that by A β ₁₋₄₂ (Grochowska et al., 2017), whilst glycosylation (addition of the monosaccharide O-linked N-acetylglucosamine (O-GlcNAc) to Ser or Thr) of APP demonstrated protective effects against A β -induced toxicity by increasing non-amyloidogenic processing of APP (Chun et al., 2015).

As demonstrated, varying species of oligomers have multiple pathways of pathology. Overall, the potential mechanisms by which these low molecular weight oligomers or dimers induce neurotoxicity has been nicely summarised, by Agrawal and Skelton, as three possibilities: **i)** interrupting cell membranes by interaction of aggregates of A β that alter the properties of the membrane, such as fluidity; **ii)** binding to cell surface receptors and **iii)** creation of pores in the cell membrane by A β oligomers (Agrawal and Skelton, 2019). The A β peptide is also suggested to interact with various other cell components, including mitochondria, lysosomes, endoplasmic reticulum and the nucleus in addition to the plasma membrane in order to evoke pathology (Picone et al., 2020).

Familial AD

Whilst sporadic AD is the most common form of AD, the pathology of Familial AD (FAD) is invaluable in helping to unravel and explore potential mechanisms behind the disease.

FAD accounts for 2-3% of all AD cases and occurs as a result of several autosomal dominant mutations passed through generations that result in the development of AD as early as 30 years of age. These mutations are found within proteins involved in the production of A β , namely APP, PSEN-1 and PSEN-2 (Rocchi et al., 2003) (Figure 3 and Table 1). Some of these mutations impact directly on the processing of APP whereas others influence the nature and aggregation propensity of the A β that is formed. An example of such includes the Arctic mutation (E693G) in APP. This pathological mutation was identified in a family living in Northern Sweden and occurs at residue 22 of A β in which Glu is mutated to Gly. This mutation increases the propensity of the peptide to aggregate and form protofibrils that do not progress to mature fibrils, a key AD phenotype. The increased aggregation observed is thought to result from the residues close proximity to the central hydrophobic

core of the peptide, the ¹⁶KLVFF²⁰ motif (Nilsberth et al., 2001). The KLVFF motif has been recognised for its importance in A β self-recognition. It is a short sequence from the centre of A β that has the ability to bind the full-length sequence. The KLVFF sequence recognises itself and forms specific interactions likely driven by hydrophobicity and is required for A β self-association and its subsequent aggregation (Watanabe et al., 2001). Incorporation of the Gly at residue 22 in the Arctic mutant is suggested to form a kink in the A β structure that creates a flatter profile compared to wildtype. This structure is more solvent exposed and therefore harbours a greater propensity to self-associate in order to shield the hydrophobic residues of A β (Hayward and Kitao, 2021).

Mutations in APP account for a small proportion of FAD cases with up to 80 % of instances of FAD being caused by mutations in the PSEN genes (Rocchi et al., 2003). PSEN-1 is the catalytic subunit of the γ -secretase enzyme that cleaves the C-terminus of A β peptide. There have been around 180 reported mutations in this gene that are suggested to increase the production of A β ₁₋₄₂ relative to A β ₁₋₄₀, a few examples of which have been listed in Table 1. Increased production of this more hydrophobic species, which acts as a seed for A β aggregation, eventually leads to increased fibril formation and consequent production of plaques associated with AD (Selkoe, Dennis J. and Hardy, 2016). Although to a lesser extent than PSEN-1, PSEN-2 mutations also impact AD. There are 38 mutations in PSEN-2 that influence AD and have been suggested to increase A β ₁₋₄₂ production to increase the A β ₁₋₄₂ to A β ₁₋₄₀ ratio and also alter Ca²⁺ signalling within the cell (Zatti et al., 2004; Walker et al., 2005).

Indirect mutations can also influence γ -secretase cleavage and the resulting length of A β peptide produced. Mutations that are close to the γ -secretase cleavage sites on APP influence the length of A β peptide released and interrupt A β ₁₋₄₂ to A β ₁₋₄₀ ratio. Various mutations have been identified in APP from residues 714-717, close to the γ -secretase sites. Mutations at earlier sites (T714I, V715A and V715M) decrease A β ₁₋₄₀ production whilst those at position 716 and 717 (I716V, V717I and V717L) increase A β ₁₋₄₂ production. Although by opposing mechanisms both types interrupt the ratio between the two A β isoforms resulting in the accumulation of A β ₁₋₄₂ and its subsequent aggregation (De Jonghe et al., 2001).

Whilst many mutations alter γ -secretase cleavage either by mutations in APP toward the C-terminus of the A β fragment or within the PSEN-1/2 gene, some have also been described that alter β - and α -secretase cleavage. The Swedish mutation is a double mutation at residues 670 and 671 of APP which sit directly before the β -secretase cleavage site. Here the residues Lys and Met are changed to Asn and Leu, respectively, and are speculated to enhance amyloidogenic cleavage of APP via β -secretase cleavage (Mullan et al., 1992). Additionally, the Uppsala deletion is the first recorded multi-codon deletion (Osaka mutation

previously identified cuts a single residue (E22) from A β resulting in A β product with a greater aggregation propensity (Tomiya et al., 2008)) to cause autosomal dominant AD and results in truncation of residues 690-695 of APP (19-24 of A β fragment) situated a few residues downstream of the α -secretase site. This deletion appears to abolish α -secretase activity at the usual cleavage site and enhances amyloidogenic processing of APP. Furthermore, the resulting A β peptide is more aggregation prone compared to wild-type A β and patients developed greater levels of Tau toxicity, corroborating the role of A β in the ACH as the driving force of Tau pathology in AD (Pagnon de la Vega et al., 2021).

Alternatively, some mutations protect against Amyloid pathology with the Icelandic mutation (A673T) being an example of this (Peacock et al., 1993). This mutation is located close to the β -secretase cleavage site of APP and hinders the activity of the β -secretase enzyme, β -site Amyloid Precursor Protein Cleaving enzyme 1 (BACE-1) (Jonsson et al., 2012). In addition to reducing cleavage of APP by BACE-1 to produce less A β , cleavage that does occur results in a peptide with a lower aggregation propensity compared to wild-type A β (Benilova et al., 2014; Maloney et al., 2014).

The various mutations mentioned (tabulated in Table 1) demonstrate the importance of FAD to determine the pathogenicity of AD and elucidate potential mechanisms by which A β presents toxicity. Although FAD occurs in less than 5 % of AD cases it is very important to study and understand the mechanisms behind these mutations as they represent excellent disease models for sporadic AD and illustrate important pathways involved in the progression of the disease (Rocchi et al., 2003). As demonstrated above, crucial mutations present within FAD point towards a causative role of A β in AD in line with the ACH. Understanding the mechanisms underlying FAD and translating these to sporadic AD is a key step in unravelling the fundamental cause of the disease and is invaluable in exploring potential therapeutics.

Table 1: Mutations involved in FAD. Mutations described for Familial AD (FAD) are vast, so some examples are provided here to demonstrate how FAD mutations speak to the role of A β in AD. All known FAD mutations occur in either Amyloid Precursor Protein (APP) or Presenilin-1 or Presenilin-2 (PSEN-1/2). Rows shaded dark blue are pathogenic mutations whilst those in light blue are protective. The β -secretase site, α -secretase and γ -secretase sites stand at residues 671, 687 and 713 (with some variation) of APP, respectively. The distribution of the APP mutations demonstrates alterations in APP processing at cleavage sites. Some mutations also sit in close proximity to the self-recognition site 'KLVFF'. The KLVFF motif is residues 16-20 of A β which represents residues 687 to 691 of APP. Further mutations in PSEN-1/2 that mostly alter γ -secretase cleavage towards production of A β ₁₋₄₂ and increase the A β ₁₋₄₂:A β ₁₋₄₀ ratio to induce toxicity are shown. Information gathered from <https://www.alzforum.org/mutations>.

FAD mutations	Synonym	Function/Mechanism	Citation
APP			
K670N+M671L	Swedish	Increases production of A β via β -secretase. Located close to β -secretase site.	(Mullan et al., 1992)
A673T	Icelandic	Reduces β -secretase activity with lower aggregation propensity of A β product. Located close to β -secretase site.	(Peacock et al., 1993; Jonsson et al., 2012)
K687Q	-	Classified as likely pathogenic with uncertain mechanism. Located close to α -secretase site.	(Jiang et al., 2019)
F690-V695 Δ	Uppsala	Abolishes non-amyloidogenic processing of APP and resulting A β peptide is more aggregation prone. Located close to α -secretase site.	(Pagnon de la Vega et al., 2021)
A692G	Flemish	Suggested to alter amyloidogenic processing of APP. Located close to recognition motif KLVFF and α -secretase site.	(Hendriks et al., 1992)
E693G	Arctic	Increases aggregation propensity of A β product. Located close to recognition motif KLVFF.	(Nilsberth et al., 2001)
E693Q	Dutch	Enhanced aggregation of A β product increasing fibril formation. Located close to recognition motif KLVFF.	(Levy et al., 1990)
E693 Δ	Osaka	Reduced overall A β production, however resulting A β product with E22 omission has higher propensity to form oligomers but not fibrils thus increasing production of toxic oligomeric forms of A β .	(Tomiya et al., 2008)
T714A	Iranian	Unknown mechanism.	(Pasalar et al., 2002)
T714I	Austrian	Decreases A β ₁₋₄₀ and increases A β ₁₋₄₂ to increase A β ₁₋₄₂ :A β ₁₋₄₀ ratio. Located close to γ -secretase site.	(Kumar-Singh et al., 2000)

V715A	German	Decreases $A\beta_{1-40}$ to increase $A\beta_{1-42}:A\beta_{1-40}$ ratio. Located close to γ -secretase site.	(Cruts et al., 2003)
V715M	French	Decreases $A\beta_{1-40}$ to increase $A\beta_{1-42}:A\beta_{1-40}$ ratio. Located close to γ -secretase site.	(Ancolio et al., 1999)
I716V	Florida	Increases $A\beta_{1-42}$ to increase $A\beta_{1-42}:A\beta_{1-40}$ ratio. Located close to γ -secretase site.	(Eckman et al., 1997)
V717G	-	Increases $A\beta_{1-42}$ and decreases $A\beta_{1-40}$ to increase $A\beta_{1-42}:A\beta_{1-40}$ ratio. Located close to γ -secretase site.	(Chartier-Harlin et al., 1991)
V717I	London	Increases $A\beta_{1-42}$ to increase $A\beta_{1-42}:A\beta_{1-40}$ ratio. Located close to γ -secretase site.	(Goate et al., 1991)
V717L	-	Increases $A\beta_{1-42}$ and decreases $A\beta_{1-40}$ to increase $A\beta_{1-42}:A\beta_{1-40}$ ratio. Located close to γ -secretase site.	(Murrell et al., 2000)
PSEN-1			
M84V	-	Increases production of $A\beta_{1-42}$ to increase $A\beta_{1-42}:A\beta_{1-40}$ ratio.	(Hooli et al., 2014)
P88L	-	Increases $A\beta_{1-42/43}:A\beta_{1-40}$ ratio.	(Liu, C.Y. et al., 2017)
F105L	-	Increases $A\beta_{1-42}:A\beta_{1-40}$ ratio.	(Finckh, Müller-Thomsen, et al., 2000)
I143T	-	Decreases $A\beta_{1-40}$ and increases $A\beta_{1-42}$ to increase $A\beta_{1-42}:A\beta_{1-40}$ ratio.	(Cruts et al., 1995)
G206A	-	Increases production of $A\beta_{1-42}$ to increase $A\beta_{1-42}:A\beta_{1-40}$ ratio.	(Athan et al., 2001)
F388L	-	Increases production of $A\beta_{1-42}$ to increase $A\beta_{1-42}:A\beta_{1-40}$ ratio.	(Zhan et al., 2017)
PSEN-2			
N141I	Volga German	Increases production of $A\beta_{1-42}$ to increase $A\beta_{1-42}:A\beta_{1-40}$ ratio.	(Levy-Lahad et al., 1995; Rogaev et al., 1995)
M239I	-	Increases production of $A\beta_{1-42}$ to increase $A\beta_{1-42}:A\beta_{1-40}$ ratio.	(Finckh, Alberici, et al., 2000)
M239V	-	Increases production of $A\beta_{1-42}$ to increase $A\beta_{1-42}:A\beta_{1-40}$ ratio.	(Rogaev et al., 1995)

Risk Factors in sporadic AD

Age is the principal risk factor for sporadic AD however there are a multitude of other risk factors involved, ranging from environmental, such as air pollution, to genetics (Killin et al., 2016). Genetic predispositions in sporadic AD are complicated, with several different genes suggested to increase the likelihood of developing the disease. This is strongly illustrated by the Apolipoprotein E (APOE) gene that encodes the ApoE protein. Physiologically, ApoE is a glycoprotein involved in the transport of cholesterol which, in the central nervous system (CNS), is suggested to have a role in the formation and maintenance of synapses (Kim, Basak and Holtzman, 2009). The APOE gene is polymorphic and various isotypes arise from point mutations at a single gene locus accounting for the three major APOE isotypes (2, 3 and 4) (Zannis, Just and Breslow, 1981). The isotype combination carried by an individual determines susceptibility to AD. Harboring an APOE ϵ 4 allele increases risk of AD whilst carrying an APOE ϵ 2 allele is seen to be protective against the disease (Corder et al., 1993; Corder et al., 1994). In addition, the dose of APOE ϵ 4 is of importance. Carrying a single APOE ϵ 4 allele decreases age of onset by 1-2 years whereas carrying two copies of the APOE ϵ 4 allele fast tracks the onset of the disease by up to 5-10 years (Corder et al., 1993). Homozygosity for APOE ϵ 4 allele is the greatest known genetic risk factor for AD with carriers being 15 times more likely to develop AD in their lifetime (Hunsberger et al., 2019). APOE isoforms have been shown to differentially contribute to AD risk by presenting variable levels of A β clearance. ApoE4 provides the least clearance accounting for the higher risk of AD associated with this isoform as a result of greater A β accumulation (Castellano et al., 2011). In addition to decreased clearance of A β , ApoE, particularly ApoE4, has been shown to accelerate A β fibril formation and act as a pathogenic chaperone promoting A β aggregation (Wisniewski et al., 1994; Sadowski et al., 2004). Furthermore, the identification of a mutation in APOE ϵ 3 in FAD, namely the Christchurch mutation, renders the usually neutral APOE ϵ 3 protective against autosomal dominant AD (Arboleda-Velasquez et al., 2019). This illustrates the importance of genetics in determining risk with a small change in a gene, in the form of a single nucleotide polymorphism (SNP), drastically altering one's potential for AD.

The risk of sporadic AD has also been linked with several other diseases. Research suggests an interplay between AD and diabetes mellitus, or type-2 diabetes with a study by Arvanitakis et al., revealing a 65% increase in the risk of AD for type-2 diabetes patients (Arvanitakis et al., 2004). So, what could explain this link between diabetes and the AD brain?

Insulin and its receptors have multiple functions within the brain, including synaptic plasticity and neurotransmission. Insulin binding to the insulin receptor activates multiple downstream signalling pathways such as phosphatidylinositol 3-kinase (PI3K)/Akt. This pathway leads

to inactivation of Glycogen synthase kinase-3 β (GSK3 β) which decreases the phosphorylation of Tau. Insulin resistance (characteristic of diabetes) causes dysregulation of these pathways leading to over activation of kinases causing the hyper-phosphorylation of Tau and production of NFT. In addition, the accumulation of insulin results in Insulin Degrading Enzymes (IDE), usually involved in the clearance of A β , being fully occupied with insulin resulting in an accumulation of A β oligomers (Chatterjee and Mudher, 2018).

Furthermore, the link between diabetes and sporadic AD has been extended by Jung et al., and their discovery of the γ -secretase modulator Stress associated ER protein 1 (SERP-1). SERP-1 is upregulated in cells experiencing ER stress, as is so in diabetes due to high glucose levels. In turn, SERP-1 increases cleavage of APP by γ -secretase resulting in increased production of A β . SERP-1 overexpression (in SH-SY5Y cells expressing APP^{swe}) increased A β secretion by up to 70 % whilst a knockout cell line of SERP-1 suppressed A β production. The group also examined post-mortem hippocampal tissue and found a 9.6-fold increase in SERP-1 in individuals affected by AD compared to control samples (Jung et al., 2020). AD has commonly been described as 'Type 3 diabetes' or 'diabetes of the brain' (de la Monte and Wands, 2008) with the link between AD and diabetes opening up potential avenues for repurposing diabetes drugs as treatments for AD (Panza et al., 2019).

In addition, a significant percentage (reports of over 50%) of Down's syndrome (DS) patients are diagnosed with AD, with almost all patients displaying AD-type pathology such as A β plaques over 35 years of age (Head et al., 2012; Castro, Zaman and Holland, 2017). This linked comorbidity of AD in DS patients likely occurs because the APP gene is located on chromosome 21 which is triplicated in individuals with DS. This trisomy of chromosome 21 leads to overexpression of APP, thus an accumulation of A β peptide, replicating AD pathology in accordance with the ACH (Castro, Zaman and Holland, 2017).

Why target A β over Tau?

As mentioned above, AD is characterised by misfolding and aggregation of the two proteins A β and Tau, so why does this study focus on A β ?

There is a fair argument for both A β and Tau and research into understanding the role and potential therapeutics targeting both proteins are essential. However, the ACH supports the notion that A β acts upstream of Tau in AD pathology. Targeting A β as opposed to Tau may be advantageous to quench pathology from both proteins. The ACH was formed following revelations regarding the genetics of FAD. When studying FAD mutations, all target either APP, PSEN-1 or PSEN-2 and are grounded around alterations in processing and production

of A β (Bekris et al., 2010). In addition, the greatest genetic risk factor in sporadic AD is APOE status. APOE isotypes differentially affect the clearance of A β in AD brain with ApoE4 providing the least clearance and the highest AD risk (Castellano et al., 2011). FAD mutations and genetic risk factors have been used to model potential mechanisms of AD and the genetics clearly point towards A β as the causative factor.

Furthermore, A β abnormalities precede those of Tau observed throughout disease progression as outlined in Figure 4, suggesting that Tau misfolding and aggregation occurs as a consequence of A β pathology. Transgenic mice studies reveal that crossing human amyloid precursor protein (hAPP) mice with human Tau (hTau) mice increases Tau pathology but has no effect on A β deposition or pathology. This supports the notion that A β activates or influences Tau pathology but not vice versa (Lewis et al., 2001). Treatments targeting Tau may not harbour the ability to alter A β toxicity, yet it may be possible to hinder Tau toxicity with A β -targeted therapies. In addition, mutations in Tau alone result in Tauopathies independent of AD, namely Frontotemporal Dementia (FTD) (Goedert, Ghetti and Spillantini, 2012). This suggests that A β is required to trigger the Tau toxicity specific to AD.

Many reports have explored how A β may execute its pathological pathways via Tau and the mechanisms by which this is done. Various articles link A β to the activation of kinases which proceed to phosphorylate Tau, leading to Tau hyperphosphorylation and pathology. A β_{56} oligomers have been reported to directly activate NMDAR (Texidó et al., 2011) which results in an influx of Ca²⁺ and the subsequent activation of Calcium-dependent Calmodulin Kinase IIa (CamKIIa), of which Tau is a substrate (Amar et al., 2017). Amar et. al demonstrate that different A β oligomer conformers target and activate distinct kinases resulting in varying phosphorylation states and alterations in Tau pathology (Amar et al., 2017). For example, whilst A β_{56} activates CamKII as described above, Larson et. al. have demonstrated the molecular mechanism by which A β leads to Tau phosphorylation via A β dimers. The group revealed that A β oligomers (notably dimers) bind to the cellular Prion Protein (PrP^c) (a membrane anchored protein) at neuronal dendritic spines. PrP^c then forms a complex with the Fyn kinase, leading to Fyn Kinase activation and subsequent phosphorylation of Tau (Larson et al., 2012).

Aside from directly activating kinases, A β oligomers have been suggested to induce Tau phosphorylation via LTD of neurons. A β oligomers were shown to cause increased, excessive release of glutamate at pre-synaptic terminals causing LTD in post-synaptic neurons. It was further demonstrated that LTD at the post-synaptic neuron resulted in an increase in Tau hyperphosphorylation (Taylor, H.B.C., Emptage and Jeans, 2021). LTD causes hyperphosphorylation of Tau irrespective of A β , i.e., if LTD is activated by other mechanisms Tau hyperphosphorylation still occurs as a result. Ultimately, A β can act by

two mechanisms to induce hyperphosphorylation of Tau. Either directly via NMDARs to activate kinases, or indirectly as a result of other A β -induced pathological mechanisms, namely LTD.

In addition to oligomeric species, the ratio of A β_{1-42} to A β_{1-40} , a key determinant in AD, has also been suggested to influence Tau pathology (Kwak et al., 2020). A high A β_{1-42} :A β_{1-40} ratio, as opposed to total amount of A β , was shown to regulate Tau pathology. Targeting this ratio could provide a therapeutic advantage over reducing total A β by successfully reducing pathology presented by both A β and Tau. Kwak et. al. demonstrated that when using A β -targeted therapeutic approaches (γ -secretase and β -secretase inhibitors) to sequester A β pathology, Tau pathology was also attenuated (Kwak et al., 2020). The ability of A β -targeted therapies to alleviate Tau pathology has also shown success in a study by Oddo et. al.. Here, the application of anti-A β antibodies in neuronal cells (mice 3xTg-AD) not only resulted in the clearance of A β but also rescued early tau pathology. Furthermore, the group demonstrated the use of a γ -secretase inhibitor that lowered early-Tau pathology, further corroborating the potential to target both A β and Tau using A β -directed therapeutics (Oddo et al., 2004). Conversely, removing Tau does not confer the same ability to rescue A β -induced toxicity and has no effect on A β production. Deletion of the gene that codes for Tau in an APP transgenic mouse line does not alter production of A β plaques but does reduce the level of change in behavioural test outcome indicating that A β utilises Tau to exert toxicity (Selkoe, D. J., 2021b). Therefore, it stands to notion that A β exists as the primary trigger for AD and is a validated target following over 25 years of research (Selkoe, Dennis J. and Hardy, 2016).

The ACH has faced debate over previous years due to the lack of successful A β -targeting therapies despite decades of research. This has raised questions regarding the validity of A β as the causative agent and whether studies have approached the correct protein target. However, the recent approval to fast-track Phase IV clinical trials of Aducanumab by the U.S Food and Drug Administration (FDA) solidifies the potential of A β as a successful therapeutic target. Although controversial, Aducanumab represents the first approved AD drug to target the cause of the disease, by reducing A β plaque burden and this opens up the avenue for further A β -targeted therapies. In agreement with Selkoe's comment, A β poses as the 'fire, not the smoke' in AD (Selkoe, D. J., 2021a).

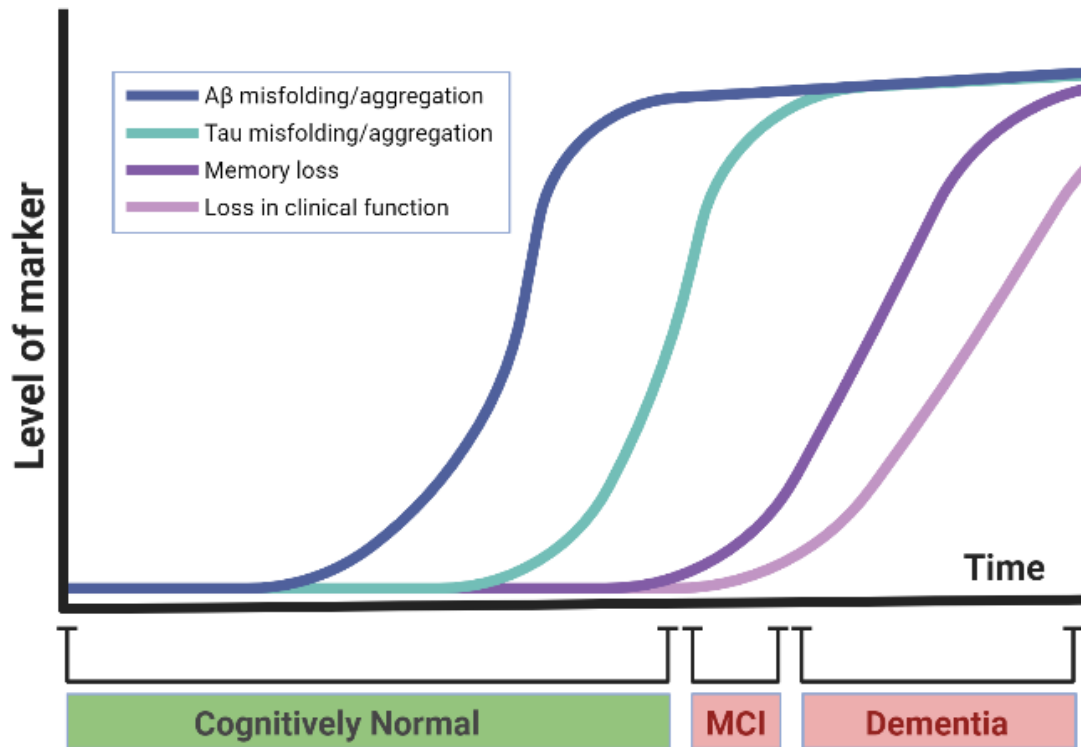


Figure 4: Protein misfolding and aggregation occurs many years before onset of clinical symptoms. Level of protein folding and aggregation, plotted against clinical diagnosis demonstrates that A β aggregation begins many years before clinical onset and is followed by Tau pathology. A β protein dysfunction can begin up to 20 years before Mild Cognitive Impairment (MCI) and display of clinical function such as memory loss and subsequent dementia diagnosis. This figure was created using BioRender.com and influenced by (Jack et al., 2013; Lista et al., 2015; Hane et al., 2017).

Structure/Fold of A β throughout aggregation

As monomers, A β peptides are intrinsically disordered in an aqueous environment or present a degree of alpha helicity in the presence of a membrane (Agrawal and Skelton, 2019). The initial step of aggregation brings two monomers together to form an A β dimer in which a β -sheet structure is adopted. The structure of this β -sheet dimer has been extensively researched and various structures have been established which mostly present an S-/C- shaped fold with an overall Greek-key like motif (Figure 1 in Chapter Three).

Oligomers are the next building block towards fibril formation and stand as the most toxic form of A β . The transient nature of A β oligomers and the large heterogeneity of oligomer conformations and sizes means that capturing the exact structure is difficult and which species presents greatest toxicity is not understood. However, attempts have been made using Nuclear magnetic resonance (NMR) and crystallography to reveal the structure of these oligomers. NMR studies demonstrated that oligomers contain a mix of parallel and anti-parallel β -sheet structures (Yu, L. et al., 2009). The oligomers used within this study

were produced *in vitro* to present long-lived oligomers in the presence of aliphatic hydrocarbon chains which may not fully represent the transient oligomers present within the human brain. X-ray crystallography has been applied to reveal that monomers initially form as trimers of β -sheet structures which further associate to form hexamers and eventually dodecamers (Spencer, Li and Nowick, 2014). Again, questions are raised with regards to the translatability of these structures to A β oligomers present in an AD brain as the study utilised synthesised peptides derived from the 17-36 fragment to mimic the fold of A β as opposed to the full sequence. There is also evidence that low n- intermediate oligomers form atypical α -sheet secondary structures (or α -pleated sheets) that may be linked to aggregation and toxicity of the oligomers (Shea et al., 2019). This intermediate α -sheet structure is thought to facilitate the transition of soluble oligomers to form β -sheet fibrils and may stand as a potential target for specifically inhibiting oligomer toxicity (Armen et al., 2004).

Oligomers of A β stack to produce protofibrils which harbour a cross- β sheet structure. These protofibrils are intertwined with another fibril and form the insoluble fibres that cluster into the amyloid plaques observed in an AD brain (Figure 5). Solid-state NMR (ssNMR) and cryogenic electron microscopy (cryo-EM) are among some of the techniques applied to reveal the structure of these insoluble amyloid molecules in fibril formation and again reveal a heterogenous mix. A β has been shown to assemble within fibrils forming either a U-shape in which two β -strands interact with a single turn (Lührs et al., 2005), an S-shape in which three β -sheet strands fold to create an S (Xiao et al., 2015), or an L/S-shape in which the N-terminus adopts an L-shape whilst the C-terminus forms an S fold (Gremer et al., 2017) (Figure 1 in Chapter Three paper). Each fibril is comprised of A β molecules arranged in either 2- or 3- fold symmetry throughout, with protofibrils intertwining to form a twisted fibril, forming a steric zipper in which the central hydrophobic core stabilises the fibril (Agrawal and Skelton, 2019). The direction in which the fibril twists differs between *in vitro* and human-derived A β samples with *in vitro* derived samples presenting a left hand twist as opposed to brain-derived samples which hold a right hand twist (Kollmer et al., 2019).

As for many amyloid proteins, A β aggregation follows a sigmoidal curve consisting of an initial lag phase, an elongation/growth phase until an equilibrium is reached at the plateau (Figure 5). The lag phase of amyloid aggregation is very slow and consists of an unfavourable primary nucleation step in which monomers and small oligomers associate to form seeds for aggregation (Chatani and Yamamoto, 2018). Once this initial energy barrier has been overcome it is followed by a rapid elongation step in which protofibrils are formed bearing a β -sheet structure. Addition of monomers to this growing fibril is more favourable and occurs rapidly with a model termed the dock and lock system. In this system an A β monomer initially reversibly docks on to the growing fibril end. Intermolecular hydrogen bonds form a β -strand that stacks on to the fibril growing end with the fibril essentially acting

as a template. Following this, intramolecular hydrogen bonds are formed to create an intermediate hairpin that aids transition of the monomer to form the s- or c-shaped structure within the fibril. Eventually the intramolecular bonds are broken down and replaced with intermolecular bonds and the monomer is bound to the adjacent molecule within the fibril in an irreversible manner, i.e. the monomer is locked on to the fibril (Esler et al., 2000; Gurry and Stultz, 2014).

Further A β oligomers form in the presence of the established fibrils throughout the elongation phase via a secondary nucleation process to allow for proliferation of amyloid aggregation. This process is much quicker than for primary nucleation and becomes the principal source for production of new oligomers which can then accelerate formation of new fibrils in an exponential manner. In this model monomers can create seeds, or a nucleus for further aggregation upon the surface of existing fibrils (Cohen et al., 2013; Törnquist et al., 2018). Secondary nucleation greatly contributes towards production of the toxic A β oligomers and may stand as a potential target for combatting AD pathology by blocking production of these oligomers.

Eventually, an equilibrium is reached in which the source of monomers and oligomers for fibril growth is depleted and aggregation is stabilised. This stage is represented as the plateau of the sigmoidal curve.

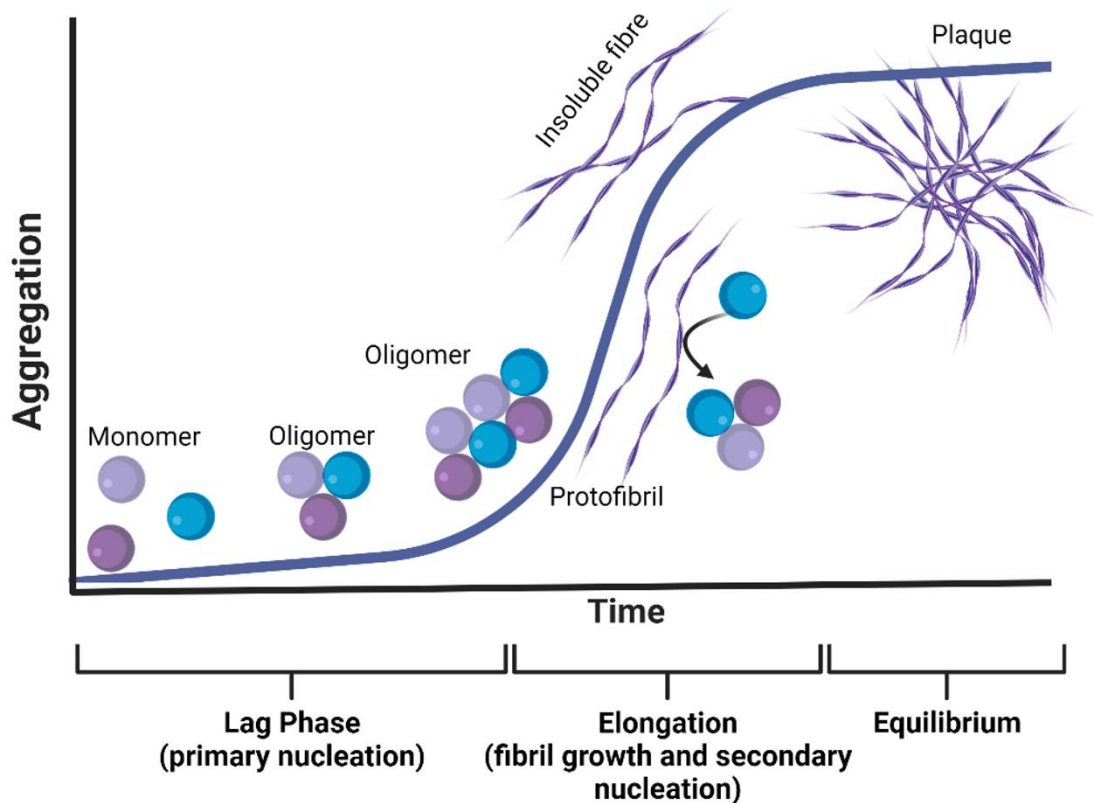


Figure 5: Misfolding and aggregation of A β in Alzheimer's disease. The aggregation process of A β from monomer to plaque is plotted along a sigmoidal curve (Blue line). An initial lag phase is the rate limiting step in which primary nucleation must occur to create seeds for aggregation. Once this step has been overcome, a rapid elongation step occurs in which rapid growth/increase in aggregation is observed until an equilibrium is reached at the plateau of the curve. Figure was created using BioRender.com and influenced from the following paper (Takahashi and Mihara, 2008).

A β – a native role?

Although A β is often associated with pathology, the peptide is present in healthy brain and is produced from the proteolytic processing of APP as described above. It is present throughout an individual's lifetime and has been identified in all vertebrates studied with a high degree of sequence conservation (Panza et al., 2019). The physiological role of A β is not fully understood, however, it is thought to have a role in neuronal cell survival. Plant et al. demonstrated that inhibiting endogenous A β resulted in increased neuronal cell death which was rescued by addition of physiological levels of A β (Plant et al., 2003). Both monomeric and oligomeric A β are found in healthy brain and are involved in numerous physiological functions from modulating synaptic function and plasticity, protecting against oxidative stress and influencing neuronal growth and survival before conversion to species conferring toxicity in AD (Bishop and Robinson, 2004; Puzzo et al., 2008; Puzzo, 2019).

Studies suggest that these contrasting functions of A β are dependent on concentration. At lower concentrations A β monomers and oligomers may have a role in aiding synaptic function, LTP and memory. However, upon accumulation of A β , thus higher concentrations, its role becomes pathological causing synaptic dysfunction characteristic of AD. This is termed the A β biphasic effect (Gulisano et al., 2018). The mechanism by which A β influences such processes could be due to its involvement in pre-synaptic vesicle release in which it behaves as a positive modulator at hippocampal synapses (Abramov et al., 2009). The A β peptide has also been implicated in a negative feedback loop that represses this synaptic vesicle release in the presence of excess A β . Kamenetz et. al., suggest that this feedback loop could cause the synaptic depression observed in AD upon accumulation of A β thus activation of this negative feedback loop (Kamenetz et al., 2003).

An additional physiological role for A β peptide has been suggested in the innate immune system where it is released as an antimicrobial peptide (AMP) in response to infection that may explain the immune component of AD (Soscia et al., 2010). Additionally, increased secretion of A β following transient acute brain injury, following a traumatic blow to the head, cerebral ischaemia or even sleep deprivation, indicate a potential role for A β in protection or repair of neurons following trauma and may be a mechanism for the brain to alleviate damage. It has been suggested that elevated levels of A β observed in AD are actually an attempt to rescue damaged neurons (Panza et al., 2019).

The various physiological roles for A β listed above may present issues when targeting this peptide for AD therapeutics. However, the intracellular nature of the screening platforms used within this study, Protein Fragment Complementation Assay (PCA) and Transcription Block Survival (TBS), will circumvent potential issues as any peptides selected must provide a growth advantage to the cells to enable selection through competition selection. Therefore, at least in *Escherichia coli* (*E.coli*), peptides selected will not confer toxicity.

Towards AD Treatments

Currently there is no treatment to cure AD, only the ability to manage the symptoms. These include the cholinesterase inhibitors, donepezil, rivastigmine and galantamine which enhance synaptic transmission by reducing the clearance of the neurotransmitter, acetylcholine, from synapses and the NMDAR antagonist, Memantine, that acts to decrease excitotoxicity caused by lack of reuptake of glutamate from the synapse. These drugs are often delivered at high doses to achieve adequate levels within the brain due to poor transport of the drugs, which results in considerable side effects. A recent exciting study explored the potential of lipid-based nanoparticles to deliver Donepezil directly to the brain

which may enhance the ability of these drugs to treat the symptoms of AD whilst evading some of the common side effects (Krishna et al., 2019).

Many studies have targeted the progressive aggregation states of A β from monomeric peptide to plaque and have addressed the various components of the APP pathway from antibodies that bind to soluble and aggregated forms of A β , to β - and γ -secretase inhibitors that reduce production of the toxic species. The failure rate of clinical trials for AD therapeutics stands at around 99 %, with reports suggesting that the lack of relevant sporadic AD models may be part of the reason for this high failure rate (Veening-Griffioen et al., 2019). In addition, AD pathology occurs many years before clinical diagnosis, by which time therapeutic intervention targeting A β may be too late (Figure 4). The development of improved cerebrospinal fluid (CSF) and blood biomarkers, and advances in Positron Emission Tomography (PET)-based imaging may allow for earlier diagnosis and the development of more successful therapeutic interventions through better patient stratification. Despite the current hurdles various promising treatments have been working their way through clinical trials recently.

Antibodies

The most recent and promising example is the monoclonal antibody Aducanumab (Aduhelm) that has recently received fast-tracked FDA approval as the first disease-modifying treatment (by clearance of A β plaques) for AD with its efficacy being tested in a Phase IV confirmatory trial. Aducanumab is a monoclonal antibody that recognises and binds to aggregated forms of A β . The human-derived Aducanumab came from a reverse translational approach in which samples from healthy, older individuals who lack AD pathology were screened as they may present some form of immune resistance to A β -induced pathology. The resulting Aducanumab binds to A β between residue 3 and 7 and selectively recognises oligomeric and aggregated forms of A β as opposed to monomers (Arndt et al., 2018). Phase III clinical trials of Aducanumab (EMERGE and ENGAGE) directly demonstrated disease modification by clearance of A β plaques, as measured by Amyloid-PET. A small number of recipients also exhibited decreased Tau pathology. The relevance of Aducanumab's ability to reduce A β plaque burden has been met with controversy due to questions of how this translates to cognitive improvement. Of the two trials, only one (EMERGE) demonstrated significant improvement in cognitive decline and met both primary and secondary endpoints, whilst ENGAGE failed to do so. Despite this, the FDA fast-tracked approval of the drug upon the premise that the clear reduction in amyloid burden is expected to result in less cognitive decline in AD patients (Selkoe, D. J., 2021b).

Although controversial, the approval of Aducanumab is the closest the AD field has come to a disease-modifying therapeutic and stands as a beacon of hope following decades of

A β -directed research and will hopefully open-up avenues for development of future therapies. Currently, various other antibodies that bind to aggregated forms of A β are working their way through Phase II to III clinical trials including Lecanemab (Swanson et al., 2021) and Gantenerumab (Ostrowitzki et al., 2017). Additionally, Donanemab, which binds a highly aggregation-prone form of A β , is also demonstrating great potential in early Phase II trials with complete clearance of amyloid plaques being observed for two-thirds of patients, along with a significant slowing in the decline of cognitive ability (Mintun et al., 2021). The potential snowball effect of Aducanumab's fast-track approval has already been demonstrated with Lilly (the pharmaceutical company that owns Donanemab) announcing plans to apply for the same fast-track approval as Aducanumab backed with reports of Donanemab's ability to clear A β plaque burden to be twice that of Aducanumab.

An issue faced in antibody therapeutics is delivery of the large drug to the brain. Studies to increase the delivery of antibodies to the brain are ongoing and some have shown success. In particular, one study presented the successful application of ultrasound to transiently open the Blood Brain Barrier (BBB) and increase the delivery of an anti-Tau antibody to the brain upon peripheral application (Janowicz et al., 2019). Whilst this is an exciting prospect to increase the delivery of antibodies to the brain, questions should be raised about the specificity of species able to cross the BBB upon opening as, although the drug can now proceed to cross the barrier, there may be potential for other, unwanted molecules to pass as well.

In addition to antibody treatments to target A β clearance directly, numerous efforts have been made to reduce production of A β by modulating β and γ -secretase cleavage of APP.

β -secretase Inhibitors

β -site amyloid precursor protein cleaving enzyme-1 (BACE-1) is the β -secretase enzyme that carries out cleavage of APP to produce A β . Thus, the potential of BACE inhibitors to prevent amyloidogenic cleavage of APP by β -secretase and thus reduce production of A β has been explored. BACE-1 inhibitors are widely toxic due to the enzyme's many substrates and so their use has proved limited with β -secretase inhibitors failing to present much success at clinical trials. Only a select few BACE inhibitors have progressed to Phase III clinical trials with Verubecestat, Atabecestat, CNP2520 and Lanabecestat all failing due to unfavourable risk-benefit ratios, toxicity, and worsened cognition in some cases upon application of the drug, with a lack of clinical benefit (Panza et al., 2019; Zhao et al., 2020).

γ -secretase inhibitors

A further approach directed at altering production of A β by modulating processing of APP targets γ -secretase cleavage. The γ -secretase enzyme complex has over 90 reported substrates including Notch proteins which play important roles in Notch signalling to

influence cell proliferation, fate, and apoptosis during neuronal development. Therefore, targeting γ -secretase with inhibitors carries several risks and off-target effects with toxicity often in the form of increased risk of skin cancer, limiting the success of these drugs (Zhao et al., 2020).

Modulating γ -secretase cleavage as opposed to inhibiting the enzyme may carry more promise. Various γ -secretase modulators in the form of non-steroidal anti-inflammatory agents, such as ibuprofen, demonstrated an ability to shift cleavage towards shorter A β peptides as opposed to the more toxic A β_{1-42} , yet the mechanism behind this was poorly understood and no successful drug emerged. Additionally, NIC5-15 (Pinitol), a natural sugar compound found in fruit, which also acts to favour the production of shorter A β fragments without altering Notch signalling, demonstrated good tolerability in Phase II clinical trials yet no follow up trials have been conducted as of yet (Zhao et al., 2020).

The lack of successful drugs culminating from studies targeting APP processing with β - and γ -secretase inhibitors raises questions of the validity of this approach. However, a recent cryo-EM structure of APP in complex with γ -secretase reveals stark contrasts between substrate binding when compared to that of Notch. This opens up the potential for the design of substrate specific inhibitors of γ -secretase to target solely APP cleavage (Zhou et al., 2019). Along with the recent revelation that higher levels of shorter A β fragments, namely A β_{1-38} , in CSF correlates with a decreased risk of AD (Cullen et al., 2021) these findings may reignite this field of study.

Other treatment avenues have been explored that target other aspects of AD pathology including anti-Tau drugs, targeting the immune system and also α -secretase modulators to promote non-amyloidogenic cleavage of APP. Additionally, the use of anti-sense oligonucleotides to quench translation of messenger RNA (mRNA) for proteins involved in AD such as APP and BACE have been explored (Chakravarthy et al., 2017). This study is however focusing on the development of peptides as an alternative method of targeting AD pathology.

Peptide Therapies to target AD

This study will focus on identifying novel peptide hits as potential therapeutics against AD. Peptides present significant benefits over small molecules and antibodies due to their lower cost of production (particularly compared to antibodies), lack of immunogenicity (due to their small size), high specificity with low toxicity and the potential to build and screen large diverse libraries. Furthermore peptides present the ability to block protein interactions by targeting binding pockets that may be out of reach for small molecules and present higher

levels of biological and chemical diversity, enabling the design of peptides with much greater specificity and the potential to form multiple points of interaction with the target than may be possible with small molecules (Mason, 2010). Additionally, peptide mimetics can be applied to modify peptides to produce more likely drug-candidates and to overcome potential drawbacks associated with peptides including cell penetrance, protease-susceptibility, rapid clearance and poor bioavailability (Ryan et al., 2018; Armiento, Spanopoulou and Kapurniotu, 2020) (Table 2).

Over the last two decades the application of peptides for therapeutics has flourished reaching over 50 approved peptide drugs and another 178 in various clinical stages of development across several therapeutic areas from diabetes to oncology in 2018 (Henninot, Collins and Nuss, 2018). Applying the success of recent applications of peptides could help overcome the lack of successful drug discoveries within the AD field. Many approaches to develop peptide inhibitors against A β pathology in AD have been carried out and are extensively reviewed in the literature. Here, we will attempt to cover a good range of peptides and their respective approaches, and all peptides mentioned are summarised in Table 3.

One approach used to identify peptides that bind to A β and prevent self-association and aggregation of the A β peptide, was to identify motifs within the sequence that are important for fibrilisation. A short binding sequence was identified between residues 16-20 with the following sequence, KLVFF, that is important for self-recognition and aggregation of A β (molecular self-recognition of KLVFF motif discussed previously). This short peptide was shown to bind full length A β and prevent aggregation (Tjernberg et al., 1996). The KLVFF binding sequence stood as a basis by which to design further, more potent peptides. In particular those of OR-1 and OR-2 which were designed to target toxic A β oligomers. Whilst both prevented fibrilisation of A β , only OR-2 was successful at targeting A β oligomers (Austen et al., 2008). Further optimisation in the form of retro-inversion of the OR2 peptide (RI-OR2) allowed for development of a more stable peptide with greater resistance to proteolysis (Taylor, M. et al., 2010). Retro-inversion of a peptide allows for conversion of all residues to D-Enantiomeric peptides (D-peptides) to resist proteolysis and reversal of the sequence means the overall shape of the peptide is conserved so as to not effect biological activity. The C-terminus of the A β peptide has also been targeted due its importance for A β dimerisation (Figure 1 (a) in Chapter Three) with successful peptides inhibiting A β -induced toxicity by stabilising non-toxic hetero-oligomers by associating with full length A β ₁₋₄₂ (Fradinger et al., 2008).

Particularly successful KLVFF sequence derived peptides are those belonging to the Proline β -sheet breaker family. Proline is an infamous β -sheet breaker peptide due to the inability of the peptide to form β -sheet conformations (Wood, S. J. et al., 1995), perhaps by

incorporating a kink in the chain thus disrupting stacking of A β molecules. Soto et al., incorporated Proline residues in to the A β sequence within the self-recognition motif and, following a sequence of peptide modifications, identified a potent inhibitor of A β aggregation, iA β ₅ (Soto et al., 1996). This iA β ₅ peptide presented the ability to not only inhibit the aggregation of A β but also breakdown preassembled fibrils *in vitro*, was capable of protecting against A β -induced toxicity in a cell model and reduced A β aggregation *in vivo* (Soto et al., 1998). Further modification of this peptide to protect iA β ₅ from proteolytic degradation demonstrated considerable reduction in amyloid deposition and ability to cross the BBB *in vivo* (Permanne et al., 2002).

Aside from sequence-derived peptides, screening of large libraries either random or semi-/rationally designed upon the A β target is an efficient method to screen large and broad peptide libraries to identify potent peptide hits against A β toxicity. One such method is phage-display which has been successfully applied by the Willbold group in identification of their D3 and subsequent RD2 peptides. Phage display uses bacteriophage particles to present library members on the surface with successful hits interacting with an immobilised protein target. Phage display identifies peptide hits consisting of L-Enantiomeric peptides (L-peptides). An advancement of the phage display technique is mirror image phage display in which the target protein is expressed with D-enantiomeric amino acids. The bacteriophage presents library members in the L-enantiomeric amino acid confirmation that bind to the D-peptide target protein. The peptide hits can then be synthesised with d-enantiomeric amino acids and will bind to the natural L-enantiomeric amino target protein due to conservation of the overall topology between D- and L- enantiomers (Schumacher et al., 1996). A randomised 12 residue library was screened covering around 1 billion members and a winning peptide hit selected, denoted D3. D3 demonstrated the ability to reduce A β aggregation and dissolve pre-formed plaques, rescue cell viability and decrease A β load *in vivo* (van Groen et al., 2008). Interestingly, D3 was also shown to specifically reduce A β oligomer levels *in vitro* (Brener et al., 2015).

Following the promise exhibited by D3, the Willbold group used the sequence as a template to rationally design D3 derivatives with greater potential to remove A β oligomers. As a result, the RD2 sequence was obtained and has been shown to possess greater bioavailability (Leithold, L.H.E. et al., 2016) and eliminated A β oligomers to a greater extent than D3 whilst retaining the ability to rescue cell viability *in vitro*. Interestingly, in transgenic mice RD2 provided a significant cognitive benefit compared to placebo with no reduction in plaque load following analysis of post mortem mice brain, further corroborating the importance of targeting A β oligomers over plaques (van Groen et al., 2017). Furthermore, RD2 reduced the ratio between A β ₁₋₄₂:A β ₁₋₄₀, the importance of which was discussed previously. RD2 stands as a promising therapeutic against AD presenting the success of

screening large, randomised peptide libraries and adopting rational design to optimise and increase the potential of peptide hits.

Aside from targeting the self-association of A β , recent studies have explored the potential of peptide inhibitors of which their design is based upon cross-amyloid formations. By targeting these cross-amyloid interactions there is potential to not only target both amyloid polypeptides with one inhibitor but to also prevent cross-amyloid interactions, or cross-seeding (Armiento, Spanopoulou and Kapurniotu, 2020). An example of this is the hetero-association of A β ₁₋₄₀, A β ₁₋₄₂ and the Islet Amyloid Polypeptide (IAPP) involved in the pathogenesis of Type-2-Diabetes. The two proteins have been shown to interact with high affinity with suggestions that this peptide interaction could provide the molecular link observed between AD and diabetes (Yan et al., 2007; Andreetto et al., 2010). Building on the identification that IAPP-GI, a mimic sequence of IAPP which is conformationally constrained by N-methylation, can bind to and prevent cytotoxicity of A β ₁₋₄₀ (Yan et al., 2007), Andreetto et. al. set out to identify short sequences, or 'hot regions', required for A β -IAPP interaction. The group used IAPP-GI as a substitute of IAPP (highly insoluble and prone to aggregation) to allow for high solubility whilst retaining the ability to behave the same as full length IAPP in binding A β ₁₋₄₀. Using membrane-bound peptide arrays they identified five short peptides based on recognition elements of A β and IAPP required for both self-association and cross-interaction between the two. The study revealed binding affinities of the peptides with the amyloid proteins and provides a scaffold for further investigation of the potential of these peptides to design potent inhibitors of amyloidosis across the diseases using the sequences as templates (Andreetto et al., 2010).

Finally, another aspect of targeting A β aggregation using a rational approach is by preventing pathological chaperoning of A β , for example by blocking interaction between A β and ApoE4, as is presented by the peptide A12-28P. A12-28P is a modified version of the original A β sequence between residues 12 and 28 (the recognition element for ApoE4 binding). Previous studies demonstrated that applying the original sequence of 12-28 peptide could block A β interaction with ApoE4 and inhibit formation of A β fibrils (Ma, Brewer and Potter, 1996). Replacing Val for Pro at position 18 (A12-28P) and incorporating d-enantiomeric amino acids with end protection created a peptide that was non-toxic, non-fibrillogenic and yielded greater protease susceptibility without effecting the peptides ability to block A β interaction with ApoE and inhibit A β aggregation to present promising results *in vitro* and *in vivo* (Sadowski et al., 2004).

Various approaches to targeting A β using peptides have been explored and demonstrates the wide application of peptides to target many protein interactions with high specificity and present exciting prospects as potential therapeutics against AD. With the increasing potential of peptides seeing over 468 peptide agents entering Phase III clinical trials and 89

approved peptide drugs across numerous disease areas towards the end of 2020 (a marked increase from figures reported in 2018), and the recent development of peptide-drug databases, such as PepTherDia providing the necessary resources to allow for further acceleration of the peptide field, it is an exciting time to apply the ever-growing potential of peptides to target A β toxicity in AD (D'Aloisio et al., 2021).

Table 2: Advantages and disadvantages of peptides as therapeutics. Summarised within the table are the various advantages and disadvantages of peptides as therapeutic agents compared to small molecules and antibodies. The following references were used to gather the information for this table (Mason, 2010; Craik et al., 2013; Recio et al., 2017).

Advantage	Disadvantages
Highly potent	Protease susceptibility
Highly selective	Poor membrane permeability
Ability to form multiple interactions with target	Low oral bioavailability
Broad range of targets	Short half-life
High chemical and biological diversity	Rapid clearance
Low immunogenicity	Potential for high production costs
Able to screen or select peptides as nucleic acids or as peptide entities	Some peptides harbour poor solubility
Limited accumulation in tissue	
Low cost of production	
Low toxicity	

Table 3: Examples of Peptides developed to target A β -induced toxicity in Alzheimer's Disease. Summarised within this table are peptide therapies mentioned within this review to demonstrate some examples of peptide therapies against A β toxicity in AD.

Name	Sequence	Method	Function	Year	Citation
A12-28P	vhhqklpffaedvgsnk	Modified sequence of A β 12-28 with addition of β -sheet breaker proline at position 18. Utilising D-amino acids, the peptide was also synthesised with end-protection (amidation of C-terminus and acetylation of N-terminus)	Increased stability and resistance to protease degradation compared to A12-28 whilst retaining the ability to block ApoE interaction with A β and block A β aggregation <i>in vitro</i> and <i>in vivo</i>	2004	(Sadowski et al., 2004)
A β 16-20	KLVFF	Derived from binding sequence identified within A β between residues 16-20. Alanine scans showed that residues 16, 17 and 20 are crucial	Binds to A β full sequence and prevents aggregation by creating atypical anti-parallel β -sheets. D-amino composed peptides based on this motif also show potential to block formation of fibrils with the added benefit of protease resistance	1996	(Tjernberg et al., 1996; Tjernberg et al., 1997)
A β 31-42/39-42	C-terminal sequence	Sequence derived from C-terminus. Screened x-42 where x = 28-39	Disrupting C-terminus association to interrupt oligomer formation showed success to inhibit A β -induced toxicity in cells by stabilising non-toxic forms of oligomers	2008	(Fradinger et al., 2008)
A β -IAPP-GI binding motif regions	A β 19-22/15-24/27-32/25-35/35-40 interact with either IAPP8-18 or 22-28	Membrane bound peptide arrays of the A β sequence in series of 10 residues identified 5 peptide sequences within A β that are required for A β association with IAPP	Five short peptide sequences required for hetero-association of A β to IAPP identified as hot regions which stand as templates to design peptide inhibitors to block the cross-amyloid interaction	2010	(Andreotti et al., 2010)
D1/D-pep	qshyrhispaqv	Mirror image phage display to identify D-peptides that bind to A β	Binds specifically to A β ₁₋₄₂ fibrils. Could act as a probe to detect amyloid in human brain and used as a carrier across the blood brain barrier for imaging	2003	(Wiesehan et al., 2003)

D3	rprrtlhthrn	Mirror image phage display with the suspected target to be dominated by small oligomers of A β	Reduced A β aggregation as determined by ThT aggregation assays, dissociated pre-formed A β aggregates, rescued cell viability of PC12 rat parenchymal cells and reduced A β load in transgenic mouse model	2008	(van Groen et al., 2008; Brener et al., 2015)
IAPP-GI	KCNTATCATQ RLANFLVHSS NNFG(N-Me)AI(N-Me)LSSTNVG SNTY	Mimic sequence of IAPP with double N-methylation (to block β -sheet formation to one side of the peptide)	Binds to A β ₁₋₄₀ to block and reverse its associated cytotoxicity	2007	(Yan et al., 2007)
iA β ₅	LPFFD	Incorporation of Proline into residues 17-21	Designed against Abeta residues 17-20 with incorporation of Proline residues presented the LPFFD peptide as a potent inhibitor of Abeta aggregation in both cell-based and <i>in vivo</i> models (rat brain model of amyloidogenesis by injecting A β in to rat brain)	1996	(Soto et al., 1996; Soto et al., 1998)
iA β _{5p}	Ac-LPFFD-Amide	iA β ₅ modification - End protected LPFFD to increase pharmacological features (acetylated at N-terminus and amidated at C-terminus to protect against proteolysis)	Improves stability of peptide and ability to cross the BBB. Demonstrates success at reducing amyloid deposition in mouse models of AD	2002	(Permann et al., 2002)
LPYFD	LPYFD	iA β ₅ derivative	Reduces cytotoxicity of A β in cell-based assays and an amide protected version of LPYFD can cross the BBB and protect synapses <i>in vivo</i>	2004	(Datki et al., 2004; Juhász et al., 2009)
OR1	H2N-RGKLVFFGR-COOH	Sequence derived from KLVFF with additional R/G soluble amino acid residues added to N and C terminus to target A β oligomers	Successfully prevented fibrilisation of A β but not oligomerisation	2008	(Austen et al., 2008)

OR2	H2N- RGKLVFFGR- NH2	Sequence derived from KLVFF with additional R/G soluble amino acid residues added to N and C terminus to target A β oligomers	Successfully prevented fibrilisation of Abeta and also oligomerisation. Also, effectively protected against toxicity in SH-SY5Y cells demonstrating importance of oligomers in toxicity	2008	(Austen et al., 2008)
RD2	ptlhthnrrrrr	Rationally designed peptide based upon rearrangement of D3 sequence to provide greater potential to remove A β oligomers	Demonstrated similar binding affinities to D3 as determined by Surface Plasmon Resonance (SPR) but greater efficiency at removing oligomers. RD2 showed cognitive improvement <i>in vivo</i> without reducing overall plaque load showing potential of targeting oligomers over plaques	2017	(van Groen et al., 2017)
RI-OR2	Ac-rGffvkGr- NH2	Retro-inversion of OR2 sequence	Provides a more stable peptide that has greater resistance to proteolysis than OR2	2010	(Taylor, M. et al., 2010)

Aim of the study

This project seeks to use semi-rationally designed libraries to target the toxic A β oligomers using peptide inhibitors selected for by intracellular screening assays. One such assay is the Protein-fragment Complementation Assay (PCA) that the study will apply to select for peptides that bind to A β . The intracellular nature of PCA selection means that only peptides capable of binding to A β and detoxifying it are ultimately selected. The project will screen two large libraries targeting regions of A β that are important for folding and aggregation of A β . The libraries will be screened against an Arctic mutant of A β ₁₋₄₂ to increase the stringency of the screen. As previously discussed, the Arctic mutant has a higher propensity to aggregate compared to wild type A β and its use allows for a higher stringency screening platform. Screening peptides against this mutant has the potential to identify more promising hits relative to those derived from targeting of wild type A β . In addition, A β ₁₋₄₂, as opposed to A β ₁₋₄₀, has elevated toxicity, a higher propensity to aggregate and acts as a seed for aggregation. Targeting A β ₁₋₄₂ could therefore be of more relevance with regards to inhibiting A β toxicity.

Once peptide hits have been identified they will be characterised using a range of biophysical techniques including Thioflavin-T (ThT) aggregation assays, circular dichroism (CD), Transmission Electron Microscopy (TEM) and protein cross-linking experiments. Within this study, a cell-based toxicity assay will be explored to demonstrate A β -induced toxicity in a cellular environment. This cell-based assay may then be used to evaluate the ability of peptide hits to rescue A β -induced toxicity to reveal their potential as therapeutic agents.

Additionally, the study will seek to both develop and explore the potential for a completely novel intracellular screening assay, known as Transcription Block Survival (TBS), that is aimed at identifying peptides that have the capability to block A β aggregation at the earliest stage, dimerisation. Initially, proof-of-principle assays will be conducted to provide proof-of-concept data to underpin the theory behind the platform, followed by an initial library test screen to evaluate the capability for TBS Assay to identify functional peptide hits that rescue A β -induced toxicity.

Chapter Two: Method
developments carried out
throughout the study to enable
optimal experimental processes

Chapter Introduction

Previous Protein Fragment Complementation Assays (PCA) report library member sizes ranging between 8,000 and ~200,000 (Acerra, Kad and Mason, 2013; Acerra, N. et al., 2014; Acerra, Nicola et al., 2014; Cheruvara et al., 2015; Baxter et al., 2017; Yu, M. et al., 2021). Here, we report the use of PCA to screen peptide libraries of 600,000 and 2.1 million member libraries which is a vast increase from those previously reported. Due to these large, ambitious library sizes, multiple stages of optimisation were required to enhance every step of peptide library building and screening to enable maximum efficiency and sufficient library coverage. Additionally, applying the library building protocol to build a subsequent library 10 – 22 within an alternative vector backbone was essential for a proof-of-principle screen for the novel Transcription Block Survival (TBS) assay, with further optimisation of the library building steps necessary within this platform. Described below are the various method development steps taken to enable successful application of the library screening process throughout the study. Subsequent to library screening, methods to purify A β protein and identified peptides hits were needed to conduct relevant biophysical characterisation of the selected hits, both aspects of which were also explored and optimised as discussed below. Furthermore, a cell-based toxicity assay was required to assess the potential of hits identified from the screen and the development of this assay also documented.

Method development steps for optimisation

Optimisation steps for Library Building

Polymerase Chain Reaction

The first stage was to develop the Deoxyribonucleic Acid (DNA) inserts that represent the library members using Polymerase Chain Reaction (PCR). Primers were designed so that all library members were incorporated, with the forward primer acting as the template for the PCR reaction. The following PCR primers were ordered from Sigma-Aldrich:

Table 1: PCR primers ordered to achieve library insert sequences from PCR.

Primer	Sequence
Library 28-42 Forward Primer	AAAG GCTAGC MRRGBNGBNVTHVTHGBNVTHATSVTHGGTG SNVTHVTHVTHGBN GGCGGCC AAAA
Library 10-22 Forward Primer	AAAG GCTAGCT ACVNKGTGNNKCATVNKAAAVNKGTGTWTTT TRYHGA AGCGGCC AAAA
Reverse Primer for both libraries	TTTT GGCGGCC

Restriction sites NheI (F primer only) and AclI (F and R primers) are highlighted in bold.

For both libraries 10-22 and 28-42, the details of which are discussed later in the thesis, a band of approximately 60 bp resulting from PCR was expected. However, following initial PCR reactions it was evident that the forward primers were self-annealing to produce two back-to-back inserts of approximately 120 bp (Figure 1 (a)). Following gel extraction, these dimer inserts were subsequently digested to form two separate library inserts at approximately 60 bp (Figure 1 (b)). The 60 bp band observed in Figure 1 (a) for the PCR lanes is most likely the primers that are added to the reaction as the difference in intensity between these bands and the Control bands is not significant. The primers are designed to be represent the full length of the insert as they also act as the template sequence which is why they appear on the gel as background. For this reason, only the dimer insert band was extracted from the gel and this digested with NheI and AclI to provide the pure library insert band, as observed in Figure 1(b). This band was extracted from the gel and the DNA ready for sticky-end ligation into vector.

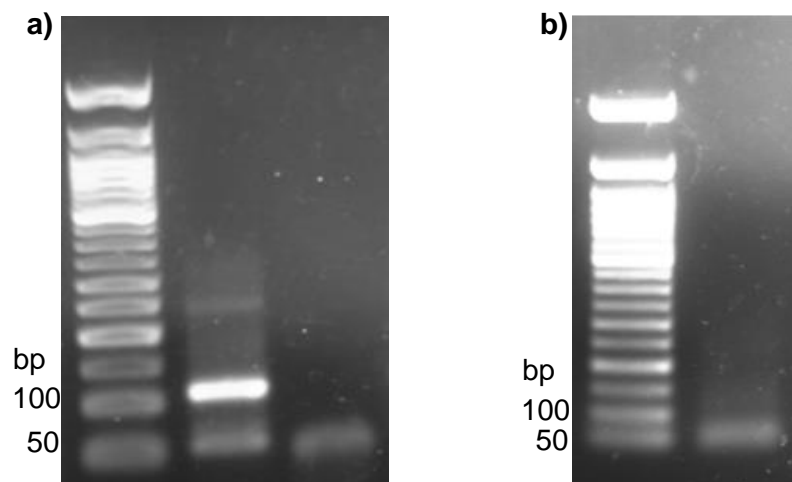


Figure 1: Polymerase Chain Reaction (PCR) to produce library dimer inserts. **a)** PCR was carried out for the libraries 10-22 and 28-42 to produce similar bands for both. The example here is for Library 10-22, but the Library 28-42 presents similar gels. Here, the forward primers self-annealed and library insert dimers at ~ 120 bp produced. Lane 2 shows PCR reaction and Lane 3 is a no Polymerase control reaction. **b)** Following gel extraction of the ~ 120 bp band the resulting DNA was digested with NheI/Ascl to cleave the dimer PCR product and digestion reaction run on electrophoresis to indicate that only a single library insert bands remain at ~ 60 bp.

Ligation and transformation of libraries within the PCA platform

Following successful PCR and restriction digest of library 10 – 22 and library 28 – 42 insert fragments to create complementary sticky ends for ligation in to the p230d-dhfr1 vector relevant for PCA, the next step was ligation and transformation to build and harvest the libraries. With standard cloning to present a single DNA product, ligation and subsequent transformation must present just a single successful colony that can be expanded in culture. However, for applications within library screening, each transformation colony will represent a library member and as such enough colonies must be produced to confidently represent the library. For at least 95 % coverage of libraries 10-22 and 28-42, ~ 2,000,000 and ~ 6,500,000 colonies were required following transformation, respectively. This required maximum efficiency at each step and extensive optimisation of ligation and transformation was carried out to achieve this, as outlined in Table 2.

For standard ligations a vector:insert ratio of 1:3 is generally adopted. However, due to the small insert size of the libraries being screened, which may present difficulty in ligation, the

initial ligations for this study utilised a vector:insert ratio above the usual at 1:6. The resulting transformation provided limited colony formation at just ~ 22 colonies. Therefore, an exaggerated vector:insert ratio of 1:50 was tested to saturate the ligation with the library inserts to potentially increase the likelihood of successful ligation of the insert to the vector. Although higher colony counts were obtained compared to the 1:6 ligation, this provided only ~ 90 colonies, contributing only a very small degree to the theoretical library size.

To potentially improve the efficiency of the cells, the optimal density of the electrocompetent cells was explored. Traditionally, following preparation of electrocompetent cells, the suspension is resuspended to an OD₆₀₀ of 0.4. Here, a range of cell densities were tested including 0.4, 0.8 and 1.0 with the highest cell density providing the greatest transformation efficiency with a considerably higher number of colony forming units presented following transformation with a positive control, fully circularised (p230d-alpha-synuclein) plasmid. Unfortunately, this did not translate towards an increase in colony formation following library transformation at this higher OD₆₀₀ with poor transformation observed, despite an improved desalt method being applied. The previous transformations employed a standard butanol desalt method to prepare ligated DNA for transformation. For Butanol desalt, the ligation mix is made up to 50 µl with ddH₂O and 500 µl Butanol added. The sample is vortexed, centrifuged and the supernatant removed to leave just the pelleted DNA, which is incubated at 37 °C until dry. Finally, the pellet is resuspended to the desired volume in ddH₂O. This desalt protocol is time-consuming and results in a loss of DNA sample. Instead, here the ligation mix was spun through a QIAquick PCR Purification Kit (Qiagen; Cat No.: 28106) to remove the salt and concentrate the DNA to provide a quick, convenient method to desalt.

Although the positive control transformation in to the applied XL1-Blue cell line provided sufficient transformation efficiency, to explore whether the cell line was limiting the success of library ligation and transformation an alternative, purchased electrocompetent cell line was tested. The NEB 10β cell line (C3020K) is a highly efficient cell line for transformation of large plasmids ideal for the library plasmid that was to be transformed. Pairing this with NEB Electroligase to circumvent the need for a desalt step, which had been a considerable point of DNA loss, provided a promising ~ 31,000 colonies following ligation and transformation. However, just 25 µl of cells, as per the manufacturer recommendations, was used with 2.5 µl of ligation mix, which may have limited the success of this transformation due to the proportion of ligase mix within the transformed cell volume. In order to increase the amount of DNA that could be applied to each transformation, the cell volume was also increased to allow for successful transformation with higher volumes of Electroligase library product. Transformation of 50 µl NEB 10β cells with 2.5 µl ligation mix presented a promising ~ 431,000 colonies, a marked improvement. Subsequently, the limit of Electroligase ligation mix volume applied to the transformation was tested and 5 µl was used to transform the 50 µl cell sample. This increased volume, thus DNA amount, greatly

improved the success of the transformation with 1,189,400 colonies which could be repeated just three times for each library to sufficiently cover libraries 10 – 22 and 28 – 42 with 99.99 % and 95.60 % confidence, respectively, following calculation with the following equation (Denault and Pelletier, 2007):

$$E = 100*(1-(1/n))^m$$

Equation 1: Library coverage where E = % of library missing, n = theoretical library size and m = colony forming units from transformation (experimental).

Simultaneously, to test the now optimised ligation protocol within the original XL1-Blue cell line, a sample of the Electroligase ligation mix was transformed in to electrocompetent XL1-Blue cells, providing only ~ 11,000 colonies compared to the 1,189,400 colonies resulting from the purchased NEB 10 β cells. This indicated that the in-house XL1-Blue electrocompetent cells were considerably less efficient in transformation than the purchased NEB 10 β cells.

For all ligations, vector only background controls were conducted and taken into consideration for final colony counts described in Table 2, in that any background, if present, was subtracted from the total colony count.

Following successful coverage of the libraries within the NEB 10 β line, the next stage was to harvest the colonies for miniprep of the library DNA for screening within the PCA platform, which is discussed later.

Table 2: Optimisation process for building libraries 10 – 22 and 28 – 42 in preparation for screening in the Protein Fragment Complementation Assay (PCA). Following successful PCR and restriction digest of library 10 – 22 and library 28 – 42 inserts to create complementary sticky ends for ligation in to p230d-dhfr1 vector, the next step was to carry out the ligation and subsequent transformation to build and harvest the libraries. This required multiple stages of optimisation which are outlined in the table below. The variable conditions included the vector:insert ratio for ligation, the type of ligase used, the cell line transformed, density of the cells and amount of DNA. Additionally, the desalt method following ligation was tested which included the traditional butanol method and an experimental method in which the ligation mix was spun through a QIAquick PCR Purification Kit (Qiagen; Cat No.: 28106) column in order to desalt and concentrate the ligated DNA, which is referred to in the table as column desalt. Two different cell lines were utilised, the XL1-Blue line which was prepared electrocompetent within the laboratory and the NEB 10 β cell line which was purchased as an electrocompetent cell. All ligations have concomitant negative (no insert) control ligations and this background, if any, has been applied to the colony counts outlined in the table.

Vector:Insert Ratio	Ligase	Desalt?	Cell line	OD ₆₀₀	DNA (ng)	Colonies (cfu)	Notes
1:6	T4	Yes (butanol)	XL1-Blue	0.4	500	22	Unsuccessful
1:50	T4	Yes (butanol)	XL1-Blue	0.4	500	89	Unsuccessful
Fully circularised positive control plasmid	T4	n/a	XL1-Blue	0.4	144	7,840,000	A higher OD ₆₀₀ provided a greater transformation efficiency
				0.8		8,660,000	
				1.0		18,260,000	
1:50	T4	Yes (column)	XL1-Blue	1.0	400	11	DNA is lost during the butanol desalt method, so used a column flow-through method to desalt ligation mix and concentrate DNA by eluting in low volume
1:50	T4	No	NEB 10 β (purchased)	n/a	62	0	Tried with no desalt to ensure all DNA is retained as DNA also lost in column desalt method Results in a low DNA concentration used in transformation and a high salt content No colonies were observed This transformation used the recommended 25 μ l of NEB 10 β that the manufacturer recommends
1:50	Electro ligase	No	NEB 10 β (purchased)	n/a	38	31,350	To entirely circumvent desalt step, Electroligase used which is compatible with transformation without desalt Used more ligation mix than the Electroligase protocol recommends (2.5 μ l as opposed to 2 μ l) to boost amount of DNA but the transformation burst Despite this, good colony count obtained
1:50	Electro ligase	No	NEB 10 β (purchased)	n/a	38	431,300	Whilst the above transformation appears promising, around 60 repeats would be required to cover the small 10 - 22 library Therefore, repeated the above transformation with a higher volume of cells to allow for increased DNA volume Using 50 μ l cells increased the transformation efficiency
1:50	Electro ligase	No	NEB 10 β (purchased)	n/a	76	1,189,400	Wanted to maximise both cell volume and DNA amount so explored how much ligation mix could be added before the salt concentration caused the transformation to pop Used 5 μ l ligation mix in 50 μ l NEB 10 β cells
1:50	Electro ligase	No	NEB 10 β (purchased)	n/a	76 (x3)	1,491,777 2,012,166 2,791,166	Did three repeats and combined to give the total colonies provided as 6,295,109 This sufficiently covered library 10 – 22
1:50	Electro ligase	No	NEB 10 β (purchased)	n/a	76 (x3)	6,641,699	Repeated above optimised transformation three times and combined at recovery stage. Library 28 – 42 sufficiently covered
1:50	Electro ligase	No	XL1-Blue	0.4	76	11,100	The NEB 10 β (purchased) are much more efficient (above) The NEB 10 β cells were used as provided so do not reflect the same cell density as the XL1-Blue which should be considered moving forward

Ligation and transformation of the libraries within the transcription-block platform

Following successful proof-of-principle analysis of the novel Transcription Block Survival (TBS) assay, described in detail in Chapter Four, the next step was to probe the potential of the platform to identify a functional peptide hit. As such library 10 – 22 was cloned in to the pQE80 plasmid, relevant for library presentation within the TBS platform. To build upon the previous library cloning and optimisation for PCA, the aim was to develop in-house NEB 10 β electrocompetent cells. Purchasing pre-prepared NEB 10 β was expensive and the cell line was difficult to obtain following covid supply issues. As previously demonstrated the XL1-Blue cell line prepared within the laboratory was less efficient than the purchased NEB 10 β cells providing ~ 11,000 colony forming units compared to the ~ 1.2 million observed following transformation of the PCA library 10 – 22 into the purchased NEB 10 β cells. When comparing the two aliquots of cells it was clear that the NEB 10 β cells were much more dense and contained many more cells than the in-house XL1-Blue electrocompetent cells, raising the question as to whether the increased transformation efficiency was due to the cell line or simply the number of cells present for transformation. Therefore, the experiment was repeated using a positive pUC19 plasmid to transform an aliquot of XL1-Blue cells ($OD_{600} = 0.4$) alongside a sample of NEB 10 β cells that had been prepared in-house, in line with the XL1-Blue cells, and also harboured an OD_{600} of 0.4. The in-house electrocompetent XL1-Blue cells produced ~ 6,000 colonies compared to ~ 16,000 for the NEB 10 β cells, indicating that the cell line used is important for transformation efficiency, with NEB 10 β proven the most competent (Table 3). Subsequently, the study sought to enhance the preparation of in-house NEB 10 β cells for application within library building for TBS screen against library 10 – 22, as outlined in Table 3.

To recapitulate the high cell density observed in the purchased NEB 10 β cells, the in-house produced NEB 10 β cells were resuspended in the residual glycerol following the final centrifugation step in the preparation of electrocompetent cells protocol and, to enhance the quality of the cells, were prepared on the day of use to avoid the harsh snap-freezing step. Following limited colony counts using DNA directly from the Electroligase mix, a large scale ligation was conducted to maximise the amount of DNA undergoing ligation. The resulting ligation mix was run through a QIAquick PCR Purification Kit (Qiagen; Cat No.: 28106) column to desalt, and most importantly, concentrate the sample by resuspending in a small volume for transformation, maximising the amount of DNA applied per transformation. This greatly increased the transformation efficiency with ~ 20,000 colonies forming as a result, compared to ~ 400 when no desalt and concentration step is performed. Despite the increase in transformation efficiency, the resulting colony numbers were not sufficient to cover the library.

Therefore, a comparison was carried out between the in-house produced NEB 10 β cells and purchased NEB 10 β cells that are electrocompetent upon purchase. This was carried out to assess the quality of the in-house produced cells and ensure that insufficient preparation of electrocompetent cells within the laboratory was not a contributing factor for the low colony counts. Reassuringly, a similar number of colony forming units were obtained for both in-house NEB 10 β and purchased NEB 10 β with ~ 25,000 and ~ 26,000 colonies, respectively.

Having ruled out the cells as the limiting factor in the ligation and transformation for the TBS library build, the study next sought to explore the DNA used for transformation. Initially, the amount of DNA used was reduced to match the amount used for the previous PCA library build as too much DNA in a single transformation can result in a reduced transformation efficiency. However, a reduced DNA amount for TBS library 10 – 22 resulted in a reduction in colony formation with higher concentrations being optimal. Therefore, the ligation conditions were altered to potentially enhance this step prior to transformation. Despite the success of overloading the ligation reaction with the insert for the previous PCA library, this was not observed for the TBS library and cloning in to the pQE80 vector. When a vector:insert ratio of 1:50 was applied a marked reduction in transformation efficiency was observed with just ~ 1,800 colonies. It was clear that saturating the ligation with the small library insert did not improve ligation efficiency within the pQE80 vector and instead the 1:10 ratio was used again but utilising an alternative ligase type. Instead, T4 DNA Ligase was employed with overnight ligation, as opposed to the Electroligase which required just 1 hour incubation at room temperature. However, the alternative ligase did not improve the colony formation.

The previous success of applying a large amount of library insert relative to the vector for PCA library building had swayed the decision to attempt higher ligation ratios for this TBS library build considering the inserts and vectors used were comparative in size. Following the lack of success here, the decision was made to step back to basics and attempt a standard 1:3 ligation which proved fruitful. This ligation condition, with T4 DNA ligase, provided ~ 74,000 colonies. Although this was an improvement compared to the 1:10 ligations, further optimisation was required to successfully cover library 10 – 22 in the TBS screen as around 28 repeats would be needed to provide confidence that the library would be sufficiently covered, which would be impractical to handle at later harvesting stages.

Ligation protocols differ in the recommended incubation temperature so, the optimal ligation incubation temperature was explored including 8 °C, 16 °C and room temperature (~ 25 °C). All transformations for this were performed using the same sample of ligation mix for library 10 – 22 and although the 8 °C ligation provided the highest number of colonies (this number has already factored the background colonies), this condition also had a higher

background in the no insert control ligation/transformation at ~ 5 % compared to the other highest colony count condition at room temperature that presented with ~ 3.5 % background colonies. Therefore, the room temperature ligation was taken as the most effective ligation condition and a large-scale ligation was conducted with subsequent column desalt and concentration to provide a high concentration sample of DNA to be used in transformation. Unfortunately, this high concentration caused the DNA to arc during electroporation and the transformation popped. Accordingly, the DNA amount used for transformation was reduced but was unable to provide sufficient colony numbers at just ~ 4,000 and further development steps were required.

For the PCA library builds, an increase in ligation efficiency was observed when applying Electroligase as opposed to T4 DNA ligase. Although Electroligase had been applied to this library build previously, since then the ligation conditions had been optimised with the identification of the lower vector:insert ratio providing promise. Therefore, the ligation was repeated again with Electroligase in place of T4 DNA Ligase, across varying ratios to identify the optimal vector:insert ratio for this alternative ligase. This experiment corroborated that, for library 10 – 22 ligation in to the pQE80 vector, a vector:insert ratio of 1:3 was optimal, but it failed to reach as high a colony counts than that for the T4 DNA ligase reactions.

Despite attempts to replicate the optimal ligation condition identified that presented ~ 74,000 colonies from a vector:insert ratio of 1:3 using T4 DNA ligase and transforming into high density NEB 10 β cells, this high count was not obtained again. Additionally, the similarity in library colony counts within both bought NEB 10 β and in-house produced NEB 10 β cells, along with the successful positive pUC19 control and the fully circularised pQE80-T7 (the original pQE80 plasmid that is digested to provide the pQE80 backbone for ligation) transformation presenting full coverage on transformation plates, indicated that the cell preparation was sufficient, but rather the DNA cloning was the restrictive factor. Within the laboratory group, various members were attempting to clone in to the pQE80 vector for various applications, also with limited success. Therefore, in the interest of time and to preserve the previous cloning efforts with the numerous transformations carried out until this point (as transformation plates can only be stored for up to two weeks before harvest), the decision was made to combine all of the obtained transformation plates to harvest and represent a sample of library 10 – 22. The initial aim with the library 10 – 22 screen within the TBS platform was to provide a proof-of-principle in the ability of TBS to identify functional peptide hits. Therefore, it seemed appropriate to continue with a sample of the library to gauge the potential of TBS before investing too much time building the full library prior to confirming the potential of the platform.

Table 3: Optimisation process for library 10 – 22 build in preparation for test screening in Transcription Block Survival (TBS) Assay. Following successful PCR and restriction digest of library 10 – 22 inserts, to create complementary sticky ends for ligation in to pQE80 backbone relevant for the TBS platform, the next step was to carry out the ligation and subsequent transformation to build and harvest the library DNA. This required multiple stages of optimisation which are outlined in the table below. The variable conditions included the vector:insert ratio for ligation, the type of ligase used, the cell line transformed, the density of the cells and amount of DNA. The desalt method used was an experimental method in which the ligation mix was spun through a QIAquick PCR Purification Kit (Qiagen; Cat No.: 28106) column in order to desalt and concentrate the ligated DNA and is referred to in the table as column desalt. Additionally, three different cell lines were utilised, the XL1-Blue line which was prepared electrocompetent within the laboratory and the NEB 10 β cell line, which was either purchased as an electrocompetent cell, referred to as NEB 10 β (purchased) or a sample of the purchased cells was taken and used for overnight incubation to inoculate a starter culture for subsequent preparation of electrocompetent cells within the laboratory, referred to as NEB 10 β (in-house). All ligations have concomitant negative (no insert) control ligations and this background, if any, has been applied to the colony counts outlined in the table.

Vector:Insert Ratio	Ligase	Desalted?	Cell line	OD ₆₀₀	DNA (ng)	Colonies (cfu)	Notes
pUC19	n/a	n/a	NEB 10 β (purchased)	0.4	0.01	15,918	To explore transformation efficiency of in-house XL1-Blue compared to NEB 10 β a sample of purchased NEB 10 β was taken for overnight incubation and subsequent preparation for electrocompetency in line with the preparation of XL1-Blue The cell type is important, not just the high density of the bought cells
			XL1-Blue			5,911	
1:10	Electroligase	Yes - column	NEB 10 β (in-house)	High density	40	470	To provide the high cell density observed with the purchased NEB 10 β the in-house produced cells were resuspended in residual glycerol following the final centrifugation step in preparation Low DNA amount used following ligation may be the limiting factor
1:10	Electroligase	Yes - column	NEB 10 β (in-house)	High density	225	19,800	To increase the amount of DNA transformed, a large scale ligation was conducted and a column desalt used to concentrate the DNA Additionally, the cells were prepared on the same day as assay to avoid harsh snap-freezing
		No			57	380	
1:10	Electroligase	Yes - column	NEB 10 β (in-house)	High density	225	25,080	The quality of the in-house produced NEB 10 β cells was assessed by transforming both in-house NEB 10 β and purchased NEB 10 β No difference in transformation efficiency between the cell types is observed
			NEB 10 β (purchased)			26,280	
1:10	Electroligase	Yes - column	NEB 10 β (in-house)	High density	45	830	Transformed with less DNA in case previously overloading but no improvement observed
1:50	Electroligase	Yes - column	NEB 10 β (in-house)	High density	225	1,766	Although for PCA libraries the overloaded ratio worked it does not appear to provide better ligation efficiency in the pQE80 system
1:10	T4	Yes - column	NEB 10 β (in-house)	High density	200	980	An alternative ligase was tested to enable overnight incubation, compared to just one hour recommended for Electroligase
1:3	T4	Yes - column	NEB 10 β (in-house)	High density	160	73,702	1:3 ratio provides better ligation efficiency but requires further optimisation Later repeats of this condition failed to provide similar colony counts
1:3	T4	No	NEB 10 β (in-house)	High density	61	RT: 1,615	Tested different temperatures for overnight ligation due to variation between protocols 8 °C ligation appears to give the most colonies, but also provided highest degree of background at 5 % compared to 3.5 % for the room temperature (RT) ligation
						14 °C: 780	
						8 °C: 1,767	
1:3	T4	Yes - column	NEB 10 β (in-house)	High density	500	19,945	Repeated the optimal condition with ligation at 1:3 at RT overnight but also with column desalt for higher DNA concentration The high concentration caused the DNA to arc during the transformation
1:3	T4	Yes - column	NEB 10 β (in-house)	High density	228	4,366	Repeated again but bought DNA concentration down Unsure what caused the low colony count
1:3	Electroligase	Yes - column	NEB 10 β (in-house)	High Density	200	3,606	Electroligase used to potentially increase ligation efficiency Confirms that 1:3 is the most efficient ligation ratio, but limited formation of colonies
1:10					1,613		
1:50					590		
1:3	Electroligase	Yes - column	NEB 10 β (in-house)	High Density	200	1,860	Repeated the 1:3 condition alongside a positive control, pQE80-T7, plasmid The cells are very competent Instead, cloning within pQE80 is the restrictive factor
pQE80-T7					58	Fully covered	

Library Screening in PCA platform

Following successful production of the libraries, the next stage was to screen the libraries within the PCA assay. The resulting library DNA from the library harvest and subsequent miniprep was transformed into BL21-Gold (BL21-G) assay cells, containing the p300d-Basic-A β target and pREP4, applying the previously optimised technique, including the use of high density electrocompetent cells. The DNA to be transformed should now represent fully circularised p230d plasmid containing the library insert and a greater transformation efficiency is expected compared to transformation following ligation. However, this was not the case with initial library transformation into BL21-G cells presenting low transformation efficiencies with just 36,313 colonies for Library 28 - 42 and 326,000 colonies resulting for Library 10 - 22 (Figure 2 (a)), compared to full, uncountable plate coverage from the pUC19 positive control. As the positive, pUC19 transformation demonstrated that the cells were sufficiently electrocompetent, the low transformation efficiency may have been as a result of poor quality DNA representing the libraries. Therefore, in order to visualise the library to ensure the expected DNA band was present and of good purity, a sample was run on agarose gel electrophoresis and imaged. Here, it was revealed that the library DNA was contaminated. A higher molecular weight band was observed that might represent genomic DNA (Figure 2 (a)). Interestingly, library 28 - 42 exhibited a higher intensity contaminating band compared to library 10 - 22. Alongside the lower transformation efficiency following transformation of library 28-42 compared to 10 - 22, this suggests that the contaminating band is interfering with the transformation efficiency potentially by masking the concentration of the library. Samples of the library were also sent for sequencing and confirmed poor representation of the library, by a lack of peak presentation at the altered residues within the library. When measuring the DNA concentration for transformation, it may be that the higher molecular weight represented a large portion of the DNA present in the measured sample and provided a falsely high DNA concentration. Therefore, each transformation, and the sample of the libraries sent for sequencing, likely contained a much lower concentration than intended, accounting for the poor library representation.

To compare the quality of the library following building and preparation in different cell types, to ensure the contamination was not presented by the cells, library 10 - 22 was simultaneously built in both NEB 10 β and XL1-Blue cells. However, both cell types presented the contaminating band (Figure 2 (b)). Additionally, the library was transformed into BL21-Nova cells with no improvement on transformation efficiency. As the type of cell presented limited improvement on library quality, the next step was to assess the harvesting method. Due to the large number of plates required to cover the libraries during the building stage, at the plate scraping stage to harvest the cells prior to miniprep the cells were incubated, at a very high density, within a conical flask for an extended time as a result of

the time consuming nature of the harvest. During this time, cell death likely occurred which may have released genomic DNA. The genomic DNA in the sample potentially accounted for the heavy contaminating band observed within the libraries. Therefore, to evade the lengthy scraping process of the harvest prior to miniprep, a small sample of library 10 - 22 was transformed into NEB 10 β cells and harvested. This small sample meant that the process of scraping the plates was considerably shorter with less plates to scrape, hence less time for the cells containing the library DNA to remain stagnant. The resulting gel electrophoresis demonstrated an improvement in library representation with a higher intensity library band and lower contamination, compared to the previous larger scale harvest. Additionally, the subsequent transformation of the small sample of library 10 – 22 presented a higher transformation efficiency with ~ 710,000 colonies (Figure 2 (c)). Although an improvement, this method still does not present a high enough transformation efficiency and is incapable of sufficiently covering the library. However, it does highlight the problematic harvesting method that results in the potential genomic DNA contamination due to cell death.

With the aim to circumvent the requirement to harvest the DNA prior to miniprep, the library was taken from glycerol stocks that were obtained following the initial successful build of the libraries. Here, the glycerol stocks, which contained sufficient cell numbers to confidently cover the libraries, were defrosted in LB media and incubated at 37 °C for one 1 hour. The cells were subsequently centrifuged and the pellet used to miniprep the library DNA. The resulting samples presented a single, clean band representing the library DNA and a significant improvement in transformation efficiency into NEB 10 β cells with up to ~ 2,000,000 colonies resulting per transformation (Figure 2 (d)). Additionally, the library samples were sequenced and presented full coverage of the library presented by variation in base peaks at altered library residue positions (Figure 2 (e)). Alongside this, the amount of library required for optimal transformation was explored by transforming with 150 ng, 300 ng and 500 ng of DNA. The 500 ng condition provided the highest colony count and was thus applied to subsequent library transformations (Figure 2 (f)).

Following multiple transformations, with all repeats combined following recovery incubation step, both library 10 – 22 and 28 – 42 were sufficiently covered within the PCA screening platform with 93.39 % and 96.48 % overall confidence coverage for library 28 – 42 and library 10 – 22, respectively, when combining the obtained coverage following library building and screening.

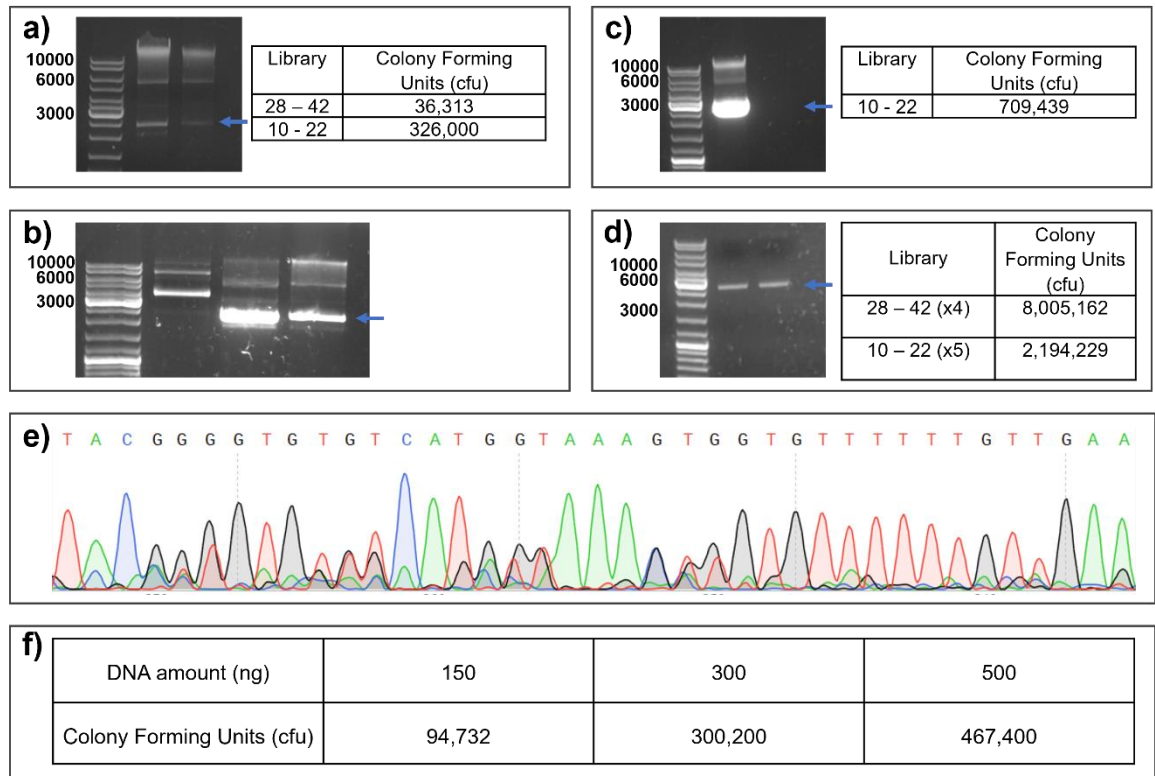


Figure 2: Optimisation of PCA screening in BL21-G cells. Following building and harvest of peptide libraries 10 – 22 and 28 – 42, the next step was to screen the libraries within the Protein Fragment Complementation Assay (PCA) with sufficient colony formation following transformation in to the BL21 – G assay cells (containing the p300d-Basic-A β and pREP4 plasmids) to allow for confidence in the library coverage. In order to do so, the quality of the library DNA was tested as a result of previously obtained low transformation efficiencies. **a)** Following library harvest, the resulting library samples were run on gel electrophoresis to ensure the expected library DNA was present and of good purity. Lane 1 contains GeneRuler DNA Ladder Mix, Lane 2 represents Library 28 – 42 whilst Lane 3 is library 10 – 22. Additionally, the table represents the colony count following transformation in to BL21-G assay cells. **b)** To compare the quality following preparation in different cell types, library 10 – 22 was built within both NEB 10 β cells (lane 4) and XL1-Blue cells (Lane 3) and the resulting harvested library ran on gel electrophoresis. Lane 1 is GeneRuler DNA Ladder Mix and Lane 2 is an unrelated sample. **c)** Following harvest of a small sample of library 10 – 22, to evade the lengthy scraping process of the harvesting step and subsequent miniprep, the resulting library sample was run on gel electrophoresis to assess the quality. Additionally, the table represents the colony count following transformation in to BL21-G assay cells. **d)** Following miniprep of defrosted library glycerol stocks, the resulting library DNA was run on gel electrophoresis and used for subsequent transformation in to BL21-G assay cells for PCA screening. The table represents the number of colonies obtained following transformation in to BL21-G with the number of transformation repeats outlined. The transformation repeats were combined after incubation for recovery following transformation. For all gels, the expected library band is marked with an arrow. **e)** Following preparation of library 10 - 22 and 28 – 42, samples were sent for sequencing by LightRun. The sequence from library 10 – 22 is shown as an example with peak variation at each base demonstrating the various residue options at those positions. **f)** The optimal amount of library DNA required for transformation to provide the highest number of colonies was explored with the transformation repeated at varying DNA concentrations. The colony numbers for each condition have been tabulated accordingly.

Peptide synthesis and purification

Two peptide libraries were designed, built, and screened using the intracellular protein fragment complementation (PCA) screening assay. Firstly, utilising recent A β structures as a template, library 28-42 was semi-rationally designed based upon those named residues. These residues are situated within the central hydrophobic core of amyloid fibres and have been shown to hold an instrumental role in the folding and interaction of A β molecules. The majority of residues within this region are incorporated into either the fold of A β (central β -sheet) or at the interface between dimers (Figure 3 (a)). Consequently, almost all residues were altered in the design of this library, resulting in a library size of 2,125,764 peptides (Figure 3 (b)). The second, smaller library is based upon a solvent-exposed β -sheet region of A β spanning residues 10 - 22. Each peptide facing into the hydrophobic core of A β was widely scrambled whilst solvent exposed residues were conserved, resulting in a library size of 655,360 peptides for library 10-22 (Figure 1 (a,f) in Chapter Three paper). Following PCA screening both libraries identified binding hits, named PCAH1 and PCAH2 for library 28-42 and library 10-22, respectively (Figure 3 (c) below & Figure 2 (a) in Chapter Three paper).

Synthesis and purification of PCAH2 was successful and characterisation of this hit has been conducted to reveal the potential of PCAH2 as a prospective AD therapeutic. This work has been prepared and written for publication and is presented in the following chapter where the work has been written towards a manuscript.

However, synthesis and purification of PCAH1 was much more complicated. Due to the design of the library, targeting the central hydrophobic core, the resulting hit was highly hydrophobic and insoluble in a range of solvents from acetonitrile to dimethyl sulfoxide (DMSO) and isopropanol. Although the synthesis of PCAH1 appeared successful, following cleavage from the resin the resulting pellet could not be sufficiently dissolved to allow for successful purification of the peptide using High Performance Liquid Chromatography (HPLC). Therefore, the cell penetrating peptide (CPP) TAT (RKKRRQRRR) was appended to the C-terminus of the PCAH1 sequence (Figure 3 (c)). The TAT-tag is a useful tool to improve the solubility of a peptide, by adding charge, to enhance dissolution of peptides for purification. An added benefit of the TAT-tag is the potential to increase cell-penetrance of the peptide for future applications within cell-based assays (Frankel and Pabo, 1988).

The modified TAT-tagged PCAH1 peptide (PCAH1-TAT) now presented solubility in DMSO, allowing for successful injection on to a HPLC column. The presence of DMSO resulted in the requirement for an extended initial buffer equilibration upon addition of the peptide to the HPLC column to ensure complete elution of DMSO following the revelation that the PCAH1-TAT elutes within the DMSO peak if the concentration gradient is applied too early.

Unfortunately, despite successful solubilisation and application on to HPLC column, the resulting HPLC trace provided a broad, unclear peak characteristic of aggregated amyloid proteins (Warner et al., 2017), that failed to present correct fragment ion or molecular ion peak assignments following Mass Spectrometry (MS) of various fractions throughout the HPLC trace (Figure 3 (d)). Despite these extensive efforts, purification remains unsuccessful for this peptide due to the hydrophobic, viscous nature of PCAH1. Therefore, the decision was made to continue solely with the PCAH2 peptide that presented promise following concurrent characterisation.

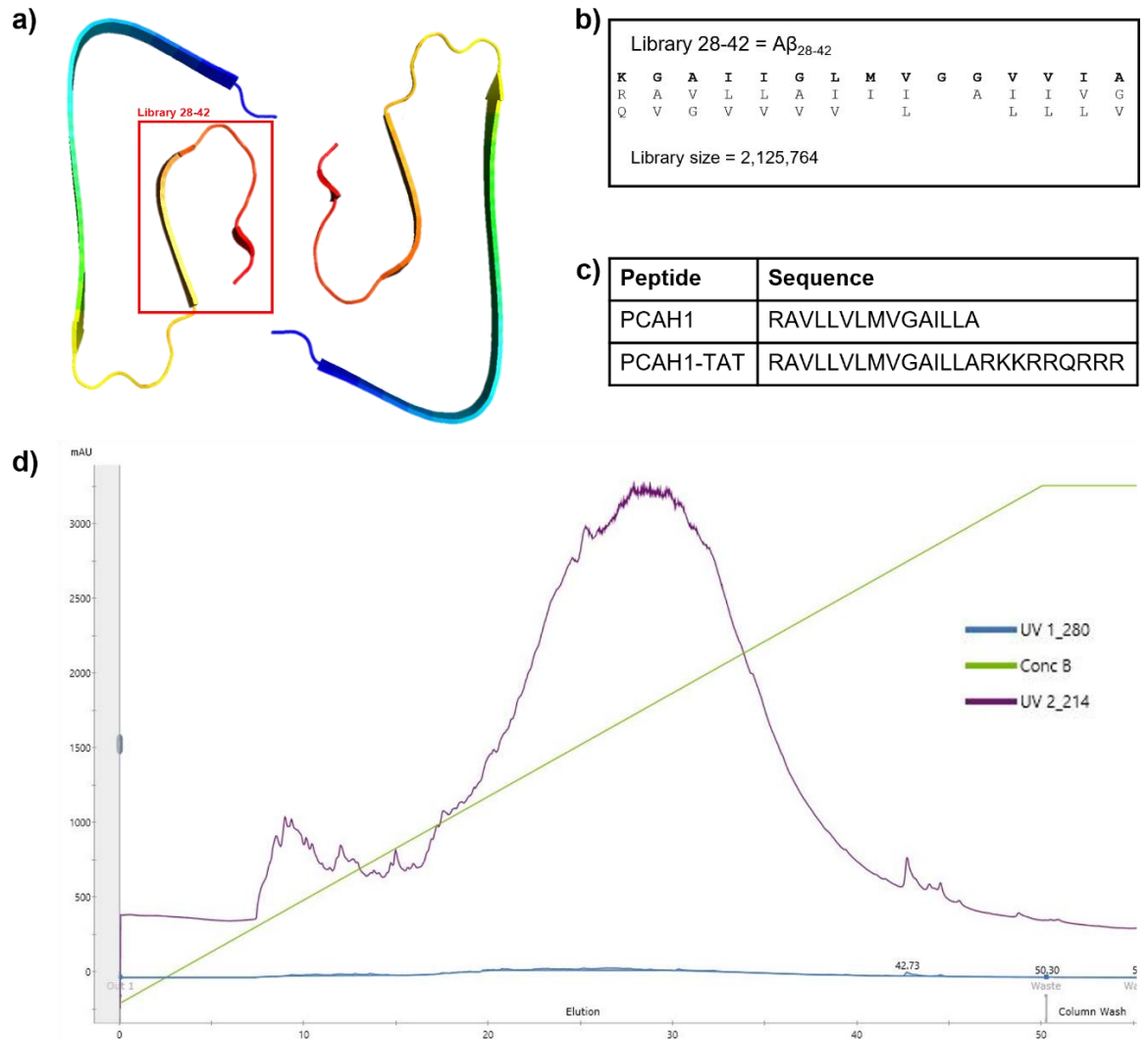


Figure 3: Design of Library 28-42 and synthesis of PCAH1 peptide hit identified following PCA screening. **a)** A Cryo-EM structure of Aβ₁₋₄₂ created with PyMol using Protein Data Bank (PDB) ID 5oqv (Gremer et al., 2017). The red box represents the region of Aβ that the library 28-42 is based upon, encompassing residues 28-42. **b)** Library design of library 28-42 targeting the sequence of Aβ₂₈₋₄₂. The top row is the wild-type sequence of residues 28-42 of Aβ. Of these residues, those conceived to have importance in folding and dimerisation of the peptide have been targeted to provide alternative residue options in these positions. Library options for each position are listed underneath the original sequence. Residues in the original sequence are included in the library. **c)** Following PCA screening, peptide PCAH1 was identified. However, handling of this hydrophobic peptide proved difficult, and a TAT-tag was added to provide greater charge, thus increased solubility. **d)** HPLC trace of PCAH1 following synthesis with both A₂₈₀ (blue) and A₂₁₅ (purple) represented along with concentration of Solvent B (ACN + 0.1 % TFA) (green).

Expression and purification of A β (M1-42)

A β (M1-42) expressed in BL21 (DE3) E.coli cells and purified with anionic exchange chromatography

Protein expression was successfully induced with 1 mM IPTG in BL21 (DE3) cells (Figure 4 (a)). A β (M1-42) is a 4.2 kDa peptide and the band between 3.5 and 6 kDa likely represents the correct protein. This band was successfully observed on a 20 % SDS-PAGE only in samples following IPTG induction, further indicating the band represents A β (M1-42). As expected, no A β (M1-42) is present in samples prior to solubilization of inclusion bodies containing the A β protein with Urea. Following this solubilization step, A β (M1-42) was present, indicated by the presence of the band between 3.5 and 6 kDa. The band was only present in the lane representing the sample that was induced by IPTG during growth. Following sonication, the sample was loaded on to a DEAE-Cellulose column and anion-exchange chromatography undertaken. A β eluted from the column between 35 – 50 % 10 mM Tris/HCl pH 8.0, 1 mM EDTA, 500 mM NaCl buffer (Buffer B), corresponding to fractions 18-24 that contain the highest concentration of A β (M1-42) with less contamination from other proteins compared to the later elution peak (Figure 4 (b-c)). These fractions were subsequently subjected to Size Exclusion Chromatography.

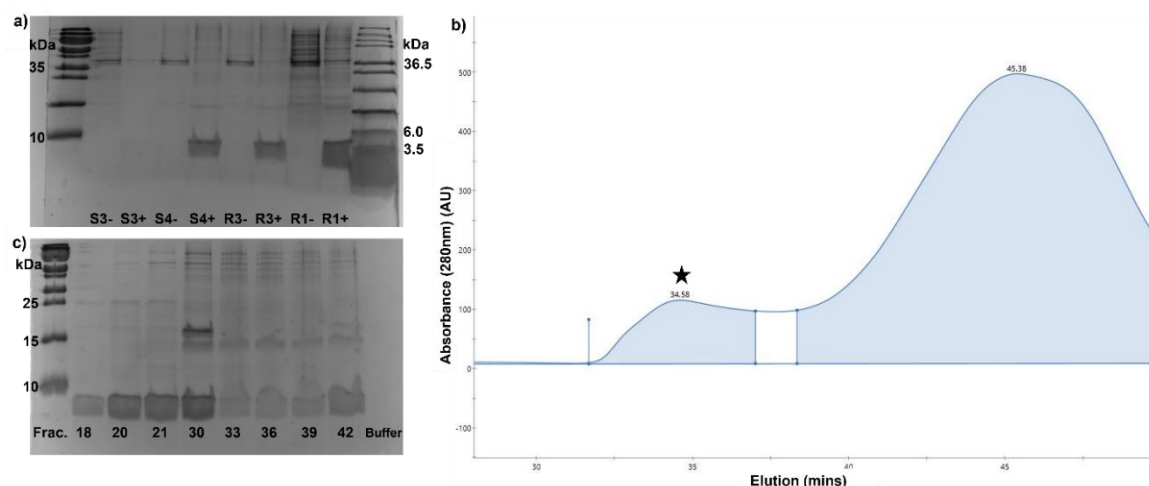


Figure 4: A β (M1-42) expression and purification to obtain monomeric A β (M1-42) peptide. a) 20 % SDS-PAGE expression gel of A β (M1-42) in BL21 (DE3) cells following induction with 1 mM IPTG. S3 is supernatant following the third sonication step during sonication and S4 is the supernatant following centrifugation after solubilisation of inclusion bodies with 8 M Urea. The samples marked + indicates samples induced with IPTG whilst – represents no IPTG induction. R1 represents resuspension of cell pellets following the first centrifugation step whilst R3 is the solution following sonication in 8 M Urea. **b)** Following solubilisation of inclusion bodies, A β (M1-42) was purified by anion-exchange chromatography. The following A280 peaks were observed. The peak marked with a star represents the A β (M1-42) elution peak. **c)** 20 % SDS-PAGE gel of peak fractions collected during A β (M1-42) purification.

Monomeric A β (M1-42) isolated with Size Exclusion Chromatography

Following purification by anion exchange chromatography, A β (M1-42) was subjected to Size Exclusion Chromatography to isolate monomeric A β . Fractions containing a peak corresponding to A β were combined (Figure 5 (a)). The absorbance peak at 280 nm is small with this likely due to the fact that A β_{42} contains just one aromatic residue for absorbance at 280 nm. Therefore, it was more effective to measure the Absorbance at 215 nm to identify amide bonds between peptide residues. Following initial purification by anion exchange, the A β -containing solution was concentrated using centrifugation filters with the flow-through and product also run on the gel to ensure no A β was lost during concentration. Following isolation of the monomeric peak by size exclusion, contaminating bands present prior to SEC were clearly removed and a single, A β monomeric band remained (Figure 5 (b)). An additional, later eluting peak was also present following size exclusion that produced no corresponding 280 nm peak raising the question as to the source of this peak. To characterise the peak it was also run on SDS-PAGE gel, yet no protein product was obtained and it was concluded that this peak was likely a breakdown product of the A β protein (Figure 5 (b)). The concentration of the resulting A β (M1-42) solution was calculated by measuring the A_{280} of the solution in a Quartz cuvette of 1 cm path length and applying Beer Lambert's Law with an extinction co-efficient (ϵ) value of 1280. The concentration of the solutions from various preparations averaged around 50 μ M.

However, upon return to the laboratory following the COVID-19 lockdown, despite the previously robust and reproducible production of A β (M1-42) that had previously been possible, this could not be replicated. Instead, low concentrations of \sim 5 μ M monomeric A β were produced and the second elution peak from SEC was exaggerated (Figure 5 (c)). As seen in timepoint aggregation experiments with A β on the SEC column, this second peak appears to increase as aggregation proceeds (Figure 7 (a)) yet, presents no evidence towards the peak forming as a result of protein presence (no absorbance at 280 nm and a lack of band presentation on SDS-PAGE gels). Therefore, this peak may result from a form of breakdown product as A β aggregates. With this in mind, the reduction in the monomeric peak observed in SEC upon return to the laboratory may have been as a result of accelerated aggregation of the samples, thus reduction in the expected monomeric A β peak and an increase in the breakdown product peak. This is also corroborated by the SEC profile from the more recent purifications of A β which also present possible oligomeric species peaks that elute prior to the desired monomeric peak (Figure 5 (c)). Efforts were made to decrease the aggregation of A β prior to application on the size exclusion column including reduced time between purification stages, avoidance of freezing samples between purifications and sonication of samples before SEC. Additionally, preincubation in 8 M Urea or 6 M Guanidine Hydrochloride (GuHCl) was carried out in an attempt to revert the A β

samples back to a monomeric state, and to prevent further aggregation. Furthermore, eluting the protein samples from anion exchange into Urea or GuHCl buffers was tested to prevent aggregation of the A β peptide straight from the column. Samples from anion exchange were also lyophilised and resuspended in 8M Urea before SEC. Additionally, the various columns were deep cleaned and tested to ensure there was no contamination present on the column that could cause the A β to aggregate upon application and a new column was also purchased. Unfortunately, following the described optimisation attempts, the same peak presentation as seen in Figure 5 (c) was observed throughout. Due to time constraints, the decision was made to purchase recombinant A β to allow for progression of peptide characterisation experiments.

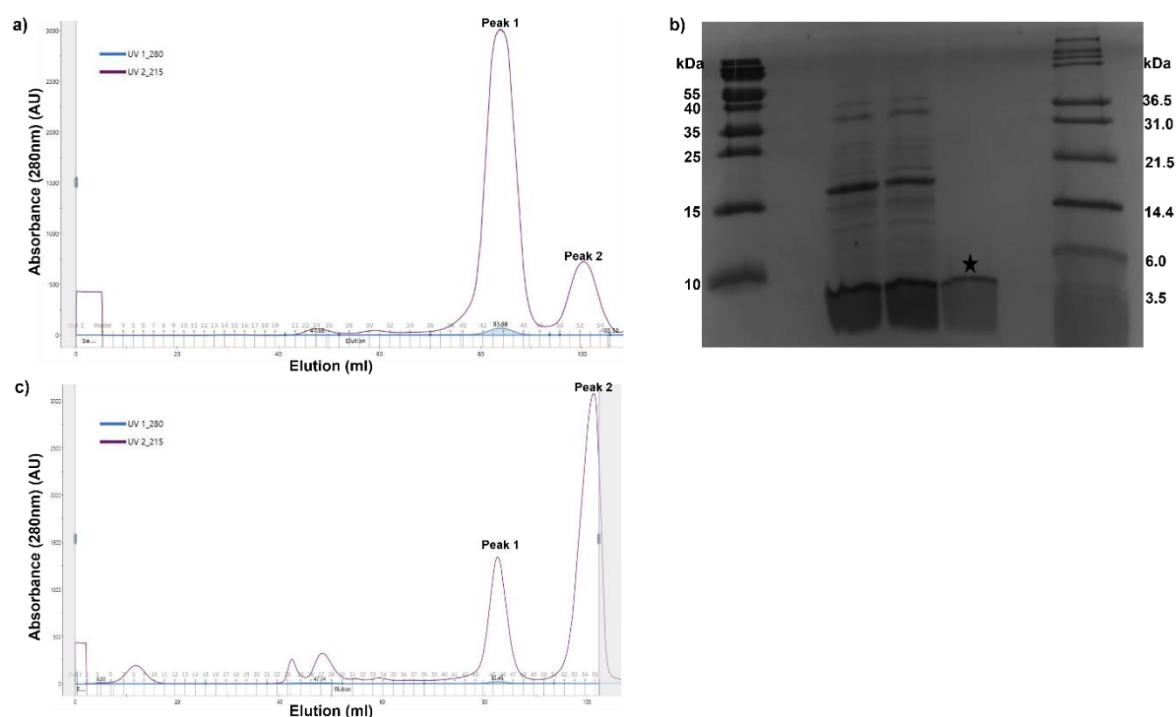


Figure 5: Monomeric A β (M1-42) obtained from Size Exclusion Chromatography. **a)** A₂₈₀ peak profile obtained from Size Exclusion Chromatography (SEC) of A β (M1-42). The peak marked peak 1 represents the monomeric A β (M1-42) peak, whilst peak 2 marks an unknown, contaminating peak. This second peak does not affect the purity of the A β produced as the monomer peak alone is isolated within the fractions collected from SEC. **b)** To confirm the presence of monomeric A β in the fractions collected that correspond to the peak a sample was run on a 20 % SDS-PAGE. The A β (M1-42) protein is approximately 4.2 kDa and is denoted by a star in Lane 5. Prior to Size exclusion, the sample from anion exchange underwent various stages to concentrate the sample. Aliquots were taken throughout the process to ensure that the A β was not lost during this process. Here, Lane 2 is the flow-through from centrifugation concentration, Lane 2 is the concentrated sample prior to filtration and Lane 4 is the filtered sample that is finally applied to the SEC column. Lane 6 is the second, contaminating peak obtained during SEC that presents no 280nm band to assess whether it contains a protein product. Lane 1 contains PageRuler 26166 ladder whilst Lane 7 is the Mark12 Ladder. **c)** Repeat of SEC to isolate monomeric A β following a sustained period outside of the laboratory with very limited, low yield of protein obtained.

Methods to explore oligomerisation state of A β throughout aggregation

Photo-induced cross-linking of unmodified proteins (PICUP)

To enable assessment of oligomeric species of A β throughout aggregation and to explore how the peptide hits identified from library screening may alter the presentation of oligomers throughout aggregation, PICUP was utilised. This is a commonly applied approach to measure protein oligomerisation, however the use of this technique within the lab required extensive optimisation. Initially, the recommended protocol, as outlined by Rahimi et. al., was adopted (Rahimi, Maiti and Bitan, 2009). In short, 18 μ l of A β sample was mixed with 1 μ l 20 mM Ammonium Persulphate (APS) (final concentration of 1 mM) and 1 mM Tris(2,2-bipyridyl)dichlororuthenium(II) hexahydrate (RuBpy) (final concentration of 0.05 mM) and exposed to 1 second irradiation before SDS-PAGE to visualise oligomeric species present. However, this proved ineffective within the laboratory setting, with no bands presenting on the subsequent gel (Figure 6 (a)). The aforementioned experiment utilised pre-aggregated A β , which may not be appropriate for monitoring the oligomerisation state of the protein as at this endpoint of aggregation the majority of protein has passed through the various oligomerisation states and most likely resides in large aggregates and plaques, which are too large to pass through the SDS-PAGE for visualisation. Therefore, a timepoint experiment was conducted to capture various stages of aggregation. However, this also proved ineffective at capturing A β oligomers to visualise on a gel, with no protein bands observed (gel not shown).

Instead, the protocol was adjusted to optimise the assay within the laboratory setting. One variable that was altered was the irradiation time, including 3, 10, 30, 60 and 120 seconds and also the source of light between torch light and ceiling light that may provide varying intensities of light that the sample is subjected to. A range of APS and RuBpy concentrations were explored with some reports suggesting the ratio of these reagents is the crucial factor, being optimal at an A β :RuBpy:APS ratio of 1:2:40 (Bitan, Gal, Lomakin and Teplow, 2001). For example, at 5 μ M A β , RuBpy and APS should be added to a final concentration of 10 μ M and 200 μ M, respectively. Previous A β PICUP experiments report optimal concentrations of A β between 10 and 50 μ M (Bitan, Gal, 2006) (Leshem et al., 2019). Within this study a lower concentration was being applied to align with previous ThT experiments that was unable to present an adequate amount of protein for successful visualisation on a gel. Perhaps, at this concentration, only a small proportion of the sample will represent each oligomeric species which may not be concentrated enough to present oligomeric bands on the gel. Therefore, a higher concentration of 50 μ M A β was tested and resulted in a feint monomer band for some wells (Figure 6 (b)) which was not present when PICUP conducted at lower concentrations where no bands were observed (Figure 6 (a)). The resulting band on this gel is likely monomer but, due to probable poor separation of the lower molecular

weight proteins on this gel, the band presents near the 10 kDa marker band. Later gels were run for longer to allow for better separation at this low molecular weight. It became apparent that concentration of protein in order to present gel bands may have been the limiting step, therefore efforts were made to increase the amount of protein loaded on to the gel.

Initially, the PICUP reaction was scaled up to 500 μ l to increase the amount of protein present in the reaction and, post-cross linking, the samples were snap-frozen and lyophilised. These samples were then resuspended in lower volumes to run on the gel at high concentrations, however, this presented messy bands or monomer only bands on gels (unsuccessful gel images not shown). Due to the harsh nature of snap-freezing and lyophilisation, the integrity of the samples was a concern as treatment of the cross-linked protein may have altered the composition of the sample and so a softer concentration technique was attempted. Following scaled up PICUP, the samples were subjected to centrifugation in a vacuum environment using the SpeedVac (Eppendorf: 5305000568) to decrease the volume to the required amount to run on an SDS-PAGE gel (20 μ l) without the requirement to snap-freeze the samples. However, this method presented no bands on the SDS-PAGE gels as opposed to the non-concentrated gels that provided monomer bands only.

To circumvent the need to increase the concentration of the samples, an alternative staining method was investigated that provided increased sensitivity. Compared to the previously utilised RunBlue (Coomassie) stain, silver staining provides greater sensitivity in the ability to visualise protein bands of just 0.25 ng as opposed to 5 ng for the Coomassie RunBlue stain. This increased sensitivity may enable the detection of transient oligomers that otherwise may not be identified if below the RunBlue staining threshold. Following the adoption of silver stain to image the gels, some potential oligomer bands were observed, yet further optimisation was required (Figure 6 (c)).

Simultaneously, complications regarding the expression and purification of the A β protein was endured, as discussed above, and the decision was made to purchase recombinant A β peptide from Stratech. This enabled a higher concentration of peptide to be applied to PICUP and 100 μ M A β proved too intense for the silver stain, however oligomeric protein was clearly present and thus demonstrates a successful A β PICUP experiment with only an adjustment to enhance imaging required (Figure 6 (d)). Therefore, a lower concentration of 50 μ M A β , along with the experimented APS and RuBpy concentrations, was applied and subjected to Coomassie staining to provide clear oligomer bands, despite this concentration of peptide previously presenting limited success with the presentation of only feint monomer bands. This previously limited presentation may be due to the multitude of factors that contributed towards the PICUP experiment including irradiation type and time, reagent

concentration, concentration method, staining method and protein concentration which over time evolved throughout the various optimisation attempts.

As there were a multitude of variable factors, each experiment explored different combinations of conditions as outlined in Table 4, until a successful protocol was achieved with 50 μM A β , 0.5 mM APS, 1 mM RuBpy, 10 second irradiation with a torch light, where clear oligomeric bands were observed on the SDS-PAGE gel with Coomassie staining (Figure 6 (e)).

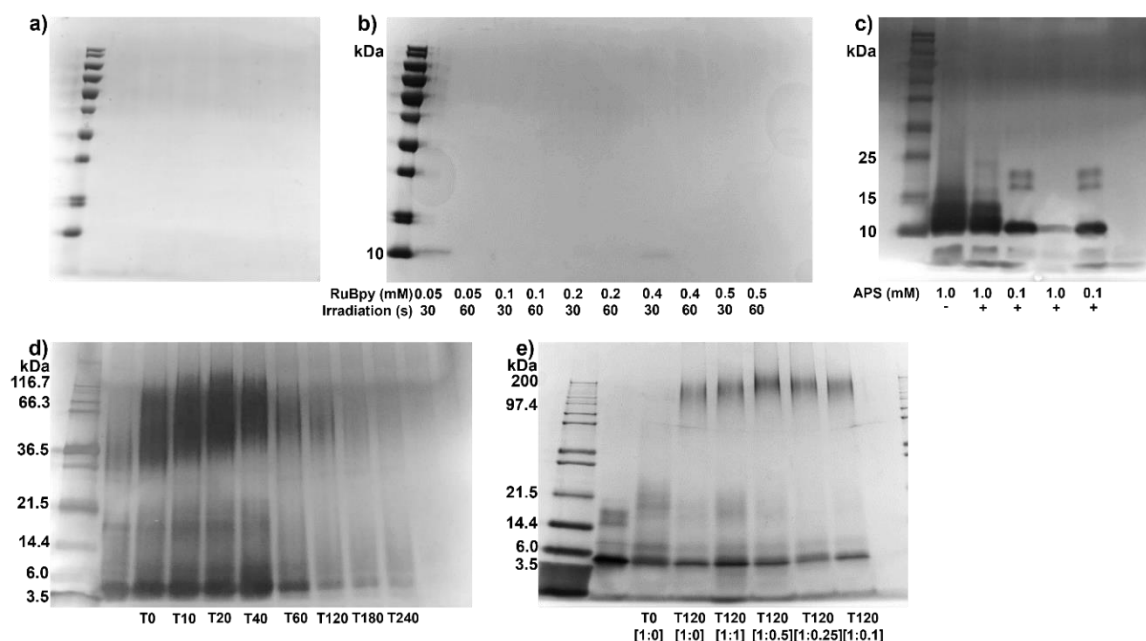


Figure 6: Optimisation of protein cross-linking to visualise oligomeric state of A β . In order to visualise A β in various states of aggregation, photo-induced cross-linking (PICUP) was conducted and the resulting sample run on SDS-PAGE to visualise the oligomeric state of A β . Multiple conditions were varied to identify the optimal conditions required for successful cross-linking and visualisation of A β oligomers on a gel. Here, some example gels are shown to demonstrate the optimisation process. **a)** SDS-PAGE gel resulting from photo cross-linking of 5 μM A β for 1 second with a final concentration of 1 mM Ammonium Persulphate (APS) and 0.05 mM Tris(2,2-bipyridyl)dichlororuthenium(II) hexahydrate (RuBpy) with subsequent Coomassie stain. Lane 1 represents PageRuler Ladder (26166), Lane 2 is pre-aggregated A β with RuBpy and Lane 3 is a no RuBpy control **b)** SDS-PAGE gel resulting from PICUP with 50 μM A β , 30 and 60 second irradiation times, APS concentration of 1 mM and a range of RuBpy concentrations from 0.05 – 0.5 mM with subsequent Coomassie stain. Lane 1 is PageRuler Ladder and Lane 12 is Buffer Only. **c)** SDS-PAGE gel following PICUP of 25 μM A β either monomeric (marked -) or pre-aggregated (incubated at 37 $^{\circ}\text{C}$, quiescent conditions for 40 minutes) (marked +) with a range of APS concentrations from 0.1 mM to 1 mM and 0.5 mM RuBpy and 60 s irradiation. Lane 1 is PageRuler Ladder, Lane 5 is no RuBpy control and Lane 7 is buffer only control. Lane 6 is a repeat of Lane 4 using an older stock of RuBpy as opposed to a fresh stock prepared on the day to test if the age of RuBpy stock impairs PICUP ability. **d)** SDS-PAGE resulting from PICUP of 100 μM A β with 1 mM APS, 0.5 mM RuBpy and 10 s irradiation. The subsequent silver stain gel is presented. Lane 1 is Mark 12 Ladder, Lane 2 is a Timepoint 0 (T0) no RuBpy control, Lane 11 is a T240 no RuBpy control and Lane 12 is the buffer only control. **e)** SDS-PAGE following optimised PICUP protocol utilising 50 μM A β , 1 mM APS and 0.5 mM RuBpy with 10 s irradiation in the presence of various A β :peptide (PCAH2) ratios.

Table 4: Optimisation process of A β protein cross-linking experiment. The table outlines the various experimental conditions and repeats conducted to reveal the optimal assay conditions to allow for successful elucidation of oligomeric state using the photo-induced cross-linking of unmodified proteins (PICUP) assay. Here, multiple factors were modified including protein concentration, Ammonium Persulphate (APS) and Tris(2,2-bipyridyl)dichlororuthenium(II) hexahydrate (RuBpy) concentrations, irradiation source and time and protein staining method used to visualise resulting protein bands on an SDS-PAGE gel. For each experiment, an SDS-PAGE gel was run and a description of the result provided. To increase the amount of protein to be loaded on the gel some samples were concentrated using either lyophilisation or centrifugation under a vacuum using an Eppendorf SpeedVac. Additionally, to capture oligomeric states at varying stages throughout A β aggregation some experiments were conducted as a timepoint assay to provide a snapshot following selected time periods throughout aggregation. Where the APS and RuBpy concentration states a ratio of 1:2:40, this denotes the concentration of A β :RuBpy:APS relative to each other. For example, at 5 μ M A β , RuBpy and APS have been added to a final concentration of 10 and 200 μ M, respectively.

[A β] (μ M)	[RuBpy] (mM)	[APS] (mM)	Irradiation time (s)	Irradiation source	Concentrated ?	Timepoint ?	Staining method	Result
5	0.05	1	1	Torch	No	No	Coomassie	No bands
5	0.5	1	3	Torch	No	No	Coomassie	No bands
5	0.5	1	3	Torch	No	Yes	Coomassie	No bands
5	0.05	1	120	Torch	Yes (lyophilisation)	No	Coomassie	No bands
50	0.05, 0.1, 0.2, 0.4, 0.5	1	30, 60	Torch	No	No	Coomassie	Feint monomer band only
5	0.05, 0.1, 0.2, 0.5, 0.5	1	10, 60	Torch	Yes (lyophilisation)	No	Coomassie	Messy gel - inconclusive
5	1:2:40	1:2:40	30	Torch	Yes (lyophilisation)	No	Coomassie	Feint monomer band only
5	1:2:40	1:2:40	60	Torch	Yes (SpeedVac)	No	Coomassie	No bands
5	1:2:40	1:2:40	60	Torch	Yes (SpeedVac)	No	Coomassie	Feint monomer band only
5	1:2:40	1:2:40	60	Torch	Yes (SpeedVac) vs. No	No	Coomassie	Monomer band only
5	1:2:40	1:2:40	60	Torch	Yes (SpeedVac) vs. No	No	Coomassie	Feint monomer for non-concentrated samples and no bands following concentration of samples
5	1:2:40	1:2:40	60	Torch	Yes (SpeedVac)	No	Coomassie	No bands
5, 25	0.5	1, 0.1, 0.2	60	Torch	Yes (SpeedVac) vs. No	No	Silver stain	No bands on 5 μ M gel Monomer and potential feint oligomer bands for 25 μ M gel with 0.1 mM APS and the 1 mM APS samples gave an intense monomer band but no oligomer band SpeedVac samples resulted in no bands
5	0.1	0.5	60	Torch	No	No	Silver stain	No bands
5, 25	0.1	0.5	60	Torch	No	No	Silver stain	Monomer and potential oligomer bands for 25 μ M gel Monomer bands only for 5 μ M
5	0.1	0.5	60	Torch	Yes (Lyophilisation)	No	Silver stain	Potential oligomer bands although bands unclear
25	0.05, 0.5	0.1, 1	10, 30	Torch vs. room light	No	Yes	Silver stain	Potential oligomer bands although bands unclear
50	0.05, 0.5	0.1, 1	10	Torch	No	No	Silver stain	Very feint oligomers bands
100	0.5	1	10	Torch	No	Yes	Silver stain	Clear oligomer bands but too much protein
50	0.5	1	10	Torch	No	Yes	Coomassie	Clear oligomers bands
50	0.5	1	10	Torch	No	No	Coomassie	Clear oligomer bands
50	0.5	1	10	Torch	No	Yes	Coomassie	Clear oligomer bands

Alongside the optimisation of PICUP, other methods to explore oligomerisation state of A β throughout aggregation were explored. Initially, the potential of an alternative cross-linking agent, Glutaraldehyde, was explored with limited success (data not shown as no bands presented on gel) (Fadouloglou, Kokkinidis and Glykos, 2008).

Size Exclusion Chromatography

Additionally, the potential to monitor the distribution of A β oligomers throughout aggregation using Size Exclusion Chromatography (SEC) was explored and demonstrated some promise. SEC was run at various timepoints throughout A β aggregation with the hope to capture the different oligomeric species present within the sample, represented as various peaks within the SEC profile. For this assay, a sample of A β was incubated under quiescent conditions at 37 °C and, at various timepoints from T0 to T35 minutes, an aliquot taken to run on SEC using the usual SEC protocol.

The potential to monitor A β aggregation alone was encouraging, particularly when observing the monomer peak as this was seen to decrease as aggregation proceeded, indicative of progression through aggregation. In terms of oligomer peaks, there are small peaks observed throughout the SEC profile that are heavier than the monomer, however these are not clear peaks (Figure 7 (a)). The inability to capture the oligomeric species present within these samples may be due to the transient nature of oligomers throughout aggregation meaning that capturing a single oligomeric species is difficult. Additionally, as there are many forms of oligomer present within a sample of A β , one conformer may not present a high enough concentration to elicit a high enough absorbance on the SEC profile for identification, with higher sensitivity required. Despite this, the change in monomer profile is valuable and may be useful in determining if the peptide may alter the aggregation of A β , with a reduction in loss of monomer peak in the presence of a peptide potentially translating to a slowing of aggregation. Therefore, the SEC experiment was repeated in the presence of the PCAH2 peptide. Standardisation between the two SEC traces is required, or a repeat of the experiment, to fully analyse the results as the profiles differ with the peptide sample trace dipping. However, a slight change in oligomer presentation and in the monomer peak is potentially evident between the two traces, but further optimisation is certainly required before drawing conclusions from this experiment to allow for confident comparison between A β SEC profiles obtained in the presence and absence of the peptide (Figure 7 (b)). The latest eluting peak on all SEC profiles (apart from the peptide only peak) is thought to be breakdown product from A β aggregation as this peak demonstrates no 280 nm absorbance and results in no bands following SDS-PAGE analysis yet appears to increase as A β aggregation proceeds (Figure 5 (b)).

Although this method demonstrated potential, for each experiment large volumes of A β samples were required. The expression and purification of A β was time consuming and

yielded small volumes compared to what was required for this experiment. Additionally, upon returning to the laboratory following Covid-19, the previously optimised protocol for A β purification was no longer successful and, despite exploring exhaustive explanations for this (described above), A β was eventually purchased to overcome this obstacle. Simultaneously, PICUP had been successfully optimised within the laboratory and, as the PICUP method used very little protein sample and provided a quick and convenient technique to analyse oligomeric status, PICUP was ultimately the preferred method for assessment of oligomerisation throughout this study.

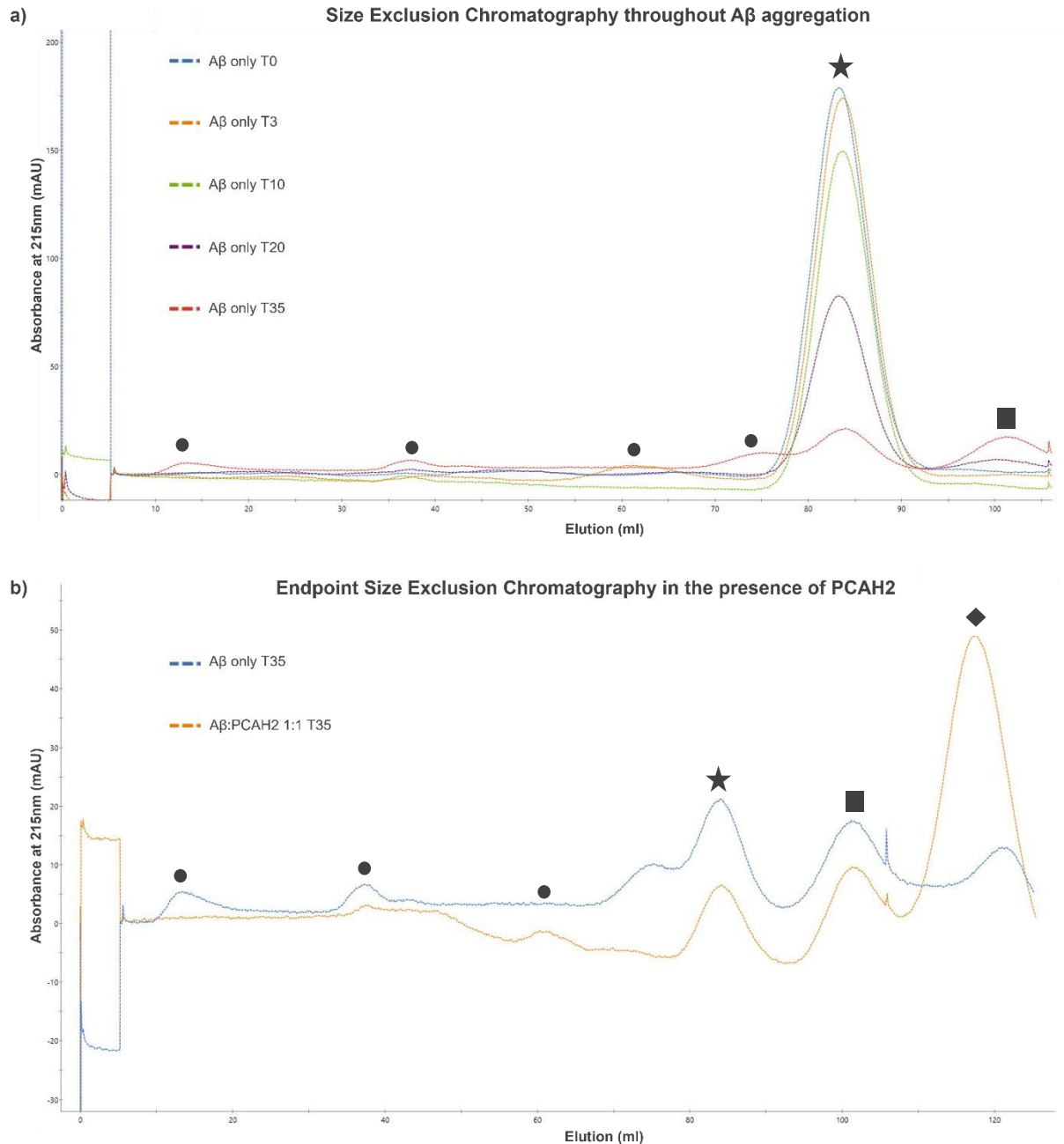


Figure 7: Timepoint Size Exclusion Chromatography (SEC) to explore oligomeric species in A β aggregation. The potential to analyse the distribution of oligomers throughout A β aggregation was explored by incubating (37 °C, quiescent) A β alone and in the presence of PCAH2 at equimolar amounts and running aliquots through SEC at various timepoints. **a)** An overlay of the SEC profiles obtained by A β alone at various timepoints from 0 minutes (T0) to 35 minutes (T35). **b)** An overlay of the SEC profiles obtained at the endpoint of aggregation, 35 minutes (T35), in the presence and absence of a PCAH2. The monomer peak is denoted by \star , various possible oligomer peaks marked with \bullet , the peptide only peak (confirmed by a peptide only control (data not shown) is represented by \blacklozenge and the breakdown product peak by \blacksquare .

Optimisation of a cell-based toxicity assay to assess A β -induced toxicity

Following biophysical characterisation of the peptide hits identified by PCA and TBS using ThT aggregation assays, CD, PICUP and TEM to reveal the potential of PCAH2 and TBSH1 to alter A β aggregation, as discussed in detail in the following chapters, the study next sought to explore how this affected A β -induced toxicity in neuronal cells. A cellular A β toxicity assay needed to be established and optimised within the laboratory with this being conducted in the neuroblastoma cell line SH-SY5Y which is a human-derived, immortal line. The work towards production and optimisation of this assay has been presented and described throughout this chapter with the application of the optimised assay described within chapters Three and Four to reveal the potential of both PCAH2 and TBSH1 to alter A β -induced toxicity. As this was an interesting line of study, the optimisation of this assay has been written up in the style of a paper but is not intended for publication.

Optimisation of an A β 1-42-induced toxicity assay in differentiated SH-SY5Y cells

Abstract

Alzheimer's Disease (AD) is the most common form of dementia with around 520,000 individuals currently diagnosed in the UK. The misfolding and aggregation of the peptide Amyloid- β (A β) is thought to be the trigger behind AD pathology. Toxic oligomeric forms of A β initiate a cascade of downstream events that eventually lead to neuronal cell death, contributing to the neurodegeneration observed in AD. This devastating disease lacks successful treatment options, and robust, reproducible A β toxicity assays are therefore needed to contribute towards effective pre-clinical screening of anti-A β targeted therapeutics. This study developed a cellular A β toxicity model to assess the potential of prospective peptide drug candidates to block A β -induced toxicity in AD. Exploring the potential of the human-derived neuroblastoma cell line (SH-SY5Y) provided a successful protocol for studying A β toxicity, particularly following differentiation of the SH-SY5Y cells. Chronic exposure to monomeric A β induced a concentration-dependent reduction in cell viability in differentiated, but not undifferentiated cells. Cell viability was measured using an MTT assay alongside morphological examination. The study has successfully established an A β toxicity model that is sensitive to low micromolar A β , in particular differentiated cells exposed to monomeric peptide, providing a screening platform for testing activity of blocking peptides.

Introduction

Alzheimer's Disease (AD) is a neurodegenerative disorder that presents as extracellular amyloid plaques and intracellular neurofibrillary tangles (NFT) composed of Amyloid- β (A β) peptide and Tau, respectively. The Amyloid Cascade Hypothesis (ACH), which is generally accepted, states that A β is the initiator of AD. The hypothesis stipulates that production of A β ₁₋₄₂ through β -secretase-mediated cleavage of the transmembrane protein Amyloidogenic Precursor Protein (APP), leads to A β misfolding, aggregation and neurotoxicity. The precise molecular mechanisms driving neuronal cell loss are not well defined, but the cascade of toxic events likely involves hyperphosphorylation of Tau and the subsequent formation of NFTs (Hardy, J.A. and Higgins, 1992; Bloom, 2014; Amar et al., 2017).

Whilst it is uncertain which precise species of A β is the most toxic to neurons it is widely accepted that a small soluble oligomeric form of A β is most likely responsible. These

oligomers have been suggested to act via multiple pathways to initiate synaptic toxicity mainly by interacting with and disrupting cell membranes, binding to cell surface receptors or creating pores in the membrane to form ion channels (Agrawal and Skelton, 2019). Synapses appear to be particularly vulnerable to A β toxicity which is likely due to A β oligomers interacting with ligand-gated ion channels, such as *N*-methyl-d-aspartate receptors (NMDAR) and α 7-nicotinic receptors, to modulate calcium levels within the cell. The resulting influx of calcium potentially activates kinases to phosphorylate Tau, induces mitochondrial stress leading to the production of Reactive Oxygen Species (ROS), initiates pro-apoptotic caspase pathways, causes neuroinflammation and eventually leads to synaptic failure and neuronal cell death (Marín et al., 2000; Calvo-Rodriguez et al., 2020).

Over 520,000 individuals are currently diagnosed with AD in the UK (Society, 2022a) and with the aging population this figure is likely set to increase. Between the years 2000 and 2019, deaths caused by AD increased by 145 % (Association, 2021) and the disease ranked 7th leading cause of death globally (WHO, 2020). Despite years of research there are currently no disease modifying therapeutics for AD, and only symptomatic treatments are available including the cholinesterase inhibitors, donepezil, rivastigmine and galantamine and the NMDAR antagonist, Memantine.

The absence of successful drug candidates may result in part from a lack of relevant research models to explore the mechanisms of A β toxicity and assess the potential of drug candidates across both *in vitro* and *in vivo* studies. It is reported that up to 99 % of prospective AD drugs progressing to clinical trials fail to reach their endpoint targets despite promising preclinical data, potentially due to the inability of the preclinical studies to sufficiently represent AD pathology relevant to humans (Veening-Griffioen et al., 2019; Slanzi et al., 2020). This study explores the potential of the human neuroblastoma cell line SH-SY5Y as a method to explore A β toxicity as relevant for AD. SH-SY5Y cells are a thrice subcloned product of the original SK-N-SH line which was derived from the bone marrow transplant of a four-year-old female in 1970 diagnosed with a metastatic neuroblastoma. SH-SY5Y cell cultures contain both substrate adherent (S-type) and neuroblast (N-type) cells despite successive cloning efforts towards the N-type cell (Forster et al., 2016). These neuroblast cells harbour non-polarised cell bodies and lack neurite outgrowths (Kovalevich and Langford, 2013).

As mentioned above, A β exerts much of its toxicity towards neuronal cells specifically, yet many cellular studies use systems that are poorly representative of neurons. For example, according to Krishtal et. al., over 81 % of studies utilising the SH-SY5Y line used undifferentiated cells (Krishtal et al., 2017). These undifferentiated cells lack crucial neuronal features required for A β toxicity such as neurites, dendrites and neuronal network connections and also do not express relevant neuronal markers, therefore failing to fully

represent differentiated neurons and thus show resistance to A β -induced neurotoxicity (Agholme et al., 2010; Xie, Hu and Li, 2010). A previous study by Krishtal et al. demonstrated an increased susceptibility to A β -induced toxicity upon differentiation of SH-SY5Y cells likely due to the development of axons, dendrites and synapses required for A β to exert neuronal damage. This addressed a crucial gap within the field and provided a good human cell line in which to study A β toxicity, which had previously been lacking (Krishtal et al., 2017). Further work also demonstrated that the differentiation route, determining the neurochemical phenotype of the cells, influenced sensitivity to A β , with cholinergic phenotypes presenting greater vulnerability to A β -induced toxicity compared to more resistant dopaminergic-like cells (Krishtal et al., 2019). This demonstrates the critical importance of selecting the appropriate growth factors and protocols for driving differentiation to the desired phenotype.

Although the lack of neuronal features and morphology of undifferentiated SH-SY5Y cells can be overcome by differentiation of the cell line there is further benefit to differentiating the line. SH-SY5Y cells often possess a heterogeneous mix of S- and N-type cells at varying stages of the cell cycle which continue to divide throughout cellular assays, impeding the ability to reliably assess cell numbers (Xie, Hu and Li, 2010; Kovalevich and Langford, 2013). However, exposure of the cells to Brain-derived Neurotrophic Factor (BDNF) upon differentiation can hinder proliferation and align the cell cycles negating this issue (Encinas et al., 2000).

Whilst differentiation and exposure to growth factors to slow proliferation can be applied to overcome these drawbacks, an additional issue for consideration is the heritage of the cells. SH-SY5Y cells are derived from a cancerous cell line so potentially harbour genetic abnormalities and properties that alter the behaviour of the cells, raising questions as to their ability to fully mirror the normal physiology of human neurons (Xicoy, Wieringa and Martens, 2017; Slanzi et al., 2020). Despite these limitations, their benefits far outweigh the disadvantages with good accessibility, cost-effectiveness and relatively labour light culture protocol that harbours a robust cell line. Furthermore, there is no requirement for animal sacrifice with the immortal SH-SY5Y line that can be continuously passaged and expanded. This easy expansion of cell number is also useful for large scale experiments where cell numbers can be increased prior to differentiation. Finally, despite conservation of post-synaptic densities observed between mammals (Bayés et al., 2011) enabling mouse neuronal cells to stand as an effective model of human neurons, the post-transcriptional landscape demonstrates vast differences between species, meaning that rodent models fail to fully reflect the human system (Somel et al., 2011; Kovalevich and Langford, 2013; Goldie, Barnett and Cairns, 2014) (Table 1). The human-derived SH-SY5Y cells better represent the AD disease model compared to rodent options (Krishtal et al., 2019) and

allows for better extrapolation of results towards human diseases with a similar genetic context (Goldie, Barnett and Cairns, 2014).

Table 1: Advantages and disadvantages of SH-SY5Y cell line as a model for neuronal diseases. The SH-SY5Y cell line has been utilised to model several neurodegenerative diseases including Parkinson’s and Alzheimer’s disease, with differentiation presenting greater potential by increasing the cells resemblance towards neurons. Within this table the advantages and disadvantages of using the line have been demonstrated. Information collated from the following references (Agholme et al., 2010; Xie, Hu and Li, 2010; Kovalevich and Langford, 2013; Xicoy, Wieringa and Martens, 2017; Slanzi et al., 2020).

Advantages and Disadvantages of SH-SY5Y cells	
Advantages	Disadvantages
No animal sacrifice is required with the immortal SH-SY5Y cell line which presents fewer ethical issues	Due to the derivation of the line from a cancerous cell they may contain genetic abnormalities or harbour cancerous properties that alter the proliferation, differentiation and viability of the cells
There is the potential to differentiate the cells towards a neuronal-like phenotype and SH-SY5Y cells can be exposed to varying differentiation protocols towards different phenotypes including cholinergic, adrenergic and dopaminergic	Undifferentiated SH-SY5Y cells lack a strong neuronal phenotype in terms of morphology, inhibition of cell proliferation and expression of neuronal and synaptic markers
The capacity for large scale expansion of cell culture prior to differentiation and assay to easily scale up experiments	Undifferentiated cell cultures contain a heterogenous mix of cells (S-type and N-type) at various stages of the cell cycle
Cells are robust and have a straightforward culture/handling protocol	SH-SY5Y cells continue to grow throughout experimental conditions which can present difficulties in tracking changes in cell number
Cost-effective model in comparison with iPSCs and primary neuronal sources	Limited neurochemical phenotype in that they cannot be differentiated to represent glutamatergic neurons
They are a human-derived line, meaning they represent/produce human proteins that may not be the case in rodent models	

The need for a robust and reliable cellular model to assess A β pathology is clear. Here we assessed A β toxicity in this SH-SY5Y human neuroblastoma cell line and also compared vulnerability between differentiated and non-differentiated cells. Sequential differentiation of SH-SY5Y with Retinoic Acid (RA) and BDNF conferred vulnerability to A β as previously described [10,11], although at a lower concentration than reported by Krishtal et al.. The study also demonstrates varying levels of A β toxicity resulting from different preparations and sources of the peptide along with the aggregation state. Application of primarily monomeric A β samples induced greater toxicity than applying fully aggregated forms of A β to cells. The optimised model described provides a robust platform by which to study the potential of A β -targeted drugs.

Materials and Methods

Expression of pET-Sac-A β (M1-42). The pET-Sac-A β (M1-42) plasmid was a gift from Dominic Walsh (Addgene Plasmid # 71875; <http://n2t.net/addgene:71875>; RRID:Addgene_71875) (Walsh et al., 2009). pET-Sac-A β (M1-42) was transformed into electrocompetent BL21 (DE3) (streaked from NEB: C257H chemically competent BL21 (DE3) cells). A single transformed colony was picked and used to inoculate 50 ml LB media (with 250 μ M Ampicillin) for an overnight culture at 37 °C. The next day 10 ml of this overnight culture was transferred in to 1 L LB media (with Amp) and incubated at 37 °C, shaking at 250 rpm, until the OD₆₀₀ reached a value of 0.6. At this point IPTG was added to a final concentration of 1 mM and the cultures incubated at 37 °C for a further 3.5 hours. The cells were harvested by centrifugation at 5,000 rpm for 15 minutes and the pellet resuspended in 50 ml 10 mM Tris/HCl pH. 8.0, 1 mM EDTA buffer with one cComplete mini Protease Inhibitor Cocktail Tablet (Roche; Cat. No.: 04693159001). This was frozen at -20 °C.

Sonication of BL21 (DE3) containing pET-Sac-A β (M1-42). The frozen cells from a 1 L culture were defrosted and diluted to a total volume of 40 ml in 10 mM Tris/HCl pH 8.0, 1 mM EDTA containing protease inhibitor. The cells were sonicated (MSE, Soniprep 150 Plus) for 2 minutes (14 Amps) on ice and subsequently centrifuged at 18,000 g for 10 minutes, 4 °C. The supernatant was removed, and the cells resuspended in 40 ml 10 mM Tris/HCl pH 8.0, 1 mM EDTA containing protease inhibitor and sonication followed by centrifugation repeated as above. This was repeated a third time and the resulting cell pellet was resuspended in 40 ml 8 M Urea, 10 mM Tris/HCl pH 8.0, 1 mM EDTA to solubilise the inclusion bodies containing A β (M1-42). The cells were sonicated as above, and the resulting solution was filtered with a 0.22 μ m filter. When sonicating the cells for 2 minutes,

every 30 seconds the sonication was paused, and the probe moved up the tube to ensure complete sonication of all cells.

Purification of A β (M1-42). Following urea solubilisation of inclusion bodies containing A β (M1-42) the resulting solution was diluted to a total volume of 50 ml with 10 mM Tris/HCl pH 8.0, 1 mM EDTA and applied to a DEAE-Cellulose column. The purification was carried out using a gradient elution on ÄKTA Pure. During the gradient elution increasing volumes of Buffer B (10 mM Tris/HCl pH 8.0, 1 mM EDTA, 500 mM NaCl) was added to Buffer A (10 mM Tris/HCl pH 8.0, 1 mM EDTA) from 0 % Buffer B to 99 % Buffer B to allow for separation of proteins within the sample. Fractions containing solutions which gave observable A₂₈₀ nm peaks were run on a 20 % SDS-PAGE gel to observe which fractions contained A β (M1-42).

Size Exclusion Chromatography (SEC) to isolate monomeric A β (M1-42). Fractions containing A β as observed on SDS-PAGE gel were pooled and subjected to SEC to isolate monomeric A β . For one round of SEC, 5 ml sample was loaded on to a HiLoad 16/600 Superdex 75 pg column (GE Healthcare: Cat. No.: 28989333) equilibrated in 20 mM Sodium Phosphate pH 8.0, 200 μ M EDTA. The SEC was run at 0.5 ml/min and protein eluted in 20 mM Sodium Phosphate pH 8.0, 200 μ M EDTA. Resulting peak fractions were run on a 20 % SDS-PAGE gel to confirm presence of monomeric A β (M1-42). Concentration of resulting A β (M1-42) was calculated by measuring Absorbance at 280nm using Varian Cary® 50 UV-Vis Spectrophotometer and applying Beer Lambert's Law with a ϵ value of 1280. A β stock solutions were snap-frozen and stored at -80 °C. Identity of protein produced was confirmed using intact MS-MS.

Commercial A β 1-42 (Stratech). In addition to purification of A β (M1-42) in the laboratory, recombinant A β ₁₋₄₂ was also purchased. Beta-Amyloid (1-42), Ultra Pure, NH₄OH was manufactured by rPeptide and purchased via Stratech (Stratech: Cat. No.: A-1167-2-RPE). Peptide was resuspended in 20 mM Sodium Phosphate pH 8.0, 200 μ M EDTA to a stock concentration of 100 μ M, aliquoted and flash frozen.

Culture of E15 primary cortical neurons. Preparation and culture of cortical neurons from E15 mouse embryos was carried out by Kim Morris prior to toxicity assays. All procedures were carried out in accordance with the United Kingdom Animal (Scientific Procedures) Act 1986 and were approved by the Bath Animal Welfare and Ethical Review Body. Protocol for preparation of cortical neurons as described previously by Hole et. al. (Hole et al., 2021). Briefly, Poly-D-Lysine (PDL) (Gibco, Cat. No.: 15230-147) at 20 μ g/ml was used to precoat plates with 0.5 ml dispensed to each well of a 24 well plate. Plates were incubated at 37 °C, 5 % CO₂ for 30-60 minutes. PDL was aspirated and wells washed twice with 0.5 ml distilled water. Wells were then washed with PBS (Gibco, DPBS (10x), Cat. No.:14200-067) and finally 0.5 ml Neurobasal media (Gibco, Cat. No.:12348-017) containing 5 % Heat

Inactivated Fetal Bovine Serum (FBS) (Gibco, Cat. No.:10500) was added to each well. Plate was incubated at 37 °C, 5 % CO₂ and serum media aspirated before plating of cells. Dissociated mouse embryonic cortical tissue from E15 brain was re-suspended in serum-free neurobasal media (with supplement B27) and dispensed into each well of the 24 well plate. The cell culture plate was incubated at 37°C, 5 % CO₂ and used at 7-8 DIV when cells were >95% differentiated neurones.

ThT toxicity assay on E15 primary cortical neurons. In order to test the potential to use A β samples directly from ThT aggregation assays to define the aggregation status of A β applied to the cells the effect of ThT on cells first needed to be determined. ThT solutions were prepared at 10 X concentration in 20 mM Sodium Phosphate buffer, 200 μ M EDTA, pH 8.0 and diluted 1:10 into each culture well (50 μ l added to 0.5 ml well) to achieve the following final ThT concentration ranges 0.5 μ M, 1 μ M, 2 μ M, 5 μ M and 10 μ M with a buffer only control included. Each condition was replicated across three wells. ThT was incubated with cells for 24 hours at 37 °C, 5 % CO₂ and an MTT assay carried out to assess cell viability.

MTT assay to assess cell viability. MTT assays are used as an indirect measure of cell viability, by measuring the conversion of MTT to formazan by mitochondrial enzymes. For the MTT assay, a 1 mg/ml MTT (in complete media) solution was prewarmed. The growth medium was aspirated, replaced with 500 μ l MTT media and incubated at 37 °C, 5 % CO₂ for 1 hour. Following this, the media was removed and 650 μ l Isopropanol added and mixed to solubilise the remaining formazan dye. 200 μ l was transferred to a single well of a clear plate in triplicate and the absorbance measured at 595 nm using a microplate reader (BioRad, Model: iMark).

Culture and differentiation of SH-SY5Y cells. Preparation and differentiation of SH-SY5Y cells was carried out with assistance from Kim Morris. SH-SY5Y, purchased from Public Health England's European Collection of Authenticated Cell Cultures (ECACC), were seeded on to Nunc™-treated cell culture plates (ThermoScientific: 142485) in Dulbecco's modified Eagle's medium (DMEM)/F12 with Phenol Red (ThermoFisher 42430082)((1:1 ratio DMEM/F12 media), 10 % FBS, 5 % Pen/strep, 5 % L-glutamine) and this stock was maintained at 37 °C, 5 % CO₂ until 80 % confluency reached. At this point cells were passaged, and this repeated up to a maximum of 20 passages at which a fresh batch of cells were used. For assay, the cell stock was seeded at 1 x 10⁵ cells/ml in a 24 well plate with 0.5 ml culture per well and incubated for 24 hours at 37 °C, 5 % CO₂. For assays utilising undifferentiated cells, A β was applied at this point. For assays requiring differentiated SH-SY5Y cells the following differentiation protocol was performed. Following the 24 hour culture of SH-SY5Y cells as described above, the culture media was removed and replaced with Serum-free DMEM/F12 with Phenol Red ((1:1 ratio DMEM/F12 media),

5 % Pen/strep, 5 % L-glutamine) media and 10 μ M Retinoic Acid (RA) (Sigma: R2625). The SH-SY5Y cells were incubated in RA media for 3 days until the RA media was removed and replaced with Neurobasal-A media (ThermoFisher: 12349015) (1 % L-Glutamine, 1 % penicillin/streptomycin, 1 % N2 neuronal supplement) and 1.85 nM Brain-Derived Neurotrophic Factor (BDNF) (Merck: B3795) and incubated for a further 4 days. After 7 days the SH-SY5Y cells were fully differentiated and ready to use. To optimise the differentiation protocol, the initial seeding density of the SH-SY5Y cells was halved and the cells were seeded at 5×10^4 cells/ml for these assays. In addition, for one experiment the presence of serum in the initial culture of the SH-SY5Y cells before differentiation was tested with serum removed following splitting of the SH-SY5Y cells and subsequent washing with serum-free media before cell plating in serum-free DMEM media containing 5 % Pen/strep, 5 % L-glutamine.

Optimisation of A β -induced toxicity in SH-SY5Y cells. For all assays A β_{1-42} was prepared in the laboratory as described with sequential anion exchange and SEC or purchased from Stratech. Upon defrosting, the A β was either directly used to achieve as close to monomeric species as possible or was incubated at 37 °C under quiescent conditions for pre-aggregation. Initially, undifferentiated SH-SY5Y cells were used in which 50 μ l A β samples, prepared at 10 X final concentration for dilution into the assay well, were applied to cells following 24 hour incubation from the initial seeding. See Table 2 for concentrations tested. For assays requiring differentiated SH-SY5Y cells, the differentiation was performed and on day 7 following start of differentiation protocol the A β samples were added in the same way. Following addition of A β , culture plates were incubated at 37 °C, 5 % CO₂ for 48 hours. See Table 2 for details of conditions tested. Following the required incubation period, an MTT assay was conducted to assess cell viability. In addition, cells were imaged using an Evos Cell imager (Auto 2) for visual observations of morphology.

Table 2: Conditions tested for optimisation of A β_{1-42} toxicity upon SH-SY5Y cells. The following assay conditions were carried out to explore the potential of A β to induce toxicity in SH-SY5Y cells.

Differentiation status	A β concentrations tested (μ M)	A β Aggregation status	Serum presence tested
Undifferentiated	0, 1, 2	Monomeric	No
Differentiated	0, 1, 2, 5	Monomeric and pre-aggregated tested at 5 μ M A β	Yes

Results and discussion

In order to evaluate the ability of peptide hits to protect against A β pathology within a cellular environment, an A β toxicity assay was required. The potential to utilise SH-SY5Y cells was explored, and the differentiation protocol is outlined below (see Figure 1).

Culture and differentiation protocol for SH-SY5Y cells established. As discussed above, differentiation of the SH-SY5Y cells enables the model to overcome many of the shortcomings associated with the undifferentiated line. As observed in Figure 1 (a), without differentiation the resulting SH-SY5Y cells have limited morphology and lack neuronal-like phenotype as shown by visual observations of morphology. There are many studies exploring the differentiation of SH-SY5Y cells using various methods. Here, an approach similar to that described by Forster et al. (Forster et al., 2016) was adopted to assess the potential to produce A β sensitive neuronal-like cells.

Overall, the resulting differentiation protocol utilised an initial seeding density of 5×10^4 cells/ml with an overnight culture in serum-supplemented media. The serum media was removed and replaced with RA media to initiate the differentiation process and incubated for 3 days before removal of the media. Subsequently, the cells were treated with BDNF, to enhance the differentiation of the cells, for a further 4 days as outlined in Figure 1. Treatment with RA, a vitamin A derivative, inhibits cell growth and proliferation whilst promoting differentiation towards cholinergic neuronal phenotypes (Melino et al., 1997; Kovalevich and Langford, 2013). Selection to sequentially differentiate with the addition of the BDNF step (some studies only apply a RA differentiation step (Oguchi et al., 2017; Mairuae et al., 2019; Chen et al., 2021; Paik et al., 2021)) presents multiple advantages. SH-SY5Y cells present a small subset of S-type cells. These cells are not sensitive to RA treatment alone and continue to proliferate, eventually over-populating the culture. Addition of BDNF enhances effects initiated by RA but also withdraws the S-type cells from the proliferative state to facilitate successful N-type differentiation towards neuronal-like cells. Although, only the N-type cells are sensitive to RA/BDNF induced differentiation (Encinas et al., 2000). Differentiation with these growth factors drives SH-SY5Y cells towards a neuronal-like differentiation so that they better represent neuronal cells, as demonstrated in the morphology analysis (Figure 1 (b)).

The study adopted various optimisation stages that aimed to improve overall differentiation of SH-SY5Y cells. Poorly or undifferentiated cells in the culture could reduce the overall sensitivity towards A β as these cells do not represent neurons to a great extent. A drawback of SH-SY5Y cells is their continued proliferation throughout differentiation. Removing serum from the initial growth culture medium could potentially slow the proliferation rate of these

cells, thus increasing efficiency of differentiation. However, this was not observed and the presence of serum did not alter susceptibility to A β toxicity (Figure S1).

A further attempt to improve overall differentiation of the cells was to alter the initial cell seeding density. This was decreased from 1×10^5 to 5×10^4 cells/ml to provide greater cell distribution towards the final stages of differentiation (by day 7). At the previous cell seeding density of 1×10^5 cells/ml, the cells appeared crowded with some presenting apoptotic-like cells bodies and less defined differentiation upon morphology analysis (Figure 2 (a)). When reducing the density, it is important to allow a high enough confluency for cells to communicate and continue to grow whilst allowing them to spread and efficiently differentiate to better present neuronal-like cells. This was achieved at half density in which, upon observation of morphology, the SH-SY5Y cells were better distributed and displayed more effective differentiation towards neuronal cells (Figure 2 (b)). Whilst not explicitly tested but rather upon observation throughout the study, the initial seeding density of SH-SY5Y cells may have an impact on susceptibility towards A β -insult. Toxicity experiments carried out at the lower seeding density generally presented a greater reduction in cell viability following exposure to A β compared to cells seeded at a higher density. This may result from the enhanced differentiation of SH-SY5Y cells seeded at half density, thus better representing neurons.

To extend this study further it would be pertinent to stain the undifferentiated and differentiated cells for specific neuronal markers to fully characterise the development and phenotype of the cells following differentiation. Undifferentiated cells present markers relevant for proliferating cells and immature neurons, such as proliferative cell nuclear antigen (PCNA) and the cell-cycle dependent marker, nestin, which is present during division of the cell (Cuende et al., 2008; Lopes et al., 2010; Kovalevich and Langford, 2013). These markers have been shown to decrease as differentiation proceeds and are substituted for neuronal markers including Neuron Specific Enolase (NSE), neuronal nuclei protein (NeuN), synaptophysin, Microtubule-associated protein (MAP) and Tau (Lopes et al., 2010; Xie, Hu and Li, 2010).

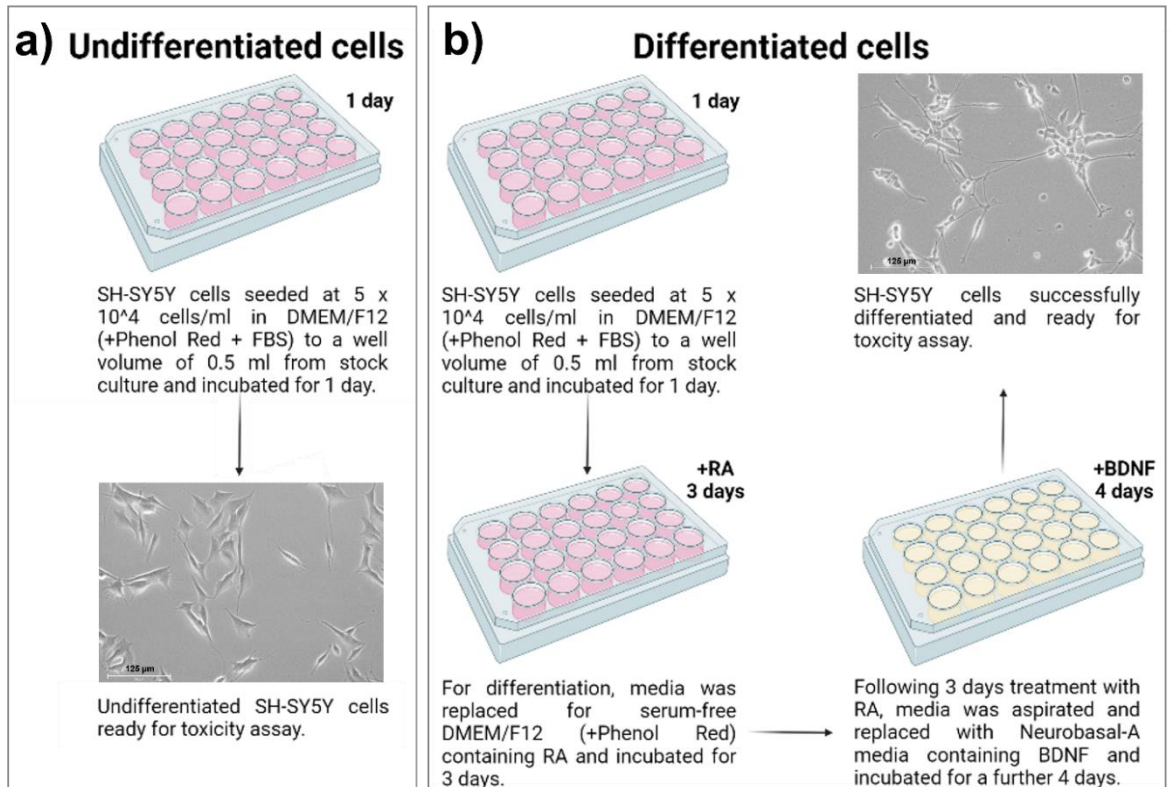


Figure 1: SH-SY5Y cell culture protocols for undifferentiated and differentiated cells.

a) Protocol for assay utilising undifferentiated cells. Here, the SH-SY5Y cells are seeded at a density of 5×10^4 cells/ml in to a 24-well cell culture plate in DMEM/F12 media with Phenol Red and Fetal Bovine Serum (FBS). The culture plate is incubated at 37°C , 5 % CO_2 for 24 hours, after which the cells are ready for assay. **b)** The SH-SY5Y cells were subjected to sequential treatment with Retinoic Acid (RA) and Brain Derived Neurotrophic Factor (BDNF) to influence progression towards more neuronal-like morphologies. Initially, cells were seeded at 5×10^4 cells/ml in DMEM media containing Phenol Red and FBS and incubated overnight as usual. The following day, the culture media was aspirated and replaced for Serum-free DMEM/F12 media containing Phenol Red with $10\ \mu\text{M}$ RA. The plate was subsequently incubated for 3 days at 37°C , 5 % CO_2 . Following 3 days incubation the RA media was aspirated and replaced with Neurobasal-A media containing $1.85\ \text{nM}$ BDNF and incubated for a further 4 days at 37°C , 5 % CO_2 .

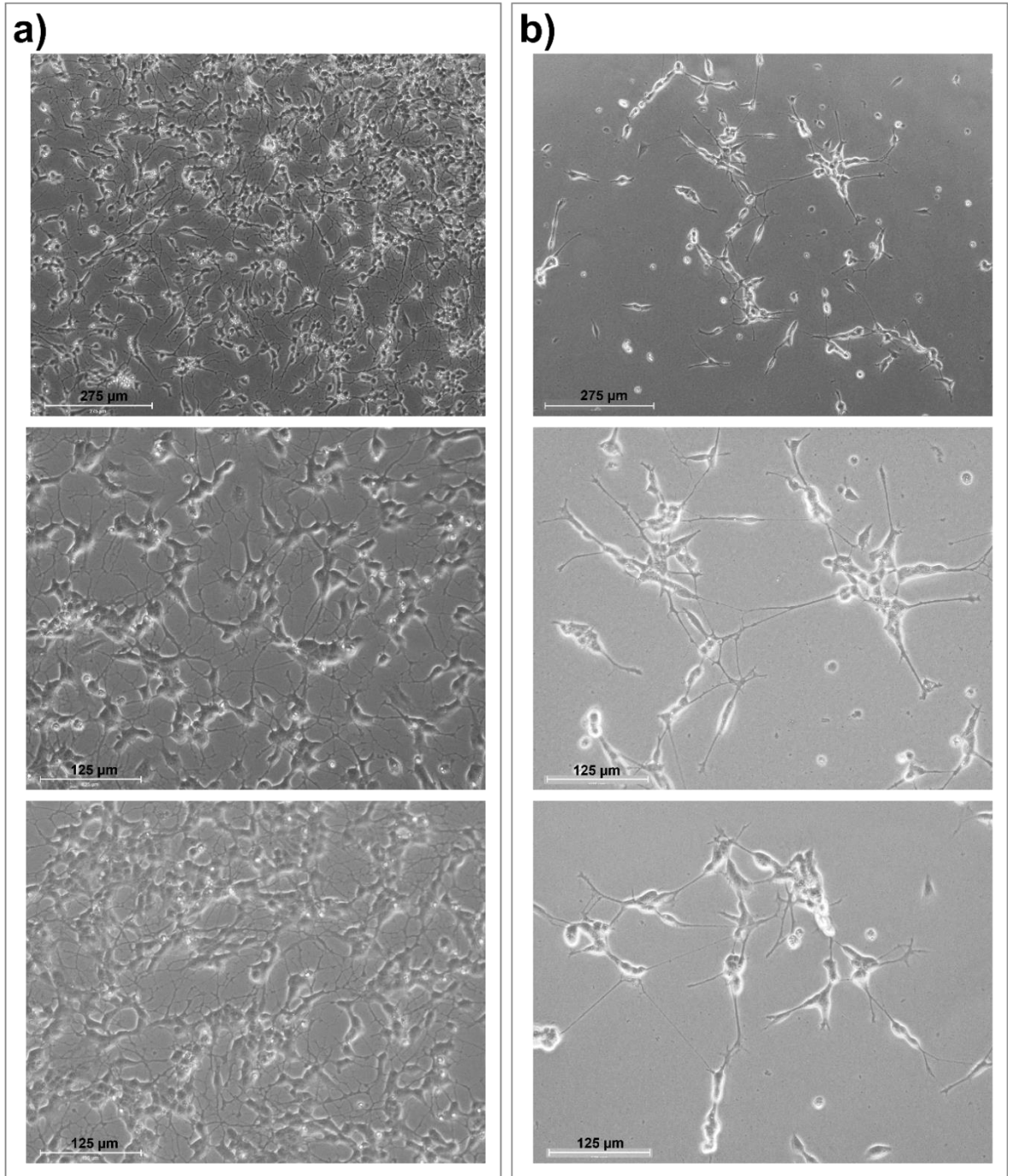


Figure 2: Cells seeded at half density present clearer differentiation. Morphological analysis captured to explore quality of differentiation at different initial seeding densities prior to differentiation. **a)** SH-SY5Y cells were seeded at a higher density (1×10^5 cells/ml) prior to differentiation with RA/BDNF. **b)** To explore whether differentiation of the SH-SY5Y cells could be more efficient, the cells were seeded at half density (5×10^4 cells/ml) with subsequent differentiation with RA/BDNF.

Differentiation of SH-SY5Y cells increases sensitivity to A β -induced toxicity. For initial experiments undifferentiated SH-SY5Y cells were utilised and following direct application of monomeric A β up to a final well concentration of 2 μ M for 48 hours, no significant toxicity was observed with a reduction in cell viability of only ~ 4 %. In detail, within the undifferentiated SH-SY5Y cells, no significant toxicity was observed with a non-significant 4 % +/- 0.90 SEM reduction in cell viability at a final well concentration of 2 μ M and only 0.4 % +/- 2.11 SEM for 1 μ M compared to vehicle control (Sodium Phosphate buffer only) (Figure 3 (a)).

However, differentiation of SH-SY5Y cells increased vulnerability of the cells to A β compared to undifferentiated cells, consistent with previous reports (Krishtal et al., 2015, 2017). An increased sensitivity to A β was observed upon differentiation of SH-SY5Y cells in which a significant reduction in cell viability of up to ~ 28 % was observed following exposure for 48 hours to a final A β concentration of 2 μ M. Due to concurrent optimisation of A β purification, assay conditions could now test up to 5 μ M A β . A concentration-dependent cell death was observed in which exposure of 5 μ M A β upon differentiated cells reduced cell viability by ~ 52 % (Figure 3 (b)). This concentration-dependent reduction in cell viability was revealed by the dose-dependent reduction in cell viability of 20.80 % +/- 6.70 SEM, 27.50 % +/- 7.51 SEM, 51.50 % +/- 5.21 SEM for 1 μ M, 2 μ M and 5 μ M, respectively. Following a one-way ANOVA with subsequent Tukey's post-hoc multiple comparison test, both 2 μ M and 5 μ M A β incurred significant reduction in cell viability compared to vehicle control where * = P<0.05; and *** = P<0.001.

The quantitative MTT measurement of cell viability is corroborated by morphology analysis. Here, differentiated SH-SY5Y cells without exposure to A β display healthy neuronal structures, whilst the differentiated SH-SY5Y cells with 5 μ M A β treatment resulted in visibly shortened, degenerating neurites and apoptotic cell bodies (Figure 3 (c)). The increased sensitivity of SH-SY5Y cells to A β upon differentiation is likely due to formation of neuron-like morphology such as axons, dendrites and synapse formation/communication between cells which were absent in undifferentiated cells (Figure 3 (c)). A β is thought to exert toxicity at neuronal synapses, which may account for differences in toxic insult between differentiated and undifferentiated cells which do not harbour neuronal structures and presents further evidence to suggest that A β interaction sites required for toxicity are located at the synapses of neurons.

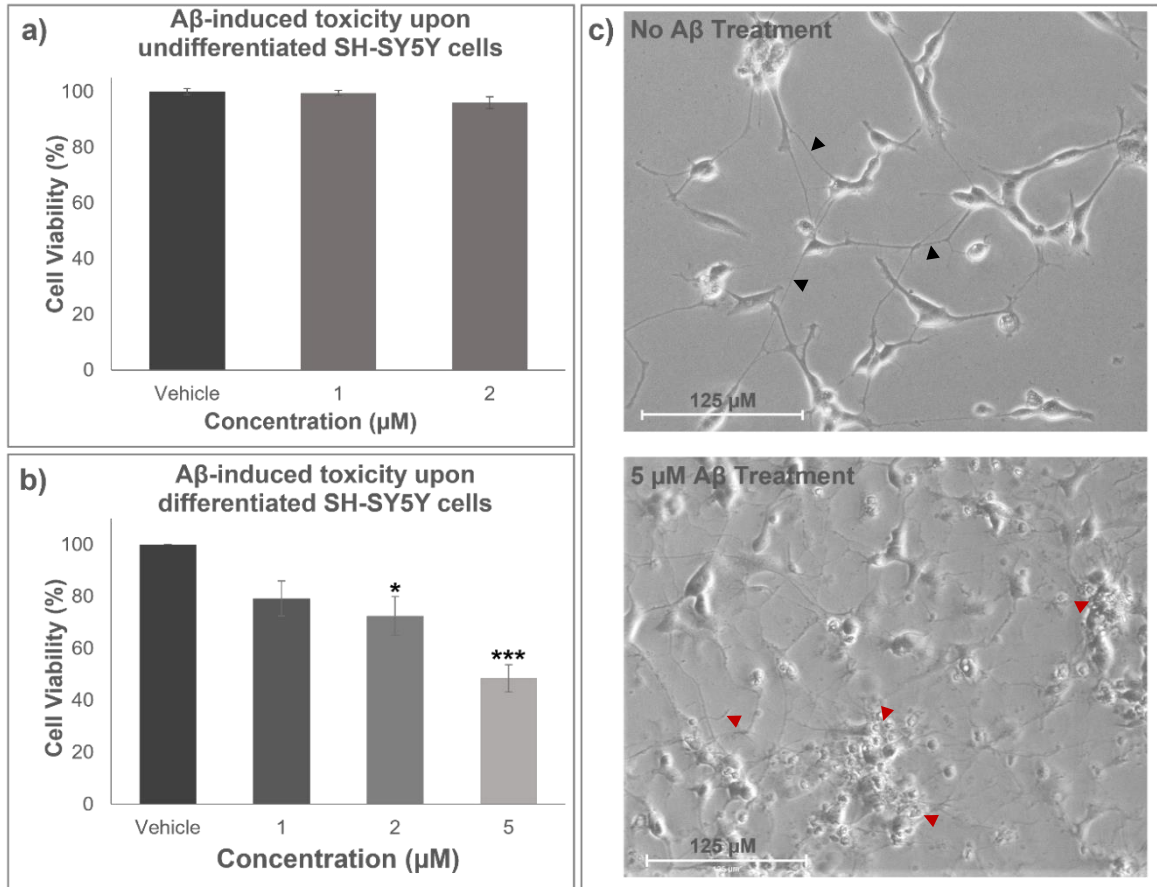


Figure 3: Differentiated SHSY5Y cells are more susceptible to Aβ-induced toxicity than undifferentiated cells. Monomeric Aβ₁₋₄₂ was applied to both undifferentiated and differentiated SH-SY5Y cells for 48 hours and cell viability measured by MTT assay. **a)** Either 1 μM monomeric Aβ, 2 μM monomeric Aβ or a Sodium Phosphate buffer only vehicle control was applied to SH-SY5Y cells and incubated for 48 hours. To measure cell viability, an MTT cell viability assay was subsequently conducted. **b)** A range of monomeric Aβ concentrations were applied to the cells and incubated for 48 hours. To measure cell viability, an MTT assay was conducted. Following a one-way ANOVA with subsequent Tukey's post-hoc multiple comparison test, both 2 μM and 5 μM Aβ incurred significant reduction in cell viability compared to vehicle control where * = P<0.05; and *** = P<0.001. Error bars represent SEM for a) and b). For each condition n = 3 with each experimental repeat containing three technical repeats. **c)** Morphology analysis was conducted to explore morphological changes in SH-SY5Y cells following exposure to Aβ. Healthy neuronal structures are denoted by black arrowheads, whilst indication of cell stress including shortened neurites and apoptotic cell bodies as shown by red arrowheads.

Source of A β and aggregation state is important for toxicity. Towards the final stages of the study recombinant A β was also purchased from Stratech. To confirm that similar levels of toxicity were observed upon addition of commercial A β to SH-SY5Y cells, a dose response of A β from a final well concentration of 1 μ M to 5 μ M was conducted. A dose dependent reduction in cell viability was observed with 32.30 % \pm 2.85 SEM, 56.75 % \pm 1.81 SEM, 59.24 % \pm 1.37 SEM following treatment with 1 μ M, 2.5 μ M and 5 μ M A β , respectively (Figure 4 (a)). Overall, recombinant A β purchased from Stratech induces toxicity, or reduction in cell viability, in differentiated SH-SY5Y cells to a greater degree compared to A β expressed and purified in house (Figure 4 (a) & Figure 3 (b)). The reduction in cell viability by the Stratech A β protein at 2.5 μ M was shown to be significant where $P < 0.0001$ following an unpaired standard student's t-test. The decision was made to conduct toxicity assays utilising the Stratech A β protein at 2.5 μ M, which provided \sim 57 % loss in cell viability, comparable to that of 5 μ M for the in house produced A β . This provides the benefit of a lower concentration of peptide required to observe a similar level of significant toxicity. This concentration is lower than seen across multiple studies within the literature which usually quote between 5 and 50 μ M to achieve a similar level of toxicity as presented here (Krishtal et al., 2017; Krishtal et al., 2019; Litwiniuk et al., 2020; Chen et al., 2021; Feng et al., 2021; Paik et al., 2021).

The source of the A β peptide, whether cell-derived, synthetic or recombinant and its subsequent preparation can influence the degree of toxicity observed (Finder et al., 2010; Reed et al., 2011; Benilova, Karran and De Strooper, 2012). Both experiments described above utilised recombinantly produced A β following different preparation protocols. The higher toxicity obtained with the Stratech A β , compared to the laboratory produced A β , may be due to the presence of particular oligomeric species within the sample as a result of the different preparation protocols. The exact species of A β oligomer that confers toxicity is not fully understood however it is believed to result from multiple different conformations of oligomer. A β preparations contain a heterogenous mix of A β isoforms and the various species populating the sample may determine the toxicity of that sample. Due to the different preparation protocols between the two protein sources, the Stratech samples may populate more toxic oligomers resulting from the preparation procedure which may encourage production of particular oligomers that present greater toxicity (Benilova, Karran and De Strooper, 2012).

To further explore the potential of varying states of A β to confer toxicity, the potential of A β in different aggregation states was explored. A β was applied to differentiated SH-SY5Y cells either as a pre-aggregated sample or as close to a monomeric sample as obtainable in the laboratory. Pre-aggregated A β was incubated at 37 °C, quiescent conditions for 3 hours to ensure full aggregation concomitant with previous ThT aggregation assays (Chapter Three). Toxicity was observed with both samples, however A β provided a greater reduction in cell

viability when applied with no pre-aggregation with ~ 26 % +/- 2.25 SEM reduction in cell viability compared to ~ 18 % +/- 1.59 SEM following treatment with pre-aggregated samples (Figure 4 (b)). This enhanced toxicity may occur due to the 'monomeric' protein aggregating, thus forming toxic oligomers, in the presence of the cell. At points during the aggregation the toxic oligomeric species must populate a high percentage of the sample which may incur greater toxicity. Whereas pre-aggregated samples have already by-passed this crucial stage of aggregation and toxic oligomers exist in an equilibrium with fibrillar A β at a lower concentration.

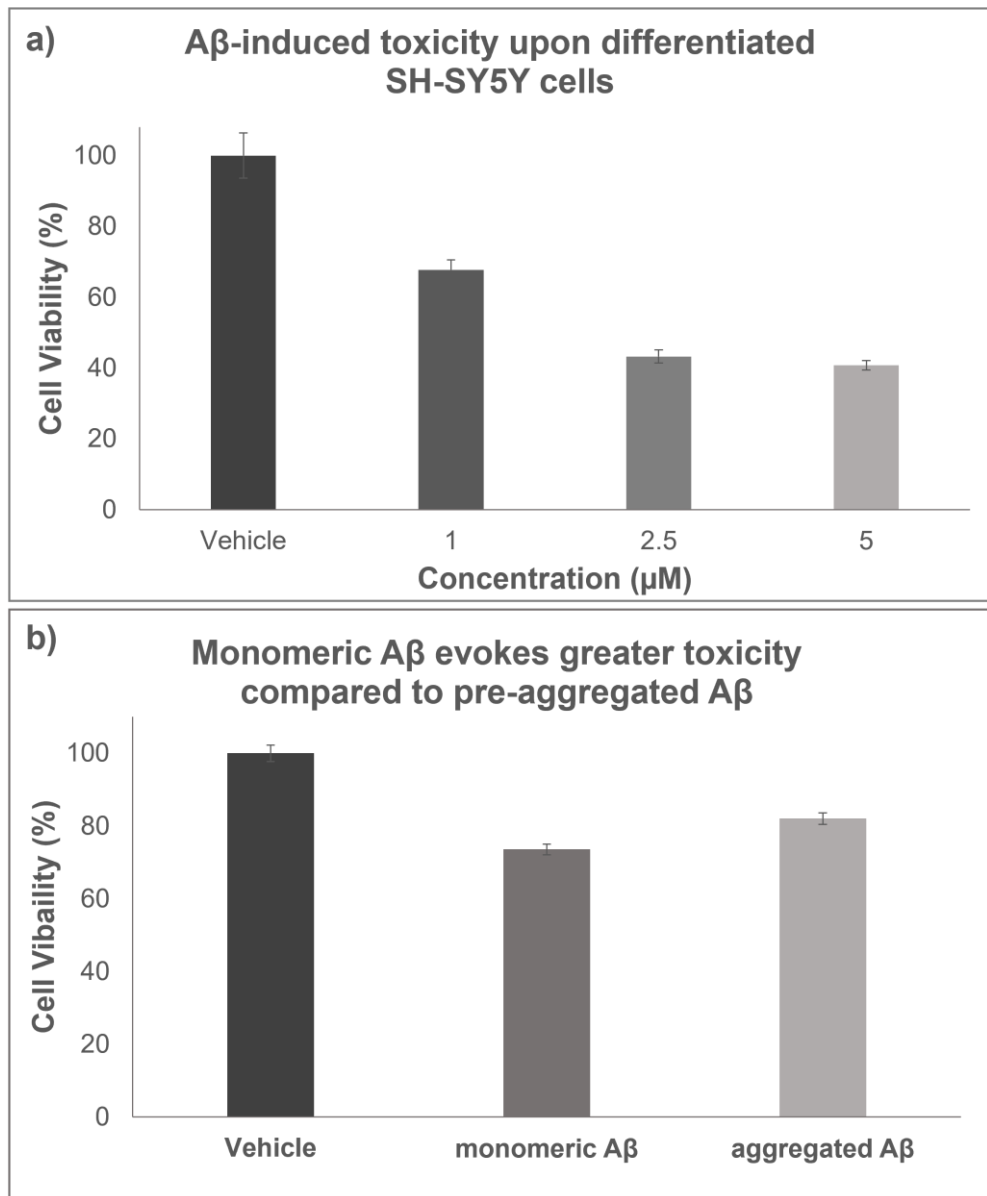


Figure 4: Oligomerisation state of Aβ influences toxicity. Differentiated SH-SY5Y cells were exposed to Aβ in various states of aggregation and sources of Aβ protein. **a)** Following previous optimisation of the differentiation protocol for SH-SY5Y cells to enhance susceptibility of the cells towards Aβ insult, the source of Aβ was altered. Here, recombinant Aβ purchased from Stratech was utilised. A range of monomeric Aβ concentrations was applied to the cells and incubated for 48 hours with an MTT assay conducted to obtain cell viability. Following subsequent repeats of the 2.5 μM Aβ condition where n = 3 experimental repeats with each repeat providing 3 technical repeats, the reduction in cell viability was shown to be significant where P<0.0001 following an unpaired standard student's t-test. **b)** Effect of aggregation status of Aβ was studied in which Aβ following 3 hours of quiescent incubation at 37 °C was applied to cells and compared to application of monomeric Aβ. Both were applied to a final well volume of 5 μM and, following incubation for 48 hours, cell viability was measured using MTT assay. Error bars represent SEM in a) and b). Both a) and b) are from a single experiment with 3 technical repeats as this was a confirmatory experiment following previous optimisation, with the exception of the 2.5 μM condition in which n = 3.

Thioflavin T (ThT) induces neurotoxicity as measured by MTT assay. Following the observation that aggregation state may alter the toxicity induced between different A β samples, the study explored the potential to apply A β directly from ThT aggregation assays such that A β aggregation could be monitored before application to cellular assays. Using A β directly from ThT experiments allows for greater knowledge of the aggregation state of A β that would subsequently be applied to the neuronal cells, as ThT fluorescence measures production of amyloid fibrils. Initial control experiments were conducted with ThT alone to assess whether ThT presented toxicity towards neuronal cells. Substantial neuronal cell death was observed upon application of ThT to the cells, even at the lowest concentration of ThT tested and as the concentration of ThT increased, cell viability decreased (Figure 5). Therefore, the potential to measure the aggregation state of A β prior to application to neurons is not possible using ThT.

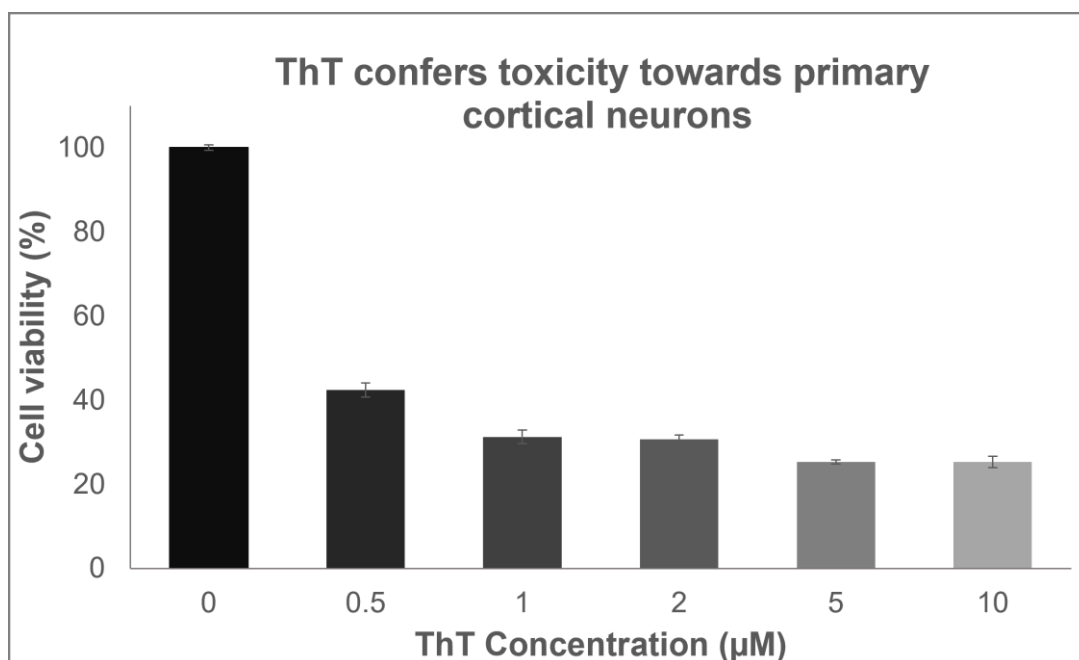


Figure 5: ThT is toxic to primary cortical neurons. Following 24 hr. incubation with varying concentrations of ThT (0.5 μM to 10 μM final well concentration), cell viability was measured using MTT assay in which absorbance at 595 nm reflects cell viability. Error bars represent SEM and data is from one experiment with three technical repeats.

Conclusions

Despite the various advantages of using SH-SY5Y cells over other commonly applied models including cost, accessibility and the human-derivation of the line, a drawback of the SH-SY5Y cell is that they are a single-cell type monolayer culture which is unable to fully represent the complexity of the human brain. Multiple cell types are involved within a 3D system in the human disease setting that cannot be recreated within a monolayer culture. Future research should be focused on developing models that better represent the complex environment of the brain.

One such study has enhanced the use of SH-SY5Y cells in this direction by pairing RA treatment with subsequent culture upon an Extracellular Matrix (ECM) gel containing several differentiation and growth factors to produce neuron-like cells within a 3D system (Agholme et al., 2010). Another exciting line of research in the pipeline sees groups developing 3D models of the human brain (neurospheroids) using human-derived stem cells (Cairns et al., 2020). These studies enable replication of the complex 3D environment provided by the use of *in vivo* mammalian models without the need for the sacrifice of an animal, with the added benefit of the human genetic component owing to the use of human-derived cells. The use of neurospheroids produced from neural progenitor and iPSCs grown upon a 3D ECM have been demonstrated to undergo neurite formation and, when genetically modified to contain AD mutations, produce both A β and Tau pathologies. These stand as very exciting and promising models by which to study AD pathology within a 3D environment relevant to, and derived from, human cells (Jorfi et al., 2018). Furthermore, there is potential to further enhance these models by considering other AD influencing factors. Kelava and Lancaster suggest incorporation of the vascular component of AD within these neurospheroids by developing the system upon vascular networks that would further expand the potential for this model to represent AD in the human system (Kelava and Lancaster, 2016). Co-culturing organoid models of the brain may also allow for mimicking of the Blood Brain Barrier (BBB) which is a crucial component of the human brain environment (Slanzi et al., 2020). Many prospective AD therapeutics are hindered by their inability to cross the BBB and developing an *in vitro* model to imitate this structure would be invaluable to pre-clinical studies.

The use of 3D organoid models to replicate the human AD system may allow for the acceleration of successful AD therapeutics, with preclinical studies potentially harbouring greater translatability in to the clinic (Slanzi et al., 2020). However, these cellular systems remain difficult to reproduce and reliably scale up to allow for drug-screening purposes (Kelava and Lancaster, 2016). Although, exciting work has begun to surface regarding 3D printing of small, spinning bioreactors to allow for cost-effective culture of these cerebral organoid systems (Qian et al., 2016).

In the meantime, however, SH-SY5Y cells present a cheaper, easily scaled and convenient model to study AD therapeutics. This study has reiterated the importance of differentiation of SH-SY5Y cells for evaluating toxicity induced by A β , as previously proposed by Krishtal et al. (Krishtal et al., 2017). Previous studies have demonstrated that application of RA inhibits proliferation and induces outgrowth of neuronal-like axons and dendrites (Cheung et al., 2009), increases Acetylcholinesterase (AChE) activity (Sidell, Lucas and Kreutzberg, 1984), enhances synaptic vesicle formation (Sarkanen et al., 2007) and increases the cells sensitivity to the neurotrophic factor BDNF which enhances final differentiation and maturation towards cholinergic phenotypes (Cheung et al., 2009; Goldie, Barnett and Cairns, 2014). The optimised differentiation and subsequent toxicity assay protocol presented here allows for SH-SY5Y sensitivity to A β at just 2.5 μ M following 48 hours A β incubation which is an improvement upon the 5-50 μ M concentration commonly described that achieve a similar level of toxicity (Krishtal et al., 2017; Krishtal et al., 2019; Litwiniuk et al., 2020; Chen et al., 2021; Feng et al., 2021; Paik et al., 2021). Another study has described A β toxicity upon differentiated SH-SY5Y cells using 2.5 μ M concentration with around 40 % loss in cell viability, as measured by MTT, compared to the 57 % described here (Oguchi et al., 2017).

Previous studies had shown treatment with 10 μ M A β to provide greater toxicity compared with 20 μ M. A lower concentration of A β allows for slower aggregation of the peptide, thus may enable longer exposure to the toxic oligomeric species as opposed to higher concentrations which aggregate faster, potentially reducing contact with intermediate oligomers as aggregation proceeds (Krishtal et al., 2019). Furthermore, Oguchi et al. described a similar finding in which 2.5 μ M A β gave a similar level of toxicity compared to 5 μ M and 10 μ M (Oguchi et al., 2017). This study has corroborated this notion that less may be more by presenting greater levels of toxicity at just a quarter of the protein concentration following 48 hour incubation. The higher degree of toxicity may also occur due to lower concentrations better representing physiological conditions and allows for more translatable assessment of A β toxicity in a relevant human-derived cell line, as opposed to saturating the system with higher concentrations of protein. The final concentration of A β within the assay accounts for the total protein concentration in the sample which contains a heterogenous mix of A β isomers in various states of aggregation. Realistically, just a fraction of the A β sample will represent the toxic species which will therefore be present at a considerably lower concentration.

Applying exogenous A β directly to SH-SY5Y cell cultures is not reflective of physiological conditions in which A β is cleaved from the cell membrane and released extracellularly. Instead, SH-SY5Y cells could be modified to endogenously produce the protein. This has been demonstrated by various groups in which the SH-SY5Y cell line has been stably transfected with APP. The APP sequence may represent the wild-type sequence or harbour

the Swedish mutation resulting in overexpression of A β . Either way, these models provide an endogenous source of A β in SH-SY5Y cells, greater reflecting the AD setting (Jämsä et al., 2011; Sun et al., 2014). The addition of a Green Fluorescent Protein (GFP) tag to endogenously produced A β has also been conducted to aid with assessment of A β aggregation and folding, where A β aggregation hinders GFP fluorescence (Chang et al., 2016; Huang, C.C. et al., 2021).

In conclusion, the protocol developed here presents a promising opportunity to successfully assess A β toxicity and the potential to explore prospective A β -targeting compounds within our laboratory. However, the current study only explores the use of the MTT assay as a measure of cell viability. Queries have been raised regarding the validity of MTT used to measure amyloid toxicity due to suggestions that the proteins may artificially decrease production of the MTT formazan product. The MTT assay relies on the reduction of the soluble tetrazolium salts to insoluble formazan crystals within the cell. The reduced MTT crystals are then displayed on the surface of the cell and, following solubilisation with isopropanol, the respective absorbance can be measured. Viable cells produce higher levels of formazan thus provide a higher readout. Reports have suggested that A β can falsely decrease this readout by enhancing exocytosis of the formazan crystals from the cells, thus falsely portraying cell death (Liu, Y., 1999; Wogulis et al., 2005). It is therefore desirable to coincide MTT with a visual observation of morphology (as done so here) along with a scrambled A β peptide control. Also, to further corroborate these findings and fully reveal the success of this study an additional cell-based assay would ideally be conducted. Work has begun to establish a Propidium Iodide-Hoe (PI/Hoe) double staining assay as an additional measure of cell viability within the laboratory. The PI/Hoe staining provides an additional measure to corroborate MTT cell viability results whilst standing as a more appropriate quantification of cell death using membrane permeable and impermeable stains to reveal apoptotic cells as opposed to mitochondrial stress, assumed to be indicative of viability as measured by in MTT (Molina-Holgado et al., 2008).

Supporting Information

Supporting Results

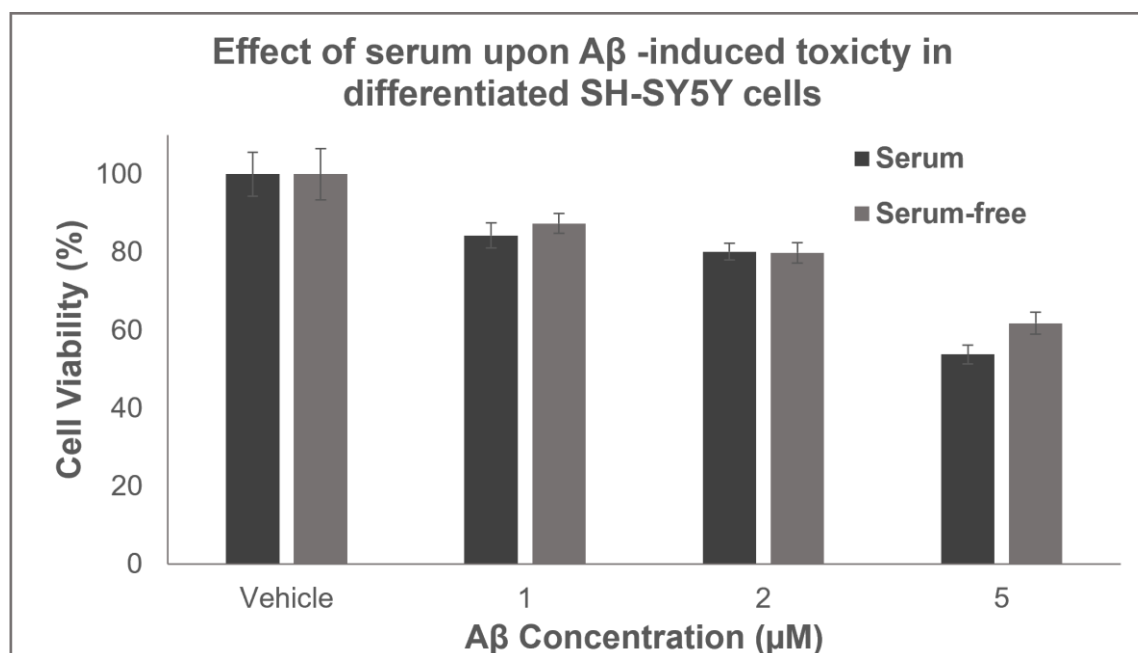


Figure S1: Presence of serum in initial growth culture media of SH-SY5Y has little effect on Aβ-induced toxicity following differentiation. Aβ was applied to SH-SY5Y cells at varying concentrations following differentiation with RA and BDNF to present more neuronal-like characteristics. In this assay, effect of serum in the initial growth culture medium of SH-SY5Y cells prior to differentiation was tested. Aβ-induced toxicity was measured using MTT cell viability assay and presence of serum was shown to hold no major effect. Perhaps serum presence in the growth culture medium prior to differentiation may slightly increase susceptibility to Aβ compared to buffer only vehicle control. However, following One-way ANOVA analysis with subsequent Tukey's multiple comparison test no significance was observed between serum and serum-free conditions.

Chapter Conclusions

Throughout the process of this study, multiple stages of optimisation have been required to allow for progression throughout the various steps from library cloning, building, screening and characterisation. A large proportion of time has been dedicated to altering laboratory processes to maximise the efficiency and success of the study to ensure that the peptide libraries can be confidently and successfully screened and that multiple, corroborating techniques could be applied to sufficiently characterise the peptides in the form of ThT, PICUP, CD, TEM and cell-based evaluations. Without these efforts, the subsequent chapters Three and Four would not be possible and so it was deemed important to expand on these efforts, as outlined in Chapter Two, to demonstrate the difficulties encountered within the laboratory, as well as the publishable, positive results described in the subsequent paper drafts, that these efforts have contributed towards. The finalised, optimised protocols applied can be found in the materials and methods of the succeeding chapters.

This section of the study has also enabled the development and optimisation of an A β toxicity assay within the differentiated SH-SY5Y cell line. In line with current literature, the study demonstrated an increased sensitivity towards A β upon differentiation as opposed to undifferentiated cells, owing to greater resemblance of neurons. Subsequent optimisation revealed the potential for the assay to induce significant toxicity at just 2.5 μ M A β . This low concentration of protein allows for better translation towards physiological conditions with the toxic oligomeric species representing a very small population of the overall sample. The optimised protocol for this A β -induced toxicity assay allows for future use towards the investigation of A β pathological mechanisms within AD and the ability to explore prospective A β -targeting therapies, as has been successfully demonstrated with the peptides described in previous chapters. Future directions of the cell-based evaluation of A β toxicity would include endogenous production of A β within SH-SY5Y cells and the development of the system upon a 3D matrix to allow for greater translatability towards the human AD setting.

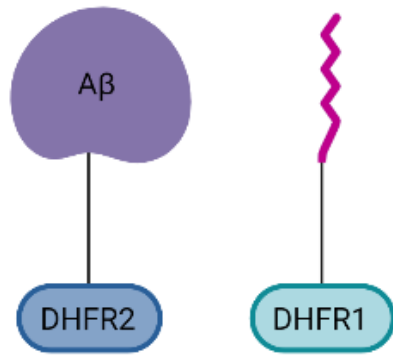
Chapter Three: Identification of in-cell derived peptide inhibitors of A β aggregation and toxicity

Chapter Introduction

Within this study, large peptide libraries were screened through the Protein Fragment Complementation Assay (PCA) to identify functional peptide hits against A β . PCA functions by recombining an artificially split murine survival gene Dihydrofolate Reductase (mDHFR), which is essential for synthesis of purine Deoxyribonucleic Acid (DNA) bases. One half of the gene is fused to the A β target and the other to the peptide library. If a given peptide does not bind to A β then mDHFR fragments remain isolated and cell survival is not possible. However, upon binding of a peptide to the A β target, the mDHFR is reconstituted and cell survival permitted (Figure 1). Endogenous bacterial DHFR is selectively inhibited by incorporation of the inhibitor Trimethoprim (TMP) such that survival of the cell depends solely on the reconstitution of mDHFR as a result of peptide binding to target. A key point is that due to the intracellular nature of PCA, hit sequences that are selected must not only bind to A β but should also detoxify the target in order for the cells to express them and the oligomer/conformers they ultimately populate. Additionally, peptide hits will potentially exhibit favourable drug-like characteristics such as low toxicity, protease resistance, target selectivity, and solubility within a cellular environment. If sufficiently small they will also be unlikely to be immunogenic since they fall below the threshold for major histocompatibility complex (MHC) presentation, aiding their potential development as therapeutic agents against AD.

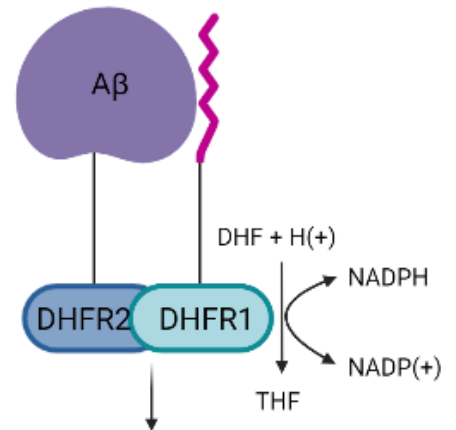
As alluded to in the previous optimisation chapter, purification of the PCAH1 peptide was complicated and remained unsuccessful. However, concurrent characterisation of the PCAH2 sequence was promising and the decision was made to advance with characterisation of this hit within a range of biophysical and cell-based assay to reveal the potential of this peptide as an AD therapeutic.

No interaction between peptide and target:



DHFR is not reconstituted so there is no cell survival or colony formation

Interaction between peptide and target:



DHFR is reconstituted allowing cell survival and colony formation

Figure 1: Mechanism of PCA Assay. Protein Fragment Complementation Assay (PCA) is a protein-interaction assay to identify peptides that bind to target proteins. A Dihydrofolate reductase enzyme (DHFR), required for survival of the cell, is cleaved in half. One half is tagged to the peptide library members with the other being tagged to the protein target A β . If no interaction between peptide and A β occurs the DHFR is not reconstituted, and the cell cannot survive. Endogenous bacterial DHFR is inhibited by Trimethoprim (TMP). If a peptide interacts with A β , DHFR is reconstituted allowing cell survival due to return of function of DHFR allowing conversion of Dihydrofolate (DHF) to Tetrahydrofolate (THF), which is an essential co-factor in the synthesis of purine bases. Image created using BioRender.com.

This declaration concerns the article entitled:			
An in-cell derived peptide inhibitor of A β aggregation and toxicity			
Publication status (tick one)			
Draft manuscript	<input checked="" type="checkbox"/>	Submitted	<input type="checkbox"/>
In review	<input type="checkbox"/>	Accepted	<input type="checkbox"/>
Published	<input type="checkbox"/>		
Publication details (reference)	N/A		
Copyright status (tick the appropriate statement) – N/A			
I hold the copyright for this material	<input type="checkbox"/>	Copyright is retained by the publisher, but I have been given permission to replicate the material here	<input type="checkbox"/>
Candidate's contribution to the paper (provide details, and also indicate as a percentage)	<p>The candidate predominantly executed the...</p> <p>Formulation of ideas: The ideas formulated within this thesis were produced between myself and my supervisor (50 %)</p> <p>Design of methodology: The design of methodology was carried out between myself and my supervisor using optimisation of previously established protocols (90 %)</p> <p>Experimental work: The majority of experimental work was carried out by myself with the exception of cell culture prior to seeding for experimentation which was carried out by Kim Morris (98 %)</p> <p>Presentation of data in journal format: Solely carried out by myself (100 %)</p>		
Statement from Candidate	This paper reports on original research I conducted during the period of my Higher Degree by Research candidature.		
Signed	Rebecca Carver	Date	07/06/2022

An in-cell derived peptide inhibitor of A β aggregation and toxicity

Abstract

Alzheimer's disease is characterised by aggregation of the amyloid- β (A β) peptide with high-resolution structural information on the precise architecture of amyloid fibres now emerging from solid-state NMR (ssNMR) and cryo-EM approaches. Here we utilise a recently identified high-resolution structure as our design guide onto which we built and screened a peptide library using an intracellular Protein-fragment Complementation screening approach. In particular, we focus our efforts on a key β -strand that is instrumental in the formation of a Greek key motif common to the majority of high-resolution structures of A $\beta_{1-40/1-42}$. We utilise ThT fluorescence aggregation experiments supported by CD, TEM and photoinduced crosslinking experiments to demonstrate that PCA derived peptides are able to impact upon A β aggregation. Finally, we demonstrate that the peptide sequence identified can rescue A β -induced toxicity using SH-SY5Y cells at low μ M concentration.

Introduction

Over 50 million individuals are affected by dementia worldwide, with Alzheimer's disease (AD) presenting as the most common form of dementia, accounting for around 70 % of cases (WHO, 2021a). With such high AD case numbers, the impact is enormous in terms of both those increasingly diagnosed with dementia and the informal carers who tend to them. It is estimated that around 16 million family members act as informal carers for loved ones diagnosed with dementia, with the disease costing around \$1 trillion globally (Association, 2018; Patterson, 2018). Currently there is no AD cure, but rather a select few drugs that can mitigate symptoms, particularly in the earlier stages. Owing to the enormous social and economic impact of the disease globally, it is clear that research towards an AD therapeutic is essential (WHO, 2020).

However, AD has a complicated disease progression that is ultimately thought to be caused by the misfolding and aggregation of two proteins, Amyloid- β (A β) and Tau, which result in the production of extracellular plaques and intracellular neurofibrillary tangles (NFT), respectively. Both proteins are considered valid, yet difficult, drug targets for AD. Although tau deposition typically better correlates with AD progression, it is long thought that A β aggregation acts upstream, initiating a cascade of events that, among others, eventually leads to Tau hyperphosphorylation and to its dysregulation and aggregation to form NFTs (Larson et al., 2012; Bloom, 2014; Amar et al., 2017; Kwak et al., 2020). Therefore, A β may

ultimately regulate Tau hyperphosphorylation, as one of many pathological pathways activated by A β . This phenomenon was dubbed the Amyloid Cascade Hypothesis (ACH) and was proposed by Hardy and Higgins in 1992 (Hardy, J.A. and Higgins, 1992).

The A β peptide is a cleavage product of the transmembrane Amyloid Precursor Protein (APP) and is produced by sequential cleavage by the β - and γ -secretases. A β is then released extracellularly and due to non-specific cleavage by γ -secretase can vary in length from ~ 36 to 43 amino acids. In a healthy brain, A β_{1-40} is the principal species with this shifting towards more production of, or a high ratio of, A β_{1-42} which can self-assemble and aggregate more readily than A β_{1-40} , deeming it the more toxic isoform (Esbjörner et al., 2014). A β deposition correlates poorly with AD progression and whilst it is not fully understood which precise oligomer or even conformer of oligomer is toxic, it is agreed that the culprit is likely to exist as a low-n oligomer that is soluble and therefore difficult to detect using conventional imaging approaches (Mroczko et al., 2018). There are various forms of oligomer, each of which exert several toxic effects ranging from blocking long term potentiation (LTP), microglia activation and the prevention of glutamate reuptake, leading to excitotoxicity (Yang, T. et al., 2017; Brinkmalm et al., 2019). It is thought there are three main mechanisms by which oligomers promote toxicity; **i)** binding cell surface receptors to activate a cascade of downstream events, **ii)** creating pores in the membrane or **iii)** interaction of aggregates of A β with the membrane that alter its property, such as fluidity (Agrawal and Skelton, 2019).

The recognised role of A β in AD pathology has led to three decades of research to target it. However, A β misfolding into amyloid is formed by a multitude of protein-protein interactions that have been historically considered 'undruggable' using conventional small molecule approaches. These are increasingly intractable aggregates as the oligomers increase in size and stability. The lack of successful drugs arising from A β research has therefore raised the question as to whether it is an appropriate drug target for AD, with many other lines of investigation being pursued, including Tau-directed therapies and drugs to prevent neuroinflammation. However, the recent Food and Drug Administration (FDA) decision to fast-track approval of Aducanumab in the United States (US) has reignited the argument that A β is a legitimate target. Indeed, although not without controversy, Aducanumab stands as the first approved drug to address the cause of AD by directly targeting A β to reduce plaque burden.

Recent improvements to a peptides half-life, stability and selectivity has led to a revival in their use as therapeutics over the last few decades with over 60 approved peptides on the market, 150 currently in clinical development and over 200 in preclinical development (Henninot, Collins and Nuss, 2018; Lau and Dunn, 2018; Armiento, Spanopoulou and Kapurniotu, 2020). The use of peptides as drugs was previously limited due to their

susceptibility to proteases, poor bioavailability and rapid clearance (Leithold, L.H. et al., 2016; Armiento, Spanopoulou and Kapurniotu, 2020). However, peptide mimetics can now be employed to overcome such shortcomings to allow the production of more drug-like candidates that evade issues such as cell penetrance and protease susceptibility (Ryan et al., 2018). Compared to small molecules and antibodies, peptides provide a middle-ground between size and specificity by providing a high specificity at a smaller size than antibodies whilst presenting low toxicity, a lack of immunogenicity (owing to their smaller size compared to antibodies) and low production costs along with providing the scope to develop and screen large, diverse libraries (Mason, 2010).

In order to target A β , a high resolution cryo-EM structure was utilised. We applied a semi-rational approach to design a library against the outer β -sheet strand incorporating residues 10–22 (Figure 1 (a)) (Gremer et al., 2017). Most recent amyloid structures hold an overall Greek key motif with an S-shaped fold validating the current design structure against recent amyloid structures despite slight variations between them (Figure 1 (a-e)) (Paravastu et al., 2008; Colvin et al., 2016; Wälti et al., 2016; Kollmer et al., 2019; Gallardo, Ranson and Radford, 2020; Sawaya et al., 2021). A β_{1-40} fibrils derived from human brain have been shown to twist in opposing directions compared to *in vitro* A β , with *in vitro* derived A β presenting a left-hand twist whilst brain derived A β are right hand twisted. In addition, the interaction between two monomers shown is suggested to present as a C-shape with four β -strand regions (β 1- β 4) (Kollmer et al., 2019). Despite these differences between brain derived and *in vitro* A β described by Koller et. al., the region that the library is designed against, residues 10-22, is still incorporated in the folding and binding of monomer and dimers in this brain-derived structure, with the main interacting strand (β 3 between residues 15 – 19 which interacts with β 4 of opposing monomer) standing at the precipice of the dimer interface. Furthermore, a recent study of human-brain derived A β_{1-42} did present differences between structures but suggested similar S-shaped folds presenting an overall Greek-key like motif in which residues 10–22 remain important for folding of the protein (Yang, Y. et al., 2022). This study indicated differences between A β structure derived from patients with Sporadic AD and Familial AD (FAD), yet both presented an overall S-shape structure. A β structures vary depending on source, whether *ex vivo* or *in vitro*, and type of AD, familial vs. sporadic, yet it is reassuring that the study confirms relevance of the library design in human derived A β from sporadic AD. Ultimately, despite various other structures having been revealed where the gross topology changes, most structures harbour this S- or C-shape (for brain derived or A β_{1-40}) meaning that the beta-strand structure is maintained, providing a firm justification for the library design on this region.

In particular we utilise Protein Fragment Complementation Assay (PCA) to identify sequences that can bind to A β in the complex environment of the cytoplasm. PCA has been successfully applied within the Mason group across a range of disease therapeutic areas

to screen peptide libraries and identify successful peptide sequences. It has previously identified peptide inhibitors of both A β and α -synuclein with the aim to prevent toxicity associated with the neurodegenerative disease AD and Parkinson's Disease and also to identify peptides with potential as therapeutics against cancer (Acerra, Kad and Mason, 2013; Acerra, N. et al., 2014; Acerra, Nicola et al., 2014; Cheruvara et al., 2015; Baxter et al., 2017; Yu, M. et al., 2021).

This study presents the successful development and screening of a large peptide library to identify a functional peptide hit that has been shown to alter A β aggregation, validated using a range of biophysical techniques, and rescue A β -induced toxicity in cellular assays.

Materials and Methods

For comprehensive materials and methods see supporting information.

Library Cloning. A self-annealing primer was designed using semi-randomised codons that corresponded to library options within the peptide such that all library members were incorporated. Following initial Polymerase Chain Reaction (PCR) it was confirmed that the primers were self-annealing to produce two inverted inserts of approximately 120 bp (Figure S1 (a)). The dimer inserts were next digested with NheI and AclI to form two separate library inserts of approximately 60 bp (Figure S1(b)). The 60 bp band observed was next extracted from the gel to provide the pure library insert band and the DNA ready for ligation with the vector.

Library ligation and transformation into NEB-10 β cell line. A p230d-alpha-synuclein-DHFR1 plasmid was digested with NheI and AclI to remove the alpha-synuclein insert. This was successfully ligated with the library inserts produced by PCR and the resulting plasmid transformed into NEB-10 β *Escherichia coli* (*E.coli*) cells since these are optimised by NEB to provide high transformation efficiencies for larger plasmids and high-quality plasmid preparations resulting from the deletion of Endonuclease I (EndA1) from the strain. A control with no insert was also conducted to indicate the level of background vector present during transformation. Taking this background into account the number of colonies obtained representing the library was used in the following calculation to ensure sufficient coverage of both libraries (equation 1) (Denault and Pelletier, 2007):

$$E = 100*(1-(1/n))^m$$

Equation 1: Library coverage where E = % of library missing, n = theoretical library size and m = colony forming units from transformation (experimental).

The colonies were harvested from the library building transformation plates and used to prepare glycerol stocks. From these glycerol stocks, the library DNA was mini-prepped and used to screen the library in the PCA assay. The library coverage was also confirmed by sequencing of library pools to ensure the ligation had been successful and all library members were fairly represented. Additionally, individual colonies were sequenced to ensure correct presentation of the library and sufficient variation at library scrambled positions across multiple sequences.

PCA Single Step Selection. BL21-Gold cells containing pREP4 plasmid (Kanamycin (Kan)) were electroporated (as described in SI) with a p300d plasmid (Chloramphenicol (Cm)) containing the target protein sequence (A β ₁₋₄₂ Arctic mutant). The cells were made electrocompetent before being transformed with the cloned p230d-library members (Ampicillin (Amp)) via electroporation. Recovered cells were spread across three plates: **i)** a set of serially diluted positive control plates on Lysogeny Broth (LB) Agar containing 250 μ M Amp, 100 μ M Kan and 100 μ M Cm were used to confirm effective transformation and library coverage (50 μ l taken from 1 ml and serially diluted to achieve up to 200,000 x dilution), **ii)** a 20x diluted (50 μ l plated of the 1 ml recovery media) M9 negative control plate containing Kan, Amp, Cm (to the same concentrations as listed above) and 2 μ M TMP but lacking Isopropyl β -D-1-thiogalactopyranoside (IPTG) to serve as a negative control. **iii)** Finally, an M9 assay plate containing Kan, Amp, Cm, TMP (all same concentrations as listed above) and 1mM IPTG to induce expression of both target and library members, which the remaining library members were plated upon. LB Agar plates were incubated at 37°C overnight and colonies subsequently counted to ensure sufficient library coverage by the screen. All M9 plates were incubated at 37°C until colonies appeared (this typically occurred within two weeks).

PCA Competition Selection. M9 media with appropriate antibiotics was used to harvest colonies from PCA single step selection. During passaging, 50 ml of M9 liquid media (containing Amp, Cm, Kan, IPTG, and TMP) was inoculated with colonies pooled from the single step (P0) selection plate to a starting OD₆₀₀ of less than 0.01. The liquid culture (P1) was next incubated at 37 °C, shaking at 250 rpm, until OD₆₀₀ = 0.4 with both the pool and individual colonies sequenced. Next, 50 μ l of the P1 culture was used to inoculate fresh M9 media with appropriate antibiotics (now P2). Passaging continued until a 'winning' sequence had been identified as verified from one clean sequence within both the pool and individual colonies. M9 media lacking IPTG was used as a control in which no growth was observed and TMP levels optimised to accommodate the growth rate of the cells at 4 μ M for liquid culture.

Thioflavin T (ThT) aggregation Assays. A β and peptide aggregation experiments were probed using ThT fluorescence studies at a range of A β and peptide concentrations. All assays were measured using a ClarioStar Microplate reader (BMG LabTech) with incubation at 37 °C under quiescent conditions. All proteins and peptides were suspended in 20 mM Sodium Phosphate Buffer, 200 μ M EDTA at pH 8.0 for A β and iA β ₅ and pH 5.8 for PCAH2 to allow for complete dissolution of the peptide into the buffer. Corning™ 96-well, non-binding, Flat Bottom, Half-area microplates (Corning: 3881) were used with 100 μ l sample per well. All plates were sealed using adhesive plate foils (ThermoFisher: AB0626). Samples were prepared in triplicate containing varying volumes of protein and peptide to obtain desired concentrations (5 μ M for A β and 0.5, 1.25, 2.5, 3.75, 5, 10 and 50 μ M for peptide), 20 μ M ThT (0.4 μ l of 5mM stock per well) and made up to final volume with 20 mM Sodium Phosphate, 200 μ M EDTA, pH 8.0. 100 μ l of sample was transferred to each well and fluorescence measured. The focal height was set to 4.2 mm and the gain adjustment to 1200. Fluorescence was measured using an excitation filter of 440 nm, an emission filter of 480 nm and read using the bottom optic with 15 flashes per well on a spiral average with a cycle scan time of 90 seconds.

Circular Dichroism (CD) experiments. To determine changes in the global secondary structure of A β in both the presence and absence of peptides circular dichroism (CD) experiments were conducted. These were either as end-point experiments following complete aggregation of A β or were undertaken in a timepoint nature in which the structure was monitored using CD throughout the A β aggregation time-course. This was achieved by capturing samples of A β at various timepoints from T₀ to the aggregation endpoint, when the ThT signal had plateaued. All samples were suspended in 20 mM Sodium Phosphate buffer, 200 μ M EDTA, pH 8.0 or pH 5.8. CD measurements were undertaken using a Chirascan™ V100 (Applied Photophysics) with the sample chamber set to 37 °C for timepoint experiments or 20 °C for endpoint experiments. A 1 mm path length quartz cuvette was used (Hellma Analytics; Cat No.: HL110-1-40) with the scan ranging from 190/200 nm - 280 nm with a 1 nm bandwidth. Three scans for each sample were taken and an average obtained.

Transmission Electron Microscopy (TEM) of aggregated A β . Following full aggregation of 50 μ M A β , samples were collected and used for TEM assessment of A β fibril morphology. TEM was carried out with the help of the University of Bath Physics Department. A drop of the aggregated A β sample was applied to a glow discharged Formvar/carbon coated, 200 mesh, copper grid and incubated at room temperature for 1 minute. The grids were then dabbed with filter paper to dry and washed twice with milli-Q water with a 1 second incubation between each wash. The sample was then stained by applying a drop of Uranyl Acetate Zero stain (Agar Scientific) and incubated for 30 seconds. Excess stain was removed by dabbing the grid with filter paper and the grids left at room temperature to air

dry for 2 hours. The samples were then applied to the Transmission Electron Microscope (JOEL; 2100 Plus) which was operating at an accelerating voltage of 200 kV.

Photo-induced Cross-linking of unmodified proteins (PICUP). PICUP protocol was adapted from Rahimi et. al. (Rahimi, Maiti and Bitan, 2009) and requires careful optimisation to work successfully for any given protein. Firstly, stock solutions of 20 mM Ammonium Persulphate (APS) and 10 mM Tris(2,2-bipyridyl)dichlororuthenium(II) hexahydrate (RuBpy) (Sigma: Cat No.: 224758) were prepared in 20 mM Sodium Phosphate, 200 μ M EDTA, pH 8.0 buffer. Both timepoint and endpoint PICUP assays were conducted in accordance with data from across the ThT monitored time-course. PICUP experiments were carried out at 50 μ M A β and with varying molar ratio of peptides (A β :PCAH2 1:1, 1:0.5, 1:0.25, 1:0.1). For the cross-linking procedure, 1 μ l 10 mM RuBpy and 1 μ l 20 mM APS were pipetted to the opposite sides of the bottom of an Eppendorf tube. 18 μ l of sample was next added to the tube and gently agitated to facilitate mixing. The tubes were then subjected to 10 seconds of light and 1 μ l 1 M Dithiothreitol (DTT) solution subsequently added to quench the reaction. The cross-linked samples were next separated by Sodium dodecyl-sulfate Polyacrylamide Gel Electrophoresis (SDS-PAGE) (150 V for 45 minutes) to distinguish different sized species of A β present.

Quantification of gel bands using ImageJ. Using ImageJ 1.53e software (<http://imagej.nih.gov/ij>), an image of the gel was opened in the software and a rectangular box drawn around the desired band. This was designated the first lane in the gels subheading under the analyse tab. The box was then dragged to the next well band, so that the size of the box remains constant, and this selected as the next well under gels subheading. This was repeated until all desired bands were highlighted. In the gels subheading, under the analyse tab, the intensity of the lanes were then plotted. Each band will result in a peak and the boundary of each peak is drawn by connecting a straight line across the base of the peak. The wand tool was then used to click within each peak to provide a reading of the area for that peak. This reading was used to roughly quantify the band intensity between lanes and the data exported to excel to calculate relative percentages of band intensities.

Preparation and Differentiation of SH-SY5Y cells. Cells were differentiated as described by Forster et. al. (Forster et al., 2016). SH-SY5Y (ECACC 94030304) cells, purchased from Public Health England's European Collection of Authenticated Cell Cultures (ECACC), were seeded on to Nunc™-treated cell culture plates (ThermoScientific: 142485) in Dulbecco's modified Eagle's medium (DMEM)/F12 with Phenol Red (ThermoFisher 42430082)((1:1 ratio DMEM/F12 media), 10 % Fetal Bovine Serum (FBS), 5 % Penicillin (Pen)/Streptomycin (Strep), 5 % L-glutamine) at a density of 5 x 10⁴ cells/ml and incubated at 37 °C, 5 % CO₂ for 1 day. Following this, the media was removed and replaced with Serum-free DMEM/F12

with Phenol Red ((1:1 ratio DMEM/F12 media), 10 % FBS, 5 % Pen/strep, 5 % L-glutamine) media and 10 μ M Retinoic Acid (RA) (Sigma: R2625). The SH-SY5Y cells were incubated in RA media for 3 days until the RA media was removed and replaced with Neurobasal-A media (ThermoFisher: 12349015) (1 % L-Glutamine, 1 % penicillin/streptomycin, 1 % N2 neuronal supplement) and 1.85 nM Brain-Derived Neurotrophic Factor (BDNF) (Merck: B3795) and incubated for a further 4 days. After 7 days the SH-SY5Y cells were fully differentiated and ready for use in assay.

Cell viability assay by MTT. 3-(4,5-dimethylthiazol-2-yl)-2,5-diphenyltetrazolium-bromide (MTT) assays stand as an indirect measure of cell viability, probing mitochondrial function by measuring the conversion of MTT to formazan by mitochondrial enzymes. For the MTT assay, a 1 mg/ml MTT (in complete media) solution was prewarmed. The assay media was aspirated, replaced with 500 μ l MTT media and incubated at 37 °C, 5 % CO₂ for 1 hour. Following this, the media was removed and 650 μ l Isopropanol added and mixed to solubilise the remaining formazan dye. 200 μ l was transferred to a single well of a clear plate in triplicate and the absorbance measured at 595 nm using a microplate reader (BioRad, Model: iMark).

Results

We report an intracellular PCA peptide library screening approach to identify those members of the peptide library that are able to bind and detoxify the 'arctic' mutant form of A β ₁₋₄₂. The E22G arctic mutant was chosen as the target to provide greater selection stringency, since this form of the protein is known to considerably accelerate AD pathology by directly leading to the population of toxic A β oligomers that do not typically progress into mature fibres (Nilsberth et al., 2001; Cheng et al., 2004). Following PCA, selected hits were characterised using a range of biophysical techniques that included ThT aggregation assays, circular dichroism (CD) and cross-linking methods as well as cell-based assays to demonstrate that the peptide binds A β to modulate aggregation as well as the potential to impact upon A β -induced toxicity.

Library designs built using a cryo-EM A β structure. The library was designed using a β -strand region within A β ₁₋₄₂ as a template, since it is important in formation of the overall Greek-key topology (Figure 1 (a)), and therefore for folding and binding of A β to form larger Protein-Protein Interaction (PPI) complexes, towards the greater goal of hindering formation of toxic oligomers (Gremer et al., 2017). In particular, the library was designed using the outer, solvent-exposed β -strand that is common to many A β structures. Sidechains facing inward towards the hydrophobic A β core were semi-scrambled whilst those facing outward into the solvent on the surface of the fibril template were unchanged to create a two-sided

peptide with a hydrophobic surface and a polar surface. Overall, the library resulting from this sequence was 655,360 peptides in size (Figure 1 (f)). Following extensive optimisation of molecular cloning techniques, the library was sufficiently built and confidently represented following transformation into NEB10 β to obtain 6,295,109 colonies, providing 99.99 % coverage of the theoretical library following the library building process (see eqn. 1).

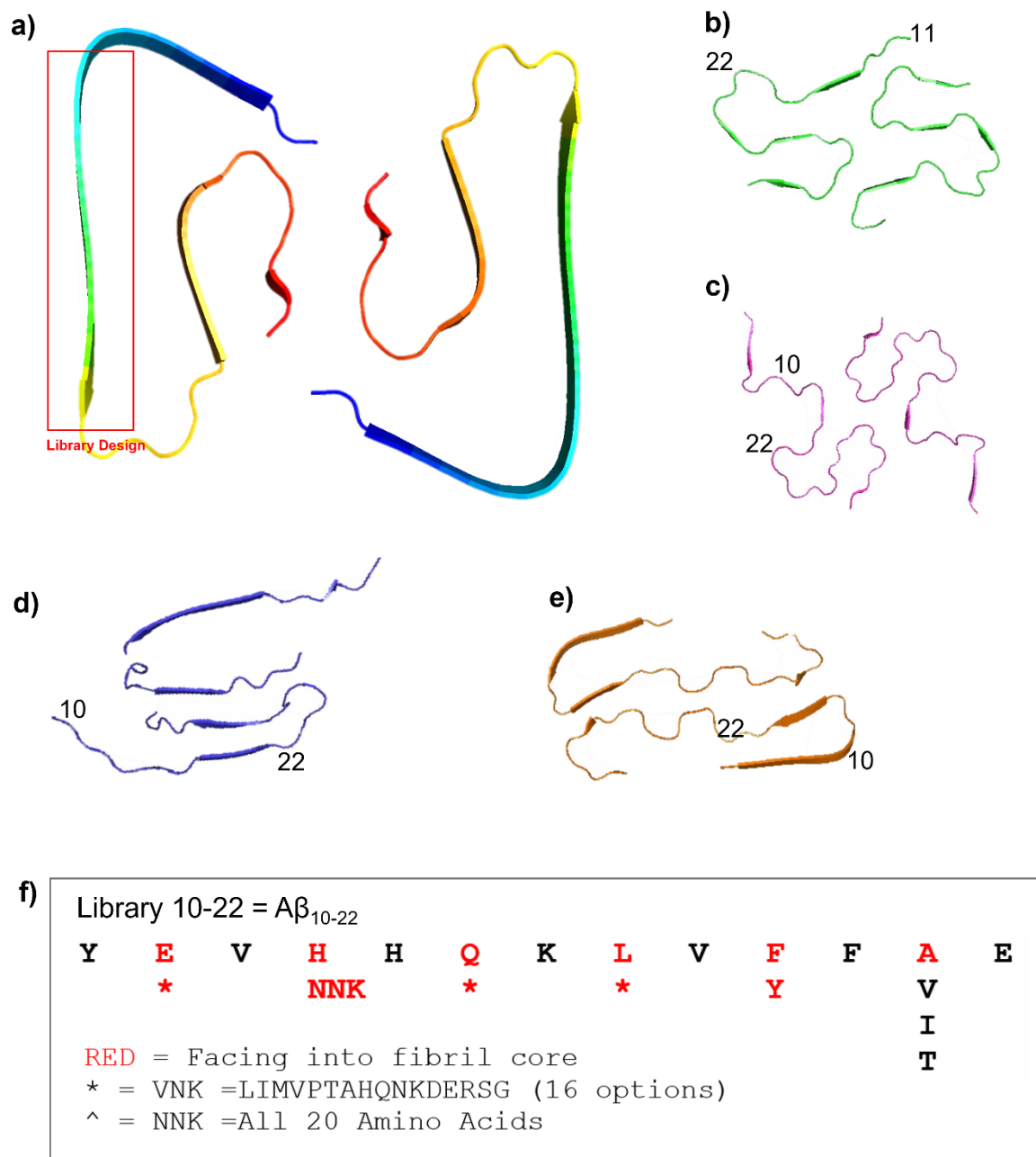


Figure 1: Library design, $A\beta$ structures and residue options for library members. **a)** Cryo-EM structure of $A\beta_{1-42}$ was created with PyMol (PDB ID 5oqv). The red box represents regions of $A\beta$ that the library is designed against using residues 10-22 (Gremer et al., 2017). **b)** Magic-angle spinning (MAS) NMR structure of $A\beta_{1-42}$ shown in green (PDB 5kk3) (Colvin et al., 2016). **c)** Solid-state NMR (ssNMR) structure of $A\beta_{1-42}$ shown in purple (PDB 2nao) (Wälti et al., 2016). **d)** ssNMR structure of $A\beta_{1-40}$ shown in blue (PDB ID 2lmn) (Paravastu et al., 2008). **e)** Cryo-EM structure of $A\beta_{1-40}$ derived from human AD brain tissue shown in orange (PDB ID 6shs) (Kollmer et al., 2019). a-f) structural images were formed in PyMol using the respective PDB ID codes and residues 10 and 22 are marked on each. **f)** Library design based on $A\beta_{10-22}$ presenting options at each residue. The top row is the original 10-22 sequence and residues marked in red are those facing into the hydrophobic core and are therefore deemed important for folding of $A\beta$. The residues in red have been scrambled and encompass a range of potential residues at each of the altered positions with * representing 16 possible residues as listed, and ^ representing NNK coding for all 20 amino acid residues.

A β interacting peptides identified by PCA. Intracellular PCA screening of the library was conducted to identify interacting peptides that not only bound to arctic A β ₁₋₄₂, but that also detoxified the target protein within the complex intracellular environment of the assay. The library was successfully screened using PCA.

Following single step PCA selection, numerous colonies were observed. TMP concentrations were optimised for this step with the final concentration of 2 μ M for the M9 agar plates obtained. Concomitant controls that lacked IPTG required for induction of protein expression within the assay were also conducted and presented no colonies, as expected. PCA colonies were next pooled and progressed further into competition selection to identify the peptide hit that provided the greatest growth advantage in liquid culture. The sequence, YAVFHPKTVFFVE, of this hit is shown in Figure 2.

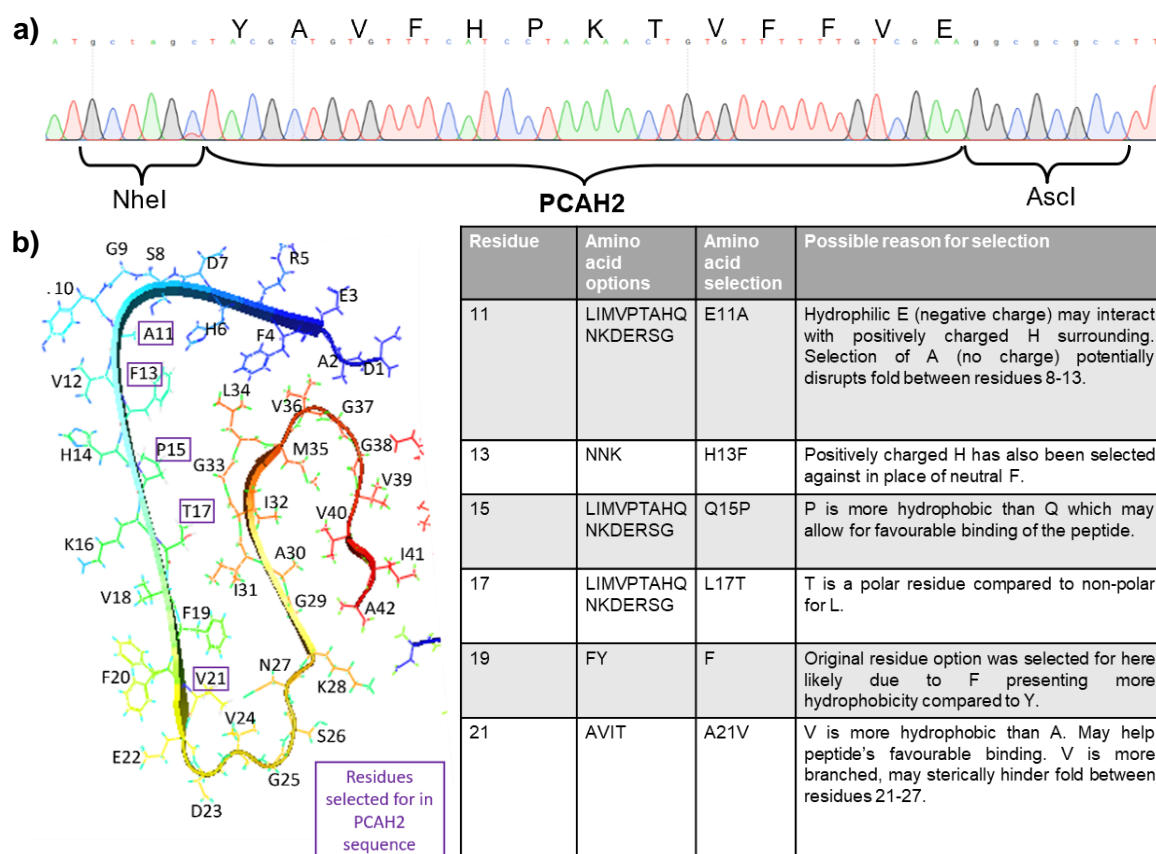


Figure 2: PCAH2 sequence resulting from PCA screening of Library 10-22. **a)** Following PCA screening, resulting hits were minipreped and sent for LightRun sequencing. **b)** Residues selected for in PCAH2 sequence overlaid with A β structure (PDB: 5oqv). Residues selected against are highlighted in purple box with selected peptide option in place and suggestions as to the property of each selection has been speculated in the table.

PCAH2 impacts upon A β aggregation and total endpoint fibrilisation. Biophysical characterisation of the PCAH2 peptide hit provides broad insight into how it interacts with A β to impact upon the aggregation process. To increase the stringency, the PCA screen was carried out against the arctic A β ₁₋₄₂ (E22G) mutant. However, to translate the selected peptides towards physiological disease conditions, the proceeding characterisation of the peptide hit employs wild type A β . PCAH2 was synthesized by solid-phase peptide synthesis (SPPS) and purified by HPLC (Figure S2) to allow for progression into biochemical exploration. Initial ThT fluorescence monitored aggregation assays were conducted and revealed a modified A β aggregation profile in the presence of PCAH2 relative to A β in isolation at a concentration of 5 μ M (Figure 3 (a)). Aggregation was also measured in the presence of an iA β ₅ peptide control (LPFFD) (Figure 3 (a)). Additionally, peptide only controls were conducted to ensure that the peptide alone did not alter ThT fluorescence, and these presented as flat lines as expected (data not shown).

Measuring A β aggregation using the ThT fluorescence assay revealed that, in the presence of the PCAH2 peptide, the lag-phase of A β aggregation is delayed. In particular, the mid-point of the ThT monitored aggregation profile confirmed PCAH2 increases the time taken to reach the sigmoidal midpoint by ~ 180 % at a ratio of 1:10 (Figure 3 (a)), although this elevated stoichiometry ultimately led to an increased ThT fluorescence profile within the stationary phase.

However, at an equimolar ratio, a delay to the midpoint time of ~ 41 % is observed along with a decrease in endpoint ThT fluorescence of ~ 24 %. These data provide evidence that, overall, PCAH2 is effective at both slowing aggregation and lowering overall amyloid load at equimolar molar ratios compared to super-stoichiometric ratios like 1:10 and 1:2. Moreover PCAH2 does so more than the iA β ₅ control which delays the midpoint of aggregation by ~ 20 % and decreases the stationary phase signal intensity endpoint (indicative of less fibrilisation) by ~ 20 % at a ratio of 1:1 (Figure 3 (a)).

Overall, although peptide ratios above 1:1 prolong the A β aggregation lag phase, over longer periods the peptide also resulted in an increase in overall ThT signal (Figure 3 (a)). To understand these results further and to expand upon the peptides potential, a lower stoichiometry was deemed required to further evaluate the ability to impact upon A β aggregation.

PCAH2 impacts upon A β aggregation and total endpoint fibrilisation at lower stoichiometries. To investigate the activity of the PCAH2 peptide at lower concentrations, ThT aggregation experiments were conducted at 5 μ M A β with equal to sub-stoichiometric ratios of peptide (Figure 3 (b)). Due to differences in time to prepare plates between experiments and the rapid aggregation time of A β (minutes), differences in lag-phase and midpoints may be observed between separate experiments meaning that comparisons

between experiments is not always appropriate, but rather is relevant in the context of each set of replicates. Reassuringly at sub-stoichiometric concentrations the fluorescence intensity at the stationary phase was found to be significantly lower unlike that for super-stoichiometric peptide ratios as described above (Figure 3 (b)). In addition, PCAH2 was found to maintain a prolonged lag-phase of aggregation, with the midpoint values increasing up to ~ 17 % (for 1:0.1), with a reduction in the fluorescence intensity of ~ 25 % (for 1:0.1) relative to A β in isolation. Although the peptide ratio of 1:1 led to the most significant midpoint increase (~ 22 %), the reduction in fluorescence intensity at the aggregation endpoint was less than for that of 1:0.1, suggesting that PCAH2 may be more beneficial at lower stoichiometries as opposed to equimolar amounts.

Following ThT monitored A β aggregation experiments, subsequent exploration was required to reveal further insight into how the peptide interacts with A β . Towards this goal we additionally studied A β secondary structure using CD and fibril formation via TEM, and also monitored for the presence of oligomeric species using PICUP. Ideally, all experiments would be carried out at 2.5 μ M using the same sample to minimise errors to reflect downstream cell-based toxicity experiments. Unfortunately, this low concentration cannot be translated to CD, TEM and PICUP which has had to be scaled up to 50 μ M for sufficient signal to noise, precluding direct comparison of matched samples with ThT.

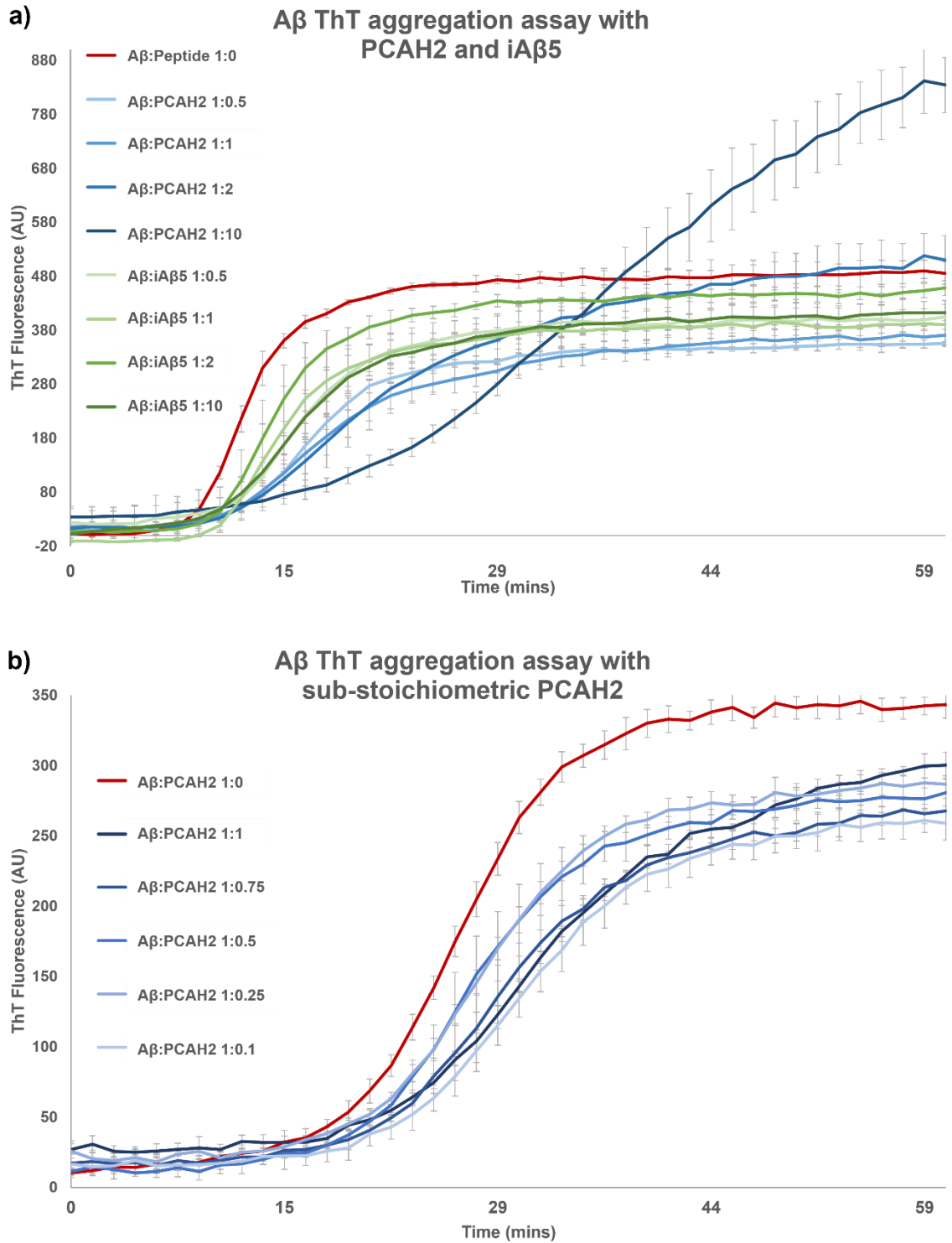


Figure 3: ThT Aggregation assays explore PCAH2 effect on A β aggregation. a) ThT aggregation assay with 5 μ M A β alone (red) and in the presence of peptide ranging from A β :PCAH2 ratios from 1:10 to 1:0.5 (blue) and A β :iA β ₅ ratios from 1:10 to 1:0.5 (green). **b)** Following revelation that molar excess of peptide results in increased overall aggregation, a range of equimolar and sub-stoichiometric ThT aggregation assays were conducted. Midpoints for both a) and b) were calculated by fitting curves to a sigmoidal fit using Origin software to reveal midpoint values in time. Endpoint values are ThT fluorescence at plateau of sigmoidal curve. Differences in time taken to prepare plates for assay accounts for differences in lag-phase length between a) and b).

Circular dichroism studies revealed that PCAH2 reduces global β -sheet content and rate of conversion. CD spectra was monitored upon addition of PCAH2, highlighting a change in the extent of β -sheet structure relative to A β alone at the endpoint of aggregation (Figure 4 (a)). As observed from aggregation experiments, the overall fibrilisation at ThT endpoint is lower upon addition of PCAH2 at stoichiometries of 1:1 and below. This is supported by CD via a corresponding reduction in the 218 nm minima.

A β adopts a β -sheet structure upon aggregation and measuring the formation of the 218 nm peak (characteristic of β -sheet) could provide a better indication of how the peptide alters A β throughout its aggregation. This time-course approach may be more relevant to understanding the peptides inhibitory effects throughout aggregation rather than at the stationary endpoint. Timepoint CD scans of A β indicate a sustained delay in formation of the 218 nm peak upon addition of PCAH2 (Figure 4 (b-d)). Initially, the peptide appears to enhance 218 nm peak formation, but over the course of the aggregation observed by CD the rate at which β -sheet forms is lower in the presence of the peptide at a ratio of 1:1.

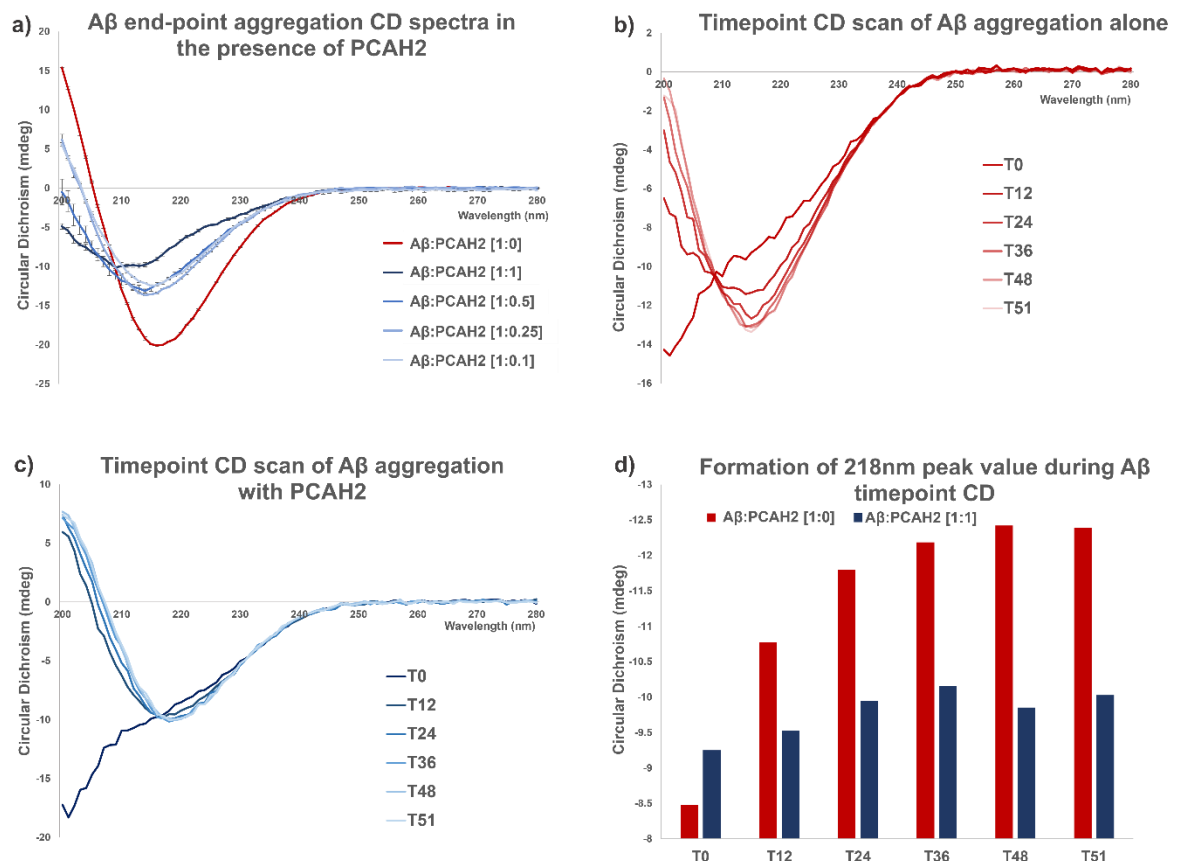


Figure 4: Circular Dichroism scan shows change in extent of β -Sheet structure of A β aggregation in the presence of PCAH2. a) Endpoint CD Scan of A β following aggregation in the presence of varying stoichiometries of PCAH2. Following full aggregation of 50 μ M A β in the presence of PCAH2 at varying stoichiometries a CD scan was taken to reveal the β -sheet structure of the protein. **b)** Timepoint CD scan throughout A β aggregation at various timepoints. **c)** Timepoint CD scan of A β aggregation in the presence of PCAH2 at equimolar amounts. **d)** Timepoint CD scans were used to determine peptide's ability to reduce formation of β -sheet fold as demonstrated by circular dichroism value at 218 nm.

Transmission Electron Microscopy suggests altered levels of A β fibrils in the presence of PCAH2. TEM was conducted to determine whether the peptide alters the appearance/morphology of A β . Samples containing either \sim 50 μ M A β alone or with two ratios of PCAH2 (1:1 and 1:2) were imaged. Samples containing PCAH2 appeared to contain more disperse fibrils with a lack of more mature, amyloid aggregates than observed in the A β only sample (bottom panel of Figure 5). This suggests a reduction in A β aggregation in the presence of the peptide (Figure 5 (a-c)). Regarding the precise fibril structures, no noticeable difference was observed by TEM at the endpoint of A β aggregation (Figure 5). Samples containing peptide only were also imaged and presented blank grid images (data not shown).

Imaging of these samples presented dense aggregates of A β (classified here as regions too thick for clear image due to inability of electrons to pass through the sample as shown

in the bottom two panels of Figure 5 (a)) in A β alone samples which were not observed in the samples containing the peptide. No dense plaques were found in samples containing the peptide. No differences were observed in A β presentation between the two peptide stoichiometries.

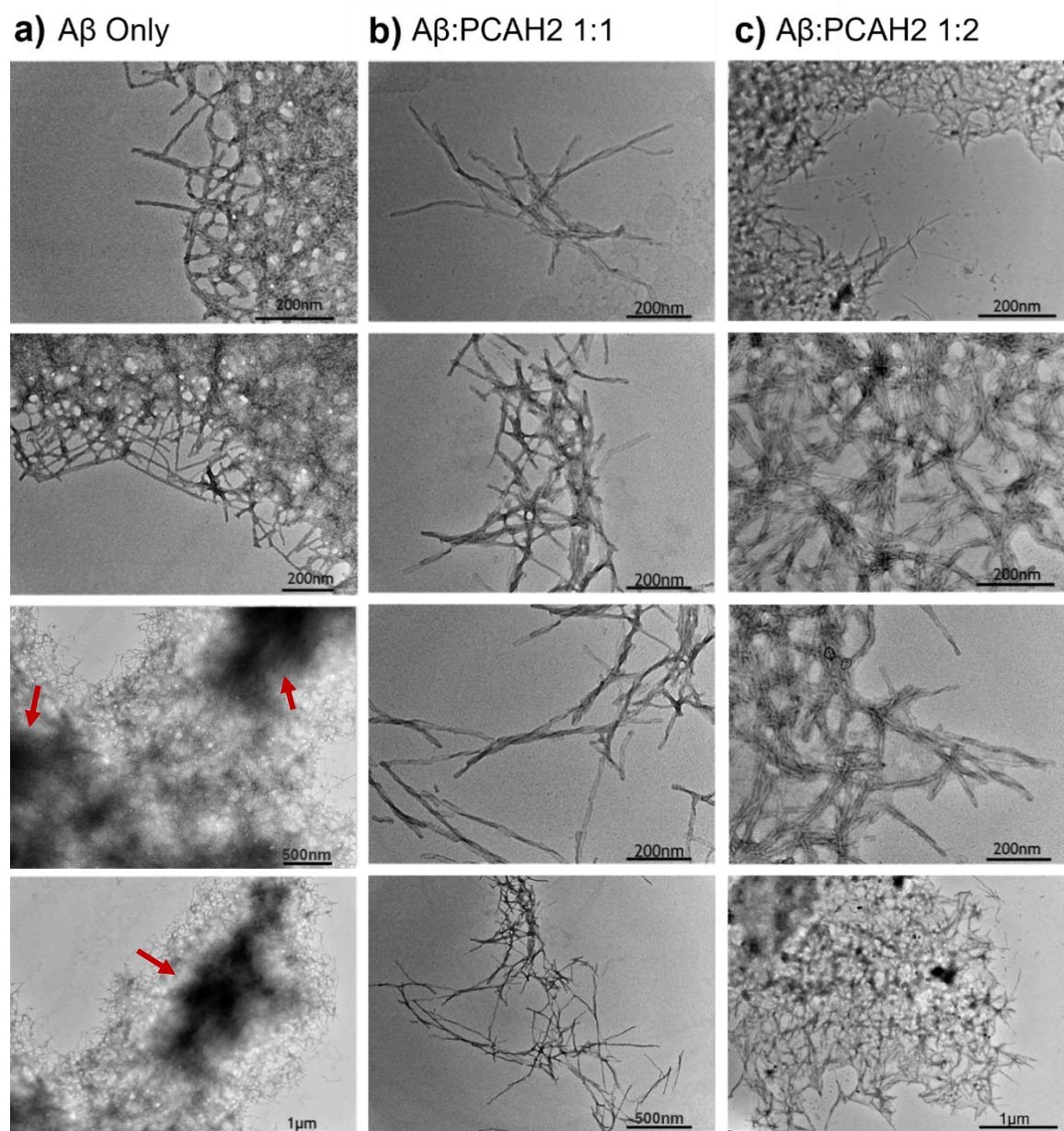


Figure 5: Transmission Electron Microscopy of end-point aggregated A β in the presence of PCAH2. Following aggregation of $\sim 50 \mu\text{M}$ A β in the presence of PCAH2 at ratios of 1:1 and 1:2 the samples were imaged using TEM to determine changes in fibril structure as a result of PCAH2. **a)** A β only **b)** A β with 1:1 PCAH2 and **c)** A β with 1:2 PCAH2. The red arrows represent dense aggregations of A β in which the sample is too thick for a clear image due to the inability of electrons to pass through the sample. The images are ordered vertically in order of magnification for each sample type. During sample collection, there was no image obtained for 1 μm for A β to peptide ratio of 1:1.

Photo-induced cross-linking of A β demonstrates that PCAH2 alters monomer and oligomer status during A β aggregation. To further corroborate the potential of PCAH2 to slow the aggregation of A β , PICUP experiments were carried out. SDS-induced artefacts are observed as expected (Bitan, G. et al., 2005; Rahimi, Maiti and Bitan, 2009), however these do not affect the observation of cross-linked oligomers, or the conclusions drawn from PICUP. 50 μ M A β was aggregated in the presence of varying ratios of PCAH2 and PICUP conducted to reveal any oligomeric species present in the samples at an endpoint of 120 minutes. An increase in intensity of monomeric A β , a single band at \sim 4.5 kDa, was observed at an A β :PCAH2 ratio of 1:1 (Figure 6 (a)). Monomer band intensity was seen to increase by \sim 12 % in the presence of PCAH2 when quantified using ImageJ software.

A potential diffuse oligomer band is also present at \sim 21.5 kDa (tetramer/pentamer) which again is more intense in the presence of equimolar PCAH2, compared to A β alone, and dose dependently decreases as the peptide ratio decreases (Figure 6 (a)).

Additionally, a higher molecular weight oligomer band is observed towards the top of the gel, ranging from \sim 100-200 kDa in accordance with the marker, upon A β aggregation across all T120 wells. This oligomer does not appear overly altered in the presence of PCAH2 and presents with around the same intensity across all endpoint wells with 1:1 again presenting the highest intensity band (Figure 6 (a)).

Subsequent timepoint PICUP experiments were conducted in which individual snapshots, relevant to the ThT-monitored A β aggregation time course, were captured in the presence and absence of the PCAH2 peptide.

When timepoint PICUP was carried out using a 1:1 ratio of A β to PCAH2, the monomer band was found to be present at higher intensity in those wells containing PCAH2 across the timepoint aggregation. At T0 the monomer band was roughly the same intensity for A β alone and with PCAH2 present, then as time proceeds the monomer band is diminished in A β only wells relative to those containing PCAH2. Band quantification of monomer at T0 vs. T120 using ImageJ demonstrated a reduction in monomer intensity of \sim 64 % for A β only compared to \sim 50 % for A β aggregated in the presence of PCAH2, indicating a slowing of aggregation (Figure 6 (b)).

The oligomer band at \sim 21.5 kDa marker fades quicker in the A β only wells compared to those containing PCAH2. Additionally, the higher molecular weight oligomer band (\sim 100-200 kDa) is not present in either A β only or A β with PCAH2 wells and then, as aggregation proceeds, appears more readily in the A β only wells relative to PCAH2 wells. This higher molecular weight oligomer band remains low across the time course of the experiment for A β in the presence of equimolar PCAH2, with a potential decrease after T60 (Figure 6 (b)).

Photo-induced cross-linking of A β demonstrates that PCAH2 also alters monomer and oligomer status during A β aggregation at lower stoichiometry. When observing A β timepoint aggregation with the sub stoichiometric ratio of PCAH2 at 1:0.5, the monomer band at ~ 4.5 kDa fades much quicker for A β only wells as time proceeds compared to those where the peptide is present. For the A β with PCAH2 the monomer band remains at a higher intensity compared to A β only at each timepoint, with the greatest distinction observed at T120 with A β alone presenting an ~ 83 % loss of monomer against T0 A β compared to just ~ 7 % as observed when PCAH2 is present (Figure 6 (d)). This further corroborates the notion that PCAH2 is slowing the aggregation of A β , even more so than the above timepoint PICUP at equimolar amounts of PCAH2.

The oligomer smear is also present in this gel at ~ 21.5 kDa. Similar to 1:1, the oligomer smear is more intense in A β with PCAH2 than A β alone and is only present in A β alone at T20 where it rapidly disappears across the timepoints as aggregation proceeds. The fading of this oligomer smear across the timepoints is slower when the PCAH2 peptide is present, suggesting that the aggregation is slowed.

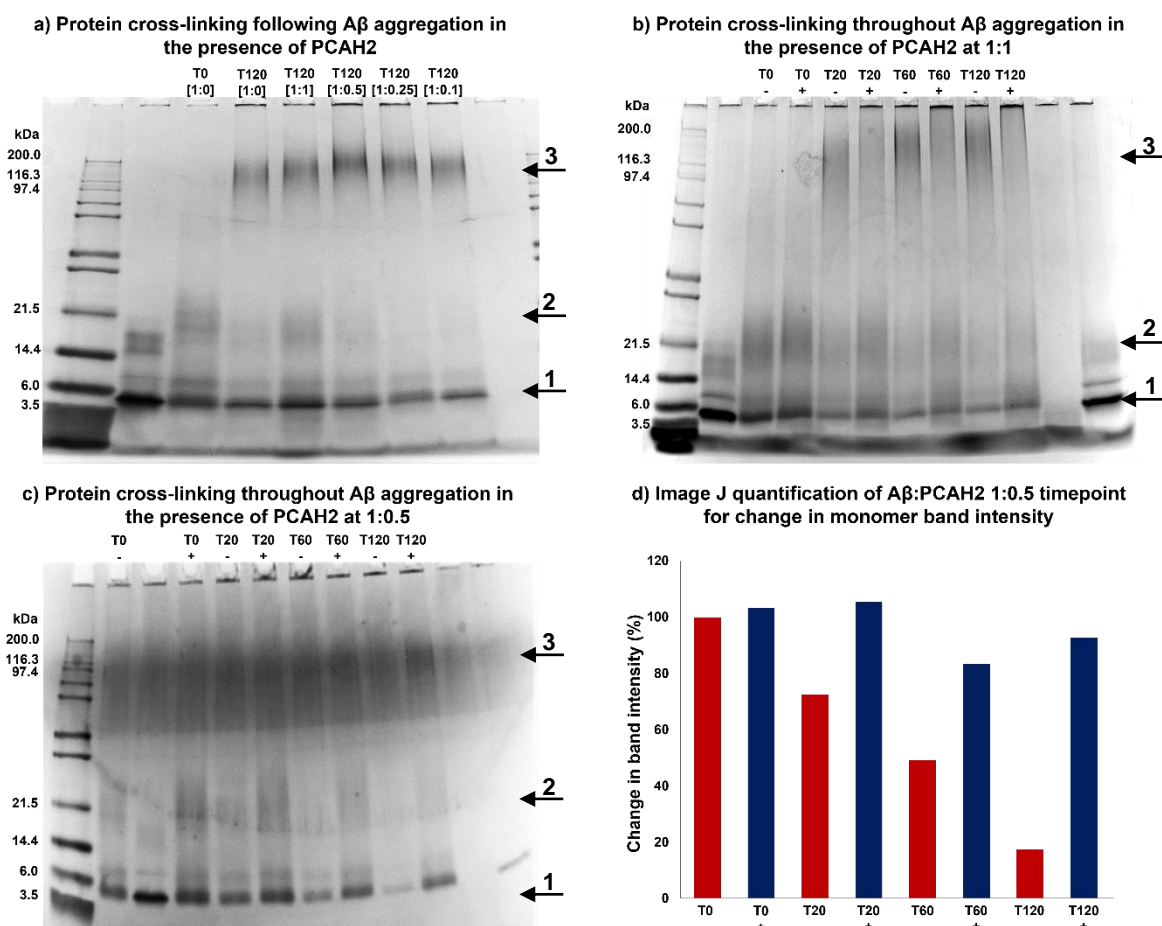


Figure 6: Photo-Induced Cross-linking of Unmodified Proteins (PICUP) of Aβ at various aggregation states with PCAH2. **a)** Following aggregation of 50 μM Aβ with varying stoichiometries of PCAH2, PICUP was carried out and samples run on 16 % SDS-PAGE gel to separate the various oligomeric species of Aβ present within the samples. A no RuBpy control was conducted in Lane 2 and an SDS-Buffer only sample in Lane 9. **b)** PICUP was carried out at various timepoints throughout aggregation of 50 μM Aβ in the presence of 1:1 Aβ:PCAH2 to create a snapshot of oligomeric species present throughout the aggregation process. A no RuBpy control was conducted in Lane 2 at T0 and Lane 12 at T120 whilst Lane 11 represents PCAH2 only at T120. Samples marked + contain PCAH2 and those with – are Aβ alone. **c)** Timepoint PICUP samples of 50 μM Aβ aggregation with 1:0.5 Aβ:PCAH2 to explore how PCAH2 alters Aβ throughout aggregation as opposed to endpoint. A no RuBpy sample is represented for T0 in Lane 3 and T120 in Lane 12. A peptide only sample at T120 is also shown in Lane 11. Samples marked + contain PCAH2 and those with – are Aβ alone. For each PICUP gel the band intensity at each monomer/oligomer band was quantified using ImageJ software (all data not shown). A dark stain on the 1:0.5 gel means that quantification of any higher weight oligomer for this gel was not possible (c). Across all gels, arrow 1 marks the 4.5 kDa band, arrow 2 marks the approximately ~ 21.5 kDa band and arrow 3 marks the ~ 100-200 kDa band. **d)** An example of ImageJ quantification analysis for c) of the monomer band using T0 Aβ only as 100 % control. Samples marked + contain PCAH2 and those with – are Aβ alone. The rate at which monomer band intensity decreases is less in the presence of PCAH2.

A β induces toxicity to differentiated but not undifferentiated SH-SY5Y cells as determined by visual observations of morphology and MTT turnover (see chapter Four). Following *in vitro* experiments that monitored broad aggregation profiles (ThT), secondary structure (CD), fibril morphology (TEM) and oligomeric state observed over the ThT-monitored time course (PICUP), we next sought to evaluate the ability of PCAH2 to protect neuronal cells against A β pathology. To do so an A β toxicity assay was optimised using the neuronal SH-SY5Y cell line using MTT assays. First, monomeric A β was directly applied to undifferentiated SH-SY5Y cells which provided only a limited toxicity profile (Figure S3 (a)). However, in agreement with Krishtal et. al., it was observed that, upon differentiation, SH-SY5Y cells were more sensitive to A β -induced toxicity, providing a promising platform in which to evaluate the potential of peptides to rescue cell viability (Krishtal et al., 2015, 2017). Treatment with monomeric A β at a final well concentration of 1 - 5 μ M on to differentiated SH-SY5Y cells provided a clear observable dose response with up to ~ 57 % toxicity (48 hrs, 2.5 μ M A β) using MTT as a measure of cell viability. This provided a sufficient toxicity window in which to evaluate the potential of PCAH2 to rescue cell viability (Figure 7 (b)). The quantitative measurement of A β toxicity on differentiated SH-SY5Y cells using MTT assays is further supported with analysis of cell morphology where there is firm evidence of cell stress, for example visibly shortened neurites and apoptotic cell bodies following 48 hr incubation with A β compared to no A β control (Figure 7 (b)).

Co-application of PCAH2 partially rescues A β -induced toxicity in differentiated SH-SY5Y cells. Following optimisation of the A β toxicity assay, PCAH2 was next applied to cells at various ratios to evaluate the ability of the peptide to restore MTT monitored cell viability. Cell-based assays were conducted at both 2.5 μ M and ~ 5 μ M A β (Figure S3 (b)) to allow for consistency with ThT analysis which was run at 5 μ M A β . Unfortunately, ThT lacks the sensitivity of MTT so running ThT at 2.5 μ M A β provided too much noise. Therefore, to confirm a similar pattern is observed, concurrent with the 5 μ M ThT data, both concentrations were run in MTT assay with the 2.5 μ M data taking precedence. Both 5 μ M and 2.5 μ M A β provide similar levels of toxicity (Figure 7 (b)) and both experimental designs demonstrate recovery in cell viability upon application of peptide however, the lower concentration of A β applied to cells is preferable.

PCAH2 was added at the same time as the monomeric A β (pre-combined) such that A β aggregates in the context of the cell in the presence of PCAH2 and reflects the ThT setup, yet at the lower concentration of 2.5 μ M A β . PCAH2 rescued cell viability by ~ 12.5 % for the optimal A β :PCAH2 ratio of 1:0.25 following treatment with 2.5 μ M A β (Figure 7 (c)). For ratios of 1:1, 1:0.5, 1:0.25 and 1:0.1 cell viability was rescued by ~ 9 %, ~ 10.4 %, ~ 12.5 % and 9 %, respectively. This implies an inverse relationship between cell rescue and

concentration of peptide between ratios or 1:1 and 1:0.25, with 1:0.1 resulting in reduced cell rescue at this very low concentration.

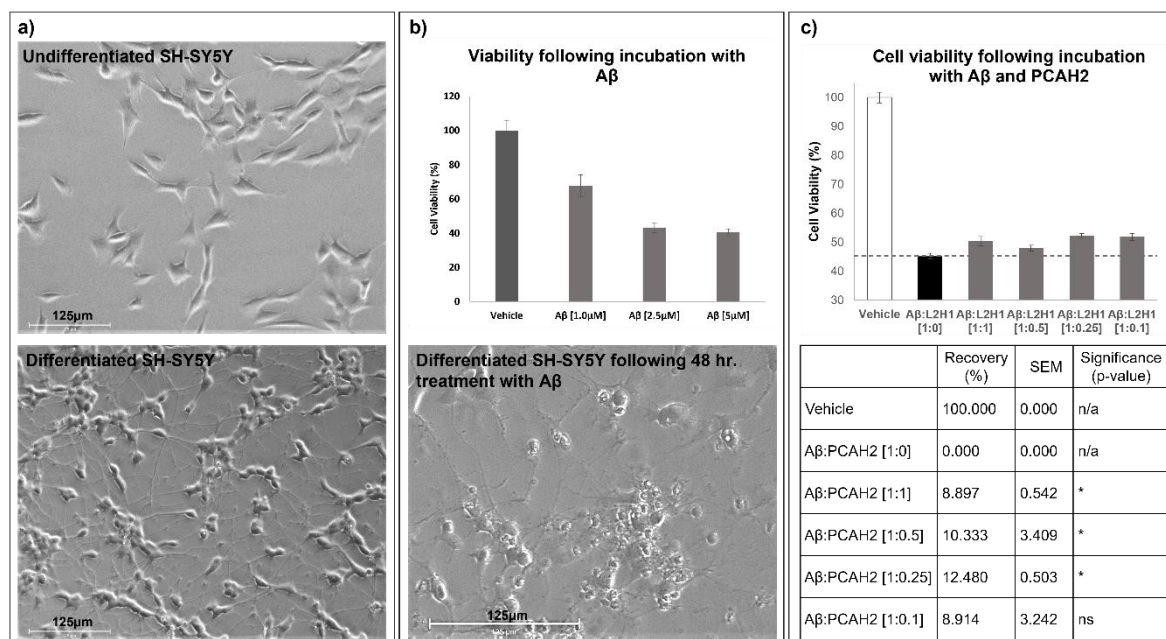


Figure 7: Aβ induces toxicity upon differentiated SH-SY5Y cells that is partially rescued in the presence of PCAH2. a) Morphometric assessment of SH-SY5Y prior to differentiation and post-differentiation with sequential treatment with RA and BDNF. **b)** Monomeric Aβ was applied to differentiated SH-SY5Y cells at varying concentrations including 1.0 μM, 2.5 μM and 5.0 μM, and, following incubation at 37 °C for 48 hours, an MTT assay conducted to evaluate cell viability. **c)** Co-application of monomeric 2.5 μM Aβ (final well concentration) with PCAH2 at varying ratios was applied to differentiated SH-SY5Y cells and, following a 48 hour incubation, cell viability was measured using an MTT. Cell viability bar chart shows one repeat of an assay due to varying toxicity windows between each repeat. Error bars represent SEM. The percentage recovery table has been calculated for assay repeats with each assay standardised to the toxicity window. For vehicle, Aβ:PCAH2 [1:0], [1:1] and [1:0.5] n=3, for Aβ:PCAH2 [1:0.25] and [1:0.1] n=2 with each experimental repeat containing three technical repeats. Following a one-way ANOVA with subsequent Tukey's post-hoc multiple comparison test on the compiled data set, significant rescue of cell viability was observed for Aβ to PCAH2 ratios of 1:1, 1:0.5 and 1:0.25 compared to Aβ only where * = P<0.05 and ns =P>0.05.

Discussion

In order to screen for peptide inhibitors of Aβ a peptide library was constructed based upon a recent cryo-EM structure of the protein. The library design incorporated a degree of scrambling at some residues that enabled residue options to remain open towards the N-terminus of the peptide. Due to the self-recognition element of residues 16-22 (KLVFF), important for Aβ self-recognition and assembly (Watanabe et al., 2001), this region was subjected to a more rational approach with incorporation of mostly hydrophobic residues

towards the C-terminus of the peptide. This was to preserve this hydrophobic binding region that is crucial for A β recognition and aggregation that is essential for the peptide to bind A β .

Following the PCA screen, residues selected within the resulting peptide sequence (YAVFHPKTVFFVE) at given positions were found to confer varying characteristics. For example, some positions led to the selection of more benign residues like that of Ala at position 11 (E11A). This was selected for from a largely scrambled pool that included the wildtype Glu. The benefit of presenting an Ala over Glu may serve by hindering charge interaction presented by the charged Glu. On the other hand, some positions selected residues with enhanced hydrophobicity like that of residue 21 in which Val was selected for over Ala (A21V). This was observed particularly at the C-terminal end of the peptide and may enhance the self-recognition properties within this region of the A β sequence. The increased hydrophobicity presented by Val may serve to guide the PCAH2 peptide in to preferentially binding to a central, hydrophobic core within the A β peptide. Additionally, the branched-chain Val may present higher steric hinderance within the fold of the protein as opposed to Ala present in the wild-type sequence. Interestingly, a central Pro (Q15P) was also selected for within a pool of largely scrambled residue options, potentially serving as a β -sheet blocker in a similar mechanism as that proposed for iA β 5 (Wood, Stephen J. et al., 1995; Soto et al., 1998) (Figure 2). The above suggestions regarding precise properties of amino acid selections are currently speculative since the properties of each residue has not been specifically explored using high resolution structural techniques.

Additionally, the peptide sequence identified by the PCA screen has selected for a c-terminal sequence similar to that of the A β (KLVFF) motif that has been identified as a key region for A β self-recognition and subsequent aggregation (Tjernberg et al., 1996). PCAH2 harbours the VFF motif followed by the library conserved Glu that may confer optimal recognition of the A β target. Tjernberg. et. al. (1996), adopted an Alanine scan to identify the crucial residues within this sequence motif and revealed residues 16, 17 and 20 as highly influential. The conservation of residue 20 within PCAH2 may therefore be important for peptide recognition towards the A β sequence. Further studies also revealed that applying the KLVFF motif as a pentapeptide against A β aggregation presented the possibility to reduce A β aggregation, with the incorporation of d-amino acids providing an additional peptide that preserved the potential to reduce A β aggregation but also allowed for greater protease stability (Tjernberg et al., 1996; Tjernberg et al., 1997). In addition, two peptides based upon the KLVFF motif, OR-1 and OR-2, along with the subsequent RI-OR2 which presents a retro-inversed version of OR-2, also contain this VFF motif and all demonstrate promising potential to inhibit A β aggregation, with OR-2 and RI-OR2 also presenting the ability to rescue A β -induced toxicity within cells (Austen et al., 2008; Taylor, M. et al., 2010). The sequence similarity between the KLVFF based peptides and the C-terminus of PCAH2 presents optimism towards the peptides potential.

Biophysical characterisation of the PCAH2 peptide hit was subsequently conducted to explore how the peptide interacts with A β to impact upon the aggregation process. The PCA screen utilised the arctic A β ₁₋₄₂ (E22G) mutant to increase the selection stringency of the screen and identify peptides that are able to detoxify this aggregation-prone mutant form. Selected peptides against this more toxic form are predicted to increase assay stringency with potential for increased effectiveness against the wild-type sequence. Therefore, the proceeding characterisation of the peptide hit employed wild type A β .

ThT fluorescence monitored aggregation assays were conducted, alongside the control peptide iA β ₅, and revealed a modified A β aggregation profile in the presence of PCAH2 relative to A β (Figure 3 (a)). The iA β ₅ peptide was identified by the Soto group where they incorporated the β -sheet breaker residue, Proline, throughout the self-recognition motif of the A β sequence (residues 16-20) (Soto et al., 1996). iA β ₅ has previously been shown to inhibit A β aggregation both *in vitro* and *in vivo* and is capable of dissolving preassembled A β fibres *in vitro* (Soto et al., 1998). The use of this control peptide is a suitable reference point for PCAH2 due to its ability to perturb aggregation and misfolding of A β as monitored by ThT, as well as a similarity in the presence of a central Pro residue that was speculated to be important in functioning as a ' β -sheet breaker.'

Not only did PCAH2 effectively slow the aggregation of A β and lower overall amyloid load at equimolar molar ratios, it did so more than the iA β ₅ control applied within our assay. Although the original iA β ₅ study documented a greater reduction in ThT fluorescence than was achieved here, with ~ 55 % reduction at the endpoint, this paper applied an outdated approach towards ThT measurements and utilised a super-stoichiometric amount of peptide, so direct comparison is difficult (Soto et al., 1996). The aforementioned KLVFF based peptides have also been applied to ThT aggregation assays to monitor their effect on A β aggregation. Austen et al., applied KLVFF as a control peptide in their exploration of the novel OR-1 and O2-1 peptides. Here, KLVFF presented no effect on A β aggregation at any concentration (Austen et al., 2008). However, the OR-1 and OR-2, including the retro-inversed R1-OR2, peptides presented complete inhibition of A β aggregation across comparable A β :peptides ratios over a 12 day period, considerably longer than applied within this study for PCAH2 (Austen et al., 2008; Taylor, M. et al., 2010). Additionally, various other peptide inhibitors have been explored using ThT and demonstrated apparently more effective reductions in ThT aggregation profiles than for the PCAH2 peptide, including the RD2 and D3 peptides (van Groen et al., 2008; Brener et al., 2015) (van Groen et al., 2017). ThT assessment for these peptides were carried out following a 6 day incubation with a final endpoint read, utilising A β :peptide ratios ranging from 1:1 up to 1:100.

Comparison between the ability of PCAH2 to alter A β aggregation as assessed by ThT is important, however none of the alternative peptides mentioned above have currently

progressed further in to clinical trials and an alternative approach may be what is required for the success of a peptide as a therapeutic. Potentially, the lessened prevention of A β by PCAH2, as measured by ThT, may provide an advantage over complete elimination of aggregation due to the proposed native function of A β oligomers within healthy, physiological conditions. Additionally, each ThT experiment carried out alternative methods, for example, for the peptides described above, each had an extended incubation time, with some up to 12 days, as opposed to the short incubations utilised in this study and many were conducted with high concentration of peptide. Therefore, direct comparison between the peptides is difficult and perhaps the most reliable way to compare the ThT aggregation profile with previous peptide sequences is through the concomitant iA β ₅ peptide control undertaken within this study, of which PCAH2 presents greater potential to alter the ThT aggregation profile.

Interestingly, the effect by PCAH2 is most promising at sub-stoichiometric conditions which provides promise for future therapeutic applications (Figure 3). Although the alteration in A β aggregation is relatively small in relation to the A β aggregation profile, it is important to note the large impact that delaying onset by just a small amount of time may have in a disease setting. It is predicted that by 2050, 9.1 million individuals in the US will have AD. By delaying the onset by just one year it is thought this number could be decreased by 14 %, while delaying onset by five years could decrease this number by 41 % (Zissimopoulos, Crimmins and St Clair, 2014). Therefore, even small delays to A β aggregation could impact significantly upon AD progression.

Applying both endpoint and timepoint CD to identify the global secondary structure of A β also provided additional evidence that PCAH2 can impact upon A β aggregation throughout aggregation and at the endpoint (Figure 4). The CD spectra also revealed that the 218 nm minima red-shifts towards 200 nm in the presence of PCAH2 which has been suggested to be due to an increase in β -strand twists. The preceding aggregation experiments revealed that A β has the greatest potential to reduce the overall fibrilisation at the endpoint at sub-stoichiometric levels as opposed to equimolar amounts (Figure 3). However, in endpoint CD experiments the 1:1 ratio appears to reduce β -sheet formation to the greatest extent (Figure 4 (a)). For acceptable signal to noise, CD scans were taken at 50 μ M A β compared to 5 μ M for ThT which may account for differences observed. Reassuringly though, the overall trend that PCAH2 alters formation of β -sheet during A β aggregation, is confirmed by both ThT and CD.

In addition, TEM suggests a reduction in A β aggregation in the presence of PCAH2 with no change in fibril morphology (Figure 5 (a-c)). It is important to note that there could be potential bias in selection of images and the inability to cover the full sample whilst searching for fibrils to image as not every species on the grid can be observed and represented.

Therefore, a lack of the dense A β aggregates in peptide samples relative to A β only samples does not provide firm evidence of a more dispersed fibrillar presentation, but rather an observation obtained upon imaging. In future TEM studies, capturing a snapshot of A β fibrils in the presence of PCAH2 at relevant time-points throughout the early stages of aggregation would be more beneficial in observing if the peptide alters the morphology of A β fibril formation and will better correlate with the ThT curves observed in which the peptide has greater effect in prolonging the lag-phase to exponential transition.

An interesting element of this study was the application of protein cross-linking studies. PICUP experiments demonstrated an increase in monomer band in wells containing A β :PCAH2 compared to the sample lacking PCAH2 at the endpoint and throughout aggregation (Figure 6). This suggests that the presence of PCAH2 is slowing the aggregation of A β as there is more monomer present at the endpoint compared to sample lacking PCAH2 and this band was shown to decrease slower throughout aggregation when the peptide was present, perhaps due to less monomer being pulled in to aggregates of A β , suggestive of a slower aggregation.

For the A β aggregation at endpoint PICUP experiment, there was also a diffuse oligomer band at ~ 21.5 kDa (potentially a tetramer/pentamer) observed that is also more intense in the presence of equimolar PCAH2 when compared to A β in isolation. This band also dose dependently decreased as the peptide ratio decreased for the endpoint PICUP gel (Figure 6 (a)). According to ThT and cell toxicity data, sub-stoichiometric ratios of PCAH2 provide the greatest reduction in endpoint aggregation and cell viability rescue, raising the question as to which species is the toxic oligomer. 1:1 shows increased intensity of the monomer and oligomer bands whilst this is not observed to the same extent in the lower stoichiometries. One possibility is that, at a ratio of 1:1, aggregation is slowed but somehow provides more toxicity compared to lower stoichiometries (yet still less overall compared to no peptide) by stabilising this oligomeric species. In contrast it is possible that lower, sub-stoichiometric concentrations of peptide, somehow avoid stabilisation of this oligomer whilst still slowing overall aggregation.

For the timepoint PICUP at A β :PCAH2 1:1, the oligomer band parallel to the ~ 21.5 kDa marker fades quicker in the A β only wells, corroborating the notion that PCAH2 is slowing the aggregation of A β as it takes longer to pass through monomer to oligomer and eventually past this oligomeric phase to higher-n species. This is also corroborated by the higher molecular weight oligomer band (~ 100-200 kDa) which appears more intense in the A β only wells as it reaches these higher molecular weight oligomers more rapidly than when peptide is present, potentially as a result of reduced aggregation rate. When observing this higher oligomer band at T0, it is not present in either A β only or A β with PCAH2 wells and then develops rapidly in the A β only wells across the timepoints relative to PCAH2 wells.

Interestingly, for A β in the presence of equimolar PCAH2 the intensity of this band remains low across the timepoints and even appears to decrease after T60 (Figure 6 (b)). One possible explanation of ThT/CD/PICUP interpreted collectively therefore is that the peptide may function by reducing/slowing the production of these higher weight oligomers.

Ultimately, PICUP corroborates the previous ThT and CD data in that the peptide appears to be altering the aggregation of A β . Pinpointing the exact oligomeric species of A β targeted is difficult since it appears to vary with A β :peptide ratio. However, collectively the experiments demonstrate that PCAH2 does impact upon A β aggregation.

In order to translate this biophysical characterisation of PCAH2 towards use as a potential AD therapeutic, a cell-based toxicity assay was established within the laboratory to explore the potential of the peptide within a neuronal cell like context. Initial cell-based experiments demonstrated an increase of susceptibility of SH-SY5Y cells to A β upon differentiation of the cell line using sequential treatment with RA and BDNF, in accordance with recent studies by the Tōugu group (Krishtal et al., 2015). The lack of toxicity observed in undifferentiated SH-SY5Y cells could be due to a lack of relevant cell morphology since differentiated cells feature better defined axons and dendrites. This lack of cell morphology was observed for the undifferentiated SH-SY5Y following morphology analysis within this study (Figure 7(a)). A β is thought to exert its pathology at synapses, which undifferentiated SH-SY5Y cells lack. Upon cell differentiation, SH-SY5Y cells consequently better represent neurons, by presenting neurites and forming interneuronal networks as observed following a visual observation of morphology, providing a platform for probing A β toxicity (Figure 7 (a)). Consequently, A β induces toxicity upon differentiated SH-SY5Y cells, as confirmed by MTT cell viability assays and morphology analysis, when applied to cells as monomer (Figure 7 (b)).

Following co-application of A β alongside PCAH2, the peptide demonstrated potential to rescue cell viability within the A β -induced toxicity experiment. Interestingly, at equimolar stoichiometries of PCAH2 the cell rescue was lower than that observed for sub-stoichiometries (Figure 7 (c)). This is in agreement with ThT assays where higher stoichiometries were found to result in increased ThT signal at the stationary phase compared to sub-stoichiometric concentrations of peptide, suggesting higher fibrilisation at the endpoint. Additionally, endpoint PICUP experiments revealed that at a peptide ratio of 1:1 a diffuse oligomer band level with a 21.5 kDa marker band (tetramer/pentamer) presented at a higher intensity than for lower stoichiometries (Figure 6 (a)). Consistent with ThT and PICUP experiments therefore, although the peptide at 1:1 was shown to slow aggregation, providing more cell recovery than in the absence of peptide, it may ultimately populate this oligomer to a greater extent than at lower peptide concentrations. This may ultimately hinder the ability of PCAH2 to rescue cell viability from A β -induced toxicity relative

to lower stoichiometries of PCAH2. Overall, the peptide demonstrated greater efficacy in MTT experiments at lower stoichiometries, which is clearly beneficial in terms of dosage for potential downstream applications.

Many previous peptides identified as potential inhibitors of A β aggregation, applied super-stoichiometric ratios of A β :peptide in order to elicit an improvement in cell viability. The D3 peptide identified by the Willbold group following a mirror-image phage display, applied MTT to assess cell viability of PC-12 cells following treatment with an A β :peptide ratio up to 1:100, with 200 μ M D3 providing complete rescue (van Groen et al., 2008; Brener et al., 2015). The ensuing RD2 peptide also presented significant rescue of cell viability in both PC-12 and SH-SY5Y cells at a ratio of 1:5 (van Groen et al., 2017). Although the extent of cell rescue within these studies is greater than that observed by PCAH2, both have been carried out at higher, super-stoichiometric ratios than that for PCAH2, which shows the greatest potential at sub-stoichiometric conditions. The lower concentrations of PCAH2 required may provide greater translatability towards a therapeutic agent with smaller doses potentially required compared to these previous peptides, despite the modest cell rescue in comparison. The above mentioned RD2 study utilised undifferentiated SH-SY5Y cells, as did that by Austen et al. for the study of OR-1 and OR-2 (Austen et al., 2008). The undifferentiated line poorly represent neuronal cells and the application of differentiated SH-SY5Y cells within this study may further improve the translatability of PCAH2 towards a more disease-like setting.

The interesting revelation that the OR-2 peptide, specifically, is capable of rescuing cell viability following A β insult, compared to OR-1 that lacks this quality, corroborates the design of the PCA screen and the likely selection of PCAH2 that potentially prevents dimer formation (Austen et al., 2008). Although only speculative, library 10 – 22 was built upon a recent cryo-EM structure of A β and hoped to target dimer formation to prevent the formation of the toxic oligomeric species of A β . Whilst both OR-1 and OR-2 demonstrated the ability to reduce A β aggregation, only OR-2 was capable of altering oligomer production, demonstrating the importance of targeting A β oligomers in order to protect against A β induced toxicity (Austen et al., 2008).

Peptide mimetic techniques may be applied in the future to increase the efficacy of the peptide to rescue cell viability following A β insult. Previous studies have demonstrated an increased potential for peptides to rescue cell viability in MTT assays upon retro-inversion in which peptides, specifically KAT, L2P1 and L2P2, were converted to their D-amino acid counterparts and the sequence reversed to maintain the topology and biological activity of the peptides whilst presenting greater protease resistance, allowing for greater efficacy within cell-based assays (Acerra, Nicola et al., 2014). This may be an exciting prospect to explore in future studies to improve the ability by which PCAH2 can rescue cell viability.

Conclusions

This study presents successful application of the intracellular library screening assay PCA to identify a winning peptide sequence (PCAH2) that binds to and detoxifies arctic A β ₁₋₄₂ within *E.coli* cells. The library was based upon a recent cryo-EM structure of A β targeting the outer β -sheet strand between residues 10 and 22 (Gremer et al., 2017). The validity of the selected hit has been supported by biophysical exploration of the peptide using ThT aggregation assays, CD, TEM and PICUP which all demonstrate interaction between wild type A β ₁₋₄₂ target and PCAH2. Each portray the overall trend that PCAH2 slows the aggregation of A β and also reduces the overall amyloid load at the endpoint. The biophysical characterisation of the peptide translates nicely into cell-based assays in which the success of the peptide is further corroborated by evidence of PCAH2 rescuing A β -induced toxicity in a differentiated SH-SY5Y cell line. An interesting observation across the experiments is that PCAH2 appears to be most efficient at lower stoichiometries which will enhance the potential of PCAH2 as a prospective therapeutic, owing to lower costs and less risk of toxicity due to potentially lower dosages. Biophysical and cell-based exploration of PCAH2 against the arctic A β (E22G) would be an interesting addition to the study. The PCAH2 was selected for against this mutant form of A β within the initial screening process. Therefore, the peptide may present greater inhibition towards arctic A β as opposed to the wild-type sequence.

The sequence of PCAH2 harbours a central Pro residue that is reminiscent of the classic 'beta-sheet breaker' peptide, iA β ₅ (Soto et al., 1998), providing a potential mechanism for the peptide. Whilst suggestions have been made as to the properties of each residue and this central proline these are just speculation. Although the design of the peptide assumed interruption to the fold of A β by mimicking β -sheet residues 10-22 with preferred characteristics, such as increased hydrophobicity being selected for, PCA and subsequent characterisation carried out in this study cannot reveal how the peptide binds or to which species of A β . PCA simply reveals peptides that bind and detoxify the A β target and future characterisation of hits, such as with computational programs like InterPep that collates known protein interactions from the Protein Data Bank (PDB) to predict protein-peptide interaction (Johansson-Åkhe, Mirabello and Wallner, 2019), are needed to reveal likely mechanisms of action.

Whilst the *in vivo* nature of PCA presents many advantages in identifying peptide hits that present favourable drug-like properties within the bacterial system it may be prudent to explore the potential of translating the current PCA system in to a mammalian cell line, preferably neuronal (Remy, Campbell-Valois and Michnick, 2007; Acerra, Nicola et al., 2014). This will increase the therapeutic relevance of the peptide screening platform and

enhance the translatability of the resulting peptide hits towards successful drug candidates where they will present within human neuronal cells.

Overall, not only does the selected PCAH2 peptide sequence provide an exciting peptide that modifies A β aggregation and toxicity in itself, there's potential also for the hit to act as a precursor for second generation libraries to identify other potent peptide sequences. There is currently no cure for AD and despite controversy surrounding A β it stands as a promising target such that the above research and future research surrounding peptide inhibitors of A β are not just exciting but needed.

Supporting Information

Supporting Materials and Methods

PCR to produce library inserts for PCA. PCR was carried out using the forward primer as the template for the library DNA with annealing temperatures of 47 °C. Primers, Polymerase, dNTPs and Buffer were added to Eppendorf's in the following amounts:

Table S1: PCR reaction reagent volumes.

Reagent	Volume (µl)	
	PCR	Control
5 x Buffer	10	10
10mM dNTPs	1	1
Forward Primer (100µM)	2	2
Polymerase	1	0
ddH2O	36	37
Total	50	50

PCR Tubes were then run through the following PCR:

Table S2: PCR Run cycles to achieve successful PCR bands.

Stage	Temperature (°C)	Time (s)
Preheat Lid	105	n/a
Initial Denaturation	98	60
Denaturation	98	20
Annealing	47	60
Extension	72	60
Final Extension	72	300
Final Hold	4	∞

} x35 cycles

Reagents used:

dNTPs: BioLine (Cat. No.: BIO-39044)

Polymerase and Buffer: NEB (Cat. No.:M0530S)

The following primers were ordered from Sigma-Aldrich:

Table S3: PCR primers ordered to achieve library insert sequences from PCR.

Primer	Sequence
A β Library (10-22) Forward Primer	AAAGCTAGCTACVNKGTGNNKCATVNKAAAVNKGTGTW TTTTTRYHGAAGGCGCGCCAAAA
A β Library (10-22) Reverse Primer	TTTTGG CGC GCC

Restriction sites NheI (F primer only) and AclI (F and R primers) are highlighted in bold.

PCR Purification. If a single PCR band was obtained the QIAquick PCR Purification Kit (Qiagen; Cat No.: 28106) was used to purify PCR products. Five volumes (one volume is the volume of PCR Product) of Buffer PB (provided with kit) was added to the PCR mix. 10 μ l of 3 M Sodium acetate added if solution is violet or orange, as opposed to yellow. DNA-Buffer mix applied to a QIAquick spin column (supplied in kit) and centrifuged at 13,000 rpm for 1 minute on a table-top centrifuge. 750 μ l Buffer PE applied to the spin column and spun in centrifuge to wash DNA. Spin column centrifuged dry to remove residual buffer and spin column placed in a sterile Eppendorf. DNA eluted by adding 20-50 μ l sterile ddH₂O, incubated at room temperature for 1 minute, then spun in a centrifuge. DNA concentration was measured using NanoDrop Spectrophotometer.

If more than one band resulting from PCR, QIAEXII Gel extraction Kit (Qiagen; Cat. No.: 20051) was used to extract the required band. For bands requiring extraction by QIAEXII, PCR products were run on a 1.5% Agarose Gel at 140 V for 45 minutes and appropriate bands extracted for purification using QIAEXII Gel Extraction Kit (Qiagen; Cat. No.: 20051). 6 volumes Buffer QXI (supplied with kit) was added to each gel slice (1 volume is weight of gel slice (mg)). Incubated at 50 °C for 10 minutes then x μ l of silica resin (provided with kit) added (dependent on amount of DNA purifying) and Eppendorf vortexed to resuspend the silica. Buffer-DNA-silica solution incubated at 50 °C for at least 5 minutes, with vortexing every 2 minutes. The solution was then centrifuged for 30 seconds at 13,000 rpm and supernatant removed. Pellet washed with 500 μ l Buffer PE (provided with kit) by applying the buffer, vortexing to resuspend pellet, then centrifuging and removing the supernatant. This process was repeated twice. Resulting pellet was air-dried at 50 °C for 10 minutes. Once dry, the pellet was resuspended in approximately 20 μ l ddH₂O and incubated at 50 °C for 5 minutes. Following this, the DNA solution was centrifuged for 30 seconds and supernatant, containing the DNA, kept. The concentration of resulting DNA was measured using NanoDrop.

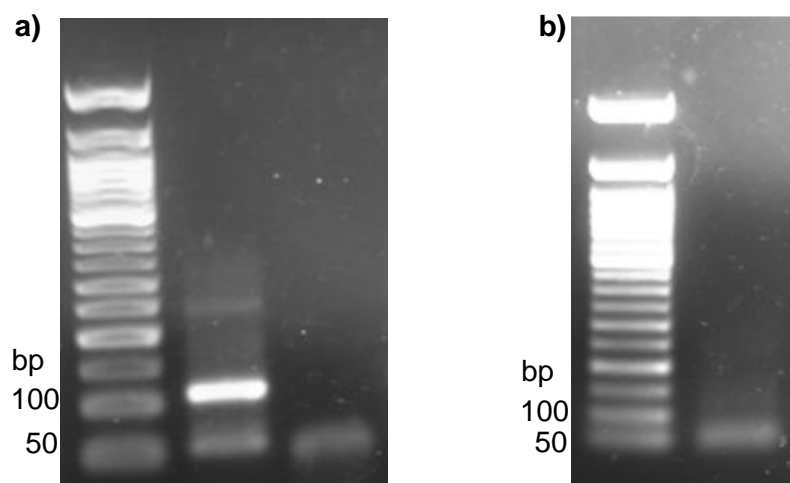


Figure S1: Library 10-22 PCR dimer insert products and resulting digest products. a) Following PCR, the forward primers self-annealed to produce library insert dimers at 120 bp. Lane 2 shows PCR reaction whilst Lane 3 represents no Polymerase control. **b)** Subsequent digestion with NheI/Ascl resulted in cleavage of the dimer PCR product and only single library insert bands remain at around 60 bp.

NanoDrop. NanoDrop 2000 (Thermofisher: Cat. No.: ND2000) was used to measure DNA concentrations. 2 μ l sample was loaded for measurement.

Restriction Digestion. Restriction digest was carried out with appropriate restriction enzymes (NheI/Ascl). The following digestion mix was used as a guideline for digestion of PCR products and plasmid DNA:

Table S4: Restriction Digest reagent volumes.

Reagent	Volume (μ l)
DNA ($\approx 2\mu$ g)	x
CutSmart Buffer	2
Restriction enzyme 1 (≈ 10 U)	1
Restriction enzyme 2 (≈ 10 U)	1
ddH ₂ O	x
Total	20

X depends on the concentration of DNA, or the volume required to make total volume up to 20 μ l.

Digestion mix was incubated at 37 °C for 3-5 hours.

Dephosphorylation of vector backbone. Following digestion of vector backbones by restriction digest enzymes, the vector backbone was dephosphorylated using the FastAP™ Thermosensitive Alkaline Phosphatase (Thermo Scientific: Cat. No.: EF0651). To a typical

digest mix the following components were added (the volumes were scaled depending on digest mix volume and amount of DNA – 1 µl of enzyme for each 1 µg of DNA):

Table S5: Reagent volumes for dephosphorylation of vector backbone.

Reagent	Volume (µl)
Restriction Digest Mix (1µg DNA)	x
10 x FastAP™ Reaction Buffer	2
FastAP™ Thermosensitive Alkaline Phosphatase	1
ddH ₂ O	x
Total	20

x depends on volume of digest mix and ddH₂O required to bring volume up to total.

The reaction was incubated at 37 °C for 10 minutes minimum.

The vector backbone was then extracted using illustra GFX DNA Extraction kit (PCA vector).

illustra GFX DNA Extraction. Following restriction digest the DNA was separated on 1 % Agarose Gel at 140 V for 45 minutes and appropriate bands extracted for purification with illustra GFX PCR DNA and Gel Band Purification Kit (GE Healthcare; Cat. No.: 28903471). To each gel slice, 500 µl Capture Buffer (provided with kit) was added and incubated at 60 °C for 30 minutes with frequent vortexing. The melted agarose-buffer solution was loaded onto a GFX Spin column (provided with kit), incubated at room temperature for 1 minute and centrifuged at 11,000 rpm for 1 minute. The column was washed with 500 µl Wash Buffer (provided with kit) and centrifuged. The column was then dried by centrifuging for 1 minute. Spin column placed in sterile Eppendorf and 15 µl ddH₂O applied to the column. This was incubated at room temperature for 2 minutes and then centrifuged at 13,000 rpm for 2 minutes. Subsequent elutions were repeated to obtain highest yield. The resulting DNA concentration was measured using NanoDrop.

QIAGEN QIAquick Gel Extraction. Following restriction digest the DNA was separated on 1 % Agarose Gel at 140 V for 45 minutes and appropriate bands extracted for purification with QIAGEN QIAquick Gel Extraction Kit (Qiagen: Cat. No.: 28704). To each gel slice, three volumes Buffer QG (provided with kit) was added to one volume gel (100 mg = 100 µl). Buffer QG/Gel slice mix was incubated at 50 °C for 10 minutes, shaking at approximately 600 rpm. Once the gel is fully dissolved, if the colour of the mixture was orange or violet (as opposed to the expected yellow) 10 µl of 10 M Sodium Acetate could be added to return the buffer colour back to yellow. The sample was then applied to a QIAquick spin column in the collection tube (both provided with kit) and centrifuged at 13,000 rpm for 1 minute (all

following centrifugation steps are carried out as described here) and flow-through discarded. 750 μ l Buffer PE (provided with kit) was then spun through the column and the flow-through discarded. To dry the column, the column was then centrifuged. 30 μ l of ddH₂O was applied to the spin column at the centre of the membrane and left to stand for 2 minutes and DNA eluted by centrifuging for 2 minutes. DNA concentration was measured using NanoDrop.

Plasmid preparation with Miniprep. Various plasmids were prepared using GeneJet Plasmid Miniprep Kit (ThermoFisher Scientific; Cat. No.: K0503). *Escherichia coli* (*E. coli*) previously transformed with desired plasmid was streaked to provide a single colony. A single colony was picked and used to inoculate 5-10 ml LB media containing the required antibiotic and incubated at 37 °C overnight, shaking at 250 rpm. The overnight culture was centrifuged at 4,500 rpm for 10 minutes and resuspended in 1 ml ddH₂O per miniprep and transferred to an Eppendorf. Cell suspension centrifuged in table-top centrifuge for 2 minutes at 8,000 rpm and supernatant removed. 250 μ l resuspension buffer (provided with kit) added to pellet and vortexed to resuspend. 250 μ l lysis buffer (provided with kit) added and Eppendorf tube inverted at least 6 times. Finally, 350 μ l neutralisation buffer added and tube inverted at least 6 times. Solution was centrifuged at 13,000 rpm for 5 minutes. The supernatant was removed and applied to a spin column (provided with kit) which was centrifuged at 13,000 rpm for 1 minute (all subsequent centrifugation as described here unless stated). 500 μ l wash buffer (provided with kit) applied to the column and centrifuged. This wash procedure was repeated twice with a subsequent centrifugation to dry the column. The DNA was eluted using ddH₂O (volume dependent on prep) by applying the ddH₂O to the centre of the column and incubating for 2 minutes followed with a 2 minute centrifugation at 13,000 rpm. Resulting DNA concentration measured using NanoDrop.

Ligation. Ligation was carried out using Electroligase (NEB; Cat. No.: M0369S) at various vector:insert ratios depending on optimised ratio. Following addition of the insert and vector the volume was made up to 5 μ l with ddH₂O and 5 μ l of 2x Reaction Buffer added. 1 μ l Electroligase enzyme was added, and the ligation mix incubated at 25 °C for 1 hour. The reaction was then inactivated by incubating at 65 °C for 15 minutes.

Preparation of electrocompetent cell lines. For library building NEB10 β (NEB; Cat. No.: C3020K) cells were used. For library screening BL21-Gold cells were used. Cell line to be made competent was streaked on LB Agar plate containing necessary antibiotics and a single colony picked to inoculate 5 ml LB Broth with antibiotics which was incubated overnight at 37 °C, shaking at 250 rpm. 50 ml 2xyt media was pre-warmed at 37 °C with appropriate antibiotics. This 50 ml starter culture was inoculated with approximately 1 ml (starting OD₆₀₀ should not be more than 0.1) of the overnight culture. This was then grown up until OD₆₀₀ = 0.6-0.8. Once sufficient growth had occurred the culture was incubated on

ice for 30 minutes with frequent inversion. The cell culture was centrifuged at 5,000 rpm for 7 minutes at 4 °C (as for all following centrifugation steps). Pellet was resuspended in 50 ml cold ddH₂O and centrifuged. Supernatant removed and pellet resuspended in 25 ml cold ddH₂O and centrifuged. Supernatant removed and pellet resuspended in 50 ml cold 15 % Glycerol and centrifuged, supernatant removed, and pellet resuspended in 25 ml cold 15 % Glycerol. A final centrifugation was carried out and the pellet resuspended in necessary volume for aliquots required (often resuspended in residual glycerol from pellet to obtain high cell density to increase transformation efficiency). Aliquots were mostly used directly for transformation to increase transformation efficiency or were snap-frozen in liquid nitrogen and stored at -80 °C.

Electroporation of DNA in to electrocompetent cells. Transformations were carried out the same for all cell lines. 990 µl 2xyt with 10 µl 100x transformation salts (0.25 M KCl, 1 MgCl₂) prewarmed at 37 °C. X µl DNA sample added to 80 µl cell aliquot (X dependent on DNA concentration and amount of DNA needed) and kept on ice. Cell-DNA mix transferred to electroporation cuvette and transformation was carried out on BioRad GenePulser II electroporation machine at 1.8 kV, 25 µF capacitance and between 200-700 Ω. Following transformation, cells were recovered in 2xyt media with electroporation salts for approximately 75 minutes and plated on M9 or LB Agar plates dependent on assay with appropriate antibiotics at suitable dilutions.

Harvesting library colonies from transformation plates. 2-10 ml LB media (or M9 if harvesting from PCA Assay plates), containing appropriate antibiotics, was applied to agar plates and the cells scraped from the surface. This step was repeated to wash the plate and ensure sufficient collection of cells. The cells were harvested into a flask and incubated at 37 °C, shaking at 250 rpm, for approximately 1 hour. The cell culture was centrifuged at 4500 rpm for 10 minutes and the pellet weight used to determine number of miniprep repeats required. The DNA was prepped using the miniprep protocol as described above.

Harvesting library colonies from glycerol stocks (used for library). A glycerol stock obtained during harvesting of library colonies from transformation plate was defrosted on ice and 50 ml 2xyt media (containing appropriate antibiotic) was pre-warmed at 37 °C. The glycerol stock was transferred in to the 2xyt media and incubated at 37 °C for 60 minutes, shaking at 250 rpm. The cell culture was then centrifuged at 4500 rpm for 10 minutes and the DNA prepared from the pellet in accordance with the usual miniprep protocol.

Expression of pET-Sac-Aβ (M1-42). The pET-Sac-Aβ (M1-42) plasmid was a gift from Dominic Walsh (Addgene Plasmid # 71875; <http://n2t.net/addgene:71875>; RRID:Addgene_71875) (Walsh et al., 2009). pET-Sac-Aβ (M1-42) was transformed in to electrocompetent BL21 (DE3) (streaked from NEB: C257H chemically competent BL21 (DE3) cells) (prepared as per protocol for preparation of electrocompetent cells previously

described). A single transformed colony was picked and used to inoculate 50 ml LB media (with Amp) for an overnight culture at 37 °C. The next day 10 ml of this overnight culture was transferred in to 1 L LB media (with Amp) and incubated at 37 °C, shaking at 250 rpm, until the OD₆₀₀ reached a value of 0.6. At this point IPTG was added to a final concentration of 1 mM and the cultures incubated at 37 °C for a further 3.5 hours. The cells were harvested by centrifugation at 5,000 rpm for 15 minutes and the pellet resuspended in 50 ml 10mM Tris/HCl pH. 8.0, 1mM EDTA buffer with one cOmplete mini Protease Inhibitor Cocktail Tablet (Roche; Cat. No.: 04693159001). This was frozen at -20 °C.

Sonication of BL21 (DE3) containing pET-Sac-A β (M1-42). The frozen cells from 1 L culture were defrosted and diluted to a total volume of 40 ml in 10 mM Tris/HCl pH 8.0, 1 mM EDTA containing protease inhibitor. The cells were sonicated (MSE, Soniprep 150 Plus) for 2 minutes (14 Amps) on ice and subsequently centrifuged at 18,000 g for 10 minutes, 4 °C. The supernatant was removed, and the cells resuspended in 40 ml 10 mM Tris/HCl pH 8.0, 1 mM EDTA containing protease inhibitor and sonication followed by centrifugation repeated as above. This was repeated a third time and the resulting cell pellet was resuspended in 40 ml 8 M Urea, 10 mM Tris/HCl pH 8.0, 1 mM EDTA to solubilise the inclusion bodies containing A β (M1-42). The cells were sonicated as above, and the resulting solution was filtered with a 0.22 μ m filter. When sonicating the cells for the 2 minutes, every 30 seconds the sonication was paused, and the probe moved up the falcon to ensure complete sonication of all cells.

Purification of A β (M1-42). Following urea solubilisation of inclusion bodies containing A β (M1-42) the resulting solution was diluted to a total volume of 50 ml with 10 mM Tris/HCl pH 8.0, 1 mM EDTA and applied to a DEAE-Cellulose column. The purification was carried out using a gradient elution on ÄKTA Pure. During the gradient elution increasing volumes of Buffer B (10 mM Tris/HCl pH 8.0, 1 mM EDTA, 500 mM NaCl) was added to Buffer A (10 mM Tris/HCl pH 8.0, 1 mM EDTA) from 0 % Buffer B to 99 % Buffer B to allow for separation of proteins within the sample. Fractions containing solutions which gave observable A₂₈₀ nm peaks were run on a 20 % SDS-PAGE gel to observe which fractions contained A β (M1-42).

Size Exclusion Chromatography (SEC) to isolate monomeric A β (M1-42). Fractions containing A β as observed on SDS-PAGE gel were pooled and subjected to SEC to isolate monomeric A β . For one round of SEC, 5 ml sample was loaded on to a HiLoad 16/600 Superdex 75 pg column (GE Healthcare: Cat. No.: 28989333) equilibrated in 20 mM Sodium Phosphate pH 8.0, 200 μ M EDTA. The SEC was run at 0.5 ml/min and protein eluted in 20 mM Sodium Phosphate pH 8.0, 200 μ M EDTA. Resulting peak fractions were run on a 20 % SDS-PAGE gel to confirm presence of monomeric A β (M1-42). Concentration of resulting A β (M1-42) was calculated by measuring Absorbance at 280 nm using Varian Cary® 50

UV-Vis Spectrophotometer and applying Beer Lambert's Law with a ϵ value of 1280. A β stock solutions were snap-frozen and stored at -80 °C. Identity of protein produced was confirmed using intact MS-MS.

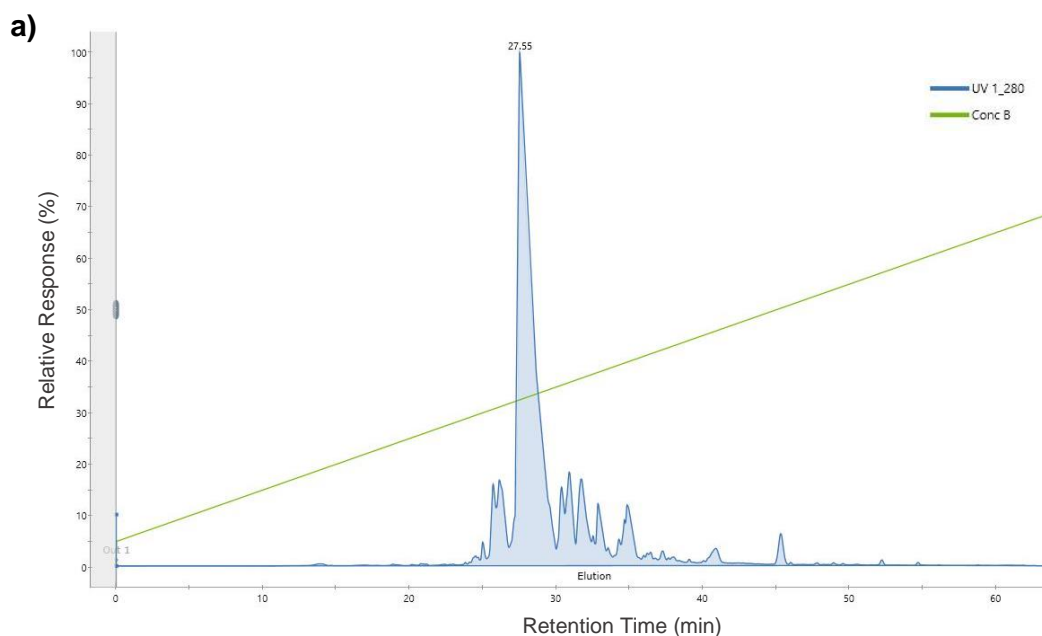
A β ₁₋₄₂ purchased from Stratech. In addition to purification of A β (M1-42) in the lab, recombinant A β ₁₋₄₂ was also purchased. Beta-Amyloid (1-42), Ultra Pure, NH₄OH was manufactured by rPeptide and purchased via Stratech (Stratech: Cat. No.: A-1167-2-RPE).

Peptide Synthesis. All Peptides were synthesised using Fmoc Solid Phase Synthesis using a Liberty Blue Automated Microwave Peptide Synthesiser (CEM: Cat No.: 925602) with the N-terminal remaining unmodified and C-terminal amidated. The peptide was built upon an H-Rink amide ChemMatrix resin (Sigma: Cat No.: 727768) with PyBop (Matrix Innovation: 1-025-0001) used as the activator base (26 g PyBop in 100 ml DMF). The deprotection reagent used was 20 % Piperidine in DMF.

The peptide was cleaved from the resin using a Trifluoroacetic acid (TFA) cleavage mix composed of 95 % TFA, 2.5 % Triisopropylsilane (TIPs), 2.5 % ddH₂O. 10 ml of cleavage mixture was added to the resin and incubated, shaking, at room temperature for 4 hours. Following this, the resin was filtered off with the TFA solution dripping into ice cold diethylether to precipitate the peptide. The diethylether/precipitated peptide mix was centrifuged at 7,800 rpm for 10 mins at -11 °C and supernatant poured off. Ice cold diethylether was added and the solution briefly vortexed and centrifuged again. This was repeated for three rounds and the final remaining peptide pellet was air-dried at room temperature overnight and then stored at -20 °C until purification by HPLC.

Purification of peptides. Peptides were purified using High Performance Liquid Chromatography (HPLC) using the C12 Jupiter® 4 μ m Proteo 90 Å, LC semi-preparative Column or preparative column (Phenomenex: Cat No.: OOG-4396-N0/OOG-4396-P0-AX). Dried pellets obtained following purification were dissolved and loaded on to the column with automatic injection by AKTA Pure HPLC system (GE Healthcare). Solvent A consisted of 0.1 % TFA in ddH₂O whilst Solvent B is 0.1 % TFA in Acetonitrile (ACN). Peptides were separated and eluted by applying a linear gradient between 5 % and 90 % Solvent B (optimised for each peptide) and fractions containing the peptide were collected with the identity of the peptide confirmed using MS. Fractions containing the peptide were lyophilised and the resulting powder stored at -20 °C until resuspension into desired buffer. Concentrations of the peptide following resuspension were confirmed using the Varian Cary® 50 UV-Vis Spectrophotometer to determine the A_{280} for peptides containing Tyrosine with an extinction coefficient of 1280 M⁻¹ cm⁻¹ or the A_{257} of Phenylalanine for peptides that lacked a Tyrosine with an extinction coefficient of 390 M⁻¹ cm⁻¹ (two phenylalanine residues).

Supporting Results



b) User Spectra

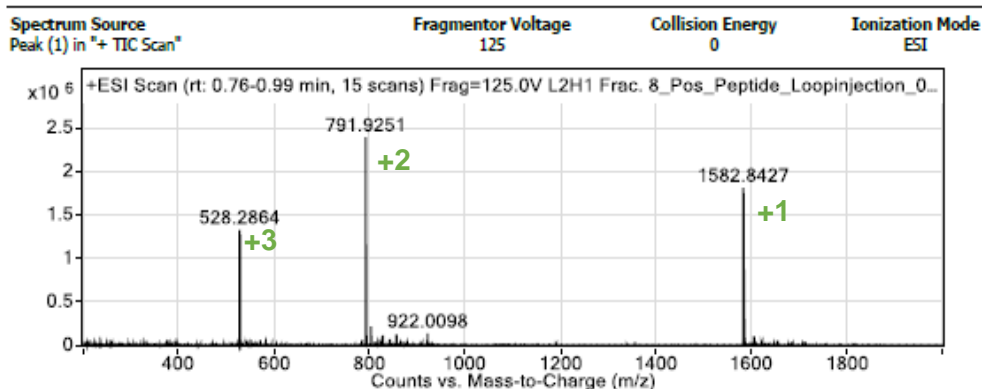
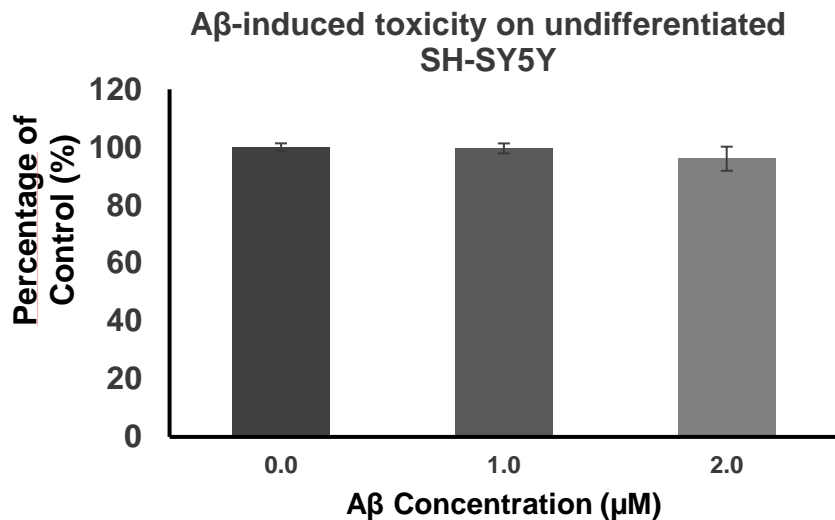


Figure S2: PCAH2 Purification by HPLC and species confirmation by Mass Spectrometry. PCAH2 was successfully produced by Fmoc solid-phase peptide synthesis (SPPS) and subsequent HPLC purification. SPPS was utilised to build the PCAH2 peptide which was subsequently cleaved and purified using a single step of HPLC. The peptide eluted with a retention time of 27.55 minutes at 32.48 % Solvent B and Mass spectrometry revealed the correct peptide had been produced. **a)** HPLC trace of PCAH2 purification. **b)** Mass Spectrometry peaks to identify PCAH2.

a)



b)

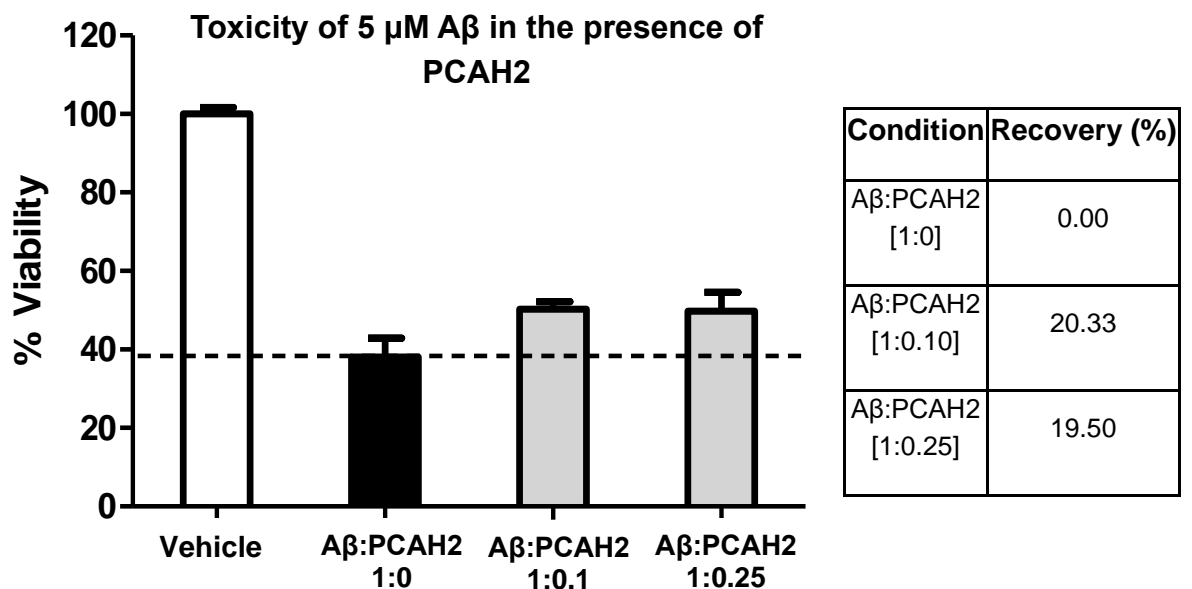


Figure S3: Optimisation of A β -induced toxicity upon SH-SY5Y cells and concurrent PCAH2 data with 5 μ M A β . **a)** Following treatment of undifferentiated SH-SY5Y cells with varying concentrations of A β , no significant toxicity was observed. **b)** Alongside the main treatment of SH-SY5Y cells with 2.5 μ M A β this concurrent assay was conducted in which differentiated SH-SY5Y cells were treated with \sim 5 μ M A β to determine whether similar trends were observed upon addition of PCAH2. PCAH2 is shown to rescue A β -induced toxicity by around 20 %.

Chapter Conclusions

The study presents the successful application of the intracellular screening assay, PCA, to identify potent, functional inhibitors of A β -induced toxicity as demonstrated through various cell-based and biochemical assays. The 655,360 member peptide library was successfully screened to identify the winning peptide sequence from PCA, PCAH2. Given the intracellular nature of PCA this was envisioned to be effective in lowering A β -driven cytotoxicity within the context of the cell. This hit was characterised and shown to hold potential for future therapeutic applications due to its ability to alter A β aggregation, as demonstrated by CD, PICUP, TEM and ThT aggregation experiments, and to reduce A β -induced toxicity in a differentiated SH-SY5Y cell line. In addition, the generated peptide sequence holds potential as a base for second generation libraries to generate more potent inhibitors of A β aggregation.

On the other hand, Library 28-42 presented limited progression despite its intriguing design targeting the dimeric interface of A β in order to theoretically thwart oligomer formation. Peptide sequences resulting from this library screen were difficult to handle throughout purification. Due to the library design targeting the central, hydrophobic core region of A β , the resulting peptide was very hydrophobic and insoluble following synthesis. Despite efforts to enhance solubilisation within a range of solvents and the addition of the CPP TAT tag, successful solubilisation was not achieved. Therefore, progression with characterisation of PCAH1 was not possible. Perhaps, second-generation libraries based upon the PCAH1 peptide sequence, modified to provide greater solubility, would be of benefit here. However, increased solubility may interfere with the ability of this peptide to target within this hydrophobic core region which is something that would need to be addressed.

To further build upon the potential to screen for peptide inhibitors of A β aggregation to identify sequences that likely prevent oligomer formation at the earliest stage, the study next sought to develop an alternative screening assay. A novel intracellular screening assay was developed that, theoretically, targets dimer formation in the form of the Transcriptional Block Survival assay, as described in the following chapter.

Chapter Four: Establishing a
Transcription Block Survival
screening assay to identify
functional peptide antagonists of
A β toxicity

Chapter Introduction

Following successful application of PCA screening we next sought to develop a novel intracellular screening assay towards specifically identifying peptides that are capable of blocking A β dimer formation. This was performed using a newly developed Transcription Block Survival (TBS) assay. To establish a proof-of-principle for the TBS assay several control experiments were conducted. Following this, a peptide library was screened within the TBS platform to explore the potential for this assay to identify 'functional' peptide hits that can impact on early A β misfolding events.

Library 28-42 holds an interesting design to be tested within this TBS assay since it maps to a region of A β ₁₋₄₂ that is located at the interface of fibrils. It also incorporates residues 41-42 that are known to be critical in converting the A β peptide to a sequence that aggregates more readily and that are strongly implicated in pathology. However, due to the significant size of the library and difficulty in synthesis and purification of the previous PCAH1 peptide along with the extensive optimisation that may be required for potential hits from this library, the decision was made to initially screen Library 10-22 as a test screen within this assay. This initial proof-of-principle screen explored the potential for the TBS platform to identify peptide sequences that can impact upon A β -induced toxicity by preventing the earliest events in the aggregation pathway. Following the initial screen, it may be worth revisiting Library 28-42 in the future. The development of this novel intracellular TBS assay, its proof of concept and application to identify peptide hits from the Library 10-22 screen has been written and prepared for publication as presented in the next section. The following manuscript refers to the previous paper outlined in Chapter Three on various occasions. The plan would be to publish the Chapter Three paper prior to the following TBS manuscript and so references would be updated to reflect this as necessary.

This declaration concerns the article entitled:			
A Transcription Block Survival screening assay to identify functional peptide antagonists of A β toxicity			
Publication status (tick one)			
Draft manuscript	<input checked="" type="checkbox"/>	Submitted	<input type="checkbox"/>
In review	<input type="checkbox"/>	Accepted	<input type="checkbox"/>
Published	<input type="checkbox"/>		<input type="checkbox"/>
Publication details (reference)	N/A		
Copyright status (tick the appropriate statement) – N/A			
I hold the copyright for this material	<input type="checkbox"/>	Copyright is retained by the publisher, but I have been given permission to replicate the material here	<input type="checkbox"/>
Candidate's contribution to the paper (provide details, and also indicate as a percentage)	<p>The candidate predominantly executed the...</p> <p>Formulation of ideas: The ideas formulated within this thesis were produced between myself and my supervisor (50 %)</p> <p>Design of methodology: The design of methodology was carried out between myself and my supervisor (80 %)</p> <p>Experimental work: The majority of experimental work was carried out by myself with the exception of cell culture prior to seeding for experimentation which was carried out by Kim Morris. Pre-Covid cell-based experiments were completed by myself. However, some elements of the cell-based assays within this section were conducted by Kim Morris as a result of post-covid laboratory restrictions (95 %)</p> <p>Presentation of data in journal format: Solely carried out by myself (100 %)</p>		
Statement from Candidate	This paper reports on original research I conducted during the period of my Higher Degree by Research candidature.		
Signed	Rebecca Carver	Date	07/06/2022

A Transcription Block Survival screening assay to identify functional peptide antagonists of A β toxicity

Abstract

It is generally accepted that a range of oligomers and their conformers of Amyloid- β (A β) impart toxicity in Alzheimer's disease (AD). Pinpointing the precise species responsible and blocking their formation has hampered the search for effective antagonists. Therefore, preventing formation of these species at the earliest point of aggregation, i.e., the formation of a dimer, to block downstream oligomer formation entirely, holds significant promise in unlocking potent inhibitors of AD. This study presents a successful proof of concept for the use of a Transcription Block Survival (TBS) assay to identify effective peptide inhibitors of A β -induced toxicity, including the use of controls. Successful application of TBS screening identified a peptide sequence that is expected to inhibit formation of dimers. This study utilised ThT aggregation measurements, protein cross-linking and circular dichroism to demonstrate that the peptide identified indeed can impact upon aggregation of A β , and when applied to cell-based assays reveals the potential of the peptide to rescue A β -induced toxicity using MTT as a measure of cell viability.

Introduction

Alzheimer's Disease (AD) accounts for around 70 % of dementia cases and effects approximately 10 % of the population over 60 (Frank et al., 2003; WHO, 2021a). AD ranks 7th leading cause of death and with no cure, only the option of drugs to alleviate symptoms, it is evident that research towards AD therapeutics are essential to address the concerning lack of disease-modifying treatments (WHO, 2020).

The lack of successful drug candidates is owing to the complicated disease progression of AD. Ultimately, the dysregulation and misfolding of two proteins, Amyloid- β (A β) and Tau, are responsible for the pathologies observed in AD brain by forming extracellular amyloid plaques and intracellular neurofibrillary tangles (NFT), respectively. Both are important targets for AD therapy however, since the formulation of the Amyloid Cascade Hypothesis (ACH) in 1992 by Hardy and Higgins (Hardy, J.A. and Higgins, 1992), much research has focused on anti-A β therapies.

The search for A β -targeted therapies has proven to be a difficult one facing much controversy with three decades of research culminating in very few to no successful drug candidates. However, the recent FDA approval to fast track Aducanumab to Phase IV trials

in the United States has reaffirmed the potential of A β -targeted therapies and the role of A β in causing AD. Aducanumab (Biogen) is dubbed the first drug to address the cause of AD, to reduce plaque burden, by directly targeting A β . Although controversial, the promise of Aducanumab indicates the potential of A β -directed therapies and opens up avenues to explore alternative methods to target A β .

It is generally accepted that the toxic isoform of A β exists as low-n soluble oligomers, although it is not known which conformer presents the highest toxicity (Mroczko et al., 2018). One approach against AD pathology is to target and prevent the formation of these oligomers. This has been attempted with small molecules and antibodies however these carry high production costs, present toxicity and often lack specificity, all of which can be overcome by the use of peptides (Mason, 2010). Whilst previous peptide studies lacked promise due to issues involving short half-life, rapid clearance, protease susceptibility and poor bioavailability, recent improvements applied to peptide mimetics overcome many of the above shortcomings and have resulted in a resurgence in research involving peptides as therapeutics (Leithold, L.H. et al., 2016; Armiento, Spanopoulou and Kapurniotu, 2020). With a peptides ability to target specific regions of interest of a protein presenting higher specificity, along with the opportunity to efficiently build and screen large, diverse peptide libraries the future of peptide therapeutics is exciting (Mason, 2010).

Numerous peptide-based approaches to target A β pathology have been explored, culminating in a lack of successful peptide drug candidates reaching clinical trials, despite exciting pre-clinical results that demonstrate alterations in A β aggregation. It is not known exactly which oligomeric conformer of A β confers toxicity and many studies created peptides based upon self-recognition elements of A β to theoretically block A β aggregation. An example of this is the sequence-derived peptides designed around the KLVFF motif, OR-1 and OR-2 aimed at targeting A β oligomer production. However, following synthesis and characterisation of the peptides it was revealed that whilst both peptides inhibited fibril formation, only one, OR2, inhibited production of oligomers. Furthermore, only OR2 rescued viability following A β -induced toxicity in cells, demonstrating the importance of targeting the production of oligomers for treatment and their relevance to AD pathology (Austen et al., 2008). Whilst peptides designed around the sequence of A β are useful tools to design peptide sequences, they require the assumption that the peptide will work as intended. It is not until the peptide has had time and money invested that the potential of the peptide is revealed and whether it influences oligomerisation as expected. Being able to select peptides for their ability to inhibit oligomer formation or know which species of A β the peptide interacts with would be of benefit.

The search for successful peptide drug candidates has been conducted within intracellular screening assays to identify peptide hits that not only bind to A β but must also detoxify it,

such as that by the Protein Fragment Complementation Assay (PCA). Accera et. al., identified the KAT, L2P1 and L2P2 peptides that demonstrated the ability to inhibit and reverse A β aggregation and their subsequent retro-inversion to aid protease resistance in mammalian cells (Acerra, Kad and Mason, 2013; Acerra, Nicola et al., 2014). However, with this PCA approach, whilst the peptide does detoxify the protein target it is not known the mechanism by which the peptide achieves this. Does it bind monomers or small oligomers to prevent oligomer formation? Or bind oligomers and push them towards inert plaques, for example? These are questions that would require exploration following identification of the hit.

Attempts have been made to screen libraries against oligomeric samples to identify hits that bind either monomer or small oligomers of A β . The Willbold group identified the D3 peptide using mirror-image phase display, an assay that utilises bacteriophage to display peptide library members on the surface (Wiesehan et al., 2003; van Groen et al., 2008). The bacteriophage is washed over a surface containing an immobilised target protein in its D-amino acid conformation. This will identify L-peptide hits that interact with the D-enantiomer of A β . Subsequent synthesis of the peptide hit sequences containing D-amino acid residues will allow for interaction with the natural L-conformer of the target protein (Schumacher et al., 1996). In retrospect, this approach proved successful following characterisation of the peptide hit using the quantitative determination of interference with A β aggregate size distribution (QIAD) assay in which density gradient centrifugation was applied to separate isomers of A β by size. Reverse-phase High Performance Liquid Chromatography (RP-HPLC) was subsequently employed to quantify the amount of each species and determine the change in size distribution of A β upon application of the peptide. This revealed the ability of D3 to specifically reduce A β oligomer levels. However, the design of the assay employed a 'low concentration' of A β in which the study 'expected' would result in monomers and small oligomers dominating the target species, rather than explicitly targeting these species (Brener et al., 2015). Furthermore, peptide binding to oligomeric samples may be too late in the aggregation process as the small, low-n oligomers recognised as the toxic conformers of A β are still allowed to form and potentially present toxicity. Being able to screen for peptide hits that are known specific binders to monomeric A β to prevent dimer formation and eliminate the production of any toxic oligomer species entirely would be ideal, something that this study addresses with the TBS assay.

In particular, the amyloid TBS assay, developed here for the first time, is utilised to screen for peptide inhibitors of A β ₁₋₄₂ dimerisation specifically. The design of TBS allows identification of peptide hits that potentially inhibit A β aggregation at the earliest stage, dimerisation, a novel and interesting prospect (Figure 2 (a)). The ability of the TBS screening platform to identify peptides that likely inhibit dimer formation holds exciting promise as successful implementation will allow for identification of peptides that intervene

before the production of any toxic oligomeric species and provides the potential to understand the form of A β that the peptide binds (the monomer). Additionally, TBS retains the intracellular advantage of PCA to provide hits that must detoxify A β to offer a growth advantage and are more likely to present protease resistance in a cellular environment. This study presents the successful development of the novel, intracellular A β TBS assay and its application to identify a peptide hit that alters A β aggregation, as demonstrated by Thioflavin-T (ThT) aggregation assays, Circular Dichroism (CD), protein cross-linking and cell-based toxicity assays.

Materials and Methods

For comprehensive materials and methods see supporting information.

TBS Assay proof-of-principle and optimisation prior to library screening.

Electrocompetent BL21-G cells were transformed with a p300d-TRE-mDHFR (Cm) plasmid and one of either p230d-A β or p230d-Basic-A β (Amp) and plated on to LB plates (Amp/Cm) (production of plasmids by PCR and ligation into relevant backbones in SI). A single colony was picked for each cell line (untagged A β and Basic-A β) and prepared electrocompetent with each cell line next transformed with an empty pQE80 (Kan) plasmid. The addition of the empty pQE80 plasmid served as a control to provide antibiotic matching to TBS screening since the library is later cloned in to pQE80 plasmid. Single colonies were picked for the two BL21-G cell lines containing pQE80-empty (untagged-A β and Basic-A β) and used to inoculate 10 ml LB (Amp/Kan/Cm) overnights. These were washed the following day with M9 media and resuspended to a final OD₆₀₀ of 0.8. Various conditions were tested in which cell volume plated was altered along with precise concentration of TMP. Conditions were explored in the following combinations:

Table 1: Combination of conditions tested to optimise TBS platform. Optimisation of TBS platform to identify optimal library screening conditions.

TMP Concentration (μ M)	4		8		16	
Volume of cells plated (μ l)	50	100	50	100	50	100

Both cell lines were plated in each condition to identify the optimal assay conditions to provide the greatest assay window for basic-A β binding to TRE sites on mDHFR (loss of colonies upon addition of the Basic tag to A β compared to untagged A β). Controls lacking protein induction by IPTG, and therefore not expected to result in cell survival, were also conducted for each condition to provide further proof that cell survival is contingent upon

the expression of the component mDHFR and A β /basic-A β proteins under control of a lac promoter.

TBS Library Screening using Single Step Selection. Electrocompetent BL21-G cells (prepared as above) were transformed with a p300d-TRE-mDHFR (Cm) plasmid and a p230d-Basic-A β plasmid (Amp) and plated on to an LB agar plate (Amp/Cm). A single colony was picked, and the cells prepared electrocompetent once more. Following library subcloning (see SI for details), the pQE80-library plasmid (Kan) was next transformed into the electrocompetent cell-line. 50 μ l of the transformed recovery media was taken for LB dilution plates (1/20th) to ensure the library was fully covered. The remaining cells were placed into a total of 10 ml LB (Amp/Kan/Cm) for overnight incubation at 37 °C. The overnight was centrifuged at 4,500 rpm for 10 minutes and washed twice with M9 media and resuspended to a final OD₆₀₀ of 0.8. 50 μ l (optimised previously as above) was then plated on to each M9 plate containing 250 μ M Amp, 100 μ M Kan, 100 μ M Cm, 8 μ M TMP (optimised previously as above) and 1 mM IPTG. A control plate lacking IPTG was also plated to ensure colonies are only observed upon induction by IPTG. The plates were sealed with parafilm and incubated at 37 °C for a minimum of 48 hours to allow for colony formation.

TBS Library Screening using Competition Selection. Liquid culture growth was optimised separately to single step selection as optimal growth conditions differ between plate culture and liquid culture. Following optimisation across a range of TMP concentrations (8 μ M, 16 μ M, 20 μ M) the best growth conditions were identified at a TMP concentration of 16 μ M, otherwise all other antibiotic concentrations remained the same as for single step selection. M9 media was used to harvest and wash the TBS-active hits from single step selection M9 plates and glycerol stocks taken. The pool of cells from the harvest was referred to as Passage 0 (P₀). P₀ pool was diluted so that OD₆₀₀ = 0.4 and 50 μ l used to inoculate 50 ml M9 media (Amp/Kan/Cm/TMP/IPTG). This was then incubated at 37 °C until OD₆₀₀ = 0.4. Then 50 μ l of cells were used to inoculate the next passage, P₁, which was grown until OD₆₀₀ = 0.4 and 50 μ l used to inoculate P₂ and so forth. Concomitant controls lacking IPTG were conducted to ensure cell survival was reliant on expression of the TBS system plasmids. After multiple passages volume of cells used to inoculate starter culture was decreased to 25 μ l to increase selection pressure. DNA sequences were monitored throughout passages to give sequence averages across the clonal population in addition to individual colonies (by plating onto LB agar). This was repeated until a single, winning sequence remained in the pool where the average pool sequence provided a clean result that matched that of the individual colonies.

ThT aggregation Assays. A β +/- TBS peptide aggregation experiments were probed first by using ThT fluorescence studies at a range of concentrations. All assays were measured using a ClarioStar Microplate reader (BMG LabTech) with incubation at 37 °C under quiescent conditions. A β protein was suspended in 20 mM Sodium Phosphate Buffer, 200 μ M EDTA (a metal ion chelator to sequester metal ions and aid stability of the protein buffer) at pH 8.0, whilst TBSH1 peptide was resuspended in 20 mM Sodium Phosphate Buffer, 200 μ M EDTA at pH 5.8 to allow for complete dissolution of the peptide into the buffer. Corning™ 96-well, non-binding, Flat Bottom, Half-area microplates (Corning: 3881) were used with 100 μ l sample per well. All plates were sealed using adhesive plate foils (ThermoFisher: AB0626). Samples were prepared in triplicate containing 17.5 μ L 100 μ M A β and varying volumes of TBSH1 peptide to obtain desired protein:peptide stoichiometries of 1:10, 1:5, 1:2, 1:1 and 1:0.5 A β :TBSH1, 20 μ M ThT (0.4 μ l of 5 mM stock per well) and made up to a final volume of 300 μ l (to allow for 3 x 100 μ l repeats) with 20 mM Sodium Phosphate, 200 μ M EDTA, pH 8.0. 100 μ l of sample was transferred to each well and fluorescence measured. The focal height was set to 4.2 mm and the gain adjustment to 1200. Fluorescence was measured using an excitation filter of 440 nm, an emission filter of 480 nm and read using the bottom optic with 15 flashes per well on a spiral average with a cycle scan time of 90 seconds.

CD experiments. To determine changes in the global secondary structure of A β in both the presence and absence of peptides CD experiments were conducted. These were either as end-point experiments following complete aggregation of A β or were undertaken in a timepoint nature in which the structure was monitored using CD throughout the A β aggregation time-course. This was achieved by capturing samples of A β at various timepoints from T₀ to the aggregation endpoint, when the ThT signal had plateaued. All samples were suspended in 20 mM Sodium Phosphate buffer, 200 μ M EDTA, pH 8.0 or pH 5.8. CD measurements were undertaken using a Chirascan™ V100 (Applied Photophysics) with the sample chamber set to 37 °C for timepoint experiments or 20 °C for endpoint experiments. A 1 mm path length quartz cuvette was used (Hellma Analytics; Cat No.: HL110-1-40) with the scan ranging from 190/200 nm - 280 nm with a 1 nm bandwidth. Three scans for each sample were taken and an average obtained.

Photo-induced Cross-linking of unmodified proteins (PICUP). PICUP protocol was adapted from Rahimi et. al. (Rahimi, Maiti and Bitan, 2009) and requires careful optimisation to work successfully for any given protein. Firstly, stock solutions of 20 mM Ammonium Persulphate (APS) and 10 mM Tris(2,2-bipyridyl)dichlororuthenium(II) hexahydrate (RuBpy) (Sigma: Cat No.: 224758) were prepared in 20 mM Sodium Phosphate, 200 μ M EDTA, pH 8.0 buffer. Both timepoint and endpoint PICUP assays were conducted in accordance with data from across the ThT monitored time-course. PICUP experiments were carried out at 50 μ M A β and with varying molar ratios of A β :TBSH1 of 1:2, 1:1 and 1:0.5.

For the cross-linking procedure, 1 μ l 10 mM RuBpy and 1 μ l 20 mM APS were pipetted to the opposite sides of the bottom of an Eppendorf tube. 18 μ l sample was next added to the tube and gently agitated to facilitate mixing. The tubes were then subjected to 10 seconds of light and 1 μ l 1 M DTT solution subsequently added to quench the reaction. The cross-linked samples were next separated by SDS-PAGE (150 V for 45 minutes) to distinguish different sized species of A β present.

Preparation and Differentiation of SH-SY5Y cells. Cells were differentiated as described by Forster et. al. (Forster et al., 2016). SH-SY5Y (ECACC 94030304) cells, purchased from Public Health England's European Collection of Authenticated Cell Cultures (ECACC), were seeded on to Nunc™-treated cell culture plates (ThermoScientific: 142485) in Dulbecco's modified Eagle's medium (DMEM)/F12 with Phenol Red (ThermoFisher 42430082)((1:1 ratio DMEM/F12 media), 10 % FBS, 5 % Pen/strep, 5 % L-glutamine) at a density of 5×10^4 cells/ml and incubated at 37 °C, 5 % CO₂ for 1 day. Following this, the media was removed and replaced with Serum-free DMEM/F12 with Phenol Red ((1:1 ratio DMEM/F12 media), 10 % FBS, 5 % Pen/strep, 5 % L-glutamine) media and 10 μ M Retinoic Acid (RA) (Sigma: R2625). The SH-SY5Y cells were incubated in RA media for 3 days until the RA media was removed and replaced with Neurobasal-A media (ThermoFisher: 12349015) (1 % L-Glutamine, 1 % pen/strep, 1 % N2 neuronal supplement) and 1.85 nM Brain-Derived Neurotrophic Factor (BDNF) (Merck: B3795) and incubated for a further 4 days. After 7 days the SH-SY5Y cells were fully differentiated and ready for use in assay.

Cell viability assay by MTT. 3-(4,5-dimethylthiazol-2-yl)-2,5-diphenyltetrazolium-bromide (MTT) assays stand as an indirect measure of cell viability, probing mitochondrial function by measuring the conversion of MTT to formazan by mitochondrial enzymes. For the MTT assay, a 1 mg/ml MTT (in complete media) solution was prewarmed. The assay media was aspirated, replaced with 500 μ l MTT media and incubated at 37 °C, 5 % CO₂ for 1 hour. Following this, the media was removed and 650 μ l Isopropanol added and mixed to solubilise the remaining formazan dye. 200 μ l was transferred to a single well of a clear plate in triplicate and the absorbance measured at 595 nm using a microplate reader (BioRad, Model: iMark).

Results

We report and explore the potential of the novel intracellular peptide library screening approach, TBS. The TBS platform is a DNA binding assay that blocks transcription of an essential gene required for cell survival. For amyloid-TBS this involves fusing a short basic DNA binding region (25 amino acids corresponding to the basic region of the cJun bZIP protein) to the N-terminus of A β ₁₋₄₂, such that the first point of aggregation (i.e., dimerisation)

aligns basic regions for cognate DNA binding (Figure 1 (a-b)). Thus, in amyloid-TBS one dimerization domain (a leucine zipper) is replaced with another ($A\beta$) in order to bring the basic regions into alignment for DNA binding. TBS readout works by incorporating 15 TPA Responsive Element (TRE) binding sites into an essential gene. Here we use murine dihydrofolate reductase (mDHFR) enzyme, which is an absolute requirement for the synthesis of purine bases thus essential for cell survival.

As a transcription factor, cJun forms heterodimers with Fos proteins via leucine zipper regions. Formation of cJun-Fos dimers brings the basic regions of the proteins together to allow 'scissor-gripping' of DNA at TRE recognition sites (Worrall and Mason, 2011) (Figure 1 (a)). For the $A\beta$ TBS assay, the leucine zipper region of cJun has been replaced with $A\beta_{1-42}$, meaning that upon $A\beta$ dimerisation the basic regions align and bind to TRE recognition sites on the TRE-mDHFR (Figure 1 (b-c)). Endogenous DHFR is selectively inhibited in the TBS assay using the antibiotic Trimethoprim (TMP), meaning that cell survival is solely dependent on transcription of this modified TRE-mDHFR. In the absence of a Basic tag, $A\beta$ is unable to bind mDHFR, meaning the sequence is available to be transcribed and translated to form the DHFR protein, allowing for cell survival and colony formation (Figure 2 (a(1))). However, upon addition of the Basic region to $A\beta$, the dimeric basic region that is formed upon $A\beta$ self-association, can insert into the major groove to selectively recognise TRE recognition sites thus blocking transcription of the mDHFR, resulting in loss of cell survival (Figure 2 (a(2))). Consequently, only inhibitors capable of preventing $A\beta$ from dimerising and docking with cognate TRE sites within the mDHFR gene will rescue gene transcription and therefore cell survival (Figure 2 (a(3))).

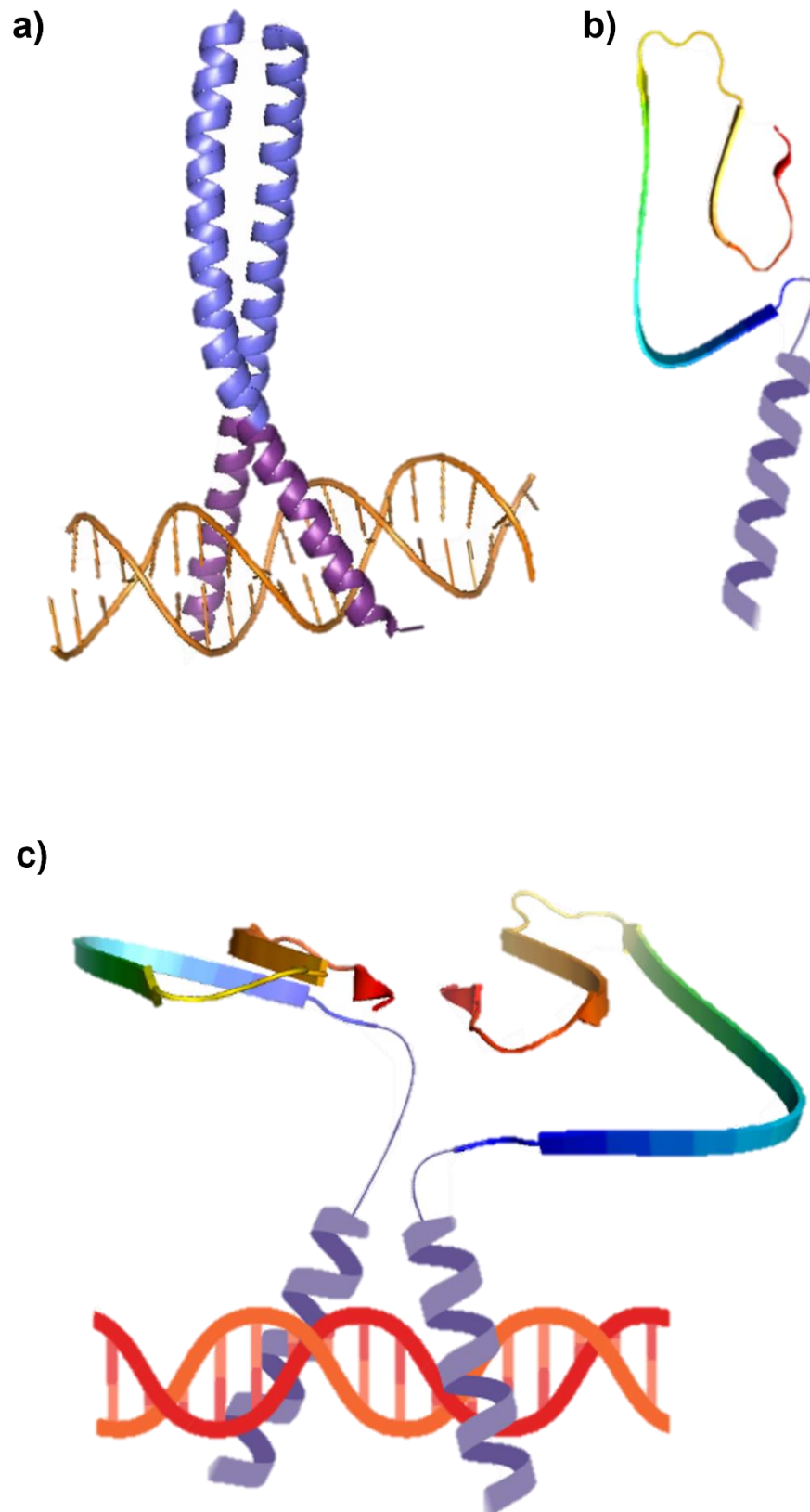


Figure 1: Concept of Transcription Block Survival Assay (TBS). **a)** cJun-cFos heterodimer scissor-gripping DNA. Image created in PyMol (PDB ID: 1FOS). **b)** Basic DNA binding region from cJun used to tag Aβ (image created using BioRender from Abeta PDB ID 5OQV). **c)** Illustration of Basic-tagged Aβ₁₋₄₂ dimerisation and scissor-gripping of DNA. This is not an accurate representation and Aβ has been rotated to demonstrate Basic-tag alignment for illustration purposes. Image created using BioRender.com.

Addition of a Basic-tag to A β inhibits cell survival in proof-of-principle assays. Prior to screening libraries using the TBS platform, proof of principle assays were required. First therefore, the ability of A β to block transcription of the survival gene TRE-mDHFR upon addition of the Basic-tag to A β_{1-42} was tested. In this assay, two cell lines were produced each containing TRE-mDHFR and either basic-A β or untagged-A β and the TBS screening platform applied. An mDHFR containing no TRE sites as a control has been conducted within the analogous bZIP TBS system and provides considerable confidence in the system by demonstrating reliance upon TRE-site recognition and binding to block transcription and cell survival.

As expected, following optimisation, loss of colonies was observed upon addition of the basic-tag to A β . The untagged-A β cell line provided an average of 75 colonies on assay plates whilst basic-A β resulted in an average of just 5 colonies, equating to an approximately 15-fold reduction and providing a firm proof-of-concept for the A β TBS Assay (Figure 2 (a(1-2) & c)).

These colonies were produced following optimisation of the assay plate conditions required to provide the largest assay window for library screening in the single step selection stage (see Materials & Methods). The optimal screening conditions identified were 8 μ M TMP with 50 μ l of OD₆₀₀ = 0.8 cell culture incubated at 37 °C for 48 hours.

TBS-active hits identified following screening of A β library 10-22. A high resolution cryo-EM structure of A β_{1-42} , harbouring a Greek-key motif common to many recent amyloid structures was used as a template to semi-rationally design a library, which has been previously discussed and screened using PCA (Chapter Three) (Gremer et al., 2017). A random sample of 100,000 members of this A β 10-22 library, has been used as a preliminary test screen to establish the potential of the TBS assay.

Following molecular cloning of the 10-22 library, this 100,000 member library was built and ~ 92 % coverage was achieved and screened through the optimised TBS platform with 100 % coverage (See Equation S1). Upon addition of the library to the TBS system concurrent untagged-A β and Basic-A β with pQE80-empty controls were repeated in which 81 and 0 colonies were observed respectively, determining the assay window for this screen. In the presence of the library with Basic-A β , 46 colonies were observed on the small M9 assay plates (representing 25 % of the total cells plated) whilst the remaining culture (75 %) was plated on to a large M9 assay plate, both of which were harvested. The presence of 46 colonies in relation to the assay window for this screen (Untagged A β (81) – Basic-A β (0)) provides ~ 57 % recovery (Figure 2 (a & c-d)).

The resulting colonies from the single-step TBS selection were harvested and taken further into competition selection in liquid M9 media. Following ten rounds of liquid competition selection passaging a final sequence was selected: YGVEHRKGVFFVE. This will be referred to from here on as TBSH1 (Table 1) (Figure 2 (b)).

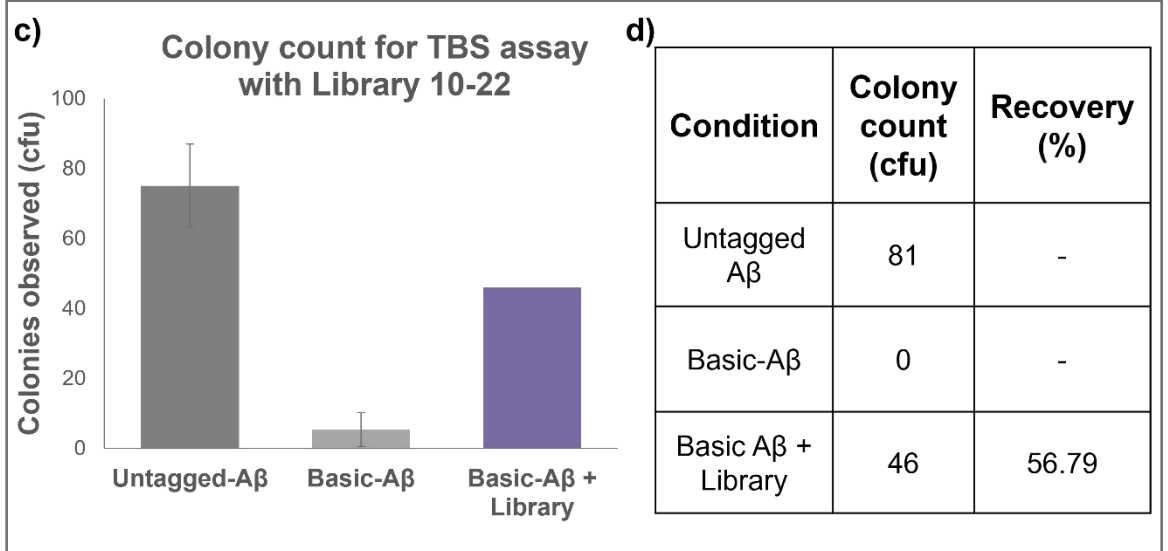
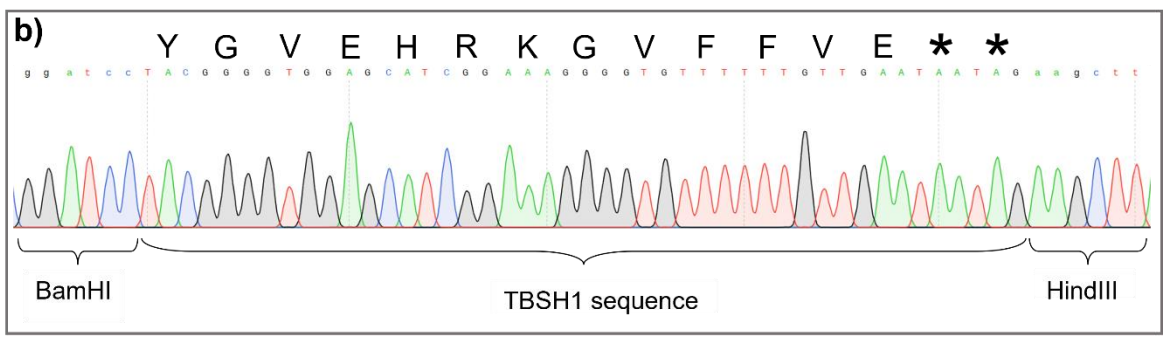
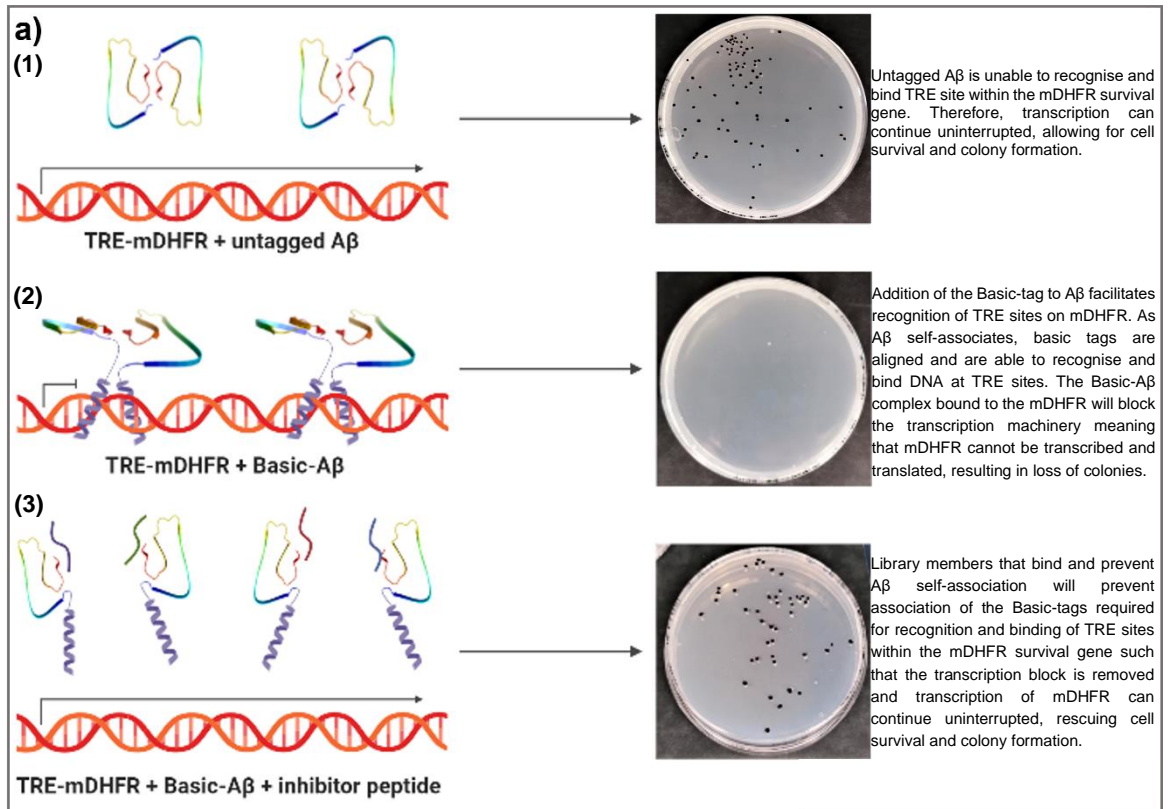


Figure legend on next page.

Figure 2: TBS Principle and application of the assay to identify a binding peptide hit.

The TBS assay is conducted within BL21-G cells containing a mutated version of the mDHFR gene with 15 TPA-Responsive Element (TRE) regions which the basic tag can recognise and bind to. Presence of the antibiotic Trimethoprim (TMP) in the assay inhibits endogenous DHFR meaning the cells survival is entirely dependent upon transcription of the TRE-mDHFR. **a)** (1) A β alone is unable to recognise and bind at the TRE mutation sites along the mDHFR sequence. Therefore, transcription is unhindered and mDHFR protein can be produced, allowing cell survival and colony formation. (2) However, upon addition of a Basic-tag to A β , dimerisation of the target protein allows for scissor-gripping of the DNA by the basic regions and blocking of transcription. This results in loss of colony formation as cell survival is dependent on transcription of this mDHFR gene. (3) Addition of peptides that block A β dimerisation will prevent the basic tags coming together, releasing the DNA for transcription of TRE-mDHFR, restoring cell survival. **b)** Sequence of TBSH1 following TBS screening of A β 10-22 library where * represents a stop codon. Resulting base peaks from LightRun sequencing are shown below the sequence, with codons aligned to relative residues. **c)** TBS proof-of-concept assays were conducted to observe loss of colonies upon addition of the Basic tag to A β . Error bars represent SEM. The library screen was conducted once hence no error bars for this condition. **d)** Representation of a single experiment to demonstrate loss of colonies upon addition of the Basic-tag to A β conducted simultaneously to the library screen to determine the assay window for that screen. Colonies counted on each assay plate is represented along with the percentage of colonies recovered with regards to the assay window.

Table 1: Sequence options throughout competition selection of A β 10-22 TBS screen.

Following single step TBS screening of A β 10-22 library, competition selection was carried out to identify the strongest TBS hit. At each passaging step the culture was pooled, minipreped and resulting DNA sent for sequencing by LightRun. The sequencing peaks obtained at each step is shown and demonstrates the variation at each position with peak colours representing different DNA bases. Restriction site bases are lower case with TAA and TAG coding for stop codons. The library template and settled sequence is shown as aligned with respective codons for each residue. The library design is shown at the top of the table where the top line is the wild type A β ₁₀₋₂₂ sequence (included as library members) and residue options shown beneath where * represents the following 16 amino acids (LIMVPTAHQNKDERSG) and ^ denotes NNK which codes for all 20 amino acid residues. Letters in black are conserved within the library design whilst red letters are altered. For passage P2 and P4 sequencing errors occurred in which no sequence was displayed, likely due to primer misalignment during sequencing.

Passage Pool	Sequence Options													
	Library 10-22 Design	Y	E	V	H	H	Q	K	L	V	F	F	A	E
		*			^		*		*		Y		V	
													I	T
		Y - V - H - K - V - F - E												
P0														
P1														
P3														
P5														
P6														
P7														
P8														
P9														
P10														
Settled sequence	Y G V E H R K G V F F V E													

TBSH1 alters course of A β aggregation as measured by ThT Fluorescence. Following successful synthesis and purification of TBSH1 (Figure S1), biophysical characterisation to reveal how the peptide might alter A β aggregation was conducted. Firstly, a ThT aggregation profile was obtained for the aggregation of 5 μ M A β with varying concentrations of TBSH1 and revealed that the peptide both increases the initial lag phase, thus slows aggregation, and reduces overall fibrilisation at the endpoint as measured by ThT.

The most effective ratio for delaying the lag phase of A β aggregation is that of 1:10 which increases the midpoint value by ~ 50 %, however at this concentration of peptide the overall fibrilisation at the endpoint is not optimal with a reduction of ~ 20 % compared to ~ 35 % for the 1:5 (Figure 3). Later cell based assays, discussed subsequently, identified the optimal A β :TBSH1 ratio to stand at 1:2. For this reason, subsequent CD and PICUP experiments were conducted using an A β :peptide ratio of 1:2.

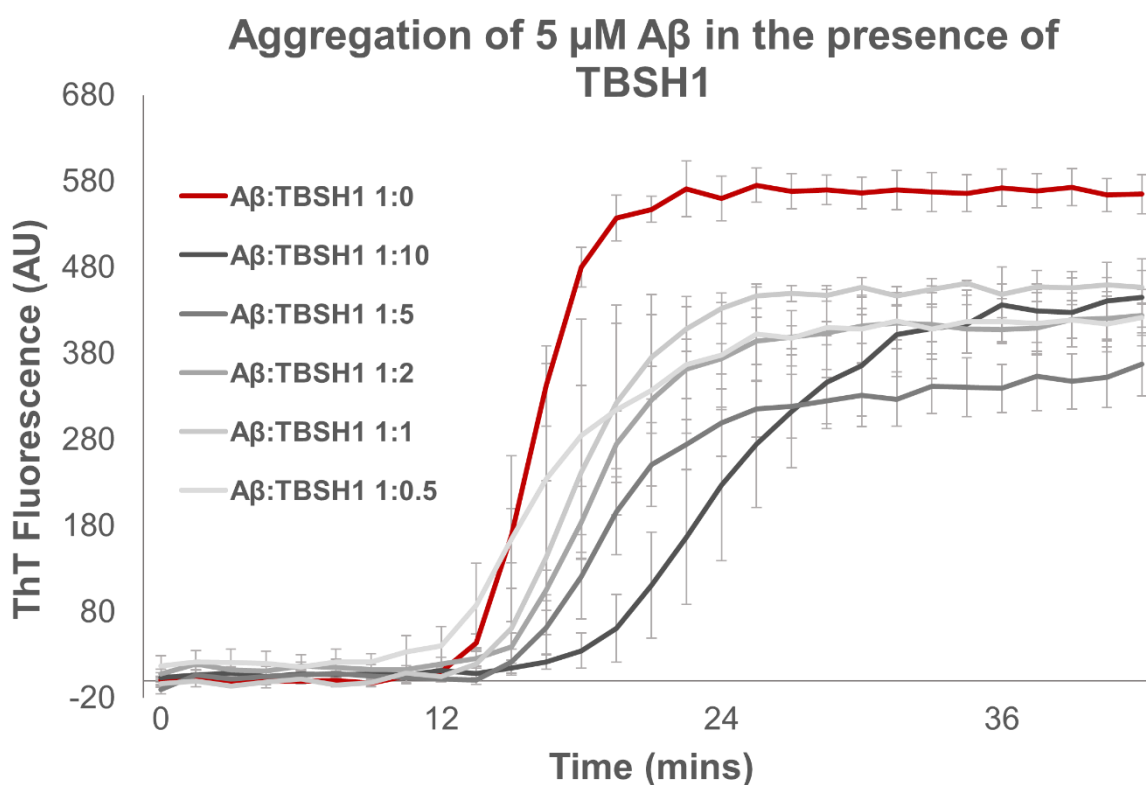


Figure 3: TBSH1 alters A β aggregation as measured with ThT fluorescence. ThT fluorescence was utilised to measure the course of A β aggregation in the presence of TBSH1. 5 μ M A β was aggregated both in the presence and absence of TBSH1 at varying ratios from 1:10 through to 1:0.5.

TBSH1 reduces global β -sheet content and rate of conversion of A β to β -sheet as measured by circular dichroism. CD experiments conducted to reveal the global secondary structure of A β at the aggregation endpoint show a reduction in the β -sheet content of A β by $\sim 18\%$ when TBSH1 is present at a ratio of 1:2 A β :TBSH1 (Figure 4 (a)).

To further explore the ability of TBSH1 to slow the aggregation of A β , as demonstrated by the prolonging of lag phase in ThT experiments (Figure 3), CD scans were conducted throughout the aggregation of A β in a timepoint manner. Timepoint CD scans reveal that TBSH1 consistently reduces the extent of β -sheet formation, as measured by formation of the 218 nm minima, throughout aggregation by between ~ 13 and 20 % across the aggregation time course with the distinction increasing as time proceeded (Figure 4 (b-d)).

Concentrations were optimised to allow successful analysis within each assay type so unfortunately ThT does not hold consistent concentrations with CD and the following PICUP experiments which were conducted at 50 μ M.

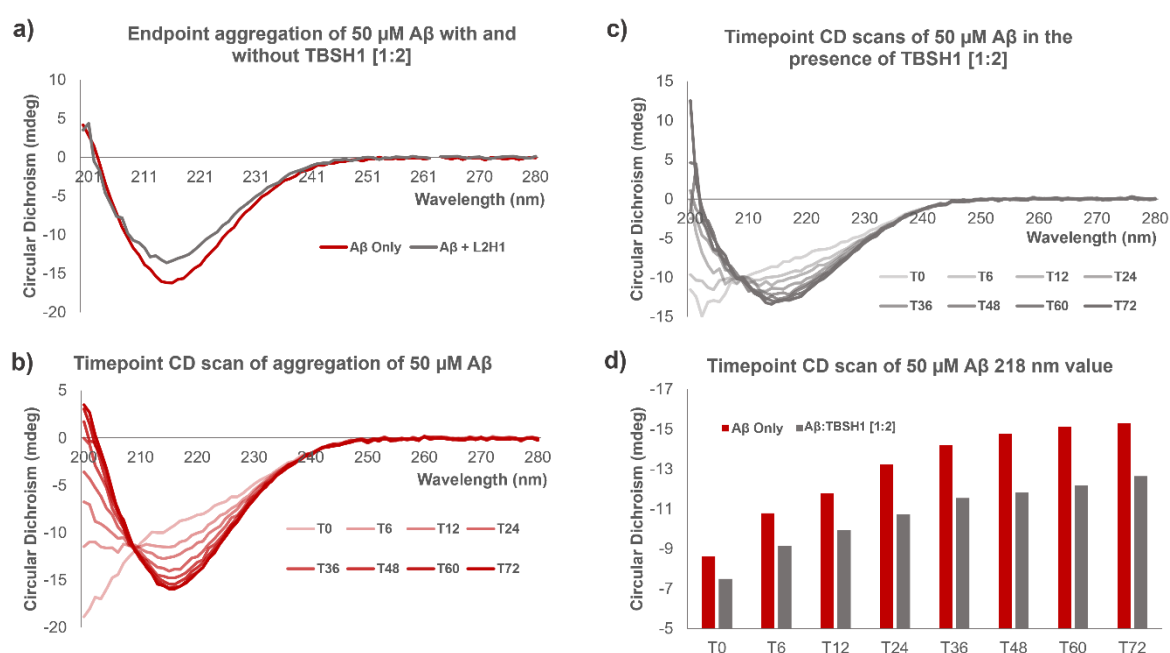


Figure 4: Circular Dichroism scans show change in extent of β -Sheet structure of A β aggregation in the presence of TBSH1. a) CD Scan of endpoint of 50 μ M A β aggregation in the presence of varying stoichiometries of TBSH1. **b)** Timepoint CD scans taken during 50 μ M A β aggregation at various timepoints. **c)** Timepoint CD scan taken during aggregation of 50 μ M A β in the presence of TBSH1 at a protein to peptide ratio of 1:2. **d)** 218 nm minima values determined by CD scans at various timepoints throughout 50 μ M A β aggregation in the presence and absence of TBSH1 reveal peptide ability to reduce β -sheet fold formation.

Photo-induced cross-linking of A β demonstrates slower aggregation of A β in the presence of TBSH1. Here, photo-induced cross-linking of unmodified proteins (PICUP) has been applied to explore the potential of TBSH1 to alter A β aggregation. An artefact created by the TBSH1 peptide, as shown in the TBSH1 only control, presents a form of cross-linked product overlapping with the size of monomeric A β at ~ 4.5 kDa. Therefore, changes in the level of monomeric A β upon addition of the TBSH1 is not possible.

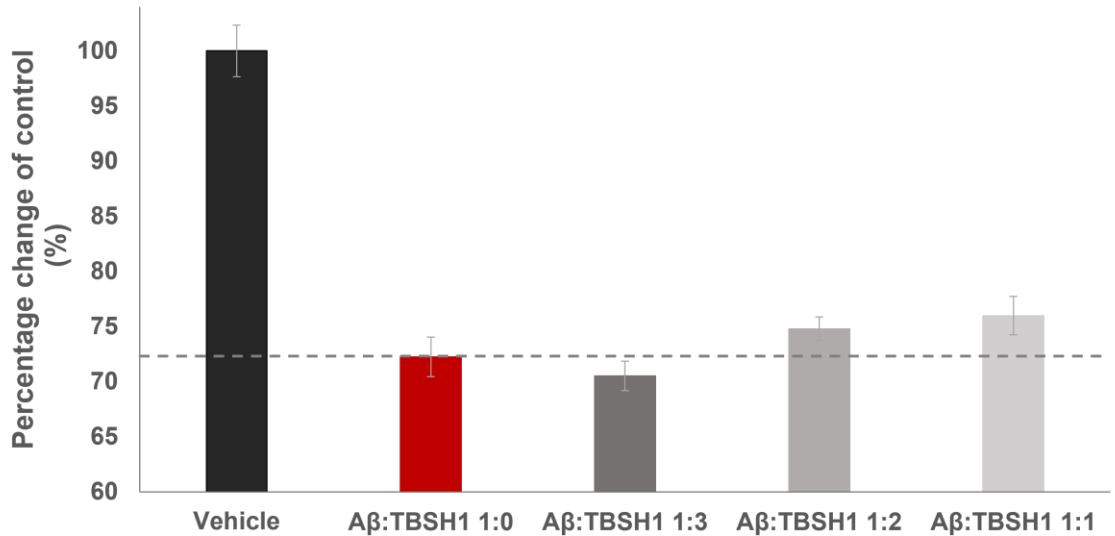
There is a dark smear present at around ~ 21.5 kDa, that increases across the timepoints of A β aggregation when the TBSH1 peptide is present at an A β :peptide ratio of 1:2. At the endpoint of aggregation, the intensity of the ~21.5 kDa band appears reduced as the peptide concentration decreases in a dose responsive manner following 120 minutes of aggregation (T120) (Figure 5).

An additional band, ranging from ~ 55 to 200 kDa, is also present towards the top of the gel. This band appears to increase in intensity throughout the timepoints as aggregation proceeds. This increase in intensity for this band appears to be thwarted in the wells containing A β in the presence of TBSH1 when compared to A β in isolation. For the TBSH1 wells, the intensity of this higher molecular weight band does not appear to change across the timepoints. At T120 the resulting band is more intense in the A β only well compared to the A β :TBSH1 well. At T120 no observable difference is observed at the higher weight oligomer band over the varying peptide (Figure 5).

TBSH1, the peptide presents some toxicity demonstrated by a reduction in cell viability by ~ 6 % +/- 1.3 SEM. Across three experimental repeats, upon co-application with TBSH1 the cell viability was rescued by ~ 14 % +/- 4.0 SEM for the optimal treatment at a 2-fold molar excess of TBSH1 (1:2) (Figure 6 (b)).

A range of A β :TBSH1 ratios were tested including 1:3, 1:2, 1:1 and 1:0.5. At a ratio of 1:3 the peptide presents toxicity and, although at equimolar amounts TBSH1 provides no alteration in cell viability at 0.4 % +/- 6.8 SEM, 1:0.5 provides partial cell rescue at ~ 9.7 % +/- 3.5 SEM recovery.

a) Cell viability of SH-SY5Y following incubation with 2.5 μ M A β with TBSH1



b)

Condition	Recovery (%)	SEM
Vehicle	100.000	n/a
A β :TBSH1 1:0	0.000	n/a
A β :TBSH1 1:3	-6.186	1.341
A β :TBSH1 1:2	14.439	4.016
A β :TBSH1 1:1	0.426	6.768
A β :TBSH1 1:0.5	9.727	3.499
A β :TBSH1 0:2	118.892	15.426
A β :TBSH1 0:3	77.384	1.923

Figure 6: TBSH1 demonstrates potential to partially rescue A β -induced toxicity in differentiated SH-SY5Y cells as measured by MTT assay. Due to differences in toxicity windows MTT values were standardised to the toxicity window and **a)** represents a single experimental repeat where, following incubation of A β at a final well concentration of 2.5 μ M for 48 hours, an MTT cell viability assay was conducted. **b)** Calculated averages across experimental repeats following standardisation to the toxicity window for each repeat with calculated SEM and significance values. Vehicle and A β :TBSH1 1:0 samples do not have SEM as standardised to 100 and 0, respectively, for toxicity window. Following One-way ANOVA analysis, no significance was observed between A β only samples and A β with co-application of TBSH1 samples. For all conditions n = 3 experimental repeats, with the exception of 1:3 and 0:3 where only one experimental repeat was conducted. Each experimental repeat has three technical repeats.

Discussion

Prior to the application of the TBS assay, proof-of-principle experiments were required to confirm that the assay worked as intended. The design of TBS implies that untagged-A β would not be expected to recognise the TRE-binding sites on the TRE-mDHFR and so transcription can continue uninterrupted. In contrast, following basic-A β dimerisation and resulting interaction of the basic regions with TRE sites within TRE-mDHFR, transcription would be blocked, impeding cell survival. This was corroborated by the proof-of-principle assays in which a loss in colonies was observed upon addition of the Basic-A β tag. Following confirmation that the assay behaved as intended, a peptide library was used to assess the potential of TBS to identify functional peptide hits.

A high resolution cryo-EM structure of A β ₁₋₄₂ that holds a Greek-key motif that is common to most recent amyloid structures was used as a template to semi-rationally design the library 10-22, which has been previously discussed and screened using PCA (Chapter Three) (Gremer et al., 2017). The outer β -sheet strand, incorporating residues 10–22, was used as the template for this library and ensured relevance across multiple structures from both *in vitro* and *in vivo* sources of A β (Figure 1 (a-e) in Chapter Three paper). Alternate residues along the β -strand (residues facing towards the hydrophobic core) were semi-scrambled to allow for selection of a peptide with potentially stronger binding properties whilst preventing self-aggregation and retaining solubility by conserving the solvent exposed residues of the β -sheet strand.

Following addition of library 10-22 to the TBS system, cell survival was recovered by ~ 57 % (Figure 2 (a & c-d)). The colonies that were rescued represent members of the library that are able to bind and revive cell survival and are therefore TBS-active, i.e., presumably bind A β to prevent dimer formation and detoxify the target. These library members underwent competition selection in order to identify a single, strongest winning hit sequence. The evolution of the sequences to emerge from TBS competition selection screening has been shown in Table 1, where relative abundance of amino acids through the selection process is represented by sequencing peaks at each residue option. The presence of various peaks at codon positions demonstrates variation in the pool for that position. As shown, the second half of the peptide sequence settled quicker than for the first half, with peak settling observed within earlier passages than for the residues closer to the C-terminus. Whilst this region of the peptide had fewer residue options incorporated in the library this is still of interest as this region is identical to that selected for in the PCA screening to reveal PCAH2 (Figure 2 (a) in Chapter Three paper). In particular the motif VFFVE was selected in both assays and potentially demonstrates the importance of this hydrophobic region for binding to A β , hence the swift settling in competition selection. Additionally, this VFFVE motif aligns well with the KLVFF sequence identified as crucial for

A β self-recognition and aggregation (Tjernberg et al., 1996). The associated pentapeptide incorporating the KLVFF motif has demonstrated the ability to reduce A β aggregation, as explored by TEM, with the incorporation of d-amino acids in the KLVFF based peptides providing additional protease stability (Tjernberg et al., 1996; Tjernberg et al., 1997). More recently, OR-1 and OR-2 have been described, along with the subsequent RI-OR2 that represents a retro-inversed version of OR-2. These peptides are also built around the KLVFF peptide and contain the VFF motif observed within both PCAH2 and TBSH1. Characterisation of OR-1, OR-2 and RI-OR2 revealed the promising potential of these peptides to inhibit A β aggregation, with the potential to rescue A β -induced toxicity within cell-based toxicity assays displayed by both OR-2 and RI-OR2, owing to their potential to inhibit oligomeric species of A β specifically (Austen et al., 2008; Taylor, M. et al., 2010). The sequence similarity between the KLVFF based peptides and the conserved sequence between PCAH2 and TBSH1 corroborate the significance of this region.

Ideally, prior to library screening a known inhibitor would have been tested in the system as a positive control exemplar. However, due to the lack of peptide inhibitors that are known to specifically interrupt dimer formation in current literature it was deemed necessary to continue with the TBS screen without such a control.

Biophysical characterisation of the TBSH1 peptide hit was conducted to explore the potential of TBS to identify functional peptide interacts that impede the aggregation of A β aggregation. Initially, ThT aggregation assays were carried out and demonstrated that TBSH1 was capable of altering the aggregation profile of A β . Whilst saturating the system with a peptide ratio of 1:10 appears to harbour the most effect in slowing the initial aggregation compared to lower ratios of peptide applied, it is important to be aware of the potential of this high concentration of peptide to result in higher overall fibrilisation at the endpoint compared to the lower ratios. Finding a suitable balance between the two factors (slowing of lag-phase and decreasing overall amyloid) was important and subsequent cell based assays, discussed later, reveal the optimum A β :TBSH1 ratio to stand at 1:2 to provide the balance between peptide toxicity and ability to rescue cell viability.

Efficacy of peptides to prevent A β aggregation encountered from ThT assays vary greatly between previously described peptides within the literature. Whilst some peptides presented limited alteration to the ThT aggregation profile of A β , namely the KLVFF based peptide, KLVFF-NH, alternative peptides such as OR1-1, OR-2 and RI-OR2 demonstrate almost complete ablation of A β aggregation as demonstrated by a flattening of the ThT profile (Austen et al., 2008). Assay conditions vary considerably between previous studies and direct comparison becomes difficult towards the ThT profile encountered here but, despite the comparably minor alteration of ThT aggregation profile presented by TBSH1, it is important to note the potentially significant impact of delaying onset by just a minimal time

may have. It has been documented that by 2050, 9.1 million individuals in the US are predicted to have an AD diagnosis. Delaying the onset by just one year could decrease this number by 14 %, whilst delaying by five years could potentially reduce this number by 41 % (Zissimopoulos, Crimmins and St Clair, 2014).

CD experiments were also conducted to reveal the global secondary structure of A β at the aggregation endpoint and reveal a reduction in the β -sheet content of A β in the presence of TBSH1 (Figure 4 (a)). A reduction in the 218 nm peak minima is indicative of extent of β -sheet formation, thus suggests a reduction in fibrilisation. This is concurrent with ThT data in which the fluorescence signal at the plateau of the ThT aggregation curves is reduced in the presence of TBSH1 (Figure 3). Additionally, timepoint CD scans corroborate ThT further by revealing a sustained reduction in 218nm minima throughout aggregation demonstrating that TBSH1 is successful in slowing the aggregation of A β .

To supplement the ThT and CD experiments, protein cross-linking was conducted to better explore the oligomeric status of A β throughout aggregation and how this changes in the presence of TBSH1. Photo-induced cross-linking of unmodified proteins (PICUP) uses the photolysis of ruthenium (II) tris-bipyridyl (RuBpy) to aid the formation of Tyrosine radicals within proteins which can then form covalent bonds with nucleophilic side chains to successfully cross-link closely associated proteins (Fancy and Kodadek, 1999). This method can be applied to amyloid proteins to provide a snapshot of different sizes of oligomer present at a certain timepoint (Rahimi, Maiti and Bitan, 2009). PICUP was utilised within this study to explore the potential of TBSH1 to alter A β aggregation.

The TBSH1 only control indicated that the peptide alone provides a form of cross-linked product, perhaps owing to the initial Tyrosine residue in the sequence of TBSH1, which overlaps with the size of monomeric A β at \sim 4.5 kDa. For this reason, changes in the level of monomeric A β upon addition of the TBSH1 could not be confidently analysed. However, when observing the dark smear around \sim 21.5 kDa, perhaps representing low-n oligomers, an increase in intensity of this smear was observed across the timepoints of A β aggregation when the TBSH1 peptide is present at an A β :peptide ratio of 1:2. Although we cannot distinguish distinct species from this broad smear, we can see that overall the rate at which this oligomer smear faded across the timepoints is quicker in the absence of TBSH1, suggesting the peptide has slowed the aggregation of A β . Furthermore, at the endpoint of aggregation, (T120), the intensity of this oligomer band appeared reduced as the peptide concentration decreased in a dose responsive manner. This suggests that the peptide is less effective at slowing the aggregation of A β at lower concentrations, concurrent with ThT data collected where this dose responsive effect is also observed; as the concentration of peptide increases the aggregation of A β is slowed to a greater extent. It must be noted that SDS-induced artefacts were observed (Bitan, G. et al., 2005; Rahimi, Maiti and Bitan, 2009)

in the no RuBpy control lane as expected which slightly overlap with this oligomer smear (Figure 5).

A higher molecular weight oligomer smear was also present towards the top of the gel ranging from ~ 55 to 200 kDa. Again, identification of a distinct oligomeric species cannot be distinguished from this band however an overall trend of these higher-n oligomers can be observed. When A β aggregates alone, as the lower weight oligomer band faded across the timepoints the intensity of this higher weight oligomer band increased, concurrent with progression through aggregation. However, in the presence of TBSH1 the intensity of this band appeared approximately the same across the timepoints such that by T120 the higher weight oligomer band is more intense in the A β only well compared to A β aggregated in the presence of 1:2 TBSH1, further indicating that TBSH1 has slowed the aggregation of A β . Across the varying peptide ratios at T120 no observable difference was observed at the higher weight oligomer band, suggesting that the peptide may take more effect upon lower weight oligomers, where a difference is observed (Figure 5).

Overall, PICUP suggests that TBSH1 has altered A β aggregation by reducing aggregation rate, in conjunction with ThT and CD data.

Following the *in vitro* experiments to measure broad aggregation profiles (ThT), oligomeric state (PICUP) and secondary structure (CD) of A β throughout aggregation in the presence of TBSH1, the study next sought to explore the effect of these changes against A β pathology in a cellular environment. The colorimetric MTT assay was used as a measure of cell viability by monitoring conversion of tetrazolium salt (MTT) (yellow) to formazan (blue) by mitochondrial activity. The greater the conversion, thus absorbance at 595 nm, reflects greater cell viability.

Co-application of A β with TBSH1 upon the SH-SY5Y cells reveals potential for TBSH1 to partially rescue cell viability, with the optimal condition resulting in ~ 14 % recovery in cell viability (Figure 6 (b)). Interestingly, upon application of a high molar ratio of TBSH1 relative to A β , the peptide becomes toxic to the cells, as observed at the ratio of 1:3 where peptide only control confers toxicity. This is an improvement on the aforementioned KLVFF-NH peptide, which decreased cell viability at a ratio of 1:1 and presented no potential to rescue A β induced toxicity within SH-SY5Y cells following an MTT cell viability assay, according to the El-Agnaf group (Austen et al., 2008). Previous studies suggest a physiological role for oligomeric A β ₁₋₄₂ enhancing long-term potentiation (LTP) in healthy brain at low, picomolar concentrations (Gulisano et al., 2018). When present at higher concentrations perhaps TBSH1 is inhibiting the native function of oligomeric A β resulting in a decrease in cell viability.

At a ratio of 1:2 the peptide no longer presents toxicity to the cell with the ratio of A β :TBSH1 of 1:2 providing the optimal recovery by ~ 14%. Whilst the 1:1 dataset is varied and results in limited rescue, 1:0.5 also partially rescues cell viability in the SH-SY5Y cell line by ~ 10 % (Figure 6 (b)). This corroborates ThT data in which 1:2 provides the greatest change in A β aggregation of the three ratios (slowing of midpoint and reduction of total fibrilisation) whilst evading toxicity in cell-based assays (Figure 3).

The theory behind the TBS platform is corroborated by cell-based toxicity assays used to explore the OR-1 and OR-2 peptides. Whilst it is important to acknowledge that suggestions as to how the TBS assay interacts and identifies A β inhibiting peptides has not been confirmed, in theory the assay should block formation of toxic oligomeric species of A β by blocking aggregation at the earliest stage, dimerisation, preceding oligomer formation. Both OR-1 and OR-2 peptides demonstrated exciting potential to prevent A β aggregation. However, only OR-2 was capable of rescuing A β -induced toxicity within the cell, owing to the ability of OR-2 to alter A β oligomers, something that OR-1 failed to do (Austen et al., 2008). This highlights the importance of blocking oligomer formation specifically and, if TBSH1 follows the theory behind the TBS platform by blocking dimer formation, should also alter oligomer formation and hold potential to rescue A β induced toxicity.

Overall, cell-based viability assays suggest the ability for the peptide to rescue A β -induced toxicity however, following assessment with a One-way ANOVA test, this rescue was not found to hold significance as a result of variance between cellular assay repeats. The insignificance presented here may occur as a result of greater variance across cellular assay plates observed following the covid lockdown, the reason for which is unclear and therefore requires further exploration to fully understand the potential of TBSH1 to rescue A β -induced toxicity in cell-based assays.

Conclusions

This study presents successful proof of principle for the novel intracellular screening assay TBS and solidifies the principles of the TBS assay as shown by loss and revival of colony growth when expected. Cloning complications encountered upon production of control peptides mean that the proof of principle lacks controls however, this issue is circumvented upon successful identification of a functional peptide hit following screening of the A β 10-22 library. Ideally, peptide controls would have been placed through the assay before library screening however this was not crucial as the lack of known inhibitors against dimerisation of A β means that inactive control peptides may not reflect an insufficient screening platform but rather that the peptides are not active within the TBS setting, i.e., presumably do not

inhibit dimer formation. Therefore, it was deemed appropriate to continue with a test library screen to explore the potential of the TBS assay.

Following screening of a random sample of 100,000 members from A β 10 – 22 library, a winning peptide sequence was identified. The ability of this peptide to alter A β aggregation and present partial recovery of A β -induced toxicity, as shown by biophysical and cell-based characterisation of the peptide, indicates potential for the TBS platform to identify functional peptide inhibitors and justifies the use of TBS as a successful screening platform. In terms of TBSH1, the characterisation of the peptide suggests some toxicity at high concentrations of the peptide but highlights potential of the peptide at an optimal ratio between 1:0.5 and 1:2, with the selected sequence standing as a good base for second generation libraries. Furthermore, future peptide modification studies of TBSH1, for example identification of essential residues within the sequence using alanine scans and removal of unnecessary residues may allow for production of smaller, less toxic peptides that enhance the potential as a therapeutic.

Whilst the theory behind TBS suggests that the peptide binds to monomeric A β to prevent dimer formation, this was not confirmed. As presented clearly from ThT analysis the peptide is able to impact upon A β aggregation and toxicity. However, it is ultimately observed that A β can still aggregate, albeit at a slower rate, in the presence of the peptide. One possibility is that the peptide functions as intended but dimers form within the $t=0$ timescale that are able to bypass the peptide, meaning that A β can 'circumvent' the point at which the peptide can intervene with the aggregation pathway. Therefore, although the peptide can slow the aggregation process, it cannot entirely thwart it. Although every effort is made to utilise monomeric samples of A β the sample is unlikely to contain 100 % monomeric species upon addition to the ThT aggregation assay. A β was snap frozen as highly monomeric samples however, upon defrosting of the sample aliquots for assay use, it cannot be ruled out that the protein begins aggregating prior to contact with TBSH1 and therefore may contain very small oligomer/dimeric species that evade inhibition by TBSH1. In addition, at lower molar ratios of A β :peptide, any excess A β is free to aggregate without peptide interference and proceed to dimer and oligomer formation. Future experiments to explore how the peptide binds to A β would be needed to address these points and, if shown to bind A β to block dimer formation, could further corroborate the principle of TBS.

Whilst it could be thought that blocking A β dimerisation would prevent formation of any further oligomeric species, presenting as a flat line on ThT upon addition of TBSH1 or lack of oligomer species in PICUP, realistically this would not be possible. In order to prevent formation of oligomeric species the peptide would need to block every single monomer as, once a single dimer molecule is formed, TBSH1 is in theory inactive against any further aggregation. Therefore, the observation of slowed aggregation (as opposed to complete

prevention) is not disappointing but rather a realistic target of the peptide. Perhaps a two-pronged therapeutic approach would be more appropriate to both slow aggregation, by reducing formation of dimers (assumed by TBS), and to target formation of later aggregates that may slip through following application of TBSH1.

A β oligomers have been shown to present physiological roles within the human brain with pathological functions taking precedent at higher concentrations resulting in a switch towards A β toxicity (Gulisano et al., 2018). Inhibiting endogenous A β has been shown to induce neuronal cell death implicating a critical role for A β in cell viability (Plant et al., 2003). Potentially, TBSH1 only slowing the initial stages of aggregation may be advantageous as the peptide may slow the formation of oligomers, presenting a smaller population of oligomers than if no peptide was present, enabling the physiological function of the peptide and prolonging the switch towards pathological A β , as opposed to thwarting production of oligomers entirely which may block any physiological functions.

In conclusion, this study presents a promising novel peptide screening platform and the identification of a peptide following initial screening. The TBSH1 peptide hit presents evidence for the use of TBS to identify potent inhibitors of A β -induced toxicity in AD and opens up potential for screening of peptide libraries rationally designed against the dimer interface (Library 28-42) whilst standing as a promising future drug candidate that is worthy of further exploration in itself.

Supporting Information

Supplementary Materials and Methods

Polymerase Chain Reaction. For the library formation, the forward primer stands as the template for the library DNA. These library members will later be transformed in to a pQE80 vector. For production of the target plasmid Basic-A β , the forward primer codes for cJUN basic tag with a short complementary site of A β following to bind to the A β sequence in the template DNA (p230d-A β -DHFR). To remove the DHFR tag from A β the reverse primers have a complementary sequence to A β and then incorporate stop codons. The following primers were ordered from Sigma-Aldrich:

Table S1: Primer sequences for TBS library 10-22 and production of proof-of-principle plasmids (Basic-A β and A β -).** Primers are written 5' to 3' and letters in bold represent restriction sites (Library restriction sites are BamHI (orange) and HindIII (purple) whilst Basic-A β and A β -** are SphI (red) and Ascl (dark blue). The A β ** F primer is Sfp8 which is a primer that anneals upstream of SphI site on p230d-A β -DHFR (so SphI is not included in the primer sequence as is incorporated from the template downstream). Letters in italics represent stop codon region. Green letters code for the cJun Basic region whilst light blue are those complementary to A β sequence.

Primer	Sequence
A β Library 10-22 Forward Primer	CTGAG GATC CTACVNKGTGNNKCATVNKAAAVNKGTGTWTTT TRYHGAA TAATAG AAGCTT TGATAA
A β Library 10-22 Reverse Primer	<i>TTATCA</i> AAGCTT <i>CTATTA</i>
Basic-A β Forward Primer	AA G CATG C GCATTAAAGCCGAACGCAAACGGATGCGCAACC GCATCGCAGCCTCCAAGTGCCGCAAACGCAAATTGGAGCGC GACGCTGAATTCGCCAC
A β -** Forward Primer	CGGATAACAATTTACACAG
A β Reverse Primer	TTTC GGCGCGCC TCATTAAGCGATAACAACGCCG

Primers, Polymerase, dNTPs, buffer and DMSO were added to Eppendorfs in the following amounts:

Table S2: Reagent volumes required for PCR reactions. For production of basic and stop plasmids X μ l template DNA also added (p230d-A β -DHFR).

Reagent	Volume (μ l)	
	PCR	Control
5 x Buffer	10	10
10mM dNTPs	2	2
Forward Primer (100 μ M)	1	1
Reverse Primer (100 μ M)	1	1
DNA Template (for target plasmids)	1	1
Polymerase	1	0
DMSO	0.75	0.75
ddH2O	33.25	34.25
Total	50	50

Product Codes: dNTPs: BioLine (Cat. No.: BIO-39044)

Polymerase, DMSO and Buffer: NEB (Cat. No.:M0530S)

The PCR ran with the following settings:

Table S3: PCR steps for production of correct PCR products.

Stage	Temperature ($^{\circ}$ C)	Time (s)
Preheat Lid	105	n/a
Initial Denaturation	98	60
Denaturation	98	20
Annealing	55/60*	60
Extension	72	60
Final Extension	72	300
Final Hold	4	∞

} x32 cycles

*The first two cycles were carried out with an annealing temperature of 55 $^{\circ}$ C with the following 30 cycles at 60 $^{\circ}$ C. For Library PCR, a gradient PCR was set between 35 $^{\circ}$ C and 40 $^{\circ}$ C and tubes combined.

PCR Purification. As more than one band occurred following PCR, QIAEXII Gel extraction Kit (Qiagen; Cat. No.: 20051) was used to extract the required band. For bands requiring extraction by QIAEXII, PCR products were run on a 1.5 % Agarose Gel at 140 V for 45 minutes and appropriate bands extracted for purification using QIAEXII Gel Extraction Kit

(Qiagen; Cat. No.: 20051). 6 volumes Buffer QXI (supplied with kit) was added to each gel slice (1 volume is weight of gel slice (mg)), incubated at 50 °C for 10 minutes then x μ l of silica resin (provided with kit) added (x is dependent on amount of DNA purifying) and Eppendorf vortexed to resuspend the silica. Buffer-DNA-silica solution incubated at 50 °C for at least 5 minutes, with vortexing every 2 minutes. The solution was then centrifuged for 30 seconds at 13,000 rpm and supernatant removed. Pellet washed with 500 μ l Buffer PE (provided with kit) by applying the buffer, vortexing to resuspend pellet, then centrifuging and removing the supernatant. This process was repeated twice. Resulting pellet was air-dried at 50 °C for 10 minutes. Once dry, the pellet was resuspended in approximately 20 μ l ddH₂O and incubated at 50 °C for 5 minutes. Following this, the DNA solution was centrifuged for 30 seconds and supernatant, containing the DNA, kept. The concentration of resulting DNA was measured using NanoDrop.

NanoDrop. NanoDrop 2000 (ThermoFisher: Cat. No.: ND2000) was used to measure DNA concentrations. 2 μ l sample was loaded for measurement.

Restriction Digestion. Restriction digest was carried out with appropriate restriction enzymes (BamHI/HindIII for library and SphI and Ascl for Basic-A β and A β -**). The following digestion mix was used as a guideline for digestion of PCR products and plasmid DNA:

Table S4: Volumes required for restriction digest of insert and vector.

Reagent	Volume (μ l)
DNA (\approx 2 μ g)	x
CutSmart Buffer	2
Restriction enzyme 1 (\approx 10 U)	1
Restriction enzyme 2 (\approx 10 U)	1
ddH ₂ O	x
Total	20

X depends on the concentration of DNA, or the volume required to make total volume up to 20 μ l.

Digestion mix was incubated at 37 °C for 3-5 hours.

Dephosphorylation of vector backbone. Following digestion of vector backbones by restriction digest enzymes, the vector backbone was dephosphorylated using the FastAP™ Thermosensitive Alkaline Phosphatase (Thermofisher Scientific: Cat. No.: EF0651). To a typical digest mix the following components were added (the volumes were scaled depending on digest mix volume and amount of DNA – 1 μ l of enzyme for each 1 μ g of DNA):

Table S5: Reagent volumes for dephosphorylation of vector backbone.

Reagent	Volume (μ l)
Restriction Digest Mix (1 μ g DNA)	x
10 x FastAP™ Reaction Buffer	2
FastAP™ Thermosensitive Alkaline Phosphatase	1
ddH ₂ O	x
Total	20

x depends on volume of digest mix and ddH₂O required to bring volume up to total.

The reaction was incubated at 37 °C for 10 minutes minimum.

The vector backbone was then extracted using QIAGEN QIAquick Gel Extraction Kit (TBS vector) as below and Qiagen QIAEXII (described above in PCR purification) kit used to extract digested library inserts as described above.

QIAGEN QIAquick Gel Extraction. Following restriction digest the DNA was separated on 1 % Agarose Gel at 140 V for 45 minutes and appropriate bands extracted for purification with QIAGEN QIAquick Gel Extraction Kit (Qiagen: Cat. No.: 28704). To each gel slice, three volumes Buffer QG (provided with kit) was added to one volume gel (100 mg = 100 μ l). Buffer QG/Gel slice mix was incubated at 50 °C for 10 minutes, shaking at approx. 600 rpm. Once the gel is fully dissolved, if the colour of the mixture was orange or violet (as opposed to the expected yellow) 10 μ l of 10 M Sodium Acetate could be added to return the buffer colour back to yellow. The sample was then applied to a QIAquick spin column in the collection tube (both provided with kit) and centrifuged at 13,000 rpm for 1 minute (all following centrifugation steps are carried out as described here) and flow-through discarded. 750 μ l Buffer PE (provided with kit) was then spun through the column and the flow-through discarded. To dry the column, the column was then centrifuged. 30 μ l of ddH₂O was applied to the spin column at the centre of the membrane and left to stand for 2 minutes and DNA eluted by centrifuging for 2 minutes. DNA concentration was measured using NanoDrop.

Plasmid preparation with Miniprep. Various plasmids were prepared using GeneJet Plasmid Miniprep Kit (ThermoFisher Scientific; Cat. No.: K0503). *Escherichia coli* (*E. coli*) previously transformed with desired plasmid was streaked to provide a single colony. A single colony was picked and used to inoculate 5-10 ml LB media containing the required antibiotic and incubated at 37 °C overnight, shaking at 250 rpm. The overnight culture was centrifuged at 4,500 rpm for 10 minutes and resuspended in 1 ml ddH₂O per miniprep and transferred to an Eppendorf. Cell suspension centrifuged in table-top centrifuge for 2 minutes at 8,000 rpm and supernatant removed. 250 μ l resuspension buffer (provided with

kit) added to pellet and vortexed to resuspend. 250 µl lysis buffer (provided with kit) added and Eppendorf tube inverted at least 6 times. Finally, 350 µl neutralisation buffer added and tube inverted at least 6 times. Solution was centrifuged at 13,000 rpm for 5 minutes. The supernatant was removed and applied to a spin column (provided with kit) which was centrifuged at 13,000 rpm for 1 minute (all subsequent centrifugation as described here unless stated). 500 µl wash buffer (provided with kit) applied to the column and centrifuged. This wash procedure was repeated twice with a subsequent centrifugation to dry the column. The DNA was eluted using ddH₂O (volume dependent on prep) by applying the ddH₂O to the centre of the column and incubating for 2 minutes followed with a 2 minute centrifugation at 13,000 rpm. Resulting DNA concentration measured using NanoDrop.

Ligation. Ligation was carried out using Electroligase (NEB: Cat. No.: M0369S) at various vector:insert ratios depending on optimised ratio. Following addition of the insert and vector, the volume was made up to 5 µl with ddH₂O and 5 µl of 2x Reaction Buffer added. 1 µl Electroligase enzyme was added, and the ligation mix incubated at 25 °C for 1 hour. The reaction was then inactivated by incubating at 65 °C for 15 minutes.

Preparation of electrocompetent cell lines. For library building NEB10β (NEB; Cat. No.: C3020K) cells were used and for library screening BL21-Gold cells were used. Cell line to be made competent was streaked on LB Agar plate containing necessary antibiotics and a single colony picked to inoculate 5 ml LB Broth with antibiotics which was incubated overnight at 37 °C, shaking at 250 rpm. 50 ml 2xyt media was pre-warmed at 37 °C with appropriate antibiotics. This 50 ml starter culture was inoculated with approximately 1 ml (starting OD₆₀₀ should not be more than 0.1) of the overnight culture. This was then grown up until OD₆₀₀ = 0.6-0.8. Once sufficient growth had occurred the culture was incubated on ice for 30 minutes with frequent inversion. The cell culture was centrifuged at 5,000 rpm for 7 minutes at 4°C (as for all following centrifugation steps). Pellet was resuspended in 50 ml cold ddH₂O and centrifuged. Supernatant removed and pellet resuspended in 25 ml cold ddH₂O and centrifuged. Supernatant removed and pellet resuspended in 50 ml cold 15 % Glycerol and centrifuged, supernatant removed, and pellet resuspended in 25 ml cold 15 % Glycerol. A final centrifugation was carried out and the pellet resuspended in necessary volume for aliquots required (often resuspended in residual glycerol from pellet to obtain high cell density to increase transformation efficiency). Aliquots were mostly used directly for transformation to increase transformation efficiency or were snap-frozen in liquid nitrogen and stored at -80 °C.

Electroporation of DNA in to electrocompetent cells. Transformations were carried out the same for all cell lines. 990 µl 2xyt with 10 µl 100x transformation salts (0.25 M KCl, 1 MgCl₂) prewarmed at 37 °C. X µl DNA sample added to 80 µl cell aliquot (X dependent on DNA concentration and amount of DNA needed) and kept on ice. Cell-DNA mix transferred

to electroporation cuvette and transformation was carried out on BioRad GenePulser II electroporation machine at 1.8 kV, 25 μ F capacitance and between 200-700 Ω . Following transformation, cells were recovered in 2xyt media with electroporation salts for approximately 75 minutes and plated on M9 or LB Agar plates dependent on assay with appropriate antibiotics at suitable dilutions.

Harvesting library colonies from transformation plates. 2-10 ml LB media (or M9 if harvesting from PCA Assay plates), containing appropriate antibiotics, was applied to agar plates and the cells scraped from the surface. This step was repeated to wash the plate and ensure sufficient collection of cells. The cells were harvested into a flask and incubated at 37 °C, shaking at 250 rpm, for approximately 1 hour. The cell culture was centrifuged at 4500 rpm for 10 minutes and the pellet weight used to determine number of miniprep repeats required. The DNA was prepped using the miniprep protocol as described above but contained contaminating bands, so library preps were taken in the future using minipreps from glycerol stocks to remove contaminant.

A β 1-42 purchased from Stratech. Recombinant A β ₁₋₄₂ was purchased from Stratech. Beta-Amyloid (1-42), Ultra Pure, NH₄OH was manufactured by rPeptide and purchased via Stratech (Stratech: Cat. No.: A-1167-2-RPE).

Peptide Synthesis. All Peptides were synthesised using Fmoc Solid Phase Synthesis using a Liberty Blue Automated Microwave Peptide Synthesiser (CEM: Cat No.: 925602) with the N-terminal remaining unmodified and C-terminal amidated. The peptide was built upon an H-Rink amide ChemMatrix resin (Sigma: Cat No.: 727768) with PyBop (Matrix Innovation: 1-025-0001) used as the activator base (26 g PyBop in 100 ml DMF). The deprotection reagent used was 20 % Piperidine in DMF.

The peptide was cleaved from the resin using a Trifluoroacetic acid (TFA) cleavage mix composed of 95 % TFA, 2.5 % Triisopropylsilane (TiPs), 2.5 % ddH₂O. 10 ml of cleavage mixture was added to the resin and incubated, shaking, at room temperature for 4 hours. Following this, the resin was filtered off with the TFA solution dripping into ice cold diethylether to precipitate the peptide. The diethylether/precipitated peptide mix was centrifuged at 7,800 rpm for 10 mins at -11 °C and supernatant poured off. Ice cold diethylether was added and the solution briefly vortexed and centrifuged again. This was repeated for three rounds and the final remaining peptide pellet was air-dried at room temperature overnight and then stored at -20 °C until purification by HPLC.

Purification of peptides. Peptides were purified using High Performance Liquid Chromatography (HPLC) using the C12 Jupiter® 4 μ m Proteo 90 Å, LC semi-preparative Column or preparative column (Phenomenex: Cat No.: OOG-4396-N0/OOG-4396-P0-AX). Dried pellets obtained following purification were dissolved and loaded on to the column

with automatic injection by Agilent HPLC. Solvent A consisted of 0.1 % TFA in ddH₂O whilst Solvent B is 0.1 % TFA in Acetonitrile (ACN). Peptides were separated and eluted by applying a linear gradient between 5 % and 90 % Solvent B (optimised for each peptide) and fractions containing the peptide were collected with the identity of the peptide confirmed using Mass Spectrometry (MS). Fractions containing the peptide were lyophilised and the resulting powder stored at -20 °C until resuspension into desired buffer. Concentrations of the peptide following resuspension were confirmed using the Varian Cary® 50 UV-Vis Spectrophotometer to determine the A₂₈₀ for peptides containing Tyrosine with an extinction coefficient of 1280 M⁻¹ cm⁻¹.

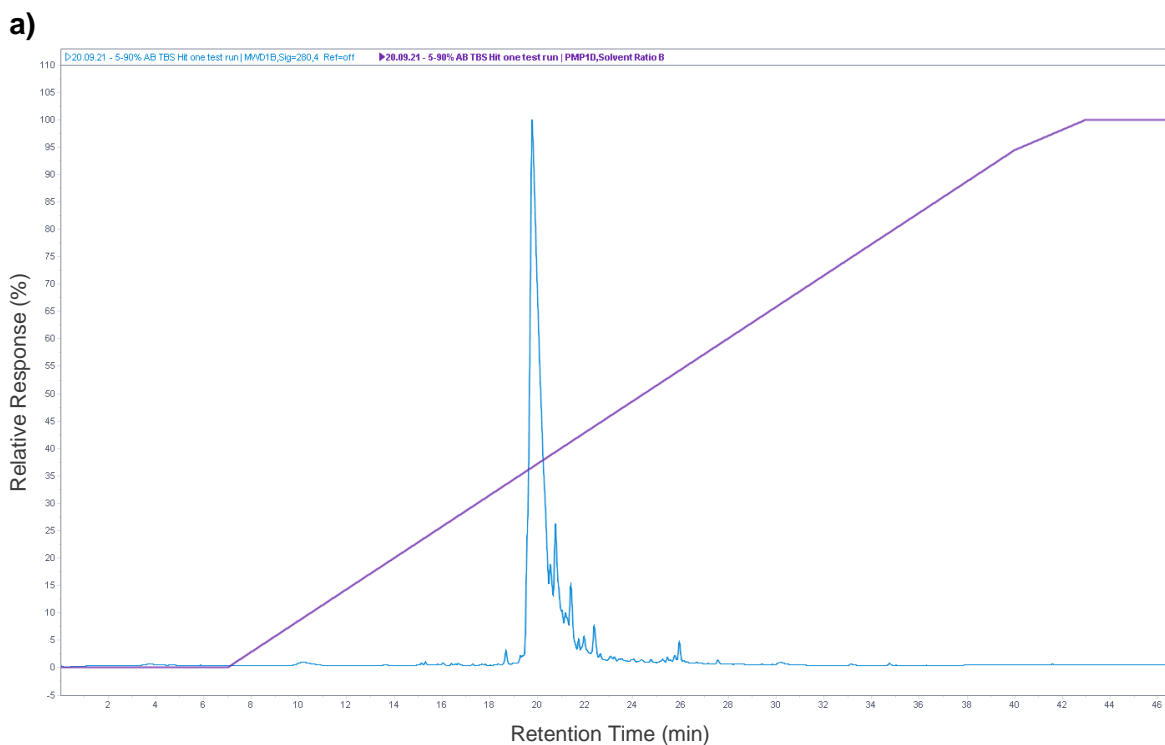
Supplementary Results

Equation S1: Following successful cloning of Aβ 10-22 library in to the pQE80 vector, a random sample of 100,000 members were successfully cloned using the following equation:

$$E = 100 \cdot (1 - (1/n))^m$$

Where E = % of library missing, n = theoretical library size and m = colony forming units from transformation (experimental).

Following transformation of the library, n = 100,000 and m = 257,782 for library cloning to provide 92.02 % coverage upon building of library. For library screening in the TBS platform, m = 116,000,000 to provide 100 % confidence of the screen. Therefore, following both library building and screening 92.02 % of the library is confidently covered.



b) User Spectra

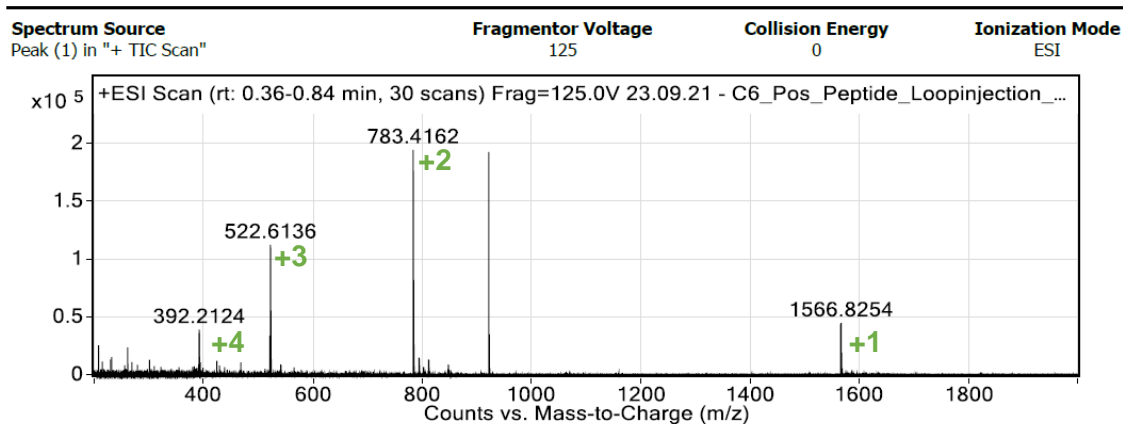


Figure S1: TBSH1 Purification by HPLC and species confirmation by Mass Spectrometry. TBSH1 was synthesised using Fmoc solid-phase synthesis and HPLC purification carried out to isolate TBSH1 product. The peptide eluted with a retention time of ~ 20 minutes at ~ 35 % Solvent B. Mass spectrometry indicates correct peptide sequence had been obtained. **a)** HPLC trace of TBSH1 purification. **b)** The peak presenting at 20 minutes was isolated and MS conducted to confirm correct sequence. TBSH1 holds a molecular weight of 1564.82 and peak assignments are shown in green. A 922 m/z standard peak is also shown.

Chapter Conclusion

Overall, this study presents the successful proof-of-concept experimentation for the TBS assay followed by its application to screen and identify peptide inhibitors. A single winning sequence was identified following single step and competition selection of the library and demonstrated ability to alter A β aggregation as determined by ThT, CD and PICUP assays. Furthermore, this peptide inhibitor showed potential to rescue A β -induced toxicity in an SH-SY5Y cell-based assay, indicating potential for translation as an AD therapeutic. The cellular aspect of the TBSH1 characterisation requires further optimisation as a result of some varied and statistically insignificant results. The insignificance presented here may occur as a result of variance across individual assay plates that was observed following the covid lockdown, the reason for which is unclear. Pre-covid data presented little variance within plates and demonstrated a promising cell rescue. However, upon replication of the experiment post-covid, cellular variance within single assay plates was observed that may contribute to the statistical insignificance. Therefore, to confidently report the ability of this peptide to rescue A β -induced toxicity within the cell-based assays, this will need to be revisited by others before publication of this data.

Despite this, following the overall successful application of the TBS platform to identify a functional peptide hit following initial test screening with Library 10-22, screening of Library 28-42 designed around the dimeric interface of A β raises exciting prospects to be pursued.

Of particular interest following the identification of TBSH1 (YGVEHRKGVFFVE) was the sequence similarity to PCAH2 (YAVFHPKTVFFVE) selected for in PCA. The C-terminal residues VFFVE are conserved between the two sequences suggesting importance of this region with the competition selection passages settling earlier within these final residues for both PCA and TBS than for residues towards the N-terminus. Previous studies have revealed importance of residues 16-20 of A β (KLVFF) for self-recognition and aggregation of A β (Tjernberg et al., 1996), with multiple peptides built upon this KLVFF motif, including OR-1, OR-2 and RI-OR2, demonstrating promise as potential therapeutic agents in their ability to reduce A β aggregation and, for OR-2 and RI-OR2, to also rescue A β -induced toxicity within cells (Austen et al., 2008; Taylor, M. et al., 2010). Both successful peptide inhibitors identified in PCA and TBS select for sequences similar to this motif, preserving the VFF sequence with an additional Val residue (perhaps for increased hydrophobicity compared to the Ala residue in wild type A β sequence) followed by the library conserved Glu. This sequence may have been chosen through the two assays as it is essential for optimal recognition of the A β target. Residues selected for throughout the rest of the two peptide sequences didn't show any favourable selection for a particular residue.

As previously discussed, PCAH2 selects for a Proline residue within the centre of the sequence which draws parallels with the β -sheet breaker peptide iA β ₅ (Soto et al., 1996; Soto et al., 1998). Interestingly, this Proline residue was not selected for following the TBS screen. Proline is incompatible within secondary β -sheet structures and disrupts their formation (Li et al., 1996) which may explain the selection of Proline within PCAH2. Perhaps, binding of PCAH2 to A β (may be monomeric, small oligomer or at fibril end) presents a kink, due to the cyclic nature of Proline, and hinders stacking of A β molecules by inhibiting association of β -sheets and further aggregation. PCA cannot reveal how a peptide binds to the target protein, so this is merely speculation, however the Proline residue appears to have importance in blocking fibril formation. For TBS, the peptide is required to block monomer interaction to prevent dimer formation. Perhaps the Proline residue is not selected here as it is less important to prevent the β -sheet fold and fibrilisation of A β but rather to interrupt the dimer interface by other means.

Chapter Five: Conclusions

Thesis Conclusions

AD is a devastating neurodegenerative disease with vast social and economic impacts across the globe. Despite a complicated disease progression, there is a long-term view supported by significant evidence that the A β protein is the trigger of toxicity within the disease. Following this revelation, decades of research has focused efforts towards A β -targeting therapies from small molecule drugs, peptide-based inhibitors and larger biologics such as anti-A β antibodies. Such molecules have been shown to target a range of aggregation states, while other molecules such as anti-sense oligonucleotides target production of proteins involved in AD, such as APP and BACE, by quenching messenger RNA (mRNA) translation (Chakravarthy et al., 2017). Despite this, there is a distinct lack of successful drug candidates progressing to the final stages of clinical trials. The lack of these may be owing to a plethora of limitations, including insufficient understanding of the toxic species of A β and the need for a relevant, translatable disease model to mimic AD in pre-clinical studies.

Firstly, a lack in our current understanding regarding the exact species of toxic oligomer and even conformer presents an enormous difficulty in replicating the precise toxic environment that successfully replicates that of a disease setting. This lack of knowledge clearly impacts upon our ability to target and produce conformer-specific drugs. Successful design of A β -targeted therapies may rely on inhibition of specific oligomeric species which have proved very hard to pinpoint. This moving target has hampered the search for effective molecules. Furthermore, current relevant disease models are limited and do not present translatable models of sporadic AD. Many *in vitro* AD models utilise cells that poorly recapitulate human neuronal cells or use rat neurons that fail to translate the post-transcriptional genetic makeup of the human neuronal system (Somel et al., 2011). *In vivo* models often harbour genetic mutations relevant to FAD as opposed to sporadic AD models, with AD pathology presenting over a number of months as opposed to physiological disease conditions in which the pathology of AD is accumulated over decades (Ameen-Ali, 2021). How well these models recapitulate what is occurring within sporadic AD in particular is unclear. Undeterred by this, recent advances in A β -targeting therapies have provided optimism and opened the avenue for further AD therapeutics. Despite clear controversy, the fast-track approval of the antibody Aducanumab has solidified ongoing interest in A β as a causative agent in AD and demonstrates the potential of A β -targeting therapies.

This study aimed to confront the lack of successful AD therapeutics with the use of a recognised intracellular screening assay and the establishment of a completely novel approach, towards identification of peptide-based inhibitors, a field of therapeutic study with increasing momentum in recent years. In addition, the study also aimed to address the lack

of appropriate cellular screening models by establishing a more relevant, robust cellular toxicity assay in which to assess the potential of peptide hits obtained throughout screening.

Peptides present promising therapeutic properties since they can achieve high specificity, have low production costs, limited immunogenicity (when shorter than ~12 residues) and can be readily modified to overcome potential shortcomings such as protease susceptibility, poor membrane permeability and rapid clearance. In this study we have attempted to identify and explore potential peptide therapies that fundamentally target A β -associated toxicity in AD, and by screening within live cells acknowledging some of these requirements. In cell screening also takes account of the fact that different oligomers and conformers of oligomers can be adopted by A β , and that ultimately peptides must both bind and detoxify A β in order for selection to occur.

The first study successfully applied the intracellular screening assay PCA to identify a peptide inhibitor of A β toxicity designed against the outer β -strand of A β as proposed by Gremer et. al. (Gremer et al., 2017). Owing to the intracellular nature of the assay, peptide hits identified and selected for present favourable drug-like characteristics. In particular, the peptide hits selected must detoxify the A β target to provide a growth advantage to the cell. A key attribute of the assay is that any lack of understanding of the toxic oligomeric species is not relevant to selection – the bacteria identify peptides from within the library that fulfil the selection criteria. Namely they must **i)** bind and **ii)** confer cell survival by detoxifying the target regardless of conformer specificity. Although the mechanism is unknown prior to full downstream characterisation, any peptide selected from the assay must both bind A β and reduce toxicity to confer survival.

The study conducted the PCA screening principle against two libraries to reveal a 'winning' peptide sequence for each, PCAH1 and PCAH2. Purification of the highly hydrophobic PCAH1 proved difficult in the absence of the DHFR1 fragment, which PCAH1 is appended to within the context of the *in vivo* assay, and progress was only achieved with PCAH2. As a result of the *in vivo* nature of PCA, the peptide hits selected often present favourable solubility. However, this is within the context of *E.coli* cells which may not fully translate outside of the assay, i.e., within purification solvents or, later in the application of peptide hits, to the environment within human neuronal cells. Therefore, there may be some benefit to exploring the possibility to transfer the established PCA screen in to a mammalian cell line, preferably a human neuronal line, in order to increase the therapeutic relevance of the screening selection and to improve translatability of resulting hits towards successful drug candidates (Remy, Campbell-Valois and Michnick, 2007; Acerra, Nicola et al., 2014). The potential of the resulting PCAH2 peptide was explored within a biophysical context and further extension of the study was carried out following optimisation of toxicity assays within a relevant human-derived cell line. PCAH2 demonstrated the ability to alter A β aggregation

by delaying initial aggregation at the lag phase and decreasing the total fibrilisation at the endpoint and also presented potential to partially rescue A β -induced toxicity in neuronal-like cells.

Many cell-based systems within the literature lack translation towards human AD and poorly represent human neuronal cells. The potential of the human neuroblastoma cell line, SH-SY5Y, was explored with susceptibility to A β observed upon differentiation of the line, in keeping with recent findings within the literature (Krishtal et al., 2017). Described within this study is a differentiation protocol with the potential to produce cells that present significant susceptibility to A β insult at concentrations as low as 2.5 μ M, as explored by MTT cell viability assay and morphology analysis of the SH-SY5Y cells in the presence and absence of A β to demonstrate toxicity encountered by the cells. The assay described provides the potential to explore A β -targeting therapies as has been demonstrated with the PCA and TBS peptide hits. Additionally, it provides a platform by which to explore A β pathology in a human-derived cellular model that represents neuronal-like cells which many studies fail to achieve.

However, the aforementioned SH-SY5Y cell cultures represent a single cell type that are present as monolayers in cultures which cannot fully represent the true complexity of the human neuronal system and the multifactorial cellular influence within AD. There is an interesting line of study currently developing 3D models of the human brain utilising SH-SY5Y cells or human derived-stem cells. Application of these 3D organoids will not only negate the requirement for mammalian sacrifice but will offer an effective model of the brain, including neurons and astrocytes. This will be of particular interest in the future for studying the efficacy of peptide-based inhibitors within a complex cellular system translatable to the environment peptides would realistically be exposed to in potential future uses as a therapeutic (Agholme et al., 2010; Cairns et al., 2020; Trujillo-Estrada et al., 2021).

In addition, a novel intracellular screening assay has been developed and is described here for the first time. The TBS platform and its potential was reinforced by the identification of the TBSH1 peptide that has been shown to successfully alter A β aggregation. Whilst PCA identifies hits that bind to A β , it is not possible to determine which species of A β is targeted following screening. The design of TBS allows for the assumption that TBS-active peptides must bind to inhibit dimer formation – the very first point of the aggregation pathway. It is important to bear in mind that this is not a proven aspect of the assay, but rather an assumption owing to the design. Moreover, any A β molecules that exist as dimeric species or higher oligomers have the potential to bypass the mode of interaction for TBS selection and can recruit more monomer, which may be a limitation of the approach.

Initial proof-of-principle assays were conducted to affirm the theory of the assay and an initial test screen was performed to assess the ability of the TBS platform to identify functional peptide hits resulting in the sequence of TBSH1. The hit sequence obtained demonstrates successful application of the TBS platform to identify peptide inhibitors that have the ability to modulate A β aggregation. The resulting screening platform therefore provides a novel means by which to select for A β -targeting peptides but may require further optimisation for effective functional readout.

Similarly to that mentioned for PCA, it would be beneficial to attempt to build the TBS platform within a neuronal cell system to greater reflect the AD environment (Remy, Campbell-Valois and Michnick, 2007; Acerra, Nicola et al., 2014). Alternatively, a mutant form of A β with increased aggregation propensity, like that of Arctic A β used within PCA, could be applied to the system to increase the stringency of the screening platform. Next, it would also be beneficial to invest future efforts towards optimisation of library cloning within the TBS pQE80. The pQE80 system was adopted to provide sufficient antibiotic resistant plasmid combinations as the BL21-Gold cells used within TBS present Tetracycline resistance, hindering the use of Tetracycline resistant plasmids. pQE80 (Kan resistance) harbours the LacI gene to regulate expression of assay proteins on plasmids and ensuring dependence of gene expression upon IPTG induction. Cloning the library in to the pQE80 plasmid means that just one plasmid is required for expression of the library and of LacI, reducing the overall number of antibiotics required in TBS. However, cloning into this plasmid proved difficult with continually low transformation efficiencies following ligation of the library into the vector. Further optimisation of this cloning system would allow for screening of larger and more relevantly designed libraries, in particular that of Library 28-42 designed around the dimeric interface of A β .

A drawback of this study is the inability of the screens to confidently reveal the form of A β that is targeted by the peptide or the mechanism by which the peptide binds as, although the libraries are semi-rationally designed against particular regions of A β , it is not possible to assume these regions are targeted. Moreover, the TBS assay design is built upon the premise that peptides will inhibit dimer formation however, this is not confirmed. Therefore, future studies applying computational analysis with programmes such as InterPep to predict protein to peptide interactions are required. InterPep is a computational programme that predicts protein residue interactions with a given peptide using templates from known protein interactions from the Protein Data Bank (PDB) (Johansson-Åkhe, Mirabello and Wallner, 2019). This theoretical prediction could be corroborated using NMR studies. Commonly, ss-NMR is applied to reveal the structure of A β and could be used to determine structural changes to A β in the presence of the peptide hits to explore the region of A β in which the peptide binds. Furthermore, in an attempt to reveal the species of A β targeted by

the resulting peptide hits, the study is next exploring the potential to apply SEC in a timepoint manner to reveal changes in peak distribution upon addition of the peptide throughout aggregation. Each peak within the SEC profile should represent a particular species of A β with monomer peaks, dimer peaks and varying oligomer peaks presenting throughout aggregation. Upon addition of the peptide, we hope to observe an alteration in some of the peak types to reveal which conformer of A β the peptide may target. This could be coupled with intact MS to confirm the molecular weight of the peaks affected. The above prospective studies may not only reveal the mechanism for the current peptide hits but could also act as a potential source to corroborate the theory behind the TBS screening platform, if the resulting hit is shown likely to bind and prevent dimer formation.

Overall, the application of these intracellular library screens provided two peptide sequences (PCAH2 and TBSH1) that present promising therapeutic prospects following successful alterations of A β aggregation as measured by ThT, CD, PICUP and TEM and partial rescue of A β -induced toxicity within our SH-SY5Y toxicity assay. The intracellular nature of the screening assays applied to identify the hit sequences mean that the peptides likely already present favourable peptide therapeutics, however peptide mimetic studies, such as retro-inversion or cyclisation to increase resistance to proteolysis or addition of CPP or N-methylation to increase cell penetrance, can now be applied to explore the potential to further enhance the translatability of these peptides into successful therapeutics. These sequences also stand as reliable scaffolds for developing second generation peptide libraries to identify more potent hits or to apply peptide mimetics in order to optimise translation of these peptides towards potential AD therapeutics. The peptide sequences selected within this study contribute to the flourishing field of peptide therapeutics and present the added benefit of selection within an *in vivo* environment, something that previous screening techniques, such as phage display, fail to achieve. The peptide hits and the avenues of future work opened up contribute towards the effort of producing an AD therapeutic, something that is currently lacking within this vital field of research.

Bibliography

Abramov, E., Dolev, I., Fogel, H., Ciccotosto, G.D., Ruff, E. and Slutsky, I., 2009. Amyloid- β as a positive endogenous regulator of release probability at hippocampal synapses. *Nature Neuroscience*, 12, p. 1567.

Acerra, N., Kad, N.M., Cheruvara, H. and Mason, J.M., 2014. Intracellular selection of peptide inhibitors that target disulphide-bridged Abeta42 oligomers. *Protein Sci*, 23(9), pp. 1262-1274.

Acerra, N., Kad, N.M., Griffith, D.A., Ott, S., Crowther, D.C. and Mason, J.M., 2014. Retro-inversal of Intracellular Selected β -Amyloid-Interacting Peptides: Implications for a Novel Alzheimer's Disease Treatment. *Biochemistry*, 53(13), pp. 2101-2111.

Acerra, N., Kad, N.M. and Mason, J.M., 2013. Combining intracellular selection with protein-fragment complementation to derive Abeta interacting peptides. *Protein Eng Des Sel*, 26(7), pp. 463-470.

Agholme, L., Lindström, T., Kågedal, K., Marcusson, J. and Hallbeck, M., 2010. An In Vitro Model for Neuroscience: Differentiation of SH-SY5Y Cells into Cells with Morphological and Biochemical Characteristics of Mature Neurons. *Journal of Alzheimer's Disease*, 20, pp. 1069-1082.

Agrawal, N. and Skelton, A.A., 2019. Structure and Function of Alzheimer's Amyloid β Proteins from Monomer to Fibrils: A Mini Review. *The Protein Journal*, 38(4), pp. 425-434.

Alves da Costa, C., Sunyach, C., Pardossi-Piquard, R., Sévalle, J., Vincent, B., Boyer, N., Kawarai, T., Girardot, N., St George-Hyslop, P. and Checler, F., 2006. Presenilin-dependent gamma-secretase-mediated control of p53-associated cell death in Alzheimer's disease. *J Neurosci*, 26(23), pp. 6377-6385.

Amar, F., Sherman, M.A., Rush, T., Larson, M., Boyle, G., Chang, L., Götz, J., Buisson, A. and Lesné, S.E., 2017. The amyloid- β oligomer A β *56 induces specific alterations in neuronal signaling that lead to tau phosphorylation and aggregation. *Science signaling*, 10(478), p. eaal2021.

Ameen-Ali, K., 2021. Has a reliance on animal models delayed progress in dementia research? Available from: <https://www.dementiaresearcher.nihr.ac.uk/has-a-reliance-on-animal-models-delayed-progress-in-dementia-research/> [Accessed 20/02/2022 2022].

Ancolio, K., Dumanchin, C., Barelli, H., Warter, J.M., Brice, A., Campion, D., Frébourg, T. and Checler, F., 1999. Unusual phenotypic alteration of beta amyloid precursor protein (betaAPP) maturation by a new Val-715 --> Met betaAPP-770 mutation responsible for probable early-onset Alzheimer's disease. *Proc Natl Acad Sci U S A*, 96(7), pp. 4119-4124.

Andreetto, E., Yan, L.M., Tatarek-Nossol, M., Velkova, A., Frank, R. and Kapurniotu, A., 2010. Identification of hot regions of the Abeta-IAPP interaction interface as high-affinity binding sites in both cross- and self-association. *Angew Chem Int Ed Engl*, 49(17), pp. 3081-3085.

Arboleda-Velasquez, J.F., Lopera, F., O'Hare, M., Delgado-Tirado, S., Marino, C., Chmielewska, N., Saez-Torres, K.L., Amarnani, D., Schultz, A.P., Sperling, R.A., Leyton-Cifuentes, D., Chen, K., Baena, A., Aguillon, D., Rios-Romenets, S., Giraldo, M., Guzmán-Vélez, E., Norton, D.J., Pardilla-Delgado, E., Artola, A., Sanchez, J.S., Acosta-Urbe, J., Lalli, M., Kosik, K.S., Huentelman, M.J., Zetterberg, H., Blennow, K., Reiman, R.A., Luo, J., Chen, Y., Thiyyagura, P., Su, Y., Jun, G.R., Naymik, M., Gai, X., Bootwalla, M., Ji, J., Shen,

- L., Miller, J.B., Kim, L.A., Tariot, P.N., Johnson, K.A., Reiman, E.M. and Quiroz, Y.T., 2019. Resistance to autosomal dominant Alzheimer's disease in an APOE3 Christchurch homozygote: a case report. *Nature Medicine*, 25(11), pp. 1680-1683.
- Armen, R.S., DeMarco, M.L., Alonso, D.O. and Daggett, V., 2004. Pauling and Corey's alpha-pleated sheet structure may define the prefibrillar amyloidogenic intermediate in amyloid disease. *Proc Natl Acad Sci U S A*, 101(32), pp. 11622-11627.
- Armiento, V., Spanopoulou, A. and Kapurniotu, A., 2020. Peptide-Based Molecular Strategies To Interfere with Protein Misfolding, Aggregation, and Cell Degeneration. *Angewandte Chemie International Edition*, 59(9), pp. 3372-3384.
- Arndt, J.W., Qian, F., Smith, B.A., Quan, C., Kilambi, K.P., Bush, M.W., Walz, T., Pepinsky, R.B., Bussi re, T., Hamann, S., Cameron, T.O. and Weinreb, P.H., 2018. Structural and kinetic basis for the selectivity of aducanumab for aggregated forms of amyloid- . *Scientific Reports*, 8(1), p. 6412.
- ARUK, 2015. #ShareTheOrange [Online]. Available from: <https://www.alzheimersresearchuk.org/orange/> [Accessed 14/02/22].
- Arvanitakis, Z., Wilson, R.S., Bienias, J.L., Evans, D.A. and Bennett, D.A., 2004. Diabetes mellitus and risk of Alzheimer disease and decline in cognitive function. *Arch Neurol*, 61(5), pp. 661-666.
- Association, A.s., 2018. 2018 Alzheimer's disease facts and figures. *Alzheimer's & Dementia*, 14(3), pp. 367-429.
- Association, A.s., 2021. 2021 Alzheimer's disease facts and figures [Online]. Available from: <https://www.alz.org/media/Documents/alzheimers-facts-and-figures-infographic.pdf> [Accessed 18/02/2022].
- Athan, E.S., Williamson, J., Ciappa, A., Santana, V., Romas, S.N., Lee, J.H., Rondon, H., Lantigua, R.A., Medrano, M., Torres, M., Arawaka, S., Rogaeva, E., Song, Y.Q., Sato, C., Kawarai, T., Fafel, K.C., Boss, M.A., Seltzer, W.K., Stern, Y., St George-Hyslop, P., Tycko, B. and Mayeux, R., 2001. A founder mutation in presenilin 1 causing early-onset Alzheimer disease in unrelated Caribbean Hispanic families. *Jama*, 286(18), pp. 2257-2263.
- Austen, B.M., Paleologou, K.E., Ali, S.A., Qureshi, M.M., Allsop, D. and El-Agnaf, O.M., 2008. Designing peptide inhibitors for oligomerization and toxicity of Alzheimer's beta-amyloid peptide. *Biochemistry*, 47(7), pp. 1984-1992.
- Baxter, D., Ullman, C.G., Frigotto, L. and Mason, J.M., 2017. Exploiting Overlapping Advantages of In Vitro and In Cellulo Selection Systems to Isolate a Novel High-Affinity cJun Antagonist. *ACS Chemical Biology*, 12(10), pp. 2579-2588.
- Bay s,  ., van de Lagemaat, L.N., Collins, M.O., Croning, M.D.R., Whittle, I.R., Choudhary, J.S. and Grant, S.G.N., 2011. Characterization of the proteome, diseases and evolution of the human postsynaptic density. *Nature Neuroscience*, 14(1), pp. 19-21.
- Bekris, L.M., Yu, C.-E., Bird, T.D. and Tsuang, D.W., 2010. Genetics of Alzheimer disease. *Journal of geriatric psychiatry and neurology*, 23(4), pp. 213-227.
- Belyaev, N.D., Kellett, K.A.B., Beckett, C., Makova, N.Z., Revett, T.J., Nalivaeva, N.N., Hooper, N.M. and Turner, A.J., 2010. The transcriptionally active amyloid precursor protein (APP) intracellular domain is preferentially produced from the 695 isoform of APP in a {beta}-secretase-dependent pathway. *The Journal of biological chemistry*, 285(53), pp. 41443-41454.

- Benilova, I., Gallardo, R., Ungureanu, A.A., Castillo Cano, V., Snellinx, A., Ramakers, M., Bartic, C., Rousseau, F., Schymkowitz, J. and De Strooper, B., 2014. The Alzheimer disease protective mutation A2T modulates kinetic and thermodynamic properties of amyloid-beta (A β) aggregation. *J Biol Chem*, 289(45), pp. 30977-30989.
- Benilova, I., Karran, E. and De Strooper, B., 2012. The toxic A β oligomer and Alzheimer's disease: an emperor in need of clothes. *Nat Neurosci*, 15(3), pp. 349-357.
- Berridge, M.J., 2010. Calcium hypothesis of Alzheimer's disease. *Pflügers Archiv - European Journal of Physiology*, 459(3), pp. 441-449.
- Bishop, G.M. and Robinson, S.R., 2004. Physiological Roles of Amyloid- β and Implications for its Removal in Alzheimer's Disease. *Drugs & Aging*, 21(10), pp. 621-630.
- Bitan, G., 2006. Structural Study of Metastable Amyloidogenic Protein Oligomers by Photo-Induced Cross-Linking of Unmodified Proteins. *Methods in Enzymology*. Academic Press, pp. 217-236.
- Bitan, G., Fradinger, E.A., Spring, S.M. and Teplow, D.B., 2005. Neurotoxic protein oligomers--what you see is not always what you get. *Amyloid*, 12(2), pp. 88-95.
- Bitan, G., Lomakin, A. and Teplow, D.B., 2001. Amyloid β -Protein Oligomerization: PRENUCLEATION INTERACTIONS REVEALED BY PHOTO-INDUCED CROSS-LINKING OF UNMODIFIED PROTEINS *. *Journal of Biological Chemistry*, 276(37), pp. 35176-35184.
- Bloom, G.S., 2014. Amyloid- β and tau: the trigger and bullet in Alzheimer disease pathogenesis. *JAMA Neurol*, 71(4), pp. 505-508.
- Brener, O., Dunkelmann, T., Gremer, L., van Groen, T., Mirecka, E.A., Kadish, I., Willuweit, A., Kutzsche, J., Jürgens, D., Rudolph, S., Tusche, M., Bongen, P., Pietruszka, J., Oesterhelt, F., Langen, K.-J., Demuth, H.-U., Janssen, A., Hoyer, W., Funke, S.A., Nagel-Steger, L. and Willbold, D., 2015. QIAD assay for quantitating a compound's efficacy in elimination of toxic A β oligomers. *Scientific Reports*, 5(1), p. 13222.
- Brinkmalm, G., Hong, W., Wang, Z., Liu, W., O'Malley, T.T., Sun, X., Frosch, M.P., Selkoe, D.J., Portelius, E., Zetterberg, H., Blennow, K. and Walsh, D.M., 2019. Identification of neurotoxic cross-linked amyloid-beta dimers in the Alzheimer's brain. *Brain*, 142(5), pp. 1441-1457.
- Cairns, D.M., Rouleau, N., Parker, R.N., Walsh, K.G., Gehrke, L. and Kaplan, D.L., 2020. A 3D human brain-like tissue model of herpes-induced Alzheimer's disease. *Sci Adv*, 6(19), p. eaay8828.
- Calvo-Rodriguez, M., Hou, S.S., Snyder, A.C., Kharitonova, E.K., Russ, A.N., Das, S., Fan, Z., Muzikansky, A., Garcia-Alloza, M., Serrano-Pozo, A., Hudry, E. and Bacskai, B.J., 2020. Increased mitochondrial calcium levels associated with neuronal death in a mouse model of Alzheimer's disease. *Nature Communications*, 11(1), p. 2146.
- Castellano, J.M., Kim, J., Stewart, F.R., Jiang, H., DeMattos, R.B., Patterson, B.W., Fagan, A.M., Morris, J.C., Mawuenyega, K.G., Cruchaga, C., Goate, A.M., Bales, K.R., Paul, S.M., Bateman, R.J. and Holtzman, D.M., 2011. Human apoE isoforms differentially regulate brain amyloid- β peptide clearance. *Science translational medicine*, 3(89), pp. 89ra57-89ra57.
- Castro, P., Zaman, S. and Holland, A., 2017. Alzheimer's disease in people with Down's syndrome: the prospects for and the challenges of developing preventative treatments. *J Neurol*, 264(4), pp. 804-813.

- Chakravarthy, M., Chen, S., Dodd, P.R. and Veedu, R.N., 2017. Nucleic Acid-Based Theranostics for Tackling Alzheimer's Disease. *Theranostics*, 7(16), pp. 3933-3947.
- Chang, K.-H., Chiu, Y.-J., Chen, S.-L., Huang, C.-H., Lin, C.-H., Lin, T.-H., Lee, C.-M., Ramesh, C., Wu, C.-H., Huang, C.-C., Fung, H.-C., Chen, Y.-C., Lin, J.-Y., Yao, C.-F., Huang, H.-J., Lee-Chen, G.-J., Lee, M.-C. and Hsieh-Li, H.M., 2016. The potential of synthetic indolyloquinoline derivatives for A β aggregation reduction by chemical chaperone activity. *Neuropharmacology*, 101, pp. 309-319.
- Chartier-Harlin, M.C., Crawford, F., Houlden, H., Warren, A., Hughes, D., Fidani, L., Goate, A., Rossor, M., Roques, P., Hardy, J. and et al., 1991. Early-onset Alzheimer's disease caused by mutations at codon 717 of the beta-amyloid precursor protein gene. *Nature*, 353(6347), pp. 844-846.
- Chatani, E. and Yamamoto, N., 2018. Recent progress on understanding the mechanisms of amyloid nucleation. *Biophysical reviews*, 10(2), pp. 527-534.
- Chatterjee, S. and Mudher, A., 2018. Alzheimer's Disease and Type 2 Diabetes: A Critical Assessment of the Shared Pathological Traits. *Frontiers in Neuroscience*, 12(383).
- Chen, W.T., Lin, G.B., Kuo, Y.Y., Hsieh, C.H., Lu, C.H., Sun, Y.K. and Chao, C.Y., 2021. Effect of high-frequency low-intensity pulsed electric field on protecting SH-SY5Y cells against hydrogen peroxide and β -amyloid-induced cell injury via ERK pathway. *PLoS One*, 16(4), p. e0250491.
- Cheng, I.H., Palop, J.J., Esposito, L.A., Bien-Ly, N., Yan, F. and Mucke, L., 2004. Aggressive amyloidosis in mice expressing human amyloid peptides with the Arctic mutation. *Nat Med*, 10(11), pp. 1190-1192.
- Cheruvuvara, H., Allen-Baume, V.L., Kad, N.M. and Mason, J.M., 2015. Intracellular screening of a peptide library to derive a potent peptide inhibitor of α -synuclein aggregation. *J Biol Chem*, 290(12), pp. 7426-7435.
- Cheung, Y.-T., Lau, W.K.-W., Yu, M.-S., Lai, C.S.-W., Yeung, S.-C., So, K.-F. and Chang, R.C.-C., 2009. Effects of all-trans-retinoic acid on human SH-SY5Y neuroblastoma as in vitro model in neurotoxicity research. *NeuroToxicology*, 30(1), pp. 127-135.
- Chow, V.W., Mattson, M.P., Wong, P.C. and Gleichmann, M., 2010. An overview of APP processing enzymes and products. *Neuromolecular medicine*, 12(1), pp. 1-12.
- Chun, Y.S., Park, Y., Oh, H.G., Kim, T.-W., Yang, H.O., Park, M.K. and Chung, S., 2015. O-GlcNAcylation Promotes Non-Amyloidogenic Processing of Amyloid- β Protein Precursor via Inhibition of Endocytosis from the Plasma Membrane. *Journal of Alzheimer's Disease*, 44, pp. 261-275.
- Cohen, S.I.A., Linse, S., Luheshi, L.M., Hellstrand, E., White, D.A., Rajah, L., Otzen, D.E., Vendruscolo, M., Dobson, C.M. and Knowles, T.P.J., 2013. Proliferation of amyloid- β 42 aggregates occurs through a secondary nucleation mechanism. *Proceedings of the National Academy of Sciences of the United States of America*, 110(24), pp. 9758-9763.
- Colvin, M.T., Silvers, R., Ni, Q.Z., Can, T.V., Sergeyev, I., Rosay, M., Donovan, K.J., Michael, B., Wall, J., Linse, S. and Griffin, R.G., 2016. Atomic Resolution Structure of Monomorphic A β 42 Amyloid Fibrils. *Journal of the American Chemical Society*, 138(30), pp. 9663-9674.
- Corder, E.H., Saunders, A.M., Risch, N.J., Strittmatter, W.J., Schmechel, D.E., Gaskell, P.C., Jr., Rimmler, J.B., Locke, P.A., Conneally, P.M., Schmechel, K.E. and et al., 1994. Protective effect of apolipoprotein E type 2 allele for late onset Alzheimer disease. *Nat Genet*, 7(2), pp. 180-184.

- Corder, E.H., Saunders, A.M., Strittmatter, W.J., Schmechel, D.E., Gaskell, P.C., Small, G.W., Roses, A.D., Haines, J.L. and Pericak-Vance, M.A., 1993. Gene Dose of Apolipoprotein E Type 4 Allele and the Risk of Alzheimer's Disease in Late Onset Families. *Science*, 261(5123), pp. 921-923.
- Craik, D.J., Fairlie, D.P., Liras, S. and Price, D., 2013. The Future of Peptide-based Drugs. *Chemical Biology & Drug Design*, 81(1), pp. 136-147.
- Cruts, M., Backhovens, H., Wang, S.Y., Van Gassen, G., Theuns, J., De Jonghe, C.D., Wehnert, A., De Voecht, J., De Winter, G., Cras, P. and et al., 1995. Molecular genetic analysis of familial early-onset Alzheimer's disease linked to chromosome 14q24.3. *Hum Mol Genet*, 4(12), pp. 2363-2371.
- Cruts, M., Dermaut, B., Rademakers, R., Van den Broeck, M., Stögbauer, F. and Van Broeckhoven, C., 2003. Novel APP mutation V715A associated with presenile Alzheimer's disease in a German family. *J Neurol*, 250(11), pp. 1374-1375.
- Cuende, J., Moreno, S., Bolaños, J.P. and Almeida, A., 2008. Retinoic acid downregulates Rae1 leading to APCCdh1 activation and neuroblastoma SH-SY5Y differentiation. *Oncogene*, 27(23), pp. 3339-3344.
- Cullen, N., Janelidze, S., Palmqvist, S., Stomrud, E., Mattsson-Carlgrén, N. and Hansson, O., 2021. Association of CSF A β 38 Levels With Risk of Alzheimer Disease-Related Decline. *Neurology*.
- D'Aloisio, V., Dognini, P., Hutcheon, G.A. and Coxon, C.R., 2021. PepTherDia: database and structural composition analysis of approved peptide therapeutics and diagnostics. *Drug Discovery Today*, 26(6), pp. 1409-1419.
- Datki, Z., Papp, R., Zádori, D., Soós, K., Fülöp, L., Juhász, A., Laskay, G., Hetényi, C., Mihalik, E., Zarándi, M. and Penke, B., 2004. In vitro model of neurotoxicity of A β 1-42 and neuroprotection by a pentapeptide: irreversible events during the first hour. *Neurobiol Dis*, 17(3), pp. 507-515.
- De Jonghe, C., Esselens, C., Kumar-Singh, S., Craessaerts, K., Serneels, S., Checler, F., Annaert, W., Van Broeckhoven, C. and De Strooper, B., 2001. Pathogenic APP mutations near the γ -secretase cleavage site differentially affect A β secretion and APP C-terminal fragment stability. *Human Molecular Genetics*, 10(16), pp. 1665-1671.
- de la Monte, S.M. and Wands, J.R., 2008. Alzheimer's disease is type 3 diabetes-evidence reviewed. *J Diabetes Sci Technol*, 2(6), pp. 1101-1113.
- Denault, M. and Pelletier, J.N., 2007. Protein Library Design and Screening. In: K.M. Arndt and K.M. Müller, eds. *Protein Engineering Protocols*. Totowa, NJ: Humana Press, pp. 127-154.
- Devkota, S., Williams, T.D. and Wolfe, M.S., 2021. Familial Alzheimer's disease mutations in amyloid protein precursor alter proteolysis by γ -secretase to increase amyloid β -peptides of ≥ 45 residues. *The Journal of biological chemistry*, 296, pp. 100281-100281.
- Eckman, C.B., Mehta, N.D., Crook, R., Perez-tur, J., Prihar, G., Pfeiffer, E., Graff-Radford, N., Hinder, P., Yager, D., Zenk, B., Refolo, L.M., Prada, C.M., Younkin, S.G., Hutton, M. and Hardy, J., 1997. A new pathogenic mutation in the APP gene (I716V) increases the relative proportion of A β 42(43). *Hum Mol Genet*, 6(12), pp. 2087-2089.
- Encinas, M., Iglesias, M., Liu, Y., Wang, H., Muhaisen, A., Ceña, V., Gallego, C. and Comella, J.X., 2000. Sequential treatment of SH-SY5Y cells with retinoic acid and brain-derived neurotrophic factor gives rise to fully differentiated, neurotrophic factor-dependent, human neuron-like cells. *J Neurochem*, 75(3), pp. 991-1003.

Esbjörner, E.K., Chan, F., Rees, E., Erdelyi, M., Luheshi, L.M., Bertoncini, C.W., Kaminski, C.F., Dobson, C.M. and Kaminski Schierle, G.S., 2014. Direct observations of amyloid β self-assembly in live cells provide insights into differences in the kinetics of A β (1-40) and A β (1-42) aggregation. *Chemistry & biology*, 21(6), pp. 732-742.

Esler, W.P., Stimson, E.R., Jennings, J.M., Vinters, H.V., Ghilardi, J.R., Lee, J.P., Mantyh, P.W. and Maggio, J.E., 2000. Alzheimer's disease amyloid propagation by a template-dependent dock-lock mechanism. *Biochemistry*, 39(21), pp. 6288-6295.

Fadoulglou, V.E., Kokkinidis, M. and Glykos, N.M., 2008. Determination of protein oligomerization state: Two approaches based on glutaraldehyde crosslinking. *Analytical Biochemistry*, 373(2), pp. 404-406.

Fancy, D.A. and Kodadek, T., 1999. Chemistry for the analysis of protein-protein interactions: rapid and efficient cross-linking triggered by long wavelength light. *Proceedings of the National Academy of Sciences of the United States of America*, 96(11), pp. 6020-6024.

Feng, J., Song, G., Shen, Q., Chen, X., Wang, Q., Guo, S. and Zhang, M., 2021. Protect Effects of Seafood-Derived Plasmalogens Against Amyloid-Beta (1-42) Induced Toxicity via Modulating the Transcripts Related to Endocytosis, Autophagy, Apoptosis, Neurotransmitter Release and Synaptic Transmission in SH-SY5Y Cells. *Front Aging Neurosci*, 13, p. 773713.

Finckh, U., Alberici, A., Antoniazzi, M., Benussi, L., Fedi, V., Giannini, C., Gal, A., Nitsch, R.M. and Binetti, G., 2000. Variable expression of familial Alzheimer disease associated with presenilin 2 mutation M239I. *Neurology*, 54(10), pp. 2006-2008.

Finckh, U., Müller-Thomsen, T., Mann, U., Eggers, C., Marksteiner, J., Meins, W., Binetti, G., Alberici, A., Hock, C., Nitsch, R.M. and Gal, A., 2000. High prevalence of pathogenic mutations in patients with early-onset dementia detected by sequence analyses of four different genes. *Am J Hum Genet*, 66(1), pp. 110-117.

Finder, V.H., Vodopivec, I., Nitsch, R.M. and Glockshuber, R., 2010. The recombinant amyloid-beta peptide Abeta1-42 aggregates faster and is more neurotoxic than synthetic Abeta1-42. *J Mol Biol*, 396(1), pp. 9-18.

Forster, J.I., Köglberger, S., Trefois, C., Boyd, O., Baumuratov, A.S., Buck, L., Balling, R. and Antony, P.M., 2016. Characterization of Differentiated SH-SY5Y as Neuronal Screening Model Reveals Increased Oxidative Vulnerability. *J Biomol Screen*, 21(5), pp. 496-509.

Fradinger, E.A., Monien, B.H., Urbanc, B., Lomakin, A., Tan, M., Li, H., Spring, S.M., Condrón, M.M., Cruz, L., Xie, C.W., Benedek, G.B. and Bitan, G., 2008. C-terminal peptides coassemble into Abeta42 oligomers and protect neurons against Abeta42-induced neurotoxicity. *Proc Natl Acad Sci U S A*, 105(37), pp. 14175-14180.

Frank, R.A., Galasko, D., Hampel, H., Hardy, J., de Leon, M.J., Mehta, P.D., Rogers, J., Siemers, E. and Trojanowski, J.Q., 2003. Biological markers for therapeutic trials in Alzheimer's disease: Proceedings of the biological markers working group; NIA initiative on neuroimaging in Alzheimer's disease. *Neurobiology of Aging*, 24(4), pp. 521-536.

Frankel, A.D. and Pabo, C.O., 1988. Cellular uptake of the tat protein from human immunodeficiency virus. *Cell*, 55(6), pp. 1189-1193.

Gallardo, R., Ranson, N.A. and Radford, S.E., 2020. Amyloid structures: much more than just a cross- β fold. *Current Opinion in Structural Biology*, 60, pp. 7-16.

- Glenner, G.G. and Wong, C.W., 1984. Alzheimer's disease: initial report of the purification and characterization of a novel cerebrovascular amyloid protein. *Biochem Biophys Res Commun*, 120(3), pp. 885-890.
- Goate, A., Chartier-Harlin, M.C., Mullan, M., Brown, J., Crawford, F., Fidani, L., Giuffra, L., Haynes, A., Irving, N., James, L. and et al., 1991. Segregation of a missense mutation in the amyloid precursor protein gene with familial Alzheimer's disease. *Nature*, 349(6311), pp. 704-706.
- Goedert, M., Ghetti, B. and Spillantini, M.G., 2012. Frontotemporal dementia: implications for understanding Alzheimer disease. *Cold Spring Harbor perspectives in medicine*, 2(2), pp. a006254-a006254.
- Goldie, B.J., Barnett, M.M. and Cairns, M.J., 2014. BDNF and the maturation of posttranscriptional regulatory networks in human SH-SY5Y neuroblast differentiation. *Frontiers in Cellular Neuroscience*, 8.
- Gremer, L., Schölzel, D., Schenk, C., Reinartz, E., Labahn, J., Ravelli, R.B.G., Tusche, M., Lopez-Iglesias, C., Hoyer, W., Heise, H., Willbold, D. and Schröder, G.F., 2017. Fibril structure of amyloid- β (1–42) by cryo-electron microscopy. *Science*, 358(6359), pp. 116-119.
- Grimm, M., Mett, J., Stahlmann, C., Grösgen, S., Hauptenthal, V., Blümel, T., Hundsdörfer, B., Zimmer, V., Mylonas, N., Tanila, H., Müller, U., Grimm, H. and Hartmann, T., 2015. APP intracellular domain derived from amyloidogenic β - and γ -secretase cleavage regulates neprilysin expression. *Frontiers in Aging Neuroscience*, 7.
- Grochowska, K.M., Yuanxiang, P., Bär, J., Raman, R., Brugal, G., Sahu, G., Schweizer, M., Bikbaev, A., Schilling, S., Demuth, H.-U. and Kreutz, M.R., 2017. Posttranslational modification impact on the mechanism by which amyloid- β induces synaptic dysfunction. *EMBO reports*, 18(6), pp. 962-981.
- Gulisano, W., Melone, M., Li Puma, D.D., Tropea, M.R., Palmeri, A., Arancio, O., Grassi, C., Conti, F. and Puzzo, D., 2018. The effect of amyloid-beta peptide on synaptic plasticity and memory is influenced by different isoforms, concentrations, and aggregation status. *Neurobiol Aging*, 71, pp. 51-60.
- Gurry, T. and Stultz, C.M., 2014. Mechanism of Amyloid- β Fibril Elongation. *Biochemistry*, 53(44), pp. 6981-6991.
- Hane, F.T., Robinson, M., Lee, B.Y., Bai, O., Leonenko, Z. and Albert, M.S., 2017. Recent Progress in Alzheimer's Disease Research, Part 3: Diagnosis and Treatment. *Journal of Alzheimer's Disease*, 57, pp. 645-665.
- Hardy, J. and Selkoe, D.J., 2002. The Amyloid Hypothesis of Alzheimer's Disease: Progress and Problems on the Road to Therapeutics. *Science*, 297(5580), p. 353.
- Hardy, J.A. and Higgins, G.A., 1992. Alzheimer's disease: the amyloid cascade hypothesis. *Science*, 256(5054), p. 184.
- Hayward, S. and Kitao, A., 2021. The role of the half-turn in determining structures of Alzheimer's A β wild-type and mutants. *Journal of Structural Biology*, 213(4), p. 107792.
- Head, E., Powell, D., Gold, B.T. and Schmitt, F.A., 2012. Alzheimer's Disease in Down Syndrome. *Eur J Neurodegener Dis*, 1(3), pp. 353-364.
- Hendriks, L., van Duijn, C.M., Cras, P., Cruts, M., Van Hul, W., van Harskamp, F., Warren, A., McInnis, M.G., Antonarakis, S.E., Martin, J.-J., Hofman, A. and Van Broeckhoven, C.,

1992. Presenile dementia and cerebral haemorrhage linked to a mutation at codon 692 of the β -amyloid precursor protein gene. *Nature Genetics*, 1(3), pp. 218-221.
- Henninot, A., Collins, J.C. and Nuss, J.M., 2018. The Current State of Peptide Drug Discovery: Back to the Future? *Journal of Medicinal Chemistry*, 61(4), pp. 1382-1414.
- Hippius, H. and Neundörfer, G., 2003. The discovery of Alzheimer's disease. *Dialogues in clinical neuroscience*, 5(1), pp. 101-108.
- Hole, K.L., Staniaszek, L.E., Menon Balan, G., Mason, J.M., Brown, J.T. and Williams, R.J., 2021. Oral (-)-Epicatechin Inhibits Progressive Tau Pathology in rTg4510 Mice Independent of Direct Actions at GSK3 β . *Frontiers in Neuroscience*, 15.
- Hooli, B.V., Kovacs-Vajna, Z.M., Mullin, K., Blumenthal, M.A., Mattheisen, M., Zhang, C., Lange, C., Mohapatra, G., Bertram, L. and Tanzi, R.E., 2014. Rare autosomal copy number variations in early-onset familial Alzheimer's disease. *Molecular Psychiatry*, 19(6), pp. 676-681.
- Huang, C.C., Chang, K.H., Chiu, Y.J., Chen, Y.R., Lung, T.H., Hsieh-Li, H.M., Su, M.T., Sun, Y.C., Chen, C.M., Lin, W. and Lee-Chen, G.J., 2021. Multi-Target Effects of Novel Synthetic Coumarin Derivatives Protecting A β -GFP SH-SY5Y Cells against A β Toxicity. *Cells*, 10(11).
- Huang, Y., Happonen, K.E., Burrola, P.G., O'Connor, C., Hah, N., Huang, L., Nimmerjahn, A. and Lemke, G., 2021. Microglia use TAM receptors to detect and engulf amyloid β plaques. *Nat Immunol*, 22(5), pp. 586-594.
- Hunsberger, H.C., Pinky, P.D., Smith, W., Suppiramaniam, V. and Reed, M.N., 2019. The role of APOE4 in Alzheimer's disease: strategies for future therapeutic interventions. *Neuronal signaling*, 3(2), pp. NS20180203-NS20180203.
- Jack, C.R., Jr., Knopman, D.S., Jagust, W.J., Petersen, R.C., Weiner, M.W., Aisen, P.S., Shaw, L.M., Vemuri, P., Wiste, H.J., Weigand, S.D., Lesnick, T.G., Pankratz, V.S., Donohue, M.C. and Trojanowski, J.Q., 2013. Tracking pathophysiological processes in Alzheimer's disease: an updated hypothetical model of dynamic biomarkers. *The Lancet. Neurology*, 12(2), pp. 207-216.
- Jämsä, A., Belda, O., Edlund, M. and Lindström, E., 2011. BACE-1 inhibition prevents the γ -secretase inhibitor evoked A β rise in human neuroblastoma SH-SY5Y cells. *Journal of Biomedical Science*, 18(1), p. 76.
- Janowicz, P.W., Leinenga, G., Götz, J. and Nisbet, R.M., 2019. Ultrasound-mediated blood-brain barrier opening enhances delivery of therapeutically relevant formats of a tau-specific antibody. *Sci Rep*, 9(1), p. 9255.
- Jiang, B., Zhou, J., Li, H.L., Chen, Y.G., Cheng, H.R., Ye, L.Q., Liu, D.S., Chen, D.F., Tao, Q.Q. and Wu, Z.Y., 2019. Mutation screening in Chinese patients with familial Alzheimer's disease by whole-exome sequencing. *Neurobiol Aging*, 76, pp. 215.e215-215.e221.
- Jin, M., Shepardson, N., Yang, T., Chen, G., Walsh, D. and Selkoe, D.J., 2011. Soluble amyloid beta-protein dimers isolated from Alzheimer cortex directly induce Tau hyperphosphorylation and neuritic degeneration. *Proc Natl Acad Sci U S A*, 108(14), pp. 5819-5824.
- Johansson-Åkhe, I., Mirabello, C. and Wallner, B., 2019. Predicting protein-peptide interaction sites using distant protein complexes as structural templates. *Scientific Reports*, 9(1), p. 4267.

- Jonsson, T., Atwal, J.K., Steinberg, S., Snaedal, J., Jonsson, P.V., Bjornsson, S., Stefansson, H., Sulem, P., Gudbjartsson, D., Maloney, J., Hoyte, K., Gustafson, A., Liu, Y., Lu, Y., Bhangale, T., Graham, R.R., Huttenlocher, J., Bjornsdottir, G., Andreassen, O.A., Jonsson, E.G., Palotie, A., Behrens, T.W., Magnusson, O.T., Kong, A., Thorsteinsdottir, U., Watts, R.J. and Stefansson, K., 2012. A mutation in APP protects against Alzheimer's disease and age-related cognitive decline. *Nature*, 488(7409), pp. 96-99.
- Jorfi, M., D'Avanzo, C., Tanzi, R.E., Kim, D.Y. and Irimia, D., 2018. Human Neurospheroid Arrays for In Vitro Studies of Alzheimer's Disease. *Sci Rep*, 8(1), p. 2450.
- Juhász, G., Márki, Á., Vass, G., Fülöp, L., Budai, D., Penke, B., Falkay, G. and Szegedi, V., 2009. An Intraperitoneally Administered Pentapeptide Protects Against A β 1–42 Induced Neuronal Excitation In Vivo. *Journal of Alzheimer's Disease*, 16, pp. 189-196.
- Jung, S., Hyun, J., Nah, J., Han, J., Kim, S.-H., Park, J., Oh, Y., Gwon, Y., Moon, S., Jo, D.-G. and Jung, Y.-K., 2020. SERP1 is an assembly regulator of γ -secretase in metabolic stress conditions. *Science Signaling*, 13(623), p. eaax8949.
- Kamenetz, F., Tomita, T., Hsieh, H., Seabrook, G., Borchelt, D., Iwatsubo, T., Sisodia, S. and Malinow, R., 2003. APP processing and synaptic function. *Neuron*, 37(6), pp. 925-937.
- Kelava, I. and Lancaster, M.A., 2016. Stem Cell Models of Human Brain Development. *Cell Stem Cell*, 18(6), pp. 736-748.
- Killin, L.O.J., Starr, J.M., Shiue, I.J. and Russ, T.C., 2016. Environmental risk factors for dementia: a systematic review. *BMC geriatrics*, 16(1), pp. 175-175.
- Kim, J., Basak, J.M. and Holtzman, D.M., 2009. The role of apolipoprotein E in Alzheimer's disease. *Neuron*, 63(3), pp. 287-303.
- Kollmer, M., Close, W., Funk, L., Rasmussen, J., Bsoul, A., Schierhorn, A., Schmidt, M., Sigurdson, C.J., Jucker, M. and Fändrich, M., 2019. Cryo-EM structure and polymorphism of A β amyloid fibrils purified from Alzheimer's brain tissue. *Nature communications*, 10(1), pp. 4760-4760.
- Kovalevich, J. and Langford, D., 2013. Considerations for the use of SH-SY5Y neuroblastoma cells in neurobiology. *Methods in molecular biology (Clifton, N.J.)*, 1078, pp. 9-21.
- Krishna, K.V., Wadhwa, G., Alexander, A., Kanojia, N., Saha, R.N., Kukreti, R., Singhvi, G. and Dubey, S.K., 2019. Design and Biological Evaluation of Lipoprotein-Based Donepezil Nanocarrier for Enhanced Brain Uptake through Oral Delivery. *ACS Chem Neurosci*, 10(9), pp. 4124-4135.
- Krishtal, J., Bragina, O., Metsla, K., Palumaa, P. and Tõugu, V., 2015. Toxicity of amyloid beta 1-40 and 1-42 on SH-SY5Y cell line. *SpringerPlus*, 4(Suppl 1), p. P19.
- Krishtal, J., Bragina, O., Metsla, K., Palumaa, P. and Tõugu, V., 2017. In situ fibrillizing amyloid-beta 1-42 induces neurite degeneration and apoptosis of differentiated SH-SY5Y cells. *PloS one*, 12(10), pp. e0186636-e0186636.
- Krishtal, J., Metsla, K., Bragina, O., Tõugu, V. and Palumaa, P., 2019. Toxicity of Amyloid- β Peptides Varies Depending on Differentiation Route of SH-SY5Y Cells. *Journal of Alzheimer's Disease*, 71(3), pp. 879-887.
- Kumar-Singh, S., De Jonghe, C., Cruts, M., Kleinert, R., Wang, R., Mercken, M., De Strooper, B., Vanderstichele, H., Löfgren, A., Vanderhoeven, I., Backhovens, H., Vanmechelen, E., Kroeisel, P.M. and Van Broeckhoven, C., 2000. Nonfibrillar diffuse amyloid

deposition due to a gamma(42)-secretase site mutation points to an essential role for N-truncated A beta(42) in Alzheimer's disease. *Hum Mol Genet*, 9(18), pp. 2589-2598.

Kumar, S. and Walter, J., 2011. Phosphorylation of amyloid beta (A β) peptides - a trigger for formation of toxic aggregates in Alzheimer's disease. *Aging (Albany NY)*, 3(8), pp. 803-812.

Kwak, S.S., Washicosky, K.J., Brand, E., von Maydell, D., Aronson, J., Kim, S., Capen, D.E., Cetinbas, M., Sadreyev, R., Ning, S., Bylykbashi, E., Xia, W., Wagner, S.L., Choi, S.H., Tanzi, R.E. and Kim, D.Y., 2020. Amyloid- β 42/40 ratio drives tau pathology in 3D human neural cell culture models of Alzheimer's disease. *Nature communications*, 11(1), pp. 1377-1377.

Larson, M., Sherman, M.A., Amar, F., Nuvolone, M., Schneider, J.A., Bennett, D.A., Aguzzi, A. and Lesné, S.E., 2012. The complex PrP(c)-Fyn couples human oligomeric A β with pathological tau changes in Alzheimer's disease. *The Journal of neuroscience : the official journal of the Society for Neuroscience*, 32(47), pp. 16857-16871a.

Lau, J.L. and Dunn, M.K., 2018. Therapeutic peptides: Historical perspectives, current development trends, and future directions. *Bioorganic & Medicinal Chemistry*, 26(10), pp. 2700-2707.

Leissring, M.A., Murphy, M.P., Mead, T.R., Akbari, Y., Sugarman, M.C., Jannatipour, M., Anliker, B., Muller, U., Saftig, P., De Strooper, B., Wolfe, M.S., Golde, T.E. and LaFerla, F.M., 2002. A physiologic signaling role for the gamma -secretase-derived intracellular fragment of APP. *Proc Natl Acad Sci U S A*, 99(7), pp. 4697-4702.

Leithold, L.H., Jiang, N., Post, J., Ziehm, T., Schartmann, E., Kutzsche, J., Shah, N.J., Breitzkreutz, J., Langen, K.J., Willuweit, A. and Willbold, D., 2016. Pharmacokinetic Properties of a Novel D-Peptide Developed to be Therapeutically Active Against Toxic β -Amyloid Oligomers. *Pharm Res*, 33(2), pp. 328-336.

Leithold, L.H.E., Jiang, N., Post, J., Ziehm, T., Schartmann, E., Kutzsche, J., Shah, N.J., Breitzkreutz, J., Langen, K.-J., Willuweit, A. and Willbold, D., 2016. Pharmacokinetic Properties of a Novel d-Peptide Developed to be Therapeutically Active Against Toxic β -Amyloid Oligomers. *Pharmaceutical Research*, 33(2), pp. 328-336.

Leshem, G., Richman, M., Lisniansky, E., Antman-Passig, M., Habashi, M., Gräslund, A., Wärmländer, S. and Rahimipour, S., 2019. Photoactive chlorin e6 is a multifunctional modulator of amyloid- β aggregation and toxicity via specific interactions with its histidine residues. *Chem Sci*, 10(1), pp. 208-217.

Levy-Lahad, E., Wasco, W., Poorkaj, P., Romano, D.M., Oshima, J., Pettingell, W.H., Yu, C.E., Jondro, P.D., Schmidt, S.D., Wang, K. and et al., 1995. Candidate gene for the chromosome 1 familial Alzheimer's disease locus. *Science*, 269(5226), pp. 973-977.

Levy, E., Carman, M.D., Fernandez-Madrid, I.J., Power, M.D., Lieberburg, I., van Duinen, S.G., Bots, G.T., Luyendijk, W. and Frangione, B., 1990. Mutation of the Alzheimer's disease amyloid gene in hereditary cerebral hemorrhage, Dutch type. *Science*, 248(4959), pp. 1124-1126.

Lewis, J., Dickson, D.W., Lin, W.L., Chisholm, L., Corral, A., Jones, G., Yen, S.H., Sahara, N., Skipper, L., Yager, D., Eckman, C., Hardy, J., Hutton, M. and McGowan, E., 2001. Enhanced neurofibrillary degeneration in transgenic mice expressing mutant tau and APP. *Science*, 293(5534), pp. 1487-1491.

Li, S.C., Goto, N.K., Williams, K.A. and Deber, C.M., 1996. Alpha-helical, but not beta-sheet, propensity of proline is determined by peptide environment. *Proc Natl Acad Sci U S A*, 93(13), pp. 6676-6681.

- Lista, S., O'Bryant, S.E., Blennow, K., Dubois, B., Hugon, J., Zetterberg, H. and Hampel, H., 2015. Biomarkers in Sporadic and Familial Alzheimer's Disease. *Journal of Alzheimer's Disease*, 47, pp. 291-317.
- Litwiniuk, A., Domańska, A., Chmielowska, M., Martyńska, L., Bik, W. and Kalisz, M., 2020. The Effects of Alpha-Linolenic Acid on the Secretory Activity of Astrocytes and β Amyloid-Associated Neurodegeneration in Differentiated SH-SY5Y Cells: Alpha-Linolenic Acid Protects the SH-SY5Y cells against β Amyloid Toxicity. *Oxid Med Cell Longev*, 2020, p. 8908901.
- Liu, C.Y., Ohki, Y., Tomita, T., Osawa, S., Reed, B.R., Jagust, W., Van Berlo, V., Jin, L.W., Chui, H.C., Coppola, G. and Ringman, J.M., 2017. Two Novel Mutations in the First Transmembrane Domain of Presenilin1 Cause Young-Onset Alzheimer's Disease. *J Alzheimers Dis*, 58(4), pp. 1035-1041.
- Liu, Y., 1999. Understanding the biological activity of amyloid proteins in vitro: from inhibited cellular MTT reduction to altered cellular cholesterol homeostasis. *Prog Neuropsychopharmacol Biol Psychiatry*, 23(3), pp. 377-395.
- Lopes, F.M., Schröder, R., Júnior, M.L.C.d.F., Zanotto-Filho, A., Müller, C.B., Pires, A.S., Meurer, R.T., Colpo, G.D., Gelain, D.P., Kapczinski, F., Moreira, J.C.F., Fernandes, M.d.C. and Klamt, F., 2010. Comparison between proliferative and neuron-like SH-SY5Y cells as an in vitro model for Parkinson disease studies. *Brain Research*, 1337, pp. 85-94.
- Lührs, T., Ritter, C., Adrian, M., Riek-Loher, D., Bohrmann, B., Döbeli, H., Schubert, D. and Riek, R., 2005. 3D structure of Alzheimer's amyloid-beta(1-42) fibrils. *Proc Natl Acad Sci U S A*, 102(48), pp. 17342-17347.
- Ma, J., Brewer, H.B., Jr. and Potter, H., 1996. Alzheimer A beta neurotoxicity: promotion by antichymotrypsin, ApoE4; inhibition by A beta-related peptides. *Neurobiol Aging*, 17(5), pp. 773-780.
- Mairuae, N., Connor, J.R., Buranrat, B. and Lee, S.Y., 2019. Oroxyllum indicum (L.) extract protects human neuroblastoma SH-SY5Y cells against β -amyloid-induced cell injury. *Mol Med Rep*, 20(2), pp. 1933-1942.
- Makin, S., 2018. The amyloid hypothesis on trial. *Nature*, 559(7715), pp. S4-s7.
- Maloney, J.A., Bainbridge, T., Gustafson, A., Zhang, S., Kyauk, R., Steiner, P., van der Brug, M., Liu, Y., Ernst, J.A., Watts, R.J. and Atwal, J.K., 2014. Molecular mechanisms of Alzheimer disease protection by the A673T allele of amyloid precursor protein. *J Biol Chem*, 289(45), pp. 30990-31000.
- Mannini, B., Mulvihill, E., Sgromo, C., Cascella, R., Khodarahmi, R., Ramazzotti, M., Dobson, C.M., Cecchi, C. and Chiti, F., 2014. Toxicity of Protein Oligomers Is Rationalized by a Function Combining Size and Surface Hydrophobicity. *ACS Chemical Biology*, 9(10), pp. 2309-2317.
- Marín, N., Romero, B., Bosch-Morell, F., Llansola, M., Felipe, V., Romá, J. and Romero, F.J., 2000. Beta-amyloid-induced activation of caspase-3 in primary cultures of rat neurons. *Mech Ageing Dev*, 119(1-2), pp. 63-67.
- Mason, J.M., 2010. Design and development of peptides and peptide mimetics as antagonists for therapeutic intervention. *Future Med Chem*, 2(12), pp. 1813-1822.
- Mattson, M.P., 1997. Cellular actions of beta-amyloid precursor protein and its soluble and fibrillogenic derivatives. *Physiological Reviews*, 77(4), pp. 1081-1132.

- Mattson, M.P., Cheng, B., Culwell, A.R., Esch, F.S., Lieberburg, I. and Rydel, R.E., 1993. Evidence for excitoprotective and intraneuronal calcium-regulating roles for secreted forms of the beta-amyloid precursor protein. *Neuron*, 10(2), pp. 243-254.
- Melino, G., Thiele, C.J., Knight, R.A. and Piacentini, M., 1997. Retinoids and the control of growth/death decisions in human neuroblastoma cell lines. *J Neurooncol*, 31(1-2), pp. 65-83.
- Mintun, M.A., Lo, A.C., Duggan Evans, C., Wessels, A.M., Ardayfio, P.A., Andersen, S.W., Shcherbinin, S., Sparks, J., Sims, J.R., Brys, M., Apostolova, L.G., Salloway, S.P. and Skovronsky, D.M., 2021. Donanemab in Early Alzheimer's Disease. *N Engl J Med*, 384(18), pp. 1691-1704.
- Molina-Holgado, F., Gaeta, A., Francis, P.T., Williams, R.J. and Hider, R.C., 2008. Neuroprotective actions of deferiprone in cultured cortical neurones and SHSY-5Y cells. *Journal of Neurochemistry*, 105(6), pp. 2466-2476.
- Möller, H.J. and Graeber, M.B., 1998. The case described by Alois Alzheimer in 1911. Historical and conceptual perspectives based on the clinical record and neurohistological sections. *Eur Arch Psychiatry Clin Neurosci*, 248(3), pp. 111-122.
- Mroczko, B., Groblewska, M., Litman-Zawadzka, A., Kornhuber, J. and Lewczuk, P., 2018. Amyloid β oligomers (A β Os) in Alzheimer's disease. *Journal of Neural Transmission*, 125(2), pp. 177-191.
- Mullan, M., Crawford, F., Axelman, K., Houlden, H., Lilius, L., Winblad, B. and Lannfelt, L., 1992. A pathogenic mutation for probable Alzheimer's disease in the APP gene at the N-terminus of beta-amyloid. *Nat Genet*, 1(5), pp. 345-347.
- Murrell, J.R., Hake, A.M., Quaid, K.A., Farlow, M.R. and Ghetti, B., 2000. Early-onset Alzheimer disease caused by a new mutation (V717L) in the amyloid precursor protein gene. *Arch Neurol*, 57(6), pp. 885-887.
- Nguyen, K.V., 2018. Special Issue: Alzheimer's disease. *AIMS neuroscience*, 5(1), pp. 74-80.
- Nikolaev, A., McLaughlin, T., O'Leary, D.D. and Tessier-Lavigne, M., 2009. APP binds DR6 to trigger axon pruning and neuron death via distinct caspases. *Nature*, 457(7232), pp. 981-989.
- Nilsberth, C., Westlind-Danielsson, A., Eckman, C.B., Condron, M.M., Axelman, K., Forsell, C., Sten, C., Luthman, J., Teplow, D.B., Younkin, S.G., Naslund, J. and Lannfelt, L., 2001. The 'Arctic' APP mutation (E693G) causes Alzheimer's disease by enhanced Abeta protofibril formation. *Nat Neurosci*, 4(9), pp. 887-893.
- Nortley, R., Korte, N., Izquierdo, P., Hirunpattarasilp, C., Mishra, A., Jaunmuktane, Z., Kyrargyri, V., Pfeiffer, T., Khennouf, L., Madry, C., Gong, H., Richard-Loendt, A., Huang, W., Saito, T., Saido, T.C., Brandner, S., Sethi, H. and Attwell, D., 2019. Amyloid β oligomers constrict human capillaries in Alzheimer's disease via signaling to pericytes. *Science (New York, N.Y.)*, 365(6450), p. eaav9518.
- Oddo, S., Billings, L., Kesslak, J.P., Cribbs, D.H. and LaFerla, F.M., 2004. Immunotherapy Leads to Clearance of Early, but Not Late, Hyperphosphorylated Tau Aggregates via the Proteasome. *Neuron*, 43(3), pp. 321-332.
- Oguchi, T., Ono, R., Tsuji, M., Shozawa, H., Somei, M., Inagaki, M., Mori, Y., Yasumoto, T., Ono, K. and Kiuchi, Y., 2017. Cilostazol Suppresses A β -induced Neurotoxicity in SH-SY5Y Cells through Inhibition of Oxidative Stress and MAPK Signaling Pathway. *Frontiers in Aging Neuroscience*, 9.

Ostrowitzki, S., Lasser, R.A., Dorflinger, E., Scheltens, P., Barkhof, F., Nikolcheva, T., Ashford, E., Retout, S., Hofmann, C., Delmar, P., Klein, G., Andjelkovic, M., Dubois, B., Boada, M., Blennow, K., Santarelli, L. and Fontoura, P., 2017. A phase III randomized trial of gantenerumab in prodromal Alzheimer's disease. *Alzheimers Res Ther*, 9(1), p. 95.

Pagnon de la Vega, M., Giedraitis, V., Michno, W., Kilander, L., Güner, G., Zielinski, M., Löwenmark, M., Brundin, R., Danfors, T., Söderberg, L., Alafuzoff, I., Nilsson, L.N.G., Erlandsson, A., Willbold, D., Müller, S.A., Schröder, G.F., Hanrieder, J., Lichtenthaler, S.F., Lannfelt, L., Sehlin, D. and Ingelsson, M., 2021. The Uppsala APP deletion causes early onset autosomal dominant Alzheimer's disease by altering APP processing and increasing amyloid β fibril formation. *Sci Transl Med*, 13(606).

Paik, S., Somvanshi, R.K., Oliveira, H.A., Zou, S. and Kumar, U., 2021. Somatostatin Ameliorates β -Amyloid-Induced Cytotoxicity via the Regulation of CRMP2 Phosphorylation and Calcium Homeostasis in SH-SY5Y Cells. *Biomedicines*, 9(1).

Panza, F., Lozupone, M., Logroscino, G. and Imbimbo, B.P., 2019. A critical appraisal of amyloid- β -targeting therapies for Alzheimer disease. *Nature Reviews Neurology*, 15(2), pp. 73-88.

Paravastu, A.K., Leapman, R.D., Yau, W.-M. and Tycko, R., 2008. Molecular structural basis for polymorphism in Alzheimer's beta-amyloid fibrils. *Proceedings of the National Academy of Sciences of the United States of America*, 105(47), pp. 18349-18354.

Pasalar, P., Najmabadi, H., Noorian, A.R., Moghimi, B., Jannati, A., Soltanzadeh, A., Krefft, T., Crook, R. and Hardy, J., 2002. An Iranian family with Alzheimer's disease caused by a novel APP mutation (Thr714Ala). *Neurology*, 58(10), pp. 1574-1575.

Patterson, C., 2018. World Alzheimer Report 2018

The state of the art of dementia research:

New frontiers.

Peacock, M.L., Warren, J.T., Jr., Roses, A.D. and Fink, J.K., 1993. Novel polymorphism in the A4 region of the amyloid precursor protein gene in a patient without Alzheimer's disease. *Neurology*, 43(6), pp. 1254-1256.

Permanne, B., Adessi, C., Saborio, G.P., Fraga, S., Frossard, M.-J., Van Dorpe, J., Dewachter, I., Banks, W.A., Van Leuven, F. and Soto, C., 2002. Reduction of amyloid load and cerebral damage in transgenic mouse model of Alzheimer's disease by treatment with a β -sheet breaker peptide. *The FASEB Journal*, 16(8), pp. 860-862.

Peters, I., Igbavboa, U., Schütt, T., Haidari, S., Hartig, U., Rosello, X., Böttner, S., Copanaki, E., Deller, T., Kögel, D., Wood, W.G., Müller, W.E. and Eckert, G.P., 2009. The interaction of beta-amyloid protein with cellular membranes stimulates its own production. *Biochimica et Biophysica Acta (BBA) - Biomembranes*, 1788(5), pp. 964-972.

Picone, P., Nuzzo, D., Giacomazza, D. and Di Carlo, M., 2020. β -Amyloid Peptide: the Cell Compartment Multi-faceted Interaction in Alzheimer's Disease. *Neurotox Res*, 37(2), pp. 250-263.

Plant, L.D., Boyle, J.P., Smith, I.F., Peers, C. and Pearson, H.A., 2003. The production of amyloid beta peptide is a critical requirement for the viability of central neurons. *J Neurosci*, 23(13), pp. 5531-5535.

Puzzo, D., 2019. A β oligomers: role at the synapse. *Aging*, 11(4), pp. 1077-1078.

Puzzo, D., Privitera, L., Leznik, E., Fà, M., Staniszewski, A., Palmeri, A. and Arancio, O., 2008. Picomolar amyloid-beta positively modulates synaptic plasticity and memory in hippocampus. *The Journal of neuroscience : the official journal of the Society for Neuroscience*, 28(53), pp. 14537-14545.

Qian, X., Nguyen, H.N., Song, M.M., Hadiono, C., Ogden, S.C., Hammack, C., Yao, B., Hamersky, G.R., Jacob, F., Zhong, C., Yoon, K.J., Jeang, W., Lin, L., Li, Y., Thakor, J., Berg, D.A., Zhang, C., Kang, E., Chickering, M., Nauen, D., Ho, C.Y., Wen, Z., Christian, K.M., Shi, P.Y., Maher, B.J., Wu, H., Jin, P., Tang, H., Song, H. and Ming, G.L., 2016. Brain-Region-Specific Organoids Using Mini-bioreactors for Modeling ZIKV Exposure. *Cell*, 165(5), pp. 1238-1254.

Rahimi, F., Maiti, P. and Bitan, G., 2009. Photo-induced cross-linking of unmodified proteins (PICUP) applied to amyloidogenic peptides. *Journal of visualized experiments : JoVE*, (23), p. 1071.

Recio, C., Maione, F., Iqbal, A.J., Mascolo, N. and De Feo, V., 2017. The Potential Therapeutic Application of Peptides and Peptidomimetics in Cardiovascular Disease. *Frontiers in pharmacology*, 7, pp. 526-526.

Reed, M.N., Hofmeister, J.J., Jungbauer, L., Welzel, A.T., Yu, C., Sherman, M.A., Lesné, S., LaDu, M.J., Walsh, D.M., Ashe, K.H. and Cleary, J.P., 2011. Cognitive effects of cell-derived and synthetically derived A β oligomers. *Neurobiol Aging*, 32(10), pp. 1784-1794.

Remy, I., Campbell-Valois, F.X. and Michnick, S.W., 2007. Detection of protein–protein interactions using a simple survival protein-fragment complementation assay based on the enzyme dihydrofolate reductase. *Nature Protocols*, 2(9), pp. 2120-2125.

Robakis, N.K., 2011. Mechanisms of AD neurodegeneration may be independent of Abeta and its derivatives. *Neurobiol Aging*, 32(3), pp. 372-379.

Rocchi, A., Pellegrini, S., Siciliano, G. and Murri, L., 2003. Causative and susceptibility genes for Alzheimer's disease: a review. *Brain Res Bull*, 61(1), pp. 1-24.

Rogaev, E.I., Sherrington, R., Rogaeva, E.A., Levesque, G., Ikeda, M., Liang, Y., Chi, H., Lin, C., Holman, K., Tsuda, T. and et al., 1995. Familial Alzheimer's disease in kindreds with missense mutations in a gene on chromosome 1 related to the Alzheimer's disease type 3 gene. *Nature*, 376(6543), pp. 775-778.

Ryan, P., Patel, B., Makwana, V., Jadhav, H.R., Kiefel, M., Davey, A., Reekie, T.A., Rudrawar, S. and Kassiou, M., 2018. Peptides, Peptidomimetics, and Carbohydrate–Peptide Conjugates as Amyloidogenic Aggregation Inhibitors for Alzheimer's Disease. *ACS Chemical Neuroscience*, 9(7), pp. 1530-1551.

Sadowski, M., Pankiewicz, J., Scholtzova, H., Ripellino, J.A., Li, Y., Schmidt, S.D., Mathews, P.M., Fryer, J.D., Holtzman, D.M., Sigurdsson, E.M. and Wisniewski, T., 2004. A synthetic peptide blocking the apolipoprotein E/beta-amyloid binding mitigates beta-amyloid toxicity and fibril formation in vitro and reduces beta-amyloid plaques in transgenic mice. *The American journal of pathology*, 165(3), pp. 937-948.

Sarkanen, J.-R., Nykky, J., Siikanen, J., Selinummi, J., Ylikomi, T. and Jalonen, T.O., 2007. Cholesterol supports the retinoic acid-induced synaptic vesicle formation in differentiating human SH-SY5Y neuroblastoma cells. *Journal of Neurochemistry*, 102(6), pp. 1941-1952.

Sawaya, M.R., Hughes, M.P., Rodriguez, J.A., Riek, R. and Eisenberg, D.S., 2021. The expanding amyloid family: Structure, stability, function, and pathogenesis. *Cell*, 184(19), pp. 4857-4873.

Scheuner, D., Eckman, C., Jensen, M., Song, X., Citron, M., Suzuki, N., Bird, T.D., Hardy, J., Hutton, M., Kukull, W., Larson, E., Levy-Lahad, E., Viitanen, M., Peskind, E., Poorkaj, P., Schellenberg, G., Tanzi, R., Wasco, W., Lannfelt, L., Selkoe, D. and Younkin, S., 1996. Secreted amyloid beta-protein similar to that in the senile plaques of Alzheimer's disease is increased in vivo by the presenilin 1 and 2 and APP mutations linked to familial Alzheimer's disease. *Nat Med*, 2(8), pp. 864-870.

Schumacher, T.N., Mayr, L.M., Minor, D.L., Jr., Milhollen, M.A., Burgess, M.W. and Kim, P.S., 1996. Identification of D-peptide ligands through mirror-image phage display. *Science*, 271(5257), pp. 1854-1857.

Selkoe, D.J., 2021a. Alzheimer's drugs: Does reducing amyloid work?—Response. *Science*, 374(6567), pp. 545-546.

Selkoe, D.J., 2021b. Treatments for Alzheimer's disease emerge. *Science*, 373(6555), pp. 624-626.

Selkoe, D.J. and Hardy, J., 2016. The amyloid hypothesis of Alzheimer's disease at 25 years. *EMBO molecular medicine*, 8(6), pp. 595-608.

Shankar, G.M., Li, S., Mehta, T.H., Garcia-Munoz, A., Shepardson, N.E., Smith, I., Brett, F.M., Farrell, M.A., Rowan, M.J., Lemere, C.A., Regan, C.M., Walsh, D.M., Sabatini, B.L. and Selkoe, D.J., 2008. Amyloid- β protein dimers isolated directly from Alzheimer's brains impair synaptic plasticity and memory. *Nature Medicine*, 14(8), pp. 837-842.

Shea, D., Hsu, C.C., Bi, T.M., Paranjapye, N., Childers, M.C., Cochran, J., Tomberlin, C.P., Wang, L., Paris, D., Zonderman, J., Varani, G., Link, C.D., Mullan, M. and Daggett, V., 2019. α -Sheet secondary structure in amyloid β -peptide drives aggregation and toxicity in Alzheimer's disease. *Proc Natl Acad Sci U S A*, 116(18), pp. 8895-8900.

Sidell, N., Lucas, C.A. and Kreutzberg, G.W., 1984. Regulation of acetylcholinesterase activity by retinoic acid in a human neuroblastoma cell line. *Experimental Cell Research*, 155(1), pp. 305-309.

Slanzi, A., Iannoto, G., Rossi, B., Zenaro, E. and Constantin, G., 2020. In vitro Models of Neurodegenerative Diseases. *Frontiers in Cell and Developmental Biology*, 8.

Society, A.s., 2022a. *Alzheimer's Disease* [Online]. Available from: <https://www.alzheimers.org.uk/about-dementia/types-dementia/alzheimers-disease> [Accessed 18/02/2022].

Society, A.s., 2022b. *Dementia and the brain* [Online]. Available from: <https://www.alzheimers.org.uk/about-dementia/symptoms-and-diagnosis/how-dementia-progresses/brain-dementia> [Accessed 14/02/22].

Somel, M., Liu, X., Tang, L., Yan, Z., Hu, H., Guo, S., Jiang, X., Zhang, X., Xu, G., Xie, G., Li, N., Hu, Y., Chen, W., Pääbo, S. and Khaitovich, P., 2011. MicroRNA-Driven Developmental Remodeling in the Brain Distinguishes Humans from Other Primates. *PLOS Biology*, 9(12), p. e1001214.

Soscia, S.J., Kirby, J.E., Washicosky, K.J., Tucker, S.M., Ingelsson, M., Hyman, B., Burton, M.A., Goldstein, L.E., Duong, S., Tanzi, R.E. and Moir, R.D., 2010. The Alzheimer's disease-associated amyloid beta-protein is an antimicrobial peptide. *PloS one*, 5(3), pp. e9505-e9505.

Soto, C., Kindy, M.S., Baumann, M. and Frangione, B., 1996. Inhibition of Alzheimer's amyloidosis by peptides that prevent beta-sheet conformation. *Biochem Biophys Res Commun*, 226(3), pp. 672-680.

- Soto, C., Sigurdsson, E.M., Morelli, L., Kumar, R.A., Castano, E.M. and Frangione, B., 1998. Beta-sheet breaker peptides inhibit fibrillogenesis in a rat brain model of amyloidosis: implications for Alzheimer's therapy. *Nat Med*, 4(7), pp. 822-826.
- Spencer, R.K., Li, H. and Nowick, J.S., 2014. X-ray crystallographic structures of trimers and higher-order oligomeric assemblies of a peptide derived from A β (17-36). *Journal of the American Chemical Society*, 136(15), pp. 5595-5598.
- Sun, P., Ding, H., Liang, M., Li, X., Mo, W., Wang, X., Liu, Y., He, R. and Hua, Q., 2014. Neuroprotective Effects of Geniposide in SH-SY5Y Cells and Primary Hippocampal Neurons Exposed to A β 42. *BioMed Research International*, 2014, p. 284314.
- Swanson, C.J., Zhang, Y., Dhadda, S., Wang, J., Kaplow, J., Lai, R.Y.K., Lannfelt, L., Bradley, H., Rabe, M., Koyama, A., Reyderman, L., Berry, D.A., Berry, S., Gordon, R., Kramer, L.D. and Cummings, J.L., 2021. A randomized, double-blind, phase 2b proof-of-concept clinical trial in early Alzheimer's disease with lecanemab, an anti-A β protofibril antibody. *Alzheimers Res Ther*, 13(1), p. 80.
- Takahashi, T. and Mihara, H., 2008. Peptide and Protein Mimetics Inhibiting Amyloid β -Peptide Aggregation. *Accounts of Chemical Research*, 41(10), pp. 1309-1318.
- Tanaka, S., Nakamura, S. and Ueda, K., 1990. [Expression of amyloid beta-protein gene in Alzheimer's disease]. *Rinsho Byori*, 38(5), pp. 489-493.
- Taylor, H.B.C., Emptage, N.J. and Jeans, A.F., 2021. Long-term depression links amyloid- β to the pathological hyperphosphorylation of tau. *Cell reports*, 36(9), pp. 109638-109638.
- Taylor, M., Moore, S., Mayes, J., Parkin, E., Beeg, M., Canovi, M., Gobbi, M., Mann, D.M. and Allsop, D., 2010. Development of a proteolytically stable retro-inverso peptide inhibitor of beta-amyloid oligomerization as a potential novel treatment for Alzheimer's disease. *Biochemistry*, 49(15), pp. 3261-3272.
- Texidó, L., Martín-Satué, M., Alberdi, E., Solsona, C. and Matute, C., 2011. Amyloid β peptide oligomers directly activate NMDA receptors. *Cell Calcium*, 49(3), pp. 184-190.
- Tjernberg, L.O., Lilliehöök, C., Callaway, D.J., Näslund, J., Hahne, S., Thyberg, J., Terenius, L. and Nordstedt, C., 1997. Controlling amyloid beta-peptide fibril formation with protease-stable ligands. *J Biol Chem*, 272(19), pp. 12601-12605.
- Tjernberg, L.O., Näslund, J., Lindqvist, F., Johansson, J., Karlström, A.R., Thyberg, J., Terenius, L. and Nordstedt, C., 1996. Arrest of beta-amyloid fibril formation by a pentapeptide ligand. *J Biol Chem*, 271(15), pp. 8545-8548.
- Tomiya, T., Nagata, T., Shimada, H., Teraoka, R., Fukushima, A., Kanemitsu, H., Takuma, H., Kuwano, R., Imagawa, M., Ataka, S., Wada, Y., Yoshioka, E., Nishizaki, T., Watanabe, Y. and Mori, H., 2008. A new amyloid beta variant favoring oligomerization in Alzheimer's-type dementia. *Ann Neurol*, 63(3), pp. 377-387.
- Törnquist, M., Michaels, T.C.T., Sanagavarapu, K., Yang, X., Meisl, G., Cohen, S.I.A., Knowles, T.P.J. and Linse, S., 2018. Secondary nucleation in amyloid formation. *Chemical Communications*, 54(63), pp. 8667-8684.
- Trujillo-Estrada, L., Sanchez-Mejias, E., Sanchez-Varo, R., Garcia-Leon, J.A., Nuñez-Diaz, C., Davila, J.C., Vitorica, J., LaFerla, F.M., Moreno-Gonzalez, I., Gutierrez, A. and Baglietto-Vargas, D., 2021. Animal and Cellular Models of Alzheimer's Disease: Progress, Promise, and Future Approaches. *The Neuroscientist*, p. 10738584211001753.

- Vadukul, D.M., Maina, M., Franklin, H., Nardecchia, A., Serpell, L.C. and Marshall, K.E., 2020. Internalisation and toxicity of amyloid- β 1-42 are influenced by its conformation and assembly state rather than size. *FEBS Lett*, 594(21), pp. 3490-3503.
- van Groen, T., Schemmert, S., Brener, O., Gremer, L., Ziehm, T., Tusche, M., Nagel-Steger, L., Kadish, I., Schartmann, E., Elfgen, A., Jürgens, D., Willuweit, A., Kutzsche, J. and Willbold, D., 2017. The A β oligomer eliminating D-enantiomeric peptide RD2 improves cognition without changing plaque pathology. *Scientific Reports*, 7(1), p. 16275.
- van Groen, T., Wiesehan, K., Funke, S.A., Kadish, I., Nagel-Steger, L. and Willbold, D., 2008. Reduction of Alzheimer's Disease Amyloid Plaque Load in Transgenic Mice by D3, a D-Enantiomeric Peptide Identified by Mirror Image Phage Display. *ChemMedChem*, 3(12), pp. 1848-1852.
- Veening-Griffioen, D.H., Ferreira, G.S., van Meer, P.J.K., Boon, W.P.C., Gispen-de Wied, C.C., Moors, E.H.M. and Schellekens, H., 2019. Are some animal models more equal than others? A case study on the translational value of animal models of efficacy for Alzheimer's disease. *Eur J Pharmacol*, 859, p. 172524.
- Walker, E.S., Martinez, M., Brunkan, A.L. and Goate, A., 2005. Presenilin 2 familial Alzheimer's disease mutations result in partial loss of function and dramatic changes in Abeta 42/40 ratios. *J Neurochem*, 92(2), pp. 294-301.
- Walsh, D.M., Thulin, E., Minogue, A.M., Gustavsson, N., Pang, E., Teplow, D.B. and Linse, S., 2009. A facile method for expression and purification of the Alzheimer's disease-associated amyloid beta-peptide. *Febs j*, 276(5), pp. 1266-1281.
- Wälti, M.A., Ravotti, F., Arai, H., Glabe, C.G., Wall, J.S., Böckmann, A., Güntert, P., Meier, B.H. and Riek, R., 2016. Atomic-resolution structure of a disease-relevant A β (1-42) amyloid fibril. *Proceedings of the National Academy of Sciences of the United States of America*, 113(34), pp. E4976-E4984.
- Wang, Y., Wu, F., Pan, H., Zheng, W., Feng, C., Wang, Y., Deng, Z., Wang, L., Luo, J. and Chen, S., 2016. Lost region in amyloid precursor protein (APP) through TALEN-mediated genome editing alters mitochondrial morphology. *Scientific Reports*, 6(1), p. 22244.
- Warner, C.J.A., Dutta, S., Foley, A.R. and Raskatov, J.A., 2017. A Tailored HPLC Purification Protocol That Yields High-purity Amyloid Beta 42 and Amyloid Beta 40 Peptides, Capable of Oligomer Formation. *Journal of visualized experiments : JoVE*, (121), p. 55482.
- Waser, M., Garn, H., Schmidt, R., Benke, T., Dal-Bianco, P., Ransmayr, G., Schmidt, H., Seiler, S., Sanin, G., Mayer, F., Caravias, G., Grossegger, D., Frühwirt, W. and Deistler, M., 2016. Quantifying synchrony patterns in the EEG of Alzheimer's patients with linear and non-linear connectivity markers. *Journal of neural transmission (Vienna, Austria : 1996)*, 123(3), pp. 297-316.
- Watanabe, K., Segawa, T., Nakamura, K., Kodaka, M., Okuno, H. and Konakahara, T., 2001. Identification of the molecular interaction site of amyloid β peptide by using a fluorescence assay. *The Journal of Peptide Research*, 58(4), pp. 342-346.
- WHO, 2020. *The top 10 causes of death* [Online]. Available from: <https://www.who.int/news-room/fact-sheets/detail/the-top-10-causes-of-death> [Accessed 11/10/2021].
- WHO, 2021a. *Dementia* [Online]. Available from: <https://www.who.int/news-room/fact-sheets/detail/dementia#:~:text=Alzheimer's%20disease%20is%20the%20most,60%E2%80%9370%25%20of%20cases> [Accessed 11/10/2021].
- WHO, 2021b. *Global status report on the public health response to dementia*. Geneva.

- Wiesehan, K., Buder, K., Linke, R.P., Patt, S., Stoldt, M., Unger, E., Schmitt, B., Bucci, E. and Willbold, D., 2003. Selection of D-Amino-Acid Peptides That Bind to Alzheimer's Disease Amyloid Peptide A β 1–42 by Mirror Image Phage Display. *ChemBioChem*, 4(8), pp. 748-753.
- Wisniewski, T., Castaño, E.M., Golabek, A., Vogel, T. and Frangione, B., 1994. Acceleration of Alzheimer's fibril formation by apolipoprotein E in vitro. *Am J Pathol*, 145(5), pp. 1030-1035.
- Wogulis, M., Wright, S., Cunningham, D., Chilcote, T., Powell, K. and Rydel, R.E., 2005. Nucleation-Dependent Polymerization Is an Essential Component of Amyloid-Mediated Neuronal Cell Death. *The Journal of Neuroscience*, 25(5), p. 1071.
- Wood, S.J., Wetzel, R., Martin, J.D. and Hurle, M.R., 1995. Prolines and Amyloidogenicity in Fragments of the Alzheimer's Peptide .beta./A4. *Biochemistry*, 34(3), pp. 724-730.
- Wood, S.J., Wetzel, R., Martin, J.D. and Hurle, M.R., 1995. Prolines and amyloidogenicity in fragments of the Alzheimer's peptide beta/A4. *Biochemistry*, 34(3), pp. 724-730.
- Worrall, J.A. and Mason, J.M., 2011. Thermodynamic analysis of Jun-Fos coiled coil peptide antagonists. *Febs j*, 278(4), pp. 663-672.
- Xiao, Y., Ma, B., McElheny, D., Parthasarathy, S., Long, F., Hoshi, M., Nussinov, R. and Ishii, Y., 2015. A β (1-42) fibril structure illuminates self-recognition and replication of amyloid in Alzheimer's disease. *Nat Struct Mol Biol*, 22(6), pp. 499-505.
- Xicoy, H., Wieringa, B. and Martens, G.J.M., 2017. The SH-SY5Y cell line in Parkinson's disease research: a systematic review. *Molecular neurodegeneration*, 12(1), pp. 10-10.
- Xie, H.-r., Hu, L.-s. and Li, G.-y., 2010. SH-SY5Y human neuroblastoma cell line: in vitro cell model of dopaminergic neurons in Parkinson's disease. *Chinese Medical Journal*, 123(8).
- Yan, L.M., Velkova, A., Tatarek-Nossol, M., Andreetto, E. and Kapurniotu, A., 2007. IAPP mimic blocks A β cytotoxic self-assembly: cross-suppression of amyloid toxicity of A β and IAPP suggests a molecular link between Alzheimer's disease and type II diabetes. *Angew Chem Int Ed Engl*, 46(8), pp. 1246-1252.
- Yang, T., Li, S., Xu, H., Walsh, D.M. and Selkoe, D.J., 2017. Large Soluble Oligomers of Amyloid β -Protein from Alzheimer Brain Are Far Less Neuroactive Than the Smaller Oligomers to Which They Dissociate. *The Journal of neuroscience : the official journal of the Society for Neuroscience*, 37(1), pp. 152-163.
- Yang, Y., Arseni, D., Zhang, W., Huang, M., Lövestam, S., Schweighauser, M., Kotecha, A., Murzin, A.G., Peak-Chew, S.Y., Macdonald, J., Lavenir, I., Garringer, H.J., Gelpi, E., Newell, K.L., Kovacs, G.G., Vidal, R., Ghetti, B., Ryskeldi-Falcon, B., Scheres, S.H.W. and Goedert, M., 2022. Cryo-EM structures of amyloid- β 42 filaments from human brains. *Science*, 375(6577), pp. 167-172.
- Yu, L., Edalji, R., Harlan, J.E., Holzman, T.F., Lopez, A.P., Labkovsky, B., Hillen, H., Barghorn, S., Ebert, U., Richardson, P.L., Miesbauer, L., Solomon, L., Bartley, D., Walter, K., Johnson, R.W., Hajduk, P.J. and Olejniczak, E.T., 2009. Structural characterization of a soluble amyloid beta-peptide oligomer. *Biochemistry*, 48(9), pp. 1870-1877.
- Yu, M., Ghamsari, L., Rotolo, J.A., Kappel, B.J. and Mason, J.M., 2021. Combined computational and intracellular peptide library screening: towards a potent and selective Fra1 inhibitor. *RSC Chemical Biology*, 2(2), pp. 656-668.

- Zannis, V.I., Just, P.W. and Breslow, J.L., 1981. Human apolipoprotein E isoprotein subclasses are genetically determined. *American journal of human genetics*, 33(1), pp. 11-24.
- Zatti, G., Ghidoni, R., Barbiero, L., Binetti, G., Pozzan, T., Fasolato, C. and Pizzo, P., 2004. The presenilin 2 M239I mutation associated with familial Alzheimer's disease reduces Ca²⁺ release from intracellular stores. *Neurobiol Dis*, 15(2), pp. 269-278.
- Zhan, Y., Zheng, H., Wang, C., Rong, Z., Xiao, N., Ma, Q. and Zhang, Y.W., 2017. A novel presenilin 1 mutation (F388L) identified in a Chinese family with early-onset Alzheimer's disease. *Neurobiol Aging*, 50, pp. 168.e161-168.e164.
- Zhao, J., Liu, X., Xia, W., Zhang, Y. and Wang, C., 2020. Targeting Amyloidogenic Processing of APP in Alzheimer's Disease. *Front Mol Neurosci*, 13, p. 137.
- Zhou, R., Yang, G., Guo, X., Zhou, Q., Lei, J. and Shi, Y., 2019. Recognition of the amyloid precursor protein by human gamma-secretase. *Science*, 363(6428).
- Zissimopoulos, J., Crimmins, E. and St Clair, P., 2014. The Value of Delaying Alzheimer's Disease Onset. *Forum for health economics & policy*, 18(1), pp. 25-39.
- Zott, B., Simon, M.M., Hong, W., Unger, F., Chen-Engerer, H.-J., Frosch, M.P., Sakmann, B., Walsh, D.M. and Konnerth, A., 2019. A vicious cycle of β amyloid-dependent neuronal hyperactivation. *Science (New York, N.Y.)*, 365(6453), pp. 559-565.